

***Xenopus laevis* as a chemical genetic screening tool
for drug discovery and development**

Adam E K Hendry

A thesis submitted for the degree of
Doctor of Philosophy
To the University of East Anglia
Norwich

School of Biological Sciences
University of East Anglia
Norwich

April 2014

Number of words: 59849

© This copy of the thesis has been supplied on condition that anyone who consults it is understood to recognise that its copyright rests with the author and that no quotation from the thesis, nor any information derived there from, may be published without the author's prior written consent.

Abstract

In this thesis we explore the applicability of the *X.laevis* chemical genetic screening model towards drug discovery and drug development. The NCI diversity set II compound library was screened to identify abnormal pigmentation generating phenotypes that may have therapeutic application towards the treatment of melanoma cancer. 13 hit compounds identified were shown to have significantly lower IC₅₀'s in the A375 melanoma cell line when compared to two control cell lines. Using the structural data of compounds screened (combined with the phenotypic data generated by the *X.laevis* screen), a report in which targets were predicted for each phenotypic category is described. Of the 10 targets predicted to generate an abnormal melanophore migration phenotype, six presented abnormal pigmentation phenotypes by compound antagonists. Two of these targets had no known previous link towards melanoma cancer. Many of the identified targets were also predicted to be targeted by nine out of 13 of the identified NCI compounds in the library screen.

Thus, through a combination of forward chemical genetic screening, appropriate cell based assays and chemoinformatical analysis we have developed an efficient and effective screening strategy for the rapid identification of hit compounds that are likely to be acting through either well known or novel targets that may have possible implications towards the treatment of melanoma cancer.

To assess the applicability of the *X.laevis* model towards drug development, in collaboration with AstraZeneca we designed a renal function toxicity assay. Renal toxicity is a serious concern in the pharmaceutical industry, being responsible for 7% of preclinical compound dropouts. I developed a biochemical assay in which renal function would be monitored by quantifying the concentration of ammonia excreted by embryos into media. A decrease in ammonia detected in the presence of nephrotoxic compounds was hypothesised to

represent a decrease in renal function, and therefore indicate toxicity. Despite promising preliminary experiments, the original salicylic acid ammonia assay detection method was inhibited by the presence of the compound solvent DMSO. A second assay (the glutamate dehydrogenase assay (GDH)) was trialled which could not detect a change in renal function in response to nephrotoxic compounds when compared to the vehicle control. In its current form, the *X.laevis* renal function assay is not capable of identifying nephrotoxic compounds and so further work is required.

Table of Contents

TITLE PAGE.....	i
ABSTRACT	ii
TABLE OF CONTENTS	iv
LIST OF FIGURES	xi
LIST OF TABLES.....	xvi
ACKNOWLEDGEMENTS.....	xvii

Contents

CHAPTER I	1
1.0 Introduction	1
1.1 Pharmaceutical drug discovery.....	2
1.1.1 The drug discovery pipeline	5
1.1.2 Lead compound identification	5
1.1.3 Preclinical assessment	8
1.1.4 Clinical testing and regulatory approval	9
1.1.5 Challenges of modern industrial drug discovery	10
1.1.6 Phenotypic versus target based chemical genetic screening	14
1.1.7 Models of phenotypic screening	19
1.1.8 Chemical genetic screening using <i>X.laevis</i> and zebrafish.....	22

1.1.9 <i>X.laevis</i> chemical genetic screening in practice	24
1.1.10 <i>Xenopus</i> melanogenesis.....	27
1.1.11 Melanoma cancer.....	28
1.1.12 Chemoinformatics	33
1.1.13 Molecular descriptors	38
1.1.14 Chemoinformatic target prediction	40
1.1.15 Summary	42
1.2 Pharmaceutical drug development	43
1.2.1 Biochemical and <i>in vitro</i> assays in preclinical toxicity testing	44
1.2.2 <i>In vivo</i> assays for drug development	46
1.2.3 <i>X.laevis</i> as a toxicity assay	47
1.2.4 Renal toxicity	50
1.2.5 Current <i>in vivo</i> and <i>in vitro</i> models of nephrotoxicity	51
1.2.6 The human kidney.....	54
1.2.7 <i>X.laevis</i> renal development and function	56
1.2.8 <i>X.laevis</i> and human differences in nitrogen excretion	57
1.2.9 <i>X.laevis</i> as a model of renal function	59
1.2.10 Summary	60
1.3 Thesis aims.....	61
CHAPTER II	62
2.0 Materials and Methods	62
2.1 Generation of <i>Xenopus laevis</i> and <i>Xenopus tropicalis</i> embryos	65
2.1.1 <i>Xenopus laevis</i> egg generation and <i>in vitro</i> fertilisation.....	65
2.1.1.1 Testes isolation	65
2.1.1.2 <i>X.laevis</i> egg generation and <i>in vitro</i> fertilization	66
2.1.1.3 Embryo dejellying.....	66
2.1.2 <i>Xenopus tropicalis</i> egg generation and <i>in vitro</i> fertilisation.....	67
2.1.2.1 Testes isolation	67

2.1.2.2 <i>X.tropicalis</i> egg generation and in vitro fertilization	67
2.1.2.3 Embryo dejellying.....	67
2.2 Chemical genetic screening	68
2.2.1 Determining the optimal screening concentrations.....	68
2.2.2 Chemical genetic screen using <i>X.laevis</i> or <i>X.tropicalis</i>	69
2.2.3 Observing embryos.....	70
2.2.4 Embryo Fixation	70
2.3 Small compounds used.....	72
2.4 Dose response assays.....	72
2.5 Cell culture assays	73
2.5.1 Cell lines used	73
2.5.2 Cell Viability assays	73
2.6 Renal function toxicity assay.....	74
2.6.1 Salicylic acid assay detection of ammonia NH ₃	74
2.6.2 Glutamate dehydrogenase assay detection of ammonia NH ₃	76
2.7 Chemoinformatical prediction of compound targets	77
2.7.1 Chemoinformatical analysis of compounds identified from the NCI Diversity set II chemical genetic screen.....	77
2.8 Statistical analysis.....	78
CHAPTER III	79
3.0 <i>Xenopus laevis</i> and <i>Xenopus tropicalis</i> as reliable models for chemical genetic screening	79
3.1 Introduction	79
3.1.1 Assessment of <i>X.laevis</i> chemical genetic screening reliability	79
3.1.2 Assessment and comparison of <i>X.tropicalis</i> as a viable chemical genetic screening model.....	81
3.2 Results	83

3.2.1 Rescreening of the original NCI diversity set I compound library	83
3.2.2 Assessment of <i>X.tropicalis</i> as a chemical genetic screening model.....	99
3.3 Discussion.....	106
CHAPTER IV	114
4.0 NCI diversity set II <i>X.laevis</i> chemical genetic screen followed by cell viability assay screening	114
4.1 Introduction	114
4.1.1 <i>X.laevis</i> as a chemical genetic screening model.....	114
4.1.2 The NCI diversity set II compound library	116
4.1.3 Screening of the NCI diversity set II compound library	117
4.2 Results	118
4.2.1 Phenotype scoring	118
4.2.2 Summary of phenotypes observed from hit compounds identified in the NCI diversity set II <i>X.laevis</i> chemical genetic screen	122
4.2.3 Summary of hit compounds identified in the NCI diversity set II <i>X.laevis</i> chemical genetic screen according to their allocated phenotypic categories.....	124
4.2.4 Melanoma cell viability screen in response to the 72 identified hit NCI diversity set II compounds.....	123
4.3 Discussion.....	156
CHAPTER V	161
5.0 Chemoinformatical analysis of the <i>X.laevis</i> NCI diversity set II compound screen	161
5.1 Introduction	161
5.2 Results	162
5.2.1 Bender laboratory chemoinformatical analysis of the NCI diversity set II chemical genetic screen.....	162

5.2.2 Summary of targets predicted to give rise to abnormal melanophore migration phenotypes when antagonised	164
5.2.3 Validation of abnormal melanophore migration predicted phenotypes.....	170
5.3 Discussion.....	184
CHAPTER VI	182
6.0 Development of the <i>X.laevis</i> renal function toxicity assay.....	194
6.1 Introduction	194
6.2 Results	197
6.2.1 Salicylic acid method of ammonia detection	197
6.2.2 Evaluation of the salicylic acid method of ammonia detection.....	198
6.2.3 Glutamate dehydrogenase assay (GDH) method of ammonia detection	204
6.2.4 Evaluation of the glutamate dehydrogenase assay method of ammonia detection.....	207
6.3 Discussion.....	210
CHAPTER VII	217
7.0 Final conclusions and future directions.....	217
7.1 Final Conclusions.....	217
7.2 Future considerations.....	220
APPENDICES.....	228
APPENDIX I	228
APPENDIX II	235
APPENDIX III	259
APPENDIX IV	241

ABBREVIATIONS269

REFERENCES270

Attached publications

I.	Chemical genetics and drug discovery in <i>Xenopus</i>	I
II.	Extensions to <i>In Silico</i> Bioactivity Predictions Using Pathway Annotations and Differential Pharmacology Analysis: Application to <i>Xenopus laevis</i> Phenotypic Readouts....	II
III.	Automated Phenotype Detection in <i>Xenopus laevis</i> Using Image Processing for Bioactivity Profile Analysis	III

List of figures and tables

Figures

Figure 1. The capacity for incorporation of the <i>X.laevis</i> animal model in the drug discovery pipeline.....	3
Figure 2. Summary of large pharma productivity between 2005-2010	10
Figure 3. Current in vitro phenotypic screening assays.....	20
Figure 4. Flow diagram of a screen using <i>X.laevis</i>	25
Figure 5. <i>Xenopus</i> melanophore migration schematic	25
Figure 6. Development of metastatic cancer	29
Figure 7. MAPK signalling cascade	29
Figure 8. Success rate as shown by development stage and therapeutic target area	31
Figure 9. Chemical space model	37
Figure 10. Schematic of the nephron.....	55
Figure 11. Common forms of ammonia excretory products	58
Figure 12. Example of <i>X.laevis</i> embryo image orientation	71
Figure 13. Phenotypic categories scored in the original Tomlinson et al., (2009) chemical genetic screen	80

Figure 14. Abnormal pigmentation phenotypes replicated using compounds identified from the original Tomlinson NCI diversity set I compound screen91

Figure 15. Abnormal melanophore morphology phenotypes replicated using compounds identified from the original Tomlinson NCI diversity set I compound screen93

Figure 16. Abnormal melanophore migration phenotypes replicated using compounds identified from the original Tomlinson NCI diversity set I compound screen94

Figure 17. Abnormal edema phenotype replicated using compounds identified from the original Tomlinson NCI diversity set I compound screen96

Figure 18. Abnormal morphology phenotypes replicated using compounds identified from the original Tomlinson NCI diversity set I compound screen97

Figure 19. Abnormal eye development phenotypes replicated using compounds identified from the original Tomlinson NCI diversity set I compound screen98

Figure 20. Comparison of NCI compounds identified in the NCI diversity set I compound screen that gave rise to a similar prominent abnormal pigmentation phenotype in both *X.laevis* and *X.tropicalis* 100

Figure 21. Comparison of NCI compounds identified in the NCI diversity set I compound screen that gave rise to a similar prominent abnormal melanophore morphology phenotype in both *X.laevis* and *X.tropicalis* 102

Figure 22. Comparison of NCI compounds identified in the NCI diversity set I compound screen that gave rise to a similar prominent abnormal melanophore migration phenotype in both *X.laevis* and *X.tropicalis* 103

Figure 23. Comparison of NCI compounds identified in the NCI diversity set I compound screen that gave rise to a similar prominent abnormal edema phenotype in both *X.laevis* and *X.tropicalis* 104

Figure 24. Comparison of NCI compounds identified in the NCI diversity set I compound screen that gave rise to a similar prominent abnormal morphology phenotype in both <i>X.laevis</i> and <i>X.tropicalis</i>	105
Figure 25. Comparison of NCI compounds identified in the NCI diversity set I compound screen that gave rise to a similar prominent abnormal eye development phenotype in both <i>X.laevis</i> and <i>X.tropicalis</i>	107
Figure 26. NCI diversity set II <i>X.laevis</i> chemical genetic screen summary figure ...	120
Figure 27. NCI compounds identified in the NCI diversity set II compound screen that gave rise to an abnormal pigmentation phenotype	125
Figure 28. NCI compounds identified in the NCI diversity set II compound screen that gave rise to a partial abnormal pigmentation phenotype	134
Figure 29. NCI compounds identified in the NCI diversity set II compound screen that gave rise to a prominent abnormal melanophore morphology phenotype	128
Figure 30. NCI compounds identified in the NCI diversity set II compound screen that gave rise to a prominent abnormal melanophore migration phenotype	134
Figure 31. NCI compounds identified in the NCI diversity set II compound screen that gave rise to a prominent edema phenotype	136
Figure 32. NCI compounds identified in the NCI diversity set II compound screen that gave rise to a prominent blistering phenotype	137
Figure 33. NCI compounds identified in the NCI diversity set II compound screen that gave rise to a prominent abnormal morphological phenotype	139
Figure 34. NCI compounds identified in the NCI diversity set II compound screen that gave rise to a prominent abnormal eye phenotype	141

Figure 35. Dose response graphs displaying cell viability (%) of A375, HEK293 and RD1 cell lines in response to the designated NCI compound over an increasing concentration range (LOG10 M).....149

Figure 36. Summary of statistical difference of 11 hit NCI compounds cell viability when screened at log10⁻⁹ M using the A375, HEK293 and RD1 cell lines to their respective in plate vehicle DMSO controls.....151

Figure 37. Data used to calculate statistical differences between IC50s generated for each of the 32 tested NCI 'hit' compounds screened upon three cell lines (A375, HEK293 and RD1)154

Figure 38. Phenotypes generated by sourced compound antagonists for melanophore migration phenotype giving targets identified the chemoinformatics report.....173

Figure 39. Stage 38 phenotype generated in response to GW5074 antagonist for predicted melanophore migration target c-Raf-1, alongside stage 38 hit NCI diversity set II compound phenotypes that were also predicted to antagonize the c-Raf-1 target175

Figure 40. Stage 38 phenotype generated in response to MIM1 antagonist for predicted melanophore migration target Mcl-1, alongside stage 38 hit NCI diversity set II compound phenotypes that were also predicted to antagonize the Mcl-1 target176

Figure 41. Stage 38 phenotype generated in response to bifemelane hydrochloride antagonist for predicted melanophore migration target MAO, alongside stage 38 hit NCI diversity set II compound phenotypes that were also predicted to antagonize the MAO target178

Figure 42. Stage 38 phenotype generated in response to AAL993 antagonist for predicted melanophore migration target VEGF-C, alongside stage 38 hit NCI diversity set II compound phenotypes that were also predicted to antagonize the VEGF-C target180

Figure 43. Stage 38 phenotype generated in response to BRD7389 antagonist for predicted melanophore migration target RSK, alongside stage 38 hit NCI diversity set II compound phenotypes that were also predicted to antagonize the RSK target	181
Figure 44. Stage 38 phenotype generated in response to PHTPP antagonist for predicted melanophore migration target ER- α , alongside stage 38 hit NCI diversity set II compound phenotypes that were also predicted to antagonize the ER- α target	183
Figure 45. Optimization of the <i>X.laevis</i> salicylic acid ammonia detection assay.....	200
Figure 46. Assessment of AstraZeneca compounds on <i>X.laevis</i> renal function using the <i>X.laevis</i> salicylic acid ammonia detection assay	205
Figure 47. Assessment of the <i>X.laevis</i> GDH ammonia detection assay	209
Appendix I Figure 1. Side by side comparison of NCI compounds identified in the NCI diversity set I compound screen that gave rise to a similar prominent abnormal pigmentation phenotype (complete list).....	210
Appendix I Figure 2. Side by side comparison of NCI compounds identified in the NCI diversity set I compound screen that gave rise to a similar prominent melanophore morphology phenotype (complete list).....	212
Appendix I Figure 3. Side by side comparison of NCI compounds identified in the NCI diversity set I compound screen that gave rise to a similar prominent melanophore migration phenotype (complete list).....	213
Appendix I Figure 4. Side by side comparison of NCI compounds identified in the NCI diversity set I compound screen that gave rise to a similar prominent eye development phenotype (complete list).....	214
Appendix III Figure 1. Dose response graphs displaying cell viability (%) of A375, HEK293 and RD1 cell lines in response to the designated NCI compound over an increasing concentration range (LOG ₁₀ M) (complete list).....	236

Appendix IV Figure 1. Data used to calculate statistical differences between IC50s generated for each of the 32 tested NCI ‘hit’ compounds screened upon three cell lines (A375, HEK293 and RD1 (complete list).	240
--	-----

Tables

Table 1. Advantages and disadvantages of forward / reverse chemical genetic screening approach towards drug discovery	16
---	----

Table 2. Advantages and disadvantages of in vitro assays used in the detection of renal toxicity.....	53
---	----

Table 3. List of reagents	62
---------------------------------	----

Table 4. List of solutions	63
----------------------------------	----

Table 5. List of equipment used	64
---------------------------------------	----

Table 6. Differences exhibited between the <i>X.laevis</i> and <i>X.tropicalis</i> animal models	82
--	----

Table 7. Hit compounds identified in the Tomlinson et al., (2005) NCI diversity set I chemical genetic screen, accompanied by their identified phenotype	84
--	----

Table 8. Collated dose response data in which embryos were exposed to hit compounds identified in the NCI diversity set II compound screen over a range of concentrations	144
---	-----

Table 9. IC50s generated screening NCI hit compounds on the A375, HEK293 and RD1 cell lines.	146
---	-----

Table 10. Summary of abnormal melanophore migration predicted targets, alongside their respective compound antagonists.....	165
---	-----

Table 11. Complete list of those compounds predicted to give rise to an abnormal melanophore migration phenotype	166
--	-----

Table 12. NCI hit compounds shown to statistically significantly reduce the A357 melanoma line when compared to their respective non melanoma controls versus the abnormal melanophore migration predicted targets.168

Table 13. Predicted abnormal melanophore migration targets are highlighted according to whether or not current literature has linked their involvement to melanoma cancer...171

Table 14. List of AstraZeneca supplied nephrotoxic and non-toxic compounds. .196

Table 15. T-test comparison of AstraZeneca compound dosed embryo media generated Delta(A340) versus vehicle control Delta(A340).208

Appendix II Table 1. Collated dose response data in which embryos were exposed to hit compounds identified in the NCI diversity set II compound screen over a range of concentrations (complete list).....215

Acknowledgements

Grant Wheeler – Thanks for all your support over the years and for putting up with my chemoinformatics stuff.

Rob Field, Sam Fountain and Duncan Armstrong – Thank you for all your help at key stages in the project, and for being so accommodating.

Vicky Hatch – That'll do pig. That'll do.

Andy Loveday – Wouldn't have been the same without you mate.

James 'Jaguar' McColl and Geoff Mok – Thanks for all the help and banter.

Kim Hanson – It couldn't have been done without you!

The Wheeler and Munsterberg groups – Thanks for being such a fun bunch of people to work with and for listening to me talk about frog urine.

Katrina Ross – Thanks for enduring. I'm still not going to tidy the desk.

The Hendry's – All that investment paid off in the end! (Sort of).

The Ross's – Thanks for all your support and letting me eat KFC in your house.

Winnie – You were irritating, and you will be missed.

Chapter I

1.0 Introduction

The primary goal of this thesis is to assess the applicability of the *Xenopus laevis* animal model towards both drug discovery and development. **Figure 1** summarises how we believe *X. laevis* can be incorporated into the pharmaceutical pipeline at various stages. It displays the points at which we believe *X. laevis* can contribute to both target based and activity based strategies, the difference being that the target based strategy requires an identified target that has been proven to be functionally involved in a disease pathway whereas an activity based strategy does not. Instead, the activity based strategy screens for lead compounds on the basis of biological activities implicated with a therapeutic benefit. The significance of this distinction and its impact on the utilisation of the *X. laevis* model towards drug discovery is discussed in the next section. **Figure 1** indicates how we believe the *X. laevis* model can be implemented at later phases in the pipeline, specifically for the purposes of this thesis preclinical development is highlighted. Preclinical development is the point at which identified hit compounds have passed the point of drug discovery and are now entering a phase of drug development. Drug development is the phase where previously identified hit compounds are assessed for their toxicity and efficacy (and is discussed in detail later in the introduction).

It has been shown previously by Tomlinson *et al.*, (2005) that *X. laevis* are highly amenable towards phenotypic chemical genetic screening having

identified numerous phenotypes. One specific compound (NCI210627) aided in the discovery of a potential new drug for the treatment of melanoma, and is currently undergoing human clinical trialling (Tomlinson et al., 2005; White et al., 2011). We aim to improve upon this process and further validate the use of *X. laevis* as a prominent model for phenotypic screening in drug discovery. A secondary aim of this thesis is to assess the value of *X. laevis* towards drug development in the form of a novel toxicity assay for the early preclinical assessment of renal toxicity, which is outlined in the next section. To emphasise the difference between assessing *X. laevis* as a tool for drug discovery and drug development, this introduction is split into two separate sections accordingly.

1.1 Pharmaceutical drug discovery

Despite increasing levels of investment from industry and governments the number of approved medicines has declined over the past three decades (Weigelt, 2009). The research and development of new drug entities however has increased over the past 10 years due to advances in technology. For example, the sequencing of the human genome has greatly expanded the list of potential “druggable” (defined as the expressed proteome believed to be applicable to modulation by compounds with drug-like properties (Cheng et al., 2007; Hopkins and Groom, 2002) expressed targets, increasing the list of known potential drug targets from around 500 to tens of thousands (Collins, 1999; Hurko, 2010). In addition, the advent of combinatorial chemistry has enabled the rapid synthesis of a large number of different, but structurally related compounds that were previously unavailable. This has allowed pharmaceutical

companies to create large (100000-1000000) novel compound libraries from which to source for drug screening (Bleicher et al., 2003).

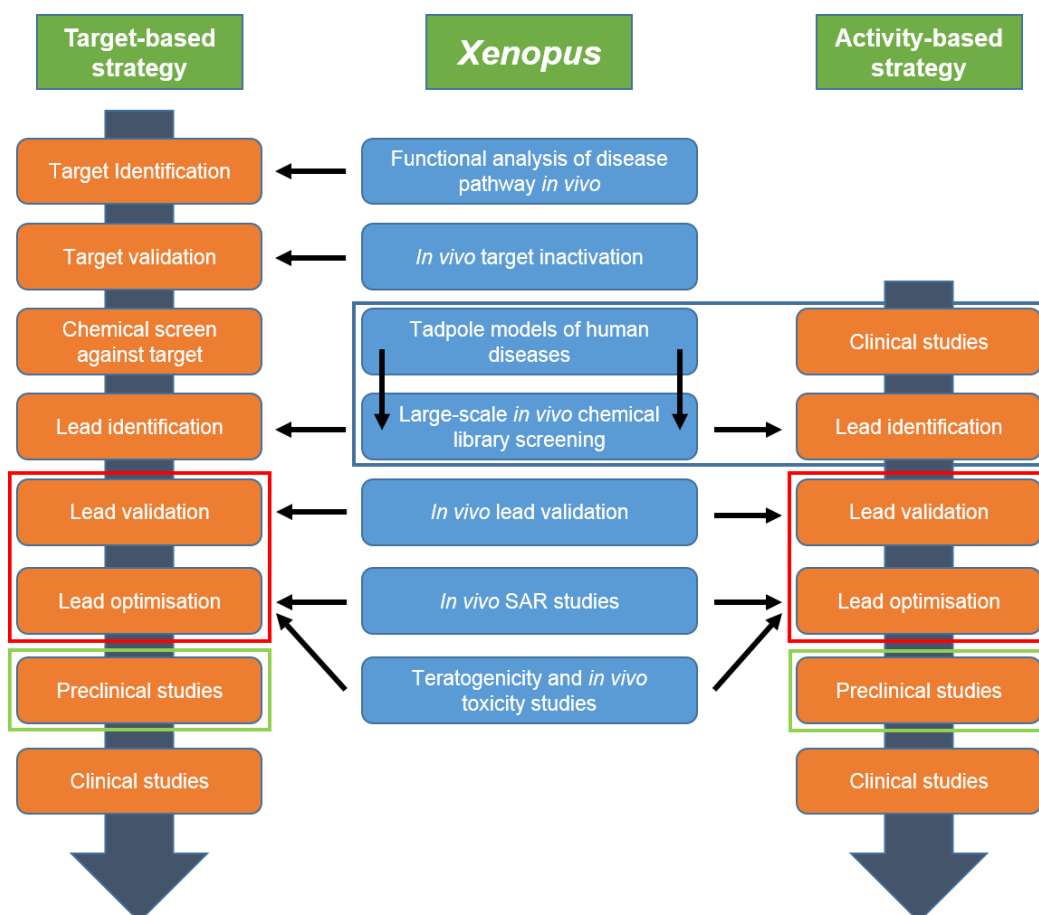


Figure 1. The capacity for incorporation of the *X. laevis* animal model in the drug discovery pipeline. Target based and activity based strategies are displayed. Arrows depict which drug development stages of both screening strategies the *X. laevis* can be incorporated. The blue box indicates where our *X. laevis* HTS incorporates into the drug discovery process. The red and green boxes indicate the drug discovery phases into which we believe using continued screening or novel assay design (such as the *X. laevis* renal assay outlined below) *X. laevis* may also be incorporated. Adapted from Wheeler and Brandli (2009).

The union of combinational chemistry and high-throughput screening (HTS) has allowed pharmaceutical companies to screen thousands of newly synthesised compounds with previously unexplored pharmacodynamic properties at an unprecedented rate (Donato and Castell, 2003; Tomlinson et al., 2005; Zon and Peterson, 2010; Zon and Peterson, 2005). HTS is able to identify those compounds that cause a desired interaction or therapeutic effect, singling them out for further screening to eventually become lead or “hit” compounds (Fox et al., 2006). HTS can be applied to cell based assays and/or model organisms ranging from *Caenorhabditis elegans* (the nematode worm) (Boyd et al., 2010b) to vertebrate models such as *Danio rerio* (zebrafish) (den Hertog, 2005; Zon and Peterson, 2005) and *X. laevis* (the African clawed frog) (Tomlinson et al., 2005; Tomlinson et al., 2009a; Tomlinson et al., 2009b).

The ultimate goal of using a chemical genetic approach is to identify specific small molecule compound inhibitors for every conceivable biochemical event (Carroll et al., 2003). However given the sheer number of possible drug targets and our current capacity to predict specific complementary binding targets of small molecules this may be a distant goal. A primary aim of this project is to assess *X. laevis* and its potential utility in the pharmaceutical industry as a model organism for chemical genetic screening. We also aim to show how *X. laevis* can be used in the pharmaceutical industry as an early preclinical toxicity screen to aid in the identification of toxic drugs that would otherwise progress further down the pipeline only to be dropped at a later time.

1.1.1 The drug discovery pipeline

Drug discovery over the past century has evolved from simple serendipitous observations of positive therapeutic effects elicited in humans towards a highly coordinated and robust production line (Hausheer et al., 2003; Swinney and Anthony, 2011). For pharmaceutical companies the efficacy and efficiency of their production line is all encompassing, ultimately determining how well they can compete with rival companies in a race to be the first to meet specific unmet market demands. While all companies will differ in their overall strategy and direction, the small molecule drug discovery pipeline is consistent when broken down into the individual stages of a compounds logical progression from initial identification to government approval (Hughes et al., 2011).

1.1.2 Lead compound identification

Over the past two decades drug development has largely focused upon using a target-based strategy (Bleicher et al., 2003; Kell, 2013; Kubinyi, 2003) . Here a target in a disease pathway will already have been identified and is believed to be critical in alleviating or curing the desired condition. Target identification is the first step in the drug discovery pipeline and is a prerequisite in the target-based strategy approach before compounds can even begin to be investigated. Industry often relies on external sources (predominantly academic literature (Bleicher et al., 2003)) when it comes to identifying novel targets associated with a disease pathway. Once a target is identified, compounds are screened against this target using reporter assay HTS technology. Compounds shown to bind to their desired target are considered lead compounds and are subsequently optimised and validated (Hughes et al., 2011).

Compound selection is a critical phase of early drug development. With the advent of combinatorial chemistry, many pharmaceutical companies in the early 1990's rapidly generated large compound libraries consisting of up to a million compounds (Bleicher et al., 2003). In addition, recent advances in HTS and reporter assay technology enabled companies to perform screens in which thousands of compounds could be screened against a target of interest over a short time period. Over time however, it became apparent that this brute force approach was inefficient. Indeed, there was no noticeable increase in lead compound identification when compared to the protocols that preceded this new approach (despite the screening of thousands more potential candidates) (Feher and Schmidt, 2003). This was attributed to the high structural complexity, poor drug like features and low product purity of the synthesised compounds (Bleicher et al., 2003; Hann et al., 2001). Rapidly the criteria by which compounds were chosen for screening shifted, where both quality and quantity of potential candidates were considered equally important (Ganesan, 2008; Villar and Hansen, 2009).

Great investment has been made into our capacity to predict which compounds may or may not be successful leads before they are even assessed (Villar and Hansen, 2009). A wide variety of algorithms are available that screen *in silico* compound structure libraries using defined descriptors to identify properties that might be considered of value or potentially risky, such as potential hERG inhibition which has been shown to lead to abnormal QT intervals which in turn induce arrhythmia and death in patients (Bender, 2010; Caldwell et al., 2009). Such "chemoinformatical analysis" are integral for efficient lead compound prediction and generation, and are discussed in detail below. A lead compound is selected based not only on positive reporter assay data (it binds to its desired

target efficiently and specifically), but also on its capacity for modification and optimisation (Song et al., 2014). Should the structure be difficult to modify this would limit the opportunities available for subsequent improvement and therefore it might be dropped despite good *in vitro* data (Avdeef, 2001).

An additional point is the use of natural products in drug discovery. Natural products are compounds that are derived from natural sources such as micro-organisms, plants and animals. Such compounds have had millions of years to evolve and therefore may represent the most biologically relevant compounds available (Harvey, 2008). Half of the new drugs approved between 1994 and 2008 were based on natural products, and this is during a time period where synthetic compound screening was heavily focused upon (Harvey, 2008). This would suggest that naturally derived compounds are an important source of novel therapeutics and remain a valuable resource for future compound screening. This is emphasised by the sharp rise in natural products currently undergoing development, and a shift to screening natural product based compound libraries (Harvey, 2008).

In summary, lead compound selection is a complex and constantly evolving process, but ultimately is aimed at providing compounds which have the best possible chance of making it through the subsequent phases of drug development.

Whilst it is essential to refine the compounds chosen for experimentation, it is equally important to focus on improving the assays used to screen the compounds themselves. If assays can be developed that detect and therefore disregard toxic compounds early in drug development then this has significant

economic implications. This has led to the research and development of numerous *in vitro* and *in vivo* high-throughput assays designed to be as reliable and robust as possible in identifying toxic compounds.

1.1.3 Preclinical assessment

Following the lead compound identification phase of drug development, compounds are subjected to preclinical efficacy and toxicity testing. Preclinical testing typically begins by subjecting lead compounds to biochemical and *in vitro* screening, followed by *in vivo* testing to identify any potential toxicity that would be undesirable in a therapeutic compound (discussed in detail below) (Han, 2010). An additional and equally important goal is to assess the efficacy of the compound by using appropriate disease models (Rick, 2009). The level of acceptable toxicity is dependent upon the severity of the toxicity manifested and the intended use of the compound. Naturally all lethally toxic compounds are unacceptable, regardless of their efficacy in binding to their desired targets (Han, 2010). However a certain level of toxicity is acceptable when treating diseases such as cancer, as the patient's life is already threatened. Chemotherapeutics have well documented side effects that can cause extreme discomfort in the short term but are acceptable due to their potential to save a patient's life. A similar approach is considered when regarding efficacy whereby a new drug must have a higher efficacy than that of a competing drug already available on the market. However some diseases may have no or limited treatment options lowering the required efficacy normally required for approval (Rick, 2009). Despite this allowance many safety regulatory bodies have become significantly more stringent in what is to be considered 'acceptable' levels of toxicity and efficacy across all compound classes. This has contributed

to the decline in approved novel therapeutic compounds as in many instances companies have failed to match these high standards (Kola and Landis, 2004).

1.1.4 Clinical testing and regulatory approval

Clinical trialling is the phase at which lead compounds are tested on human patients. Compounds which have reached this phase have strong preclinical data which infer low toxicity and high efficacy to minimise risk and maximise patient benefit as much as possible. Clinical trials are heavily regulated, with local governing bodies only permitting them to be carried out if preclinical data strongly supports the value of the study. Clinical trialling can be split into four separate phases, with sequential progression through each stage edging the prospective drug closer to approval. Phase zero clinical trialling is the first in human trial, in which single low doses of the compounds are administered to a small subject group (typically 10-15 participants) to assess the pharmacodynamic and pharmacokinetic properties of the compounds in the human system. Phase one clinical trialling uses a larger group (20-80 participants), testing the compound over a range of concentrations to assess any potential toxicity and determine safe dosage. Phase two and phase three clinical trialling expands the participant group (100-300 and 1000-3000 participants respectively) to further assess safety and also efficacy when compared to other compounds on the market targeted towards the same disease. If the compound is shown to have minimal (or acceptable) levels of toxicity and the efficacy is sufficiently high, it will then be approved by the appropriate local regulatory body (Hackshaw, 2009).

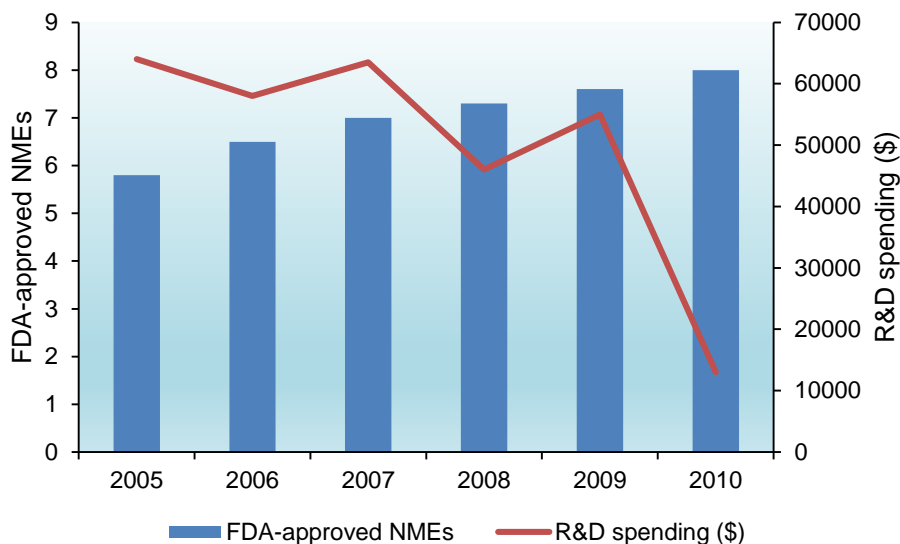


Figure 2. Summary of large pharma productivity between 2005-2010 (includes Eli Lilly, GlaxoSmithKline, Merck, Novartis, AstraZeneca, Bristol-Myers Squibb, Sanofi-Aventis, Pfizer and Roche). \$M represents millions of US Dollars. Taken from (Bunnage, 2011).

1.1.5 Challenges of modern industrial drug discovery

The reward for generating a “first in class” compound is substantial. The highest grossing drug in United States history is the cholesterol lowering statin Atorvastatin (marketed under the trade name Lipitor), which through its patent lifespan earned an estimated total of \$123 billion in global sales for its parent company Pfizer (King, 2013). Whilst Lipitor has eclipsed most other block buster drugs in terms of revenue (over double that of its closest competitor Plavix (Bristol-Myers Squibb and Sanofi)), it is still significant that profits such as these that have enabled pharmaceutical companies to become recognised global industrial giants in their own right. It should be noted however that drug development is not without risk. A successful drug candidate takes an estimated

10 years to be approved through clinical trialling and regulatory approval (not including preclinical development time) and costs an estimated \$1.32 billion per newly approved drug (including failures) before any financial return can be expected (Kaitin, 2010; Silber, 2010). An additional constant concern associated with pharmaceutical drug discovery is commonly referred to as the “patent cliff”. This is the point at which a drug is no longer protected by the parent company’s patent. With its exclusivity lost and open to competition from other companies, cheaply made competing generics significantly reduce the revenue of the original compound (2011; Cahn, 2012). Over the past two decades this concern has been compounded by the relative drop in successfully approved novel therapeutic compounds accompanied by the concerning lack of prospective entities in many of the larger pharmaceutical companies pipelines (Kaitin, 2010; Kola and Landis, 2004; Swinney and Anthony, 2011). One notable cause for the drop in newly approved compounds is increasingly high attrition rates. This has been attributed to a number of factors such as a focus on more complex diseases (Pammolli et al., 2011), increasingly stringent regulatory approval towards efficacy and toxicity (Paul et al., 2010) and the insufficient capacity of preclinical assays to accurately predict toxicity prior to clinical trials (Bleicher et al., 2003; Kaitin, 2010; Munos, 2009; Scannell et al., 2012; Wienkers and Heath, 2005).

Currently large pharmaceutical companies are actively investing into the research and development process, with the world’s leading companies investing an average \$10-50 billion between 1998 and 2004 (Tollman et al., 2011). This is emphasised in **Figure 2** in which large pharmaceutical company productivity between 2005-2010 is displayed, comparing new molecular entities approved (NMEs) versus year on year research and development spending

(Bunnage, 2011). Given the stated rise in compound development attrition and research expenditure this model of pharmaceutical development is clearly unsustainable. A change is required in the way pharmaceutical companies function, both in their research and development strategies and in their overall structure and role in the drug development process.

A clear shift in industry attitude toward drug development has been observed in the past 10 years, ranging from moving primary research facilities to cheaper locations (i.e. Asia (Li, 2008; Wood, 2012)) and intriguingly a number of large scale acquisitions of small specialised biotech companies (such as AstraZeneca's reported \$15 billion acquisition of MedImmune in 2007 (Zimm, 2007) or Pfizer's unprecedented \$68 billion acquisition of Wyeth in 2009 (Sorkin, 2009)) (Drews, 2003; LaMattina, 2011). Such major acquisitions represent an attempt to diversify their research and development by utilising small and specialised biotech companies that have greater expertise in particular scientific fields or disease areas and are more flexible in adopting new technology than traditional large pharmaceutical powerhouses (Comanor and Scherer, 2013; Drews, 2003; LaMattina, 2011). There has also been a move towards open source collaboration between pharmaceutical competitors (Mullard, 2011) as well as academics in an attempt to share information and facilities with the admirable attitude that it is possible to achieve more through collaboration (Portilla and Alving, 2010).

Academic institutions (much like small biotech companies) have the advantage of being extremely flexible in their approach to drug development, which has not gone unnoticed by large pharmaceutical companies who now commonly

collaborate with academic laboratories and academia based small biotechs. In the US there are now 78 academic or non-profit situated dedicated small drug discovery facilities (Frye et al., 2011). Such academic facilities in both the US and UK tend to focus on targets that lie outside of the traditional pathways typically focused upon by pharmaceutical companies, with roughly 50% of these *targets being based on new discoveries (Frye et al., 2011; Tralau-Stewart et al., 2013). Indeed, there is strong support for the utility of academia in drug discovery, which between 1998 and 2007 contributed intellectual property towards 56% of the new therapeutic compounds and biologics judged by the FDA to warrant priority review (Frye, 2013; Kneller, 2010; Silber, 2010). Academic projects have a key advantage in novel target discovery due to their project aims being rooted in furthering our knowledge of biology (Frye, 2013; Slusher et al., 2013). These projects are free to pursue obscure or untested targets and pathways without the risk of said target being discovered to have poor druggability (and therefore possess no monetary value) despite being important biologically in their own right (Slusher et al., 2013). This also allows academics to pursue low profile diseases which may affect a significantly smaller population group (such as rare genetic diseases) rather than high profile diseases (such as cancer and cardiovascular disease) (Kneller, 2010; Stevens et al., 2011).*

The direction and strategy to which large pharma has undertaken drug discovery is being forced to change significantly for the first time in its history. Never before has the sector been faced with the genuine prospect of failure to regularly bring new drugs to market, and whilst for the larger elite companies it is not yet a time of crisis, clear steps are being made to address what could soon become a precarious situation. Aside from a large shift in business

strategy, it is clear that the drug discovery process itself also needs to be overhauled to improve its diminished productivity. One approach that is gaining support within the literature is a return to phenotypic screening (Abdulla et al., 2009; Dar et al., 2012; Kell, 2013; Lee et al., 2012; Sykes and Avery, 2013) via the adoption of 'network pharmacology' (Ho and Lieu, 2008; Hopkins, 2008; Schrattenholz and Soskic, 2008). Both of these concepts can be addressed through chemical genetic screening.

1.1.6 Phenotypic versus target based chemical genetic screening

Chemical genetic assays study biology by using small molecular compounds to modulate protein function and can be split into two types; phenotypic (forward) chemical genetics and target based (reverse) chemical genetics (Cong et al., 2012). The latter refers to an assay in which the genetic or protein target is known and small molecules are screened against it to assess binding efficacy. Once a compound that is shown to interact with the known target is identified, the resulting phenotype is studied to determine the role the target gene or protein has in the model system (Spring, 2005). Forward chemical genetic assays screen compounds without a specific (or known) genetic or protein target. Those compounds that give rise to interesting or predicted phenotypes are identified as "hits" and undergo further investigation to identify the relevant genes involved (Spring, 2005). The advantages of using either a forward or reverse chemical genetic screening approach are outlined in **Table 1**.

Whilst both forward and reverse chemical genetics have significant advantages and disadvantages in their application, in the context of compound screening for drug development, the past 20 years have been dominated by a reverse genetic

approach (Abdulla et al., 2009; Butcher, 2005; Kell, 2013; Kubinyi, 2003). This was due to the original belief that following the sequencing of the human genome it would be possible to identify the function of each of the 30000-40000 identified genes by knocking each down separately so as to subsequently determine its biological role and assess its potential as a therapeutic target (Lander et al., 2001). This has since been shown to be impractical, not least because it is very rare that a small molecular compound binds to only a single target (Lee et al., 2012). Many commonly prescribed drugs on the market today have either numerous targets or their primary targets are unknown. For example lithium and valproic acid are widely used for the treatment of bipolar affective disorder and as a local anaesthetic respectively and have no universally accepted mechanism(s) of action (Williams, 2003). A consideration for the application of a forward chemical genetic approach to compound screening is the reintroduction of serendipity into the scientific process (Hausheer et al., 2003; Proschak, 2013). For example, early antihistamines were noticed purely by chance to have significant antipsychotic and antidepressant effects, an observation that ultimately gave rise to the field of psychopharmaceuticals (Benson, 1996; Butcher, 2005).

It has been observed in a variety of model organisms that single gene knockouts often present no overt observable phenotype and in fact only around 19% of genes are considered essential for survival (Austin et al., 2004; Giaever et al., 2002; Hopkins, 2008; Winzeler et al., 1999). This is almost certainly a natural defence mechanism towards random deletion events. Redundancies in most biological pathways have been well characterised and are often compensated for by alternative signalling routes (Kitano, 2007). It has been suggested therefore that in some cases it may be necessary to target multiple “nodes” of a

Table 1. Advantages and disadvantages of forward / reverse chemical genetic screening approach towards drug discovery

Strategy	Advantages	Disadvantages
Forward chemical genetic screening	<ul style="list-style-type: none"> - Allows for multiple target binding - Identifies promiscuous compounds - Optimisation of polypharmacological profile possible (Dar et al., 2012) - Identification of novel (multiple) targets or pathways in a disease - Contributed >50% of novel molecular mechanisms of action identified in approved small compounds over the past decade (Swinney and Anthony, 2011) 	<ul style="list-style-type: none"> - Difficult to optimise due to numerous targets involved - Mechanism of action may not always be known
Reverse chemical genetic screening	<ul style="list-style-type: none"> - Pipeline is geared towards generating target focused compounds - Single known target (simplifies mechanism of action) - Potential to be highly specific towards target (low off target toxicity) 	<ul style="list-style-type: none"> - Extremely difficult to make 100% selective for single target - Does not take into account multiple targets / pathways involved in disease - Has a poor track record for drug development with high attrition rates - Requires extensive validation of biological target. - Potential for adverse drug – drug interactions when combined (Buçşa C, 2013)

pathway (or pathways) before a phenotype may be induced (Zhao and Iyengar, 2012).

This is particularly relevant for diseases in which the primary targets are also present in otherwise healthy cells (Tang and Aittokallio, 2014). The goal of target based drug discovery is to identify and exploit differentially expressed targets (such as BRAF in cancer) to treat the disease whilst minimalizing toxicity towards healthy cells (Cong et al., 2012; Hopkins, 2008; Joyce et al., 2012). However this is not always possible, as can be seen in many forms of chemotherapy where severe toxicity can be observed in patients due to the cytotoxicity of the dosed compounds inhibiting essential functions present in both healthy and cancerous cells simultaneously (Tang and Aittokallio, 2014). It has been suggested that a more prudent approach may be to better understand the subtle ways in which pathways are perturbed in cancer (Bhadriraju and Chen, 2002; Tang and Aittokallio, 2014). For example, two proteins that may be non-lethal to cancer when knocked down alone may be essential for survival when knocked down simultaneously due to their combined importance in a cancer specific pathway. These small fluctuations in endogenous pathway expression between cancerous and healthy cells, may explain the clear difference in their observed cell fate despite their common genetic lineage (Gascoigne and Taylor, 2008; Hopkins, 2008; Tang and Aittokallio, 2014).

Phenotypic screening can be used as a powerful tool in developing this polypharmacological approach. Compounds screened can bind multiple targets to generate a phenotype (thereby having a desired polypharmacological profile). It is then possible using chemoinformatics to predict (and then biologically validate) any number of potential targets that only in combination elicit the observed effect (Feng et al., 2009; Liggi, 2013). In this way it is possible to generate a target profile of the disease and subsequently optimise the compound identified in the phenotypic screen towards each of those targets.

A study by Dar *et al.*, (2012) provides an elegant example of how both target and phenotypic chemical genetic screening can be used in combination to discover numerous targets in cancer, which can be successfully antagonised simultaneously to develop a selectively promiscuous compound with a strong therapeutic effect. Dar *et al.*, (2012) used a target based chemical genetic screen (utilising the *Drosophila* multiple endocrine neoplasia type 2 (MEN2B) model) to identify one compound (AD57) that rescued oncogenic Ret induced lethality (Read *et al.*, 2005; Vidal *et al.*, 2006). Structurally related Ret inhibitors showed reduced efficacy and increased toxicity when compared to AD57. Phenotypic compound screening using the *Drosophila* wing assay (where overexpressed Ret in the wing leads to over proliferation and abnormal cell migration), showed that optimal survival in the model occurred when Ret, Src, Raf and S6K were inhibited. It was also shown that inhibition of Tor led to increased toxicity (Read *et al.*, 2005). Using this knowledge two compounds were synthesised (AD80 and AD81) based on the previous AD57 scaffold that were selectively potent for all three desired targets (whilst selectively avoiding Tor binding), resulting in lowered toxicity and improved efficacy in *Drosophila* and mammalian MEN2 models. This included mouse xenografts, which when compared to previously screened isomers (i.e. AD57) and even currently available drugs (such as vandetanib) showed improved inhibition of tumour growth (Dar *et al.*, 2012). This screen highlighted the strong advantages of using chemical genetic screening to both identify lead compounds towards a specific target (through target based screening) and develop an optimal polypharmacological profile (through phenotypic screening) for optimised compound efficacy with minimal toxicity (Dar *et al.*, 2012; Hopkins, 2008). This

study provided significant support for the role of phenotypic based screening and polypharmacology towards successful drug development.

1.1.7 Models of phenotypic screening

It is important to pick an appropriate model when developing a phenotypic screen as this often determines the throughput capacity. For example, over the past two decades cell based assays have been used to great effect in phenotypic screens due to significant advances in high throughput screening technology. Using *in vitro* model systems it is possible to screen vast numbers of compounds and/or end points over a short time period (summarised in **Figure 3** and reviewed in (Feng et al., 2009; Michelini et al., 2010)). As a model system, the practical advantages of using an *in vitro* assay (depending on the assay chosen) is unparalleled in its capacity for application towards high throughput screening (Feng et al., 2009). As such, cell based assays play an important role in early drug discovery by rapidly identifying lead compounds. All cell based assays however share one common flaw, their inability to accurately represent a fully functional three-dimensional model organism. This is significant, as failure to accurately predict efficacy and toxicity in humans has been well documented as a contributor to the currently high levels of compound development attrition (Hopkins, 2008; Kola and Landis, 2004).

One alternative to *in vitro* screening is to use invertebrate models in the form of *C. elegans* and *Drosophila melanogaster*, which retain the capacity for high throughput screening with the advantages associated with using an *in vivo*

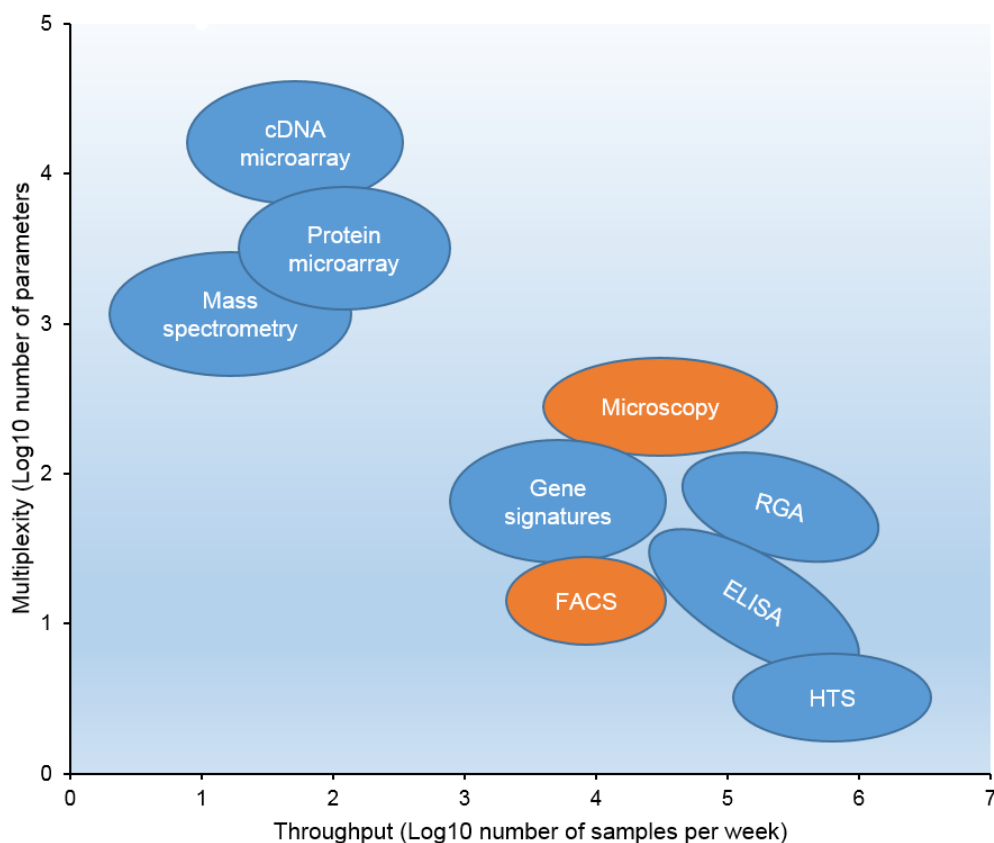


Figure 3. Current *in vitro* phenotypic screening assays. Throughput is defined by the number of compounds screened per week (Log_{10}). Multiplicity is defined by the number of parameters (Log_{10}) an assay format can assess. HTS represents HTS assays with a single output (and therefore producing the highest throughput). RGA and ELISA assays shown are considered to be multiplexed, (many HTS assays running simultaneously at lower throughput). Assay formats shown in orange are imaged based assays. Assay formats shown in blue are non-imaged based assays. Assay multiplicity is inversely correlated with throughput. cDNA, (complementary DNA). ELISA, (enzyme-linked immunosorbent assays). RGA, (reporter gene assays). FACS, (fluorescence-activated cell sorting). HTS, (high throughput screening). Adapted from (Feng et al., 2009)

system (Segalat, 2007). *C. elegans* was first introduced as a viable animal model by Sidney Brenner in the 1960's and has contributed greatly to our understanding of the molecular biology behind many critical biological events, such as senescence, early development, apoptosis and neuronal function (Brenner, 1974; Giacomotto and Segalat, 2010). Their short life cycle, low cost, ease of husbandry and small size (~50µM in length) make them highly amenable towards high-throughput phenotypic chemical genetic screening (Boyd et al., 2010a; Boyd et al., 2010b; Helmcke et al., 2010). However, *C. elegans* have several drawbacks towards their use as a model of a human system. For example, they are genetically distant from humans and as such cannot replicate a number of diseases. Also, whilst they have functioning organ systems their anatomy and physiology may be too different to reliably predict efficacy or toxicity in a human equivalent (Bier, 2004; Mushegian et al., 1998). The fruit fly model *Drosophila melanogaster* is similar in its advantages and disadvantages towards chemical genetic screening (Arias, 2008; Brenner, 1974; Manev and Dimitrijevic, 2004; Stilwell et al., 2006). Whilst both models have been shown to have potential in drug discovery (reviewed in (Artal-Sanz et al., 2006), (Nichols, 2006) and (Segalat, 2007)), it remains that their physiology may be too different to humans to be a representative screening model (Wheeler, 2012).

Commonly used model of the human system is the mouse (*Mus murinae*) (West et al., 2000). However mice are large, have relatively low fecundity, long life spans and high husbandry costs. As such the mouse model is obviously not suited towards optimised medium to high throughput compound screening. A compromise between the evolutionary and physiological relevance of the mouse and the practical high though put screening advantages elicited by *C. elegans*

and *D.melanogaster* can be found in the form of Zebrafish and *X. laevis*. Both models are significantly more relevant towards human physiology than the invertebrate models whilst retaining their high fecundity and screening capacity (Brenner, 1974; Wheeler and Brandli, 2009; Zon and Peterson, 2010; Zon and Peterson, 2005).

1.1.8 Chemical genetic screening using *X. laevis* and zebrafish

Peterson *et al.* conducted the first successful HTS using the zebrafish vertebrate animal model (Peterson et al., 2000). The HTS was performed using a chemical genetic approach, screening 1100 small molecules selected randomly from a small molecular library. To maximise screening output, 4 organ systems were observed; the central nervous system, the cardiovascular system, pigmentation and ear development, which differ significantly from invertebrates. Visual examination of all four systems for abnormal phenotypic defects allowed a single experimenter to screen roughly 400 compounds per day. Around 1% of compounds screened affected a single feature of one of the organ systems observed (Peterson et al., 2000). Since then, in a screen conducted by Tomlinson *et al.*, (2005), it has also been shown that the classical animal model *X. laevis* is equally amenable to HTS. The experiment subjected *X. laevis* embryo samples to much the same compounds and screening methods used upon zebrafish in the Peterson *et al.* (2000) HTS. Results revealed compounds that were shown to give a particular phenotype in zebrafish also gave a very similar phenotype in *X. laevis* (Tomlinson et al., 2005).

The advantages to using both zebrafish and *X. laevis* as a screening animal model are highly comparable. The main practical advantage of using *X. laevis* is

that hundreds of eggs can be produced at a controlled time by a single female following hormone stimulation (zebrafish require no hormone stimulation but females produce fewer eggs). *X. laevis* eggs are easily fertilized via *in vitro* fertilization, which allows for the rapid generation of viable embryos in a relatively short amount of time. The embryos are also small enough to be arrayed out into 96 or 48 well plates as desired, but large enough so that development can be easily observed under a light microscope. As both of these organisms are aquatic, compounds can be dosed into the media and are passively or actively absorbed (Berger and Currie, 2007; Wheeler, 2012). These practical advantages make *X. laevis* highly suited towards HTS. Whilst these practical advantages are shared by both *X. laevis* and zebrafish, it is notable that *X. laevis* is evolutionary several hundred million years closer to humans (Kumar and Hedges, 1998). Also the *X. laevis* animal model contains organs that are more representative of the human system, such as lungs instead of gills, their immune system and a two chambered atrium which the zebrafish lacks (Wheeler and Brandli, 2009). As a genetic model *X. laevis* has proven to be inapplicable to techniques commonly utilised in the zebrafish due to its polytetraploid genome (Wheeler and Brandli, 2009). However, an evolutionary very close model to *X. laevis*, *Xenopus tropicalis*, has a diploid genome that was sequenced in 2012 (Hellsten et al., 2010). It is also worth noting that the *X. laevis* genome is currently being sequenced, the first draft of which has been published on Xenbase, the *Xenopus* model organism online data base (<http://xenbase.org>) (Bowes et al., 2013; Bowes et al., 2008; Bowes et al., 2010; James-Zorn et al., 2013). Both *X. laevis* and *X. tropicalis* have proven to give very similar results when screened with the same set of compounds, suggesting *X. tropicalis* in the future may be used instead of or in conjunction with *X. laevis* (Fort et al., 2004; Wheeler and Brandli, 2009).

1.1.9 *X. laevis* chemical genetic screening in practice

The value of *X. laevis* as a HTS vertebrate animal model was emphasized in a highly successful HTS carried out by Tomlinson *et al.*, (2009) (**Figure 4**) (Tomlinson *et al.*, 2009b). The screen observed the phenotypic effects of 3000 arrayed compounds (sourced from either the NCI Diversity I or the MicroSource Gen-Plus collection) placed in 96 well plates with five *X. laevis* embryos per well. The embryos were allowed to develop over 3 days until they reached stage 38. Phenotypic abnormalities were primarily scored depending on pigmentation defects observed. Of the 3000 compounds screened 40 provided reproducible abnormal phenotypes considered to be a “hit” (Tomlinson *et al.*, 2009b). The 40 reported “hits” could be broken down into common abnormal phenotypic categories of which included edema (8%), general development (8%), melanophore morphology (12%), eye development (13%), melanophore migration (17%) and pigmentation (42%) (Tomlinson *et al.*, 2005).

Further analysis of the identified hit compound NCI 84093 (which was shown to cause marked inhibition of melanophore migration), showed it to be a matrix metalloproteinase (MMP) inhibitor (Tomlinson *et al.*, 2009a). MMPs consist of a large family of zinc dependant endopeptidases that can cleave the vast majority of constituents in the extracellular matrix (Wang *et al.*, 2011). They also have a number of other roles in human systems such as cell migration and have been heavily linked to cancer progression (Hofmann *et al.*, 2000). Specifically NCI/84093 was shown to inhibit MMP-14 and MMP-2, which have been identified as being required for melanophore migration, an important factor in melanoma (Tomlinson *et al.*, 2009a). Melanoma is a very aggressive and invasive form of cancer that shows poor prognosis on diagnosis

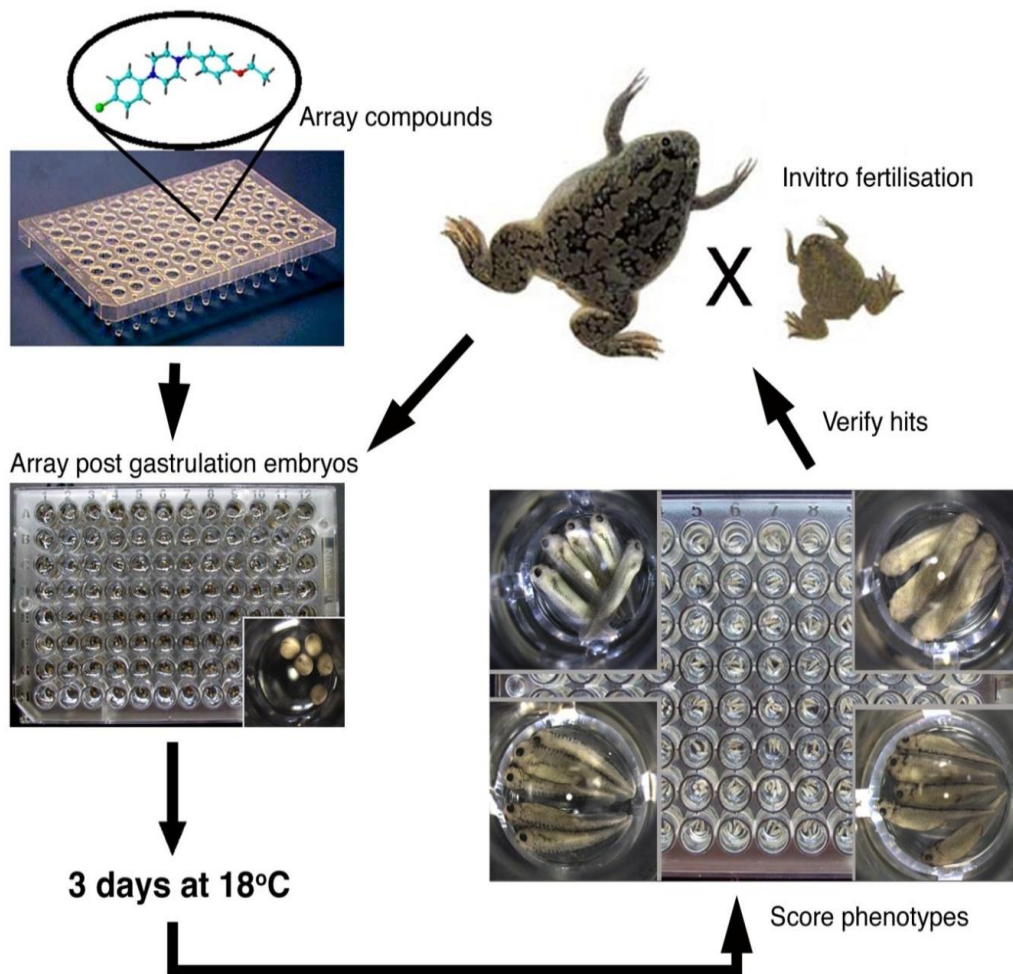


Figure 4. Flow diagram of a screen using *X. laevis*. Compounds are arrayed out into 96 well plates. Embryo's are collected and arrayed out into well plates, 5 embryos per well. Plates are incubated at 18°C for three days and phenotypes are subsequently scored. Those compounds that generate abnormal phenotypes are screened again using the same process to verify hits and/or to produce dose response data with a range of concentrations of the same compound. Adapted from (Tomlinson et al., 2009a).

(Eide et al., 2009). It has been suggested that its highly invasive qualities are due to the fact that the melanocytes from which the melanoma is derived are extremely migratory themselves. Thus previous results suggest that inhibiting melanophore migration could pose an effective treatment of melanoma, as was shown with a second hit compound NCI 210627.

Using similarity searching chemoinformatical algorithms, further analysis of NCI 210627 found it to be structurally highly related to the dihydroorotate dehydrogenase (DHODH) inhibitor Brequinar (Tomlinson et al., 2005; White et al., 2011). It was subsequently found that the anti-arthritic drug Leflunomide was also an inhibitor of DHODH despite being structurally unrelated to both NCI 210627 and Brequinar. As Leflunomide was already an FDA approved drug it was quickly taken on for further testing as there is little chance of off target toxicity due to its already approved status. Since this discovery, Leflunomide has been shown to have very promising implications as an anti-melanoma chemotherapeutic (White et al., 2011). By inhibiting DHODH it is believed that Leflunomide causes the inhibition of transcriptional elongation in melanoma cells which was shown to cause a rapid reduction in primary melanoma tumor size, a mechanism of action that would not have been identified were it not for the original *X. laevis* screen (White et al., 2011). These results emphasize the potential of *X. laevis* HTS as a tool for identifying new drugs with novel mechanisms of action. It also goes some way to help validate *X. laevis* as a valuable asset to drug discovery.

Since the initial Tomlinson screen a number of other successful chemical genetic screens have also contributed towards validating *X. laevis* as model for phenotypic chemical genetic screening (Adams et al., 2006; Dush et al., 2011;

Kalin et al., 2009). These assays focused upon different end points including angiogenesis, lymphangiogenesis, left right asymmetry and TGF- β signaling (Dush et al., 2011; Kalin et al., 2009). For the purpose of this thesis I will concentrate upon *X. laevis* melanocyte abnormalities as my primary screening endpoint. We hope to replicate the original success of the initial Tomlinson screen by identifying novel compounds for the treatment of melanoma, but also to expand the screens remit to better identify and validate the potentially novel targets involved.

1.1.10 *Xenopus* melanogenesis

Xenopus melanophores (known as melanocytes in higher vertebrates) are derived from pluripotent neural crest cells which arise in the developing neural tube. Neural crest cells can also differentiate into bone, cartilage, neurons and endocrine, adipose and connective tissue (Kumasaka et al., 2005). Melanophore migration begins as a wave, starting at the anterior of the embryo and ending at the posterior trunk. Between stages 26 and 30, *Xenopus* melanophores migrate from the dorsal side of the neural tube and finish migrating by stage 41, forming two distinctive lateral and dorsal pigment stripes (**Figure 5**) (Collazo et al., 1993). Melanophore development has been shown to play a role in a number of different disease states. For example, absence of the melanocytes in humans is indicative of piebaldism. Another example includes vitiligo, an autoimmune disease which leads to the destruction of melanocytes in patches of the patients skin (Granato et al., 1996). Perhaps more significantly, accumulated mutations in melanocytes promoting uncontrolled cell growth can give rise to the formation of melanoma. For example, the transcription factor *Mitf* has been shown to be essential towards melanocyte development, with Loss of

Mitf function leading to a total failure of melanocyte differentiation (Kumasaka et al., 2005). *Mitf* however has also been shown to play a significant role in the progression of human melanoma growth by promoting cell division and survival through CDK2 and BCL2 respectively (Garraway et al., 2005). The inhibition of the formation of melanophores and their subsequent migration in *Xenopus* has been used as an indicator of potential therapeutic compounds for the treatment of melanoma in humans (White et al., 2011).

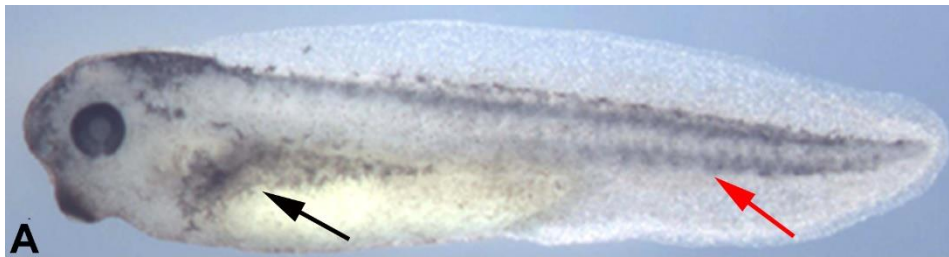


Figure 5. *Xenopus* melanophore migration schematic. The dorsal (red arrow) and lateral pigment (black arrow) stripes of a stage 38 wild type embryo.

1.1.11 Melanoma

Melanoma is a cancer of the skin, arising from melanocytes that have undergone numerous mutations to become cancerous (**Figure 6**). It is a particularly aggressive form of cancer with poor prognosis rates past stage 1 of tumour development (Braeuer, 2013; Garbe and Leiter, 2009). Melanocytes reside within the basal layer of the epidermis, which on occasion give rise to

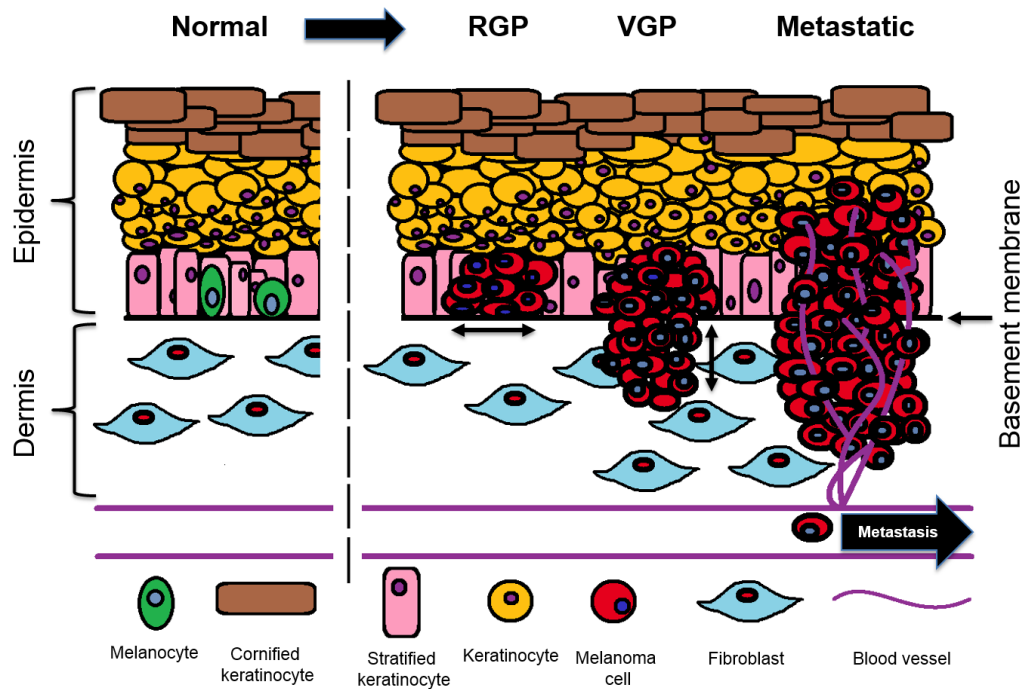


Figure 6. Development of metastatic cancer. Summarises the various phases involved in the progression of a melanocyte to a malignant melanoma. Adapted from (Gaggioli and Sahai, 2007).

naevi through abnormal increased proliferation. Not all naevi will become cancerous but some may show increasing signs of dysplasia, which begin to spread. The initial radial growth phase (RGP) tends to occur laterally and close to the epidermis and is still associated with good prognosis if diagnosed at this phase. As the melanoma begins to grow vertically (the vertical growth phase (VGP)), melanoma cells penetrate the basement membrane and invade the dermis, the majority of which still remaining in clusters. The VGP is often associated with the cancer possessing metastatic potential, which when accompanied by increasing vasculogenesis signals the cancer is now aggressive and will begin to spread to different sites (Gaggioli and Sahai, 2007).

Reported melanoma incident rates have risen over the past decade and this has recently been accompanied by a number of new treatment options that have successfully improved patient survival rates (Garbe and Leiter, 2009). It is now well established that a mutation in the B-Raf oncogene, which is present in 41% of melanomas, plays a significant role in the progression of the disease (Bis, 2013; Lee, 2011). B-Raf activates the MAP kinase / ERK pathway thereby promoting uncontrolled cell division (Braeuer, 2013; Wan et al., 2004). The MAPK pathway has been shown to play a significant role in the proliferation and survival cancer cells, particularly in melanoma (**Figure 7**). The activation of RAS GTPase promotes the activation of the ARAF, BRAF and CRAF kinases. RAF kinases promote the phosphorylation and activation of MEK, which subsequently phosphorylates and activates ERK. ERK proteins translocate into the nucleus where they begin to upregulate a number of cell survival proteins and transcription factors. This includes the upregulation of CCND1, which is known to promote cell proliferation and cell survival. In this way, the MEK pathway plays a significant role towards the promotion and survival of melanoma. This also explains why such great effort has been made into the development of inhibitors specific to this pathway, as clearly they have strong therapeutic potential. Current example inhibitors are shown in **Figure 7**.

The significance of the MAPK pathway in melanoma is emphasised by the numerous studies and therapeutics that are targeted towards B-Raf in an attempt to inhibit its proliferative effects (Sabbatino et al., 2013). Two notable examples are Vermurafenib and Debrafenib, compounds that specifically interfere with the B-Raf/MEK pathway resulting in cell death (Chapman et al., 2011). Whilst these compounds represent a significant step forward in our capacity to treat melanoma (replacing decarbazine as the front line treatment

option (Chapman et al., 2011)), they are only effective against tumours that contain the B-Raf mutation (Chapman et al., 2011). This is important as 41% of melanoma patients with wild type B-Raf must rely on less effective treatment options (Bis, 2013). Moreover, it is not uncommon for those patients possessing B-Raf mutant containing tumours to develop resistance within a year, resulting in remission (Fedorenko et al., 2011).

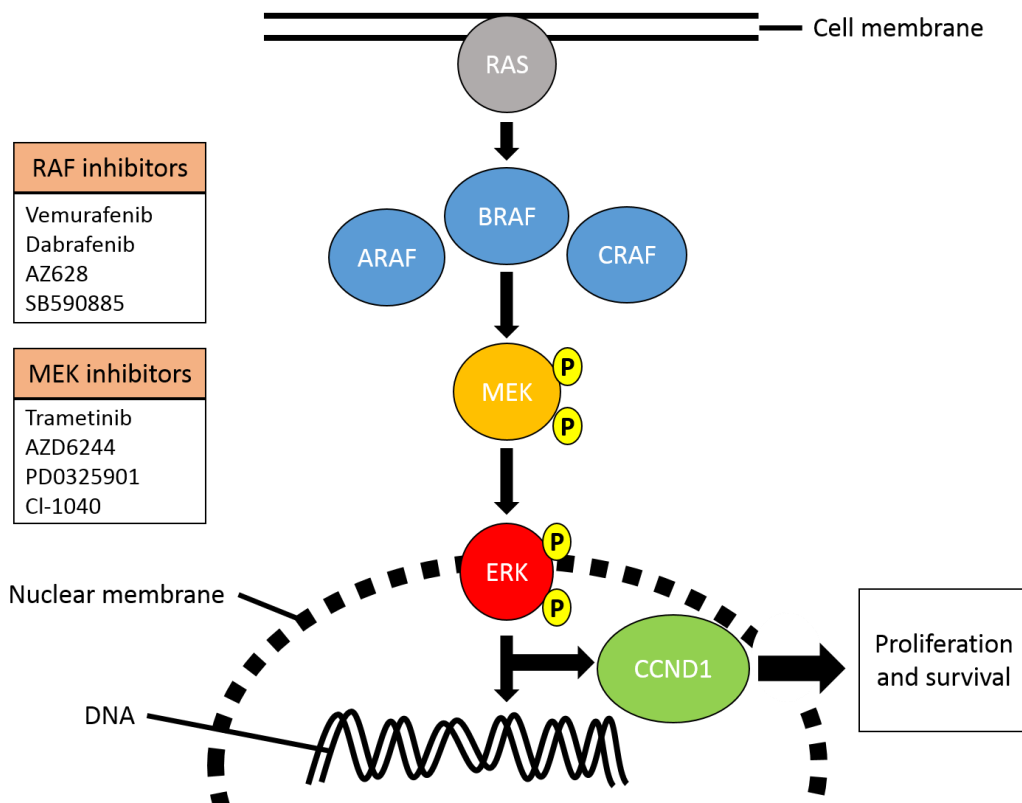


Figure 7. MAPK signalling cascade. Example inhibitors of the RAF and MEK elements of the MAPK pathway are indicated. ARAF, v-raf murine sarcoma 3611 viral oncogene homolog; BRAF, v-raf murine sarcoma viral oncogene B1; CCND1, cyclin D1; CRAF, v-raf-1 murine leukemia viral oncogene homolog 1; ERK, extracellular signal-regulated kin-ase; MEK mitogen-activated protein kinase kinase (adapted from (Siddiqui and Piperdi, 2010)).

This has led to numerous combinatorial studies in an attempt to target the cancer at multiple target sights to inhibit it rapidly via multiple pathways before it can acquire resistance (reviewed in (Kwong and Davies, 2014)).

It is evident that alternative targets need to be identified if melanoma is to be treated effectively, particularly for those patients who possess B-Raf wild type tumours. Whilst there are numerous candidates (such as the PI3K-AKT pathway or CDK4 (Davies, 2012; Kwong et al., 2012; Kwong and Davies, 2014)) for alternate targets acting independently to the MAP kinase / ERK pathway it has yet to be shown which targets in combination with B-RAF result in the best chance of survival (Kwong and Davies, 2014). Recent studies have shown that the addition of a MEK inhibitor combined with a B-Raf antagonist has promising effects in reducing melanoma tumour size and proliferation (Greger et al., 2012; Grimaldi et al., 2014). MEK inhibitors however have proven themselves to have significant toxic side effects in humans as their mechanism of action results in global cytotoxicity (Menzies and Long, 2013). It is likely that given the high variation of mutations observed between melanoma patients any combinatorial treatment will ultimately have to be personalised (Madureira and de Mello, 2014).

It is also worth noting the recent success of antibiotic treatments such as PD-1 and MDX-101 (Ipilimumab). Ipilimumab activates the immune system by targeting CTLA-4. Inhibiting CTLA-4 allows cytotoxic T lymphocytes to recognise and destroy the melanoma cells. Novel treatments such as these in combination with small compound therapy may in the future prove to be an effective tool for the treatment of melanoma (Cha et al., 2014).

Whilst progress has been made in our capacity to treat melanoma, it is clear that both new drugs and novel targets (that are differentially expressed in cancer cells when compared to healthy cells) are required. One way to quickly identify novel therapeutic compounds is to predict them *in silico* by screening virtual compound libraries against a target of interest to predict binding potential (Kortagere et al., 2012; Vogt and Bajorath, 2012). By using known structural alerts and previous biological and chemical data it is also possible to predict those compounds that might be particularly toxic or difficult to optimise, as well as other important drug characteristics such as solubility, absorption and potential metabolic and excretory routes (Tan et al., 2013; Valerio and Choudhuri, 2012). Likewise, it is also possible to predict which targets might give rise to an exhibited phenotype by combining biological and structural data (Liggi, 2013). In this way *in silico* predictions (known as chemoinformatics) can refine the selection process by which screening compounds are chosen (Vogt and Bajorath, 2012).

1.1.12 Chemoinformatics

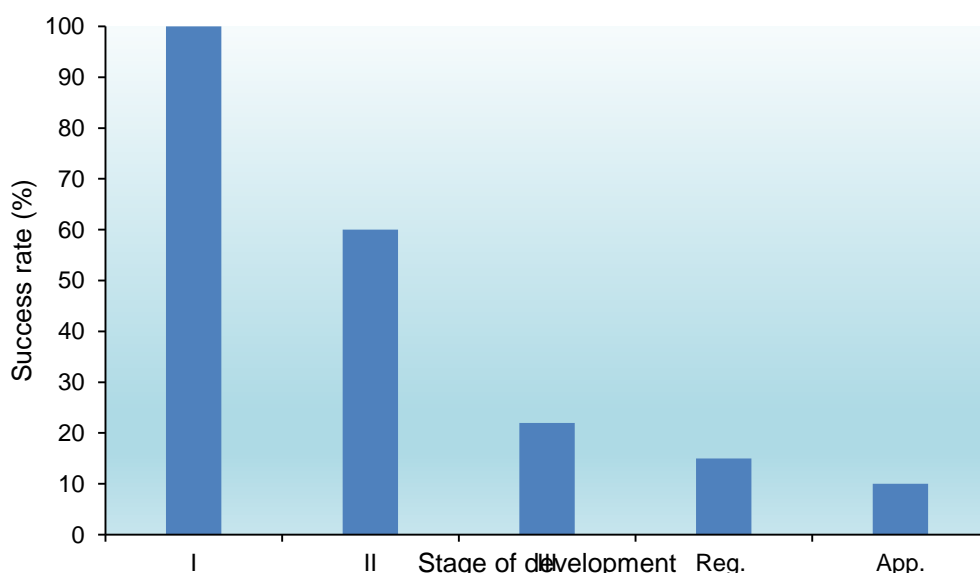
The field of chemoinformatics has shown great potential for the prediction of both compounds with good 'drug like' qualities and novel disease targets, thereby being of great use towards chemical genetic screening experimental design and analysis (Chen et al., 2012). Defined in 1998 by Brown, "Chemoinformatics is the mixing of those information resources to transform data into information and information into knowledge for the intended purpose of making better decisions faster in the area of drug lead identification and optimization" (Brown, 1998). In respect to drug discovery the value of

chemoinformatics increased in the 1990's due to the use of HTS methods combined with the advent of click chemistry and the large number of 'druggable' targets' identified as a consequence of the human genome project (Dobson, 2004; Feher and Schmidt, 2003; Lander et al., 2001). The identification of thousands of new potential druggable targets widened the scope for drug screening, yet the majority of suspected targets have never been pharmacologically proven in their inferred disease pathway (Dobson, 2004). Indeed, hindsight has shown that care should be taken in the interpretation of this explosion of targets, which has led to the concept of a "druggable genome" (Cheng et al., 2007). This term, which is now commonly cited in literature, is misleading in the context of small molecule drug discovery as the target of such molecules is almost always a protein complex and not the genes themselves. When this is taken into account the number of potential druggable targets increases from ~30,000 genes to several hundred thousand proteins (when alternative splicing and post-translational modifications are also considered (Kubinyi, 2003)). It still remains today that the great majority of these proteins have very little information regarding their functions in the human system, let alone their potential role in disease pathways (Kola and Landis, 2004). It has been estimated that theory precedes empirical validation of new proposed drug targets by at least a decade (Hurko, 2010).

It follows that despite a dramatic increase in available compounds and the capacity through which to screen them, the number of approved medicines has steadily declined over the past 30 years (Drews, 2003; Frantz, 2004; Weigelt, 2009). In 1998 it was estimated that of 7,000,000 compounds screened, just one will become a fully approved drug (Hurko, 2010) In **Figure 8** compounds can clearly be seen to have significantly lower success rates at later clinical

stages, emphasizing the current rate of compounds attrition. In addition the drug discovery process takes between 8-12 years, costing \$1.2 billion dollars (Hurko, 2010). If it is also considered that only three in ten medicines that make it to market recover the original investment made into them, it becomes clear that such attrition is unacceptable and unsustainable (Kola and Landis, 2004).

Compounds tend to fail at very late stages in the drug discovery pipeline, typically in phase 1 or phase 2 clinical trials (Kola and Landis, 2004). This has led to the belief that whilst high-throughput screening of compound libraries provides numerous "hit" lead compounds, the quality of these lead compounds must be drastically improved so as to not subject them to expensive clinical trailing that will inevitably fail (Kubinyi, 2003). This has promoted much research into the development of improved compound screening. Due primarily to the



advent of combinational chemistry there has been a dramatic rise in the quantity

Figure 8. Success rate as shown by development stage and therapeutic target area. App, approval; Reg, Registration. Adapted from (Kola and Landis, 2004).

of chemical information available (Kodadek, 2011; Lopez-Vallejo et al., 2011). Chemoinformatics are commonly employed as a computational solution to help organise and refine this data to make the most of the available information. The capacity to organise and segregate vast quantities of data based on defined chemical descriptors provides an opportunity to greatly refine compounds chosen for HTS (Bender, 2010; Bender et al., 2009; Xue and Bajorath, 2000). This therefore leads to the production of a higher quality “hit” that is more likely to progress through late stage clinical trialling where most compounds currently fail. There are four primary areas in which chemoinformatics can be applied to the design of a HTS experiment; compound library design, compound similarity searching and clustering, data modelling and the design of screening strategies (Parker and Schreyer, 2004). Whilst all of these areas have significance in the design of successful HTS, library design and selection is particularly important (Goodnow et al., 2003).

The failure of large newly synthesised compound libraries in the 1990’s to produce an increase in identified lead compounds suggests that such a method is inefficient (Feher and Schmidt, 2003; Goodnow et al., 2003). It is now widely accepted that this random synthesis approach failed because the compounds generated did not represent an appropriate area of chemical space (Feher and Schmidt, 2003; Ganesan, 2008; Lipinski and Hopkins, 2004; Lipinski et al., 2001). Chemical space is a term intended to represent all possible (not necessarily existing) compounds, which is proposed to resemble the cosmological universe in its vastness. **Figure 9** depicts a model representing all of chemical space. The light blue space represents all possible compounds. If it is assumed that within this model that proximity between compounds is

dependent upon similarity, so that the most similar compounds are adjacent to each other, it is possible to predict discrete areas of chemical space with particular properties. This is illustrated by the coloured areas (Lipinski and Hopkins, 2004). Such diversity makes screening compounds and compiling compound libraries randomly highly inefficient and may contribute greatly to the high attrition described in the later stages of the drug discovery process (Feher and Schmidt, 2003). In light of this, significant efforts have been made by pharmaceutical companies to create more focused screens and libraries. This can be achieved by using chemoinformatical algorithms to select discrete areas of chemical space to sample compounds from, which often depends on what

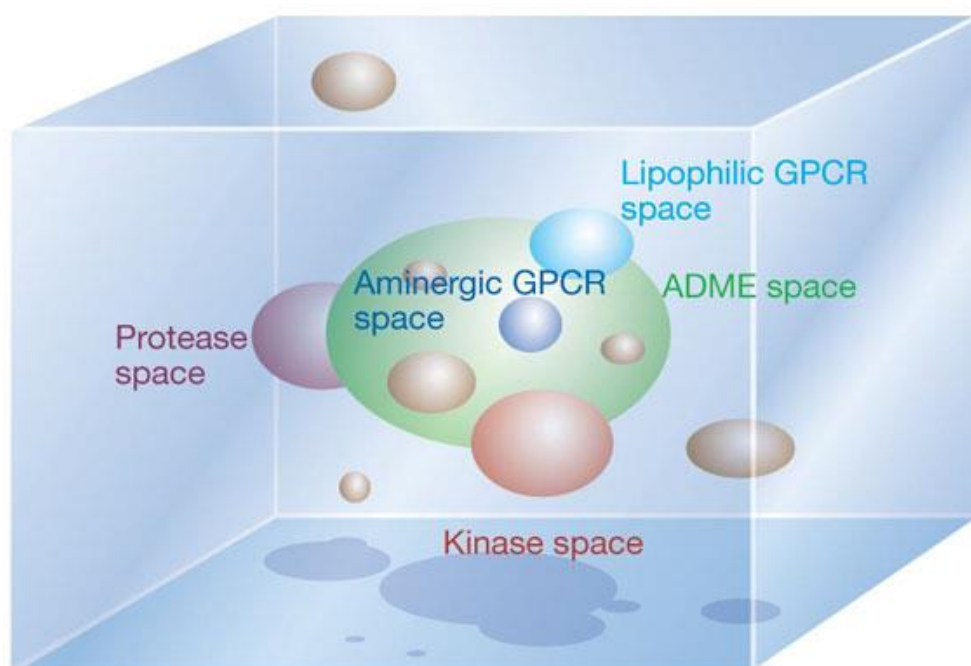


Figure 9. Chemical space model. Blue space represents all possible compounds. Coloured regions represent chemical space occupied by compounds sharing similar specified features. ADME; absorption, distribution, metabolism and excretion. Figure taken from (Lipinski and Hopkins, 2004).

characteristics or “descriptors” it is believed the molecule should have to be an effective drug for the target therapeutic area (Gedeck et al., 2006; Lipinski and Hopkins, 2004; Reymond et al., 2010).

1.1.13 Molecular descriptors

Lipinski's rule of five is an example of a commonly applied general rule of thumb as to what characteristics (or descriptors) a molecule should have (Maldonado et al., 2006). These assumptions are based on past research that has shown that 90% of orally absorbed drugs have less than ten hydrogen-bond acceptors, less than five hydrogen-bond donors, a molecular weight of less than 500 Da and a log P (measure of hydrophilicity) of less than five (Lipinski et al., 2001). By disregarding all compounds that do not abide by these rules the experimenter is left with a chemical space containing compounds that are predicted to be more likely to become successful drug candidates. However, if one considers all the possible organic “drug-like” compounds below 500 Da (roughly 10^{60} compounds (Bohacek et al., 1996)), there would not be enough matter in the universe to synthesise just one of every molecule (Bender et al., 2006). Much research has been focused on the creation of more focused descriptors; however these typically depend on the desired therapeutic application (Bender, 2010; Maldonado et al., 2006). For example as an alternative to the Lipinski rules, oral absorption and blood brain barrier penetration can be partially predicted by observing the polar surface area (Bergstrom et al., 2003; Ertl et al., 2000) or VolSurf parameters (Cruciani et al., 2000; Ertl et al., 2000; Kubinyi, 2003). Certain properties are integral for an effective drug regardless of binding efficiency and are said to require acceptable ADME (absorption, distribution, metabolism and excretion) properties (Beresford et al., 2002; Geerts and

Vander Heyden, 2011; Tian et al., 2011). Positive ADME properties relate directly to effective drug efficacy. For example a compound must be hydrophilic enough so that it is efficiently absorbed and distributed around the body, but hydrophobic enough so that it can easily diffuse across the required cell membranes to reach the intended target (Tian et al., 2011).

Appropriate descriptors are integral to effective chemoinformatic analysis and are determined by the desired use of the compound in question. Many drugs need to be metabolised to be transformed into their active form (also known as prodrugs) (Rautio et al., 2008). Prodrugs are designed like this because the parent compound may be more stable or easily administered than its active form, thereby making them more efficient as a therapeutic agent (Rautio et al., 2008). For example the pain alleviating drug codeine is in fact an inactive parent compound which when metabolised creates the substrate morphine, a potent opiate analgesic (Solomon, 1974). The metabolic fate of the compound is particularly important factor in drug development. It is imperative that the compound can be metabolised and/or excreted easily from the system once it has achieved its intended goal (Boobis et al., 2002; Murphy, 2001). This requires the compound to be small enough and polar enough to be excreted in the urine or faeces. If the compound aggregates in a tissue and cannot be cleared, or produces toxic metabolites following its degradation then it cannot be used as an approved drug regardless of its efficacy (Caldwell et al., 2009). By using descriptors that indicate a compound will be broken down safely (or activate appropriately), chemoinformatic analytical descriptors are integral in directing this selection process (Boobis et al., 2002).

1.1.14 Chemoinformatic target prediction

One disadvantage of utilising a phenotypic screen is the bottleneck that occurs when trying to understand the mechanism of action elicited by an identified lead (Kalin et al., 2009; Wheeler and Brandli, 2009). Given that compounds used in such screens often have little information regarding their biological (and potentially novel) targets, understanding the underlying root cause of the elicited phenotype is comparable to searching for a needle in haystack. This fact is compounded by the possibility that numerous pathways and targets may likely be involved (Kell, 2013). Target prediction methods use databases (such as ChEMBL (Gaulton et al., 2012), PubChem (Wang et al., 2009) and WOMBAT (Schreiber, 2008)), to link small molecules to bioactivity data (Liggi, 2013). Molecules are selected and their known information are extrapolated onto those molecules whose biological activity is unknown (Liggi, 2013). Utilising chemoinformatical analysis combined with ligand data it is possible to predict targets for compounds *in silico* that have been proven to be accurate when validated in a biological system (Cortes-Ciriano, 2013; Liggi, 2013; Schreiber, 2008). For example, a study by Lemieux *et al.*, (2013) used chemoinformatics to predict targets for compounds shown to give abnormal feeding phenotypes in *C. elegans*. By using ligand binding data, numerous pathways were predicted and subsequently biologically validated *in vitro*. In total, four pathways that were previously unknown to effect feeding in *C. elegans* were predicted and validated (Lemieux et al., 2013).

To predict mechanisms of action, compounds with known mechanisms of action are typically used as activity landmarks (to which it might be inferred that compounds of similar structure might elicit their phenotype via the same

mechanism of action). This approach is limited in that it relies on the availability of a relevant landmark compound that has a clear and specific mechanism of action. It also does not take into account phenotypes that arise through the inhibition of more than one target. One approach to circumvent this issue is to integrate chemical similarity comparisons with phenotypic data. Training statistical models (using compound structural information that are associated with known targets) can reveal new relationships between phenotypes and compounds. It is also possible to integrate relevant signalling pathways and disease information into the analysis. For example, compounds that perturb different targets in the same pathway are expected to generate a similar phenotype. A study by Loukine *et al.*, (2012) constructed a bioactivity profile network by screening 656 FDA approved drugs *in silico* against 73 targets. By combining *in silico* target prediction, *in vitro* tests, adverse drug reaction annotation, pharmacodynamic and pharmacokinetic properties a drug-target-adverse effect network was created. This network predicted new off targets (247 drug-target-side effect links) for the screened compounds that explained a number of side effects known to be elicited by the drugs. For example, tremors are known side effect of diphenhydramine, which was predicted to interfere with an off target dopamine transporter, and was subsequently biologically validated (Liggi, 2013; Loukine *et al.*, 2012). This study emphasises the power of chemoinformatic analysis as a tool for the prediction of novel targets using phenotypic screening data. It also demonstrates how such an approach can significantly reduce the bottle neck seen in phenotypic screening by rapidly predicting numerous novel targets to explain abnormal phenotypes which may be multi-targeted in nature (Liggi, 2013; Zhao and Iyengar, 2012). In collaboration with Andreas Bender I used the phenotypic data generated in our

X. laevis screen in conjunction with chemoinformatical analysis to predict novel targets and pathways for the potential treatment of melanoma.

1.1.15 Summary

It has been shown previously by Tomlinson *et al.*, (2005) that *X. laevis* are highly amenable towards phenotypic chemical genetic screening having identified numerous hit compounds, one of which aiding in the discovery of a new drug for the treatment of melanoma that is currently undergoing human clinical trialling (Tomlinson *et al.*, 2005; White *et al.*, 2011). We aim to improve upon this process and further validate the use of *X. laevis* as a prominent model for phenotypic screening in drug discovery.

We aim to screen the NCI diversity set II compound library and expand upon the previous Tomlinson screen by first utilising cell based assays to better understand the effect *in vivo* identified abnormal phenotype compounds might have towards melanoma cell viability. In collaboration with Andreas Bender (Unilever, Cambridge), we will then use a chemoinformatical approach to predict potential targets for each of the phenotypic hit compounds identified *in vivo*. These predicted targets will then be subsequently validated biologically by using known inhibitors in an attempt to replicate the original identified phenotype.

A secondary aim of this thesis is to assess the value of *X. laevis* towards drug development. This was attempted by developing a novel toxicity assay for the early preclinical assessment of renal toxicity. The significance of drug development and the amenability of the *X. laevis* model towards improving its current capabilities are discussed in the next section.

1.2 Pharmaceutical drug development

Toxicity testing in drug discovery is unavoidable both from a legal and ethical standpoint. It is illegal to market drugs that have not been approved by the regional safety regulatory body and therefore all pharmaceutical compounds must abide by the established safety parameter laws. Safety regulatory bodies are a necessity as they provide expert independent reviews of drug toxicity data and form the mediating barrier between profit seeking companies and the health of their patients.

The importance of safety testing in pharmaceuticals is exemplified by the 1950s thalidomide tragedy. Between 1956-1962 pregnant women were prescribed thalidomide as an anti-emetic, resulting in over 9000 children in Europe and Africa being born with severe deformities (Franks et al., 2004). The USA escaped this tragedy because the Food and Drug Administration (the FDA) refused to approve the drug due to a lack of sufficient safety data (Weir, 2009). The United States FDA was formed in the early 19th century in response to deaths from dangerous formulations, and is integral in ensuring that clinical trials are conducted safely and provide safe and efficacious drugs. Whilst discrepancies do exist between what different countries regulatory bodies consider as permissible with regards to toxicity, it is hoped that such authorities have significantly reduced the chance of another event on the scale of thalidomide ever occurring again.

Over the past two decades regulatory body safety parameters have become increasingly stringent, making their standards of high efficacy and low levels of off target toxicity difficult to achieve (Lorman, 2001). This has contributed to the

documented decrease in pharmaceutical productivity and subsequent drop in the number of novel therapeutic compounds coming to market (Kola and Landis, 2004). Increasingly compounds are failing at very late stages of drug development due to previously undiagnosed toxicity and/or lack of efficacy, resulting in great expenditure with little return (Kola and Landis, 2004; Swinney and Anthony, 2011). To combat this, pharmaceutical companies have incorporated a plethora of biochemical, *in vivo* and *in vitro* assays as standard practice within their pipelines that are critical for the prediction of toxicity and optimisation of prospective compounds.

1.2.1 Biochemical and *in vitro* assays in preclinical toxicity testing

A considerable amount of effort has been made in attempting to create economical, high-throughput pre-clinical assays that can be used to assess compound toxicity and ADME (absorption, distribution, metabolism and excretion) characteristics before they can progress further into development. The early prediction of whether a compound might exhibit toxic side effects (such as unwanted drug-drug interactions or off target effects), poses a significant challenge in drug development. *In vitro* biochemical based assays have been implemented as a method of predicting potential compound toxicity. In 1998, the number of serious adverse drug-drug interactions reported in the U.S.A. was estimated to be as high two million per year (Lazarou et al., 1998). It was proposed that many of the reported adverse drug-drug reactions were caused by one drug inhibiting the metabolism of the other, the first administered compound resulting in high plasma concentration levels of the second resulting in a subsequent toxic effect (Wienkers and Heath, 2005). To address this problem a simple biochemical assay was implemented that assessed the

inhibition of specific cytochrome P450 (CYP) function. Cytochrome P450s are a superfamily of enzymes that play an important role in the phase one metabolism of the majority of organic compounds in the body. Therefore by measuring their activity and production in the presence of a compound it is possible to assess metabolic state and potential toxicity. To achieve this, a probe substrate that produces a quantifiable product (such as fluorescence) when metabolised can be added to the desired isolated specific CYP (as well as the suspected CYP inhibitor compound). The measured rate of metabolism of the probe substrate (which can be assessed by a fluorometric or liquid chromatography-mass spectroscopy assay) indicated whether or not the suspected compound might be a toxic CYP inhibitor (Donato and Castell, 2003; Wienkers and Heath, 2005). This biochemical assay was an excellent example of current toxicity assay development, in that it provides a quick, simple and quantifiable assessment of a compounds toxicity that would typically only usually be observed at a much later stage in drug development. However, such biochemical assays are not without their disadvantages, mainly because by their very nature they do not adequately represent a functional biological system.

This concern led to the implementation of cell based assays in early preclinical protocols, which have subsequently been used to assess toxicity, proliferation, activation of signalling pathways and morphological changes (Michelini et al., 2010). For example, a simple high-throughput procedure that quantifies cell death (and therefore potential toxicity) is the terminal deoxynucleotidyl transferase dUTP nick end labelling (TUNEL) assay which accurately measures cell culture apoptosis by labelling the terminal end of nucleic acids to determine DNA fragmentation (Kasagi et al., 1994). As well as modelling toxicity, studies have shown that primary human cell systems can be manufactured to closely

represent a number of different disease states (Bhadriraju and Chen, 2002; Butcher, 2005). In addition, these prospective assays can be automated in 96 or 384 well plates, and are therefore easily amenable to HTS (it was estimated that approximately 500 compounds a week can be tested in a fully automated system (Butcher, 2005)). Hence cell-based assays can be used as a screening tool to search for potential drug compounds at a previously unprecedented rate in a model that can replicate an extensive range of disease states (Michelini et al., 2010). They can also equally be used from a toxicological perspective to identify compounds that might also exacerbate or trigger a disease or condition. However, cell based assays are limited in a number of ways. For example, despite the wide variety of disease modelling cell lines available, this list is by no means comprehensive. The primary issue with all cell based assays however is that they are still inadequate as a model of a three dimensional organism. Such assays in practice are two dimensional and therefore cannot mimic the known complicated matrix of signals that comprise a three dimensional organ tissue. Similarly, cell based assays cannot replicate whole body or multiple tissue disease states that require a complete animal system, such as abnormal hormone regulation and neuronal disorders (Butcher, 2005). Despite these issues, cell based screening has an important place in early preclinical prediction of *in vivo* toxicity and represents an economical high-throughput option for initial compound screening.

1.2.2 *In vivo* assays for drug development

Many of the benefits ascribed to cell based assays arise because experimentally they are infeasible in more traditional animal models such as *Rattus norvegicus* (rats), *mus musculus* (mice), *Canis lupus* (dogs), *sus scrota* (pigs) and non-

human primates (Hornberg et al., 2013). Such animal models are expensive, far from high-throughput and therefore restricted to late stage preclinical testing despite their *in vivo* relevance (Zbinden, 1991). This is unfortunate as such species are evolutionary the closest (easily available) experimental animal models of the human system. Invertebrate animal models (such as the classic nematode worm and *Drosophila*) can easily be incorporated into screening assays, but their protein divergence from humans results in a high rate of false negatives making them unsuitable despite their practical advantages (Segalat, 2007). Zebrafish and *X. laevis* have proven themselves to be highly amenable to HTS (Peterson et al., 2000; Taylor et al., 2010; Tomlinson et al., 2005; Tomlinson et al., 2009a; White et al., 2011). Both also have also been used for toxicity testing, in particular *X. laevis*, which has a long history of use in the identification of toxic compounds.

1.2.3 *X. laevis* as a toxicity assay

X. laevis has historically been used as a toxicity assay for three decades. The 'Frog Embryo Teratogenesis Assay – *Xenopus*' (FETAX) assay was originally developed by Dumont *et al.*, (1983) and this protocol has been the basis of thousands of toxicity assays to date (Dumont, 1983). The majority of these experiments have focused upon using the FETAX assay as a model for environmental toxicity, using *X. laevis* as a surrogate model for other amphibians. This once again is due to the practical advantages of utilising the *X. laevis* model (such as year round fecundity and ease of husbandry), which would be extremely difficult if not impossible with other native amphibians.

The FETAX assay is a straightforward toxicity screen. Blastula (stage 12) embryos are subjected to compounds at varying concentrations (alongside appropriate negative, positive and vehicle controls) for 96 hours, subsequently fixed and observed using a light microscope for any overt signs of toxicity (Davies, 1995). The endpoint of the experiment is normally dependant on the hypothesis, but can include and is not limited to: mortality and malformation (Mouche et al., 2011), developmental stage, head-to-tail length (Hoke and Ankley, 2005), motility (behaviour), pigmentation (Dumont, 1983), malformations of the major organs (such as the gut, eyes and brain), and so on. Other endpoints could also include chromosomal damage or RNA, DNA, protein synthesis and enzyme levels (Davies, 1995).

The FETAX assay has great scope as a toxicity assay but is not without its caveats. The *X. laevis* model has been noted as being somewhat insensitive compared to other aquatic models (such as other amphibians, *daphnia rosea*, salmon, rainbow trout, etc.). A study by Hoke and Ankley (2005) showed that these species when subjected to the same compound concentrations as *X. laevis* are less tolerant and therefore perhaps better environmental markers (Hoke and Ankley, 2005). This study however was primarily focused upon *X. laevis* as an environmental marker of toxicity and also only used lethality as an endpoint. This by no means discounts the FETAX assay as a viable pharmaceutical toxicity assay and instead suggests that species native to the environment containing the contaminant may be more viable models for environmental toxicity testing.

One specific aim of this project is to develop a novel toxicity assay that would improve the development of compounds within a pharmaceutical pipeline. This

would ideally identify toxic compounds sooner and therefore permit them to be disregarded quicker, allowing resources to be spent on stronger candidates. The goal was to produce an *in vivo*, medium throughput, vertebrate toxicity assay using the *X. laevis* model that either meets an unmet current demand or improves upon an assay that is currently in place. The belief is that such an assay would begin to bridge the gap between preclinical *in vitro* and subsequent *in vivo* toxicity screening. This is important, as *in vivo* screening is extremely costly and relatively slow. Previous chemical genetic screening in our laboratory has already shown that the *X. laevis* model is highly amenable to such a screening platform, whereby many compounds could be tested in quick succession (Tomlinson et al., 2005; Tomlinson et al., 2009a; White et al., 2011). The strong history of the FETAX assay is also evidence that *X. laevis* can successfully be used as a model for toxicity (albeit so far only primarily in an environmental context), utilising many different endpoints.

It is important to note that, as mentioned above, if this assay is to be industrially relevant it must either meet an unmet demand or improve upon assays that are already in place. In collaboration with our part sponsors AstraZeneca we considered several suggestions for toxicity end points that were thought to be 'desirable' (assuming my assay could determine them in an efficient and efficacious manner). These suggested toxicity end points included liver toxicity, structural cardio toxins, macrophage infiltration and finally renal toxicity. After searching the relevant literature coupled with preliminary assays I decided to focus on developing a *X. laevis* renal toxicity assay.

1.2.4 Renal toxicity

Renal toxicity is a serious concern in the pharmaceutical industry, being responsible for 7% of preclinical compound failures (Desrochers et al., 2013; Fuchs and Hewitt, 2011). In addition, 30-50% of reported kidney failure in patients is due to adverse drug reactions (Desrochers et al., 2013; Fuchs and Hewitt, 2011; Pannu and Nadim, 2008). Clearly nephrotoxicity is a serious concern that has yet to be fully addressed using the current technology available (Desrochers et al., 2013). Despite being less than 1% of our total body weight, the kidney receives 20-25% of our total cardiac output making it highly susceptible to blood borne toxicants (such as drugs) due to overwhelming exposure (Choudhury and Ahmed, 2006). Given that the kidney is a specialised filtration organ, it also rapidly concentrates compounds to levels that were previously non-toxic when diluted by the blood. Proximal tubule deterioration is commonly associated with nephrotoxicity because it is the first section of the nephron to come into contact with the toxic filtrate (Lash, 2009). Furthermore, the kidney expresses many of the enzymes that are associated with toxic bioactivation of compounds more commonly associated with liver toxicity (such as members of the cytochrome P450 or glutathione families) (Lash, 2009). All of these factors contribute to a high level of nephrotoxicity during drug development.

Nephrotoxicity can be broken down into two subtypes; acute renal failure and chronic renal failure. Acute renal failure occurs rapidly following toxicant exposure and can manifest itself through numerous mechanisms. For example, hypofiltration or hypoperfusion is a result of renal vasoconstriction or glomerular injury. Acute tubular necrosis arises from direct tubular injury and in some

cases intratubular obstruction causes rapid determination of renal function (Lash, 2009). Chronic renal failure arises gradually over time through prolonged low level toxicant exposure and can result in chronic tubulointstitial fibrosis through immunological or inflammatory reactions, or papillary necrosis through chronic ischemia or cell injury (Lash, 2009). Whilst this list is by no means exhaustive it gives an insight into the many specific ways in which nephrotoxicity can manifest.

1.2.5 Current *in vivo* and *in vitro* models of nephrotoxicity

In an attempt to assess potential renal toxicity in prospective compounds a number of preclinical *in vitro* and *in vivo* assays have been generated. *In vivo* assays have a number of advantages over *in vitro* assays, the most obvious and important of which being that they represent a fully functioning organism and therefore are far more representative of human physiology. One typical *in vivo* assay for example is to observe the glomerular filtration rate (GFR) as a measure of renal function (National Kidney, 2002; Stevens et al., 2006). The GFR can be defined as the volume of blood removed substance per unit of time. One common indirect measure of the GFR is to observe creatinine concentration in the blood. Creatinine in normal healthy animals (including humans) is produced at a constant rate and it is excreted continually. Abnormal creatinine concentrations in the blood and/or urine would therefore imply abnormal renal function (National Kidney, 2002; Stevens et al., 2006). One significant limitation with this assay is its relative insensitivity whereby extensive damage often occurs before creatinine levels change at which point irreparable damage may have occurred (National Kidney, 2002). Other common *in vivo* assessments of renal function often included detection of abnormalities present

within the urine such as osmolality and overall volume, which are indicative of a disruption to normal fluid homeostasis. Other potential indicators in the urine that may signify abnormal renal function include acid/base balance, solute concentration and the presence of proteins/enzymes (Waring and Moonie, 2011).

The classic limitations associated with *in vivo* assays are their high expense and relatively low throughput when compared to *in vitro* capabilities (Zbinden, 1991). In an attempt to address this, a number of *in vitro* assays have been generated to increase the throughput of drug development whilst rapidly identifying potentially nephrotoxic compounds (Desrochers et al., 2013; Lash, 2009) (summarised in **Table 2**).

A large number of *in vitro* assays have been generated which range greatly in complexity. The use of isolated perfused kidneys for example represent the best *in vitro* model available that can closely replicate *in vivo* conditions. Naturally however, this is an expensive and low throughput procedure when compared to primary and immortalised cell culture screening, which sacrifices *in vivo* relevance for high throughput potential. Both of these assays have relevance in the prediction of nephrotoxicity and their individual application is determined by the situation at hand. For example earlier in preclinical screening when significantly more compounds are being explored the high throughput capacity of cell based assays takes precedent over their respective lack of *in vivo* relevance. Later in preclinical testing when only a relatively few number of

Table 2. Advantages and disadvantages of *in vitro* assays used in the detection of renal toxicity

<i>In vitro</i> assay	Advantages	Disadvantages
Isolated perfused kidney	<ul style="list-style-type: none"> - Highly representative of <i>in vivo</i> system 	<ul style="list-style-type: none"> - <2 hours viability - Limited amount of repeated use per sample - Incomplete structure - Expensive and low throughput
Renal slices	<ul style="list-style-type: none"> - Simple - Intact structure - High throughput 	<ul style="list-style-type: none"> - <2 hours viability - Lumen can collapse - Poor oxygenation can result in death of section
Isolated perfused tubules	<ul style="list-style-type: none"> - Intact tubules - Can determine site of action in tubules - Possible to quantitate viability 	<ul style="list-style-type: none"> - <2 hours viability - Can be difficult to isolate and set up
Renal cell suspensions	<ul style="list-style-type: none"> - Simple - High throughput 	<ul style="list-style-type: none"> - <4 hours viability - Loss of cell polarisation - Loss of extracellular transport mechanisms
Primary cell lines	<ul style="list-style-type: none"> - Similar to <i>in vivo</i> - Maintains cell polarity - Long time viability 	<ul style="list-style-type: none"> - Easily contaminated with other cell types - Dedifferentiation can occur - Tricky to maintain
Renal cell cultures	<ul style="list-style-type: none"> - Standardised protocol improves reproducibility - Immortalised - Easy to transfect and genetically manipulate - Simple to use 	<ul style="list-style-type: none"> - Dedifferentiation can occur - Can have an ill-defined origin

prospective compounds are remaining (but accurate prediction of nephrotoxicity is essential prior to *in vivo* screening), the isolated perfused kidney assay is more appropriate with its high relevance to an *in vivo* system (despite its low throughput capacity).

1.2.6 The human kidney

Mammalian kidneys are bilateral organs whose primary role is to regulate the composition and volume of bodily fluids, and remove metabolic waste products from the blood by filtration. All vertebrate kidney development undergoes three phases, starting as a pronephros, progressing into a mesonephros and finally the metanephros (a fully developed adult kidney) (Vize, 2003). Each phase increases in complexity in both the number and organisation of the nephrons. The pronephros is non-functioning in higher vertebrates and consists of a 6-10 pairs of tubules in humans. These tubules lead into a pair of primary ducts that extend caudally into the cloaca. The structure completely disappears by the fourth week of human development to be replaced by the mesonephros. The mesonephros consists of mesonephric tubules derived from the mesoderm and is the primary excretory organ in the first 4-8 weeks of human development. Towards week 8, the structure degenerates and is replaced by the metanephros which begins developing at week 5. The metanephros is the permanent higher vertebrate kidney and is also derived from the intermediate mesoderm. The human metanephros is distinct from its previous incarnations in that it contains a much larger number of nephrons (around 300 million), and contains an extensively branched duct system (Vize, 2003).

Each nephron consists of a glomerulus (also known as the Bowman's capsule) that is connected to a tubule, which is in turn connected to a collecting duct (**Figure 10**). The glomerulus is the first stage in the filtration process and is comprised of a capillary tuft surrounded by a group of specialised epithelial cells known as podocytes. The glomerulus is responsible for blood ultrafiltration in which podocytes play a critical role (Vize, 2003).

The purpose of the tubule is to enable reabsorption of metabolically useful solutes as well as reuptake of water. The tubule can be divided into three segments known as the proximal, intermediate and distal tubule. Each tubule partition is unique unto each other in that they contain distinct cellular morphologies and express unique solute transporters (Vize, 2003).

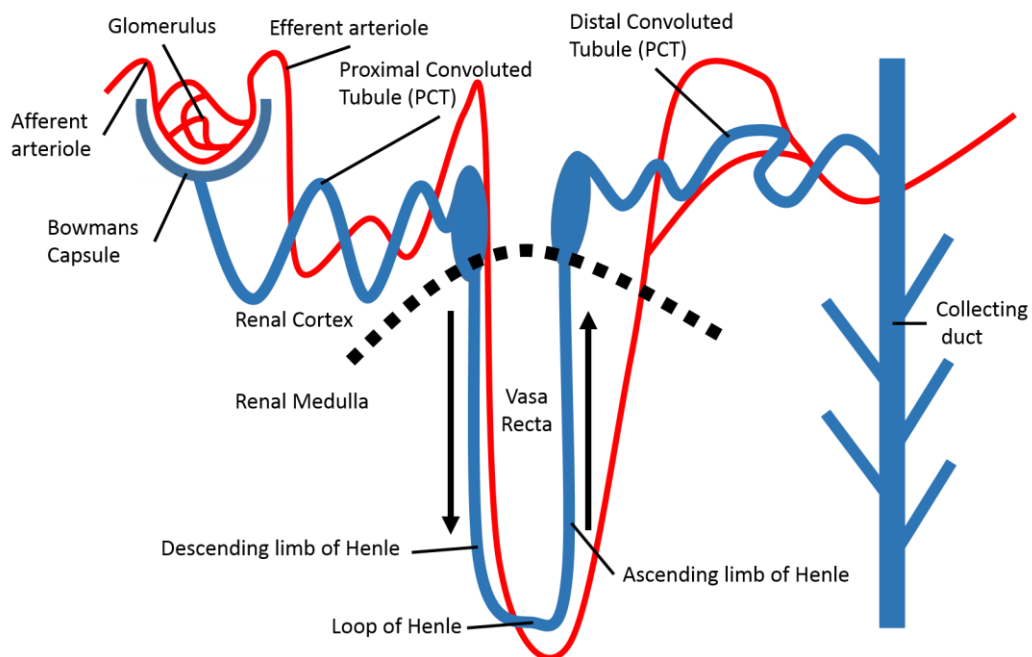


Figure 10. Schematic of the nephron.

1.2.7 *X. laevis* renal development and function

As mentioned previously, the higher vertebrate kidney has three separate phases of development in which three structures are formed in sequence, with the preceding structure being superseded by the next (the pronephros to the mesonephros to finally the metanephros). In higher vertebrates the pronephros is non-functioning and is considered to be a vestigial organ (Vize, 2003). In *X. laevis* however the pronephros acts as a functioning organ from 6 days post fertilisation and is critical in maintaining blood solute levels (Jones, 2005). *X. laevis*, like most aquatic organisms, passively absorb water through their skin via their environment; thereby blood osmolality is an important concern even at early stages in development. The early *X. laevis* pronephros functions as any vertebrate kidney would by filtering and actively reabsorbing solutes to maintain acceptable blood solute levels and prevent ion depletion. The *X. laevis* pronephros is a relatively simple paired organ (with respect to the metanephros), in that it consists of only three major components: the glomus, the tubules and the duct. It is in essence, a single functioning nephron.

In early development the mesodermally derived pronephros is formed between the lateral plate and the paraxial mesoderm ventral to somites three and five (Jones, 2005; Vize, 2003). The nephritic field is quickly established and final patterning occurs by stage 26 (tail bud) of development (Jones, 2005). At this point the specific structures of the pronephros begin to arise, with the glomus becoming distinct from the tubules and the duct and the intermediate mesoderm being separated into the somatic and splanchnic mesoderm via the formation of the coelom (Jones, 2005; Vize, 2003). By Stage 30, the lumen of the nephrons has formed and the pronephros is fully functional by stage 38 (Jones, 2005).

Blood is filtered via the glomus, entering the coelomic space and subsequently the nephron via the nephrostomes (ciliated funnels which push the urine into the tubules). The tubules actively reuptake salts by creating an electrochemical gradient by using a number of different transporters to efficiently reabsorb useful solutes.

Despite the simplicity of the pronephros compared to the adult metanephros their primary function is analogous, making it an excellent model of renal development and also potentially renal function.

1.2.8 *X. laevis* and human differences in nitrogen excretion

Whilst the *X. laevis* renal system has many similarities to humans, one key difference is the primary urinary product. *X. laevis* being aquatic organisms excrete ammonia as opposed to urea in the case of terrestrial animals such as humans. Both products are essential in the removal of excess nitrogen, which is highly toxic if not disposed of effectively.

Ammonia in animals is produced by dietary amino acids broken down by gut bacteria as well as the catabolism of amino acids, nucleic acids, and amines (etc.) in peripheral tissues. Ammonia in most tetrapod's is highly toxic, and so the majority produced is rapidly converted into urea. Evolution has led to the synthesis of three different dominant nitrogen products in the pursuit of efficient nitrogen excretion in animals in the form of ammonia, urea and uric acid (**Figure 11**).

The nitrogen product produced is dependent upon the environment in which the organism inhabits, the deciding factor commonly hinging on the organisms requirement for water retention. For example, most aquatic animals such as teleost fish, aquatic invertebrates and larval amphibians excrete ammonia (Wright, 1995). This is primarily due to the high solubility of ammonia allowing for easy excretion into the surrounding media, with some animals capable of excreting some ammonia passively through the skin as well as via the kidney (Cruz et al., 2013). Aquatic animals have subsequently evolved a much higher tolerance to ammonia blood levels than terrestrial animals (Wright, 1995). For example teleost fish are capable of tolerating between 0.05mM - 1mM ammonia plasma concentrations (Wright, 1995) when compared to most mammals, which exhibit central nervous damage at plasma concentrations as low as 0.05mM (Meijer et al., 1990). The ability to excrete ammonia easily into their environment is unique to aquatic animals, as due to its high solubility 1mg of ammonia requires 400ml of water to maintain ammonia below toxic levels. In contrast, urea excretion requires 10 times less water than ammonia excretion and uric acid excretion requires 50 times less water (Wright, 1995). This is significant for terrestrial animals that are far more dependent upon efficient water retention than their aquatic counterparts. It is for this reason that terrestrial animals

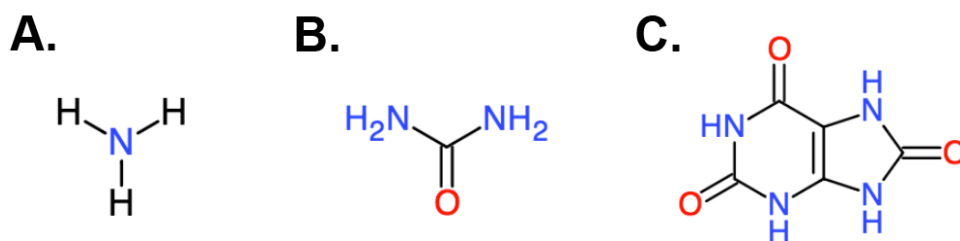


Figure 11. Common forms of ammonia excretory products. A. Ammonia. B. Urea. C. Uric acid. (Wright, 1995)

convert ammonia to either urea or uric acid despite the respective increase in metabolic cost.

X. laevis, despite technically belonging to a family of amphibians, only excrete ammonia. This is almost certainly due to a critical time point in their evolution in which *X. laevis* moved back to being wholly aquatic organisms, never venturing onto land (Balinsky, 1961; Underhay, 1955). This would explain why the primary *X. laevis* urinary metabolite is ammonia; whereas other closely related species of truly amphibious frogs in their adult form produce urea (Underhay, 1955). It is interesting that *X. laevis* retain the ability to produce urea but do so only in times of drought when water is scarce. This is presumably a defensive response in an attempt to preserve water under stressful environmental conditions (Balinsky, 1961; Underhay, 1955).

1.2.9 *X. laevis* as a model of renal function

Whilst most nephrotoxicity typically concerns the adult metanephros, there is still great benefit to be had in studying the nephrotoxic effects of compounds on the *X. laevis* embryo pronephros. *X. laevis* have successfully been used to model kidney development and interrogate the complex developmental mechanisms that govern it (Jones, 2005). For example using the animal cap assay (where mesodermal cells are dissected from a blastula stage embryo), it is possible to differentiate mesodermal cells into pronephric tubules when treated with the growth factor activin and retinoic acid (Moriya, 1993). It is now also possible to differentiate these cells into the pronephric glomus and duct (Brennan et al., 1999; Osafune et al., 2002). Such assays have been used to identify the exact time at which parts of the pronephros are formed (Seufert et al., 1999).

Morpholino knock down experiments have also been used to identify a number of genes critical in pronephros development (Jones, 2005). Such interrogation of early kidney development is extremely difficult in other vertebrate amniotes and exemplifies *X. laevis* as an excellent model of early kidney development. Renal function as opposed to renal development however, is an area that has yet to be explored in *X. laevis*.

1.2.10 Summary

There is currently no literature in which renal function in *X. laevis* has been cited as a predictor for nephrotoxicity. This niche combined with the described advantages of using the *X. laevis* model suggest the proposed assay (if successfully developed) has the potential to be of significant benefit to the drug discovery process. It is known that the *X. laevis* pronephros is functional from as early as stage 38, actively excreting ammonia into the surrounding media. Using a simple biochemical assay we believe that it may be possible to quantify the amount of ammonia excreted into the media as an indirect measure of active renal function. Our hypothesis is that any nephrotoxic compounds introduced into the *X. laevis* system could result in a significant change in the amount of ammonia excreted thereby indicating abnormal renal function as a result of nephrotoxicity.

1.3 Thesis aims

The primary goal of this thesis is to assess the applicability of *X. laevis* as a model for drug discovery and development (Summarised in **Figure 1**). The secondary aim of this thesis is to assess the value of *X. laevis* towards drug development in the form of a novel toxicity assay for the early preclinical assessment of renal toxicity. In collaboration with our part sponsors AstraZeneca, I have attempted to design a novel preclinical toxicity assay for the detection of renal toxicity. Using simple biochemical assays (utilising the salicylic acid and glutamate dehydrogenase assay methods of ammonia detection), I go on to show that it is possible to detect excreted ammonia in the *X. laevis* media. The assay however may not be sensitive enough to detect changes in renal function as an indicator of nephrotoxicity. Further refinement of the assay may lead to increased sensitivity. In summary, this thesis shows the potential of the *X. laevis* animal model across all phases of preclinical development towards drug discovery and development as a high throughput, high content, vertebrate screening model organism.

Chapter II

2.0 Materials and Methods

Table 3. List of reagents

Reagents	Supplier details
L15	Sigma L5520
Gentamycin sulphate	Sigma G1397.
Bovine serum albumin	Fisher Scientific BPE9703-100.
Ethyl 3-aminobenzoate methane sulfonate	Sigma A5040-25G.
Human Chorionic gonadotropin (HCG)	www.animeddirect.co.uk 804745.
Pregnant mare serum gonadotrophin (PMSG)	www.animeddirect.co.uk 859448.
Poly-L-Lysine	Sigma P4832
Cytochalasin D	Sigma C8273
Penicillin Streptomycin (Pen Strep)	Gibco 15070-063
L-Glutamine	Gibco 25030-024
0.25% Trypsin-EDTA (1X)	Gibco 25200-072
Trypan blue solution	Fluka 93595

Dimethyl sulphoxide (DMSO) Hybri-Max	Sigma D2650
RPMI – 1640 Medium (1X)	Hyclone SH30096.01
DMEM + GlutaMAX	Gibco 21885-025
CellTitre-glo Luminescent Cell Viability assay	Promega G7572
JBL NH ₄ Test	JBL www.JBL.de
Tetra Test NH ₃ / NH ₄	Tetra www.miscota.co.uk
API Ammonia Test Kit	API www.apifishcare.co.uk
Glutamate dehydrogenase (GDH) activity assay	Sigma AA0100

Table 4. List of solutions

Solutions	Formulation
BSA solution	1% BSA in 1XMMR.
1XMMR	100mM NaCl, 2mM KCL, 1mM MgCl ₂ , 2mM CaCl ₂ , 5mM HEPES.
0.1XMMR	10mM NaCl, 0.2mM KCL, 0.1mM MgCl ₂ , 0.2mM CaCl ₂ , 0.5mM HEPES.
0.05XMMR	5mM NaCl, 0.1mM KCL, 0.05mM MgCl ₂ , 0.1mM CaCl ₂ , 0.25mM HEPES.
HCG 100U/ml	HCG was prepared in PBS and stored at 4°C.

PMSG 1000U/ml	PMSG was prepared in PBS and stored at 4°C.
<i>X. laevis</i> testis buffer	80% fetal calf serum, 20% 1XMMR.
<i>X. tropicalis</i> testis buffer	L15 with 10% FBS.
A375 media	RPMI – 1640 Medium (1X) supplemented with 10% FBS, 1% Pen strep and 1% L-Glutamate.
HEK293 media	DMEM + GlutaMAX supplemented with 10% FBS, 1% Pen Strep and 1% L-Glutamate.
RD1 media	DMEM + GlutaMAX supplemented with 10% FBS and 1% Pen Strep,
Ammonia assay standards	All solutions were prepared using 0.1 X MMR buffered with 10mM TRIS

Table 5. List of equipment used

Equipment	Supplier
Plate reader	BMG LabTech Omega Series (Data analysed using OMEGA software)
Spectrophotometer	Biochrom WPA Biowave II UV/Visible Spectrophotometer

2.1 Generation of *Xenopus laevis* and *Xenopus tropicalis* embryos

X. laevis and *X. tropicalis* adult frogs were kept at 18°C and 25°C in 40 litre and 20 litre tanks (maximum of 15 frogs per tank) respectively, with 12:12 hour light:dark cycles.

All experiments involving *X. laevis* and *X. tropicalis* were in compliance with the relevant laws and guidelines installed by the UEA. This research has been approved by an ethical review board in accordance with UK Home Office regulations under the project license number PPL 80/2499. *X. laevis* embryos were generated and staged according to Nieuwkoop and Faber (Nieuwkoop, 1956).

2.1.1 *X. laevis* egg generation and *in vitro* fertilisation

2.1.1.1 Testes isolation

A live *X. laevis* male was isolated and immersed in 0.5g of 1.6% ethyl 3-aminobenzoate methane sulfonate dissolved in 300ml reverse osmosis water in a 500ml beaker. The beaker was wrapped in tin foil and placed in the dark at 4°C for one hour. The testes were surgically removed and stored in *X. laevis* testes buffer at 4°C, remaining viable for a maximum of 1 week. The carcass was disposed of via incineration.

2.1.1.2 *X. laevis* egg generation and *in vitro* fertilization

Female frogs were primed 4 days prior to the experiment by injecting 100U PMSG into one pericardial sac in an isolated priming tank. The female *X. laevis* were not fed and were isolated until the day of the experiment. 14 hours prior to the experiment pre-primed female *X. laevis* were induced with 500U human chorionic gonadotrophin (HCG) by injecting 250U into each pericardial sac and left overnight at RT. The following day *X. laevis* eggs were collected by gently squeezing the animals with a massaging action ensuring eggs were deposited into a 25ml Petri dish. Excess water was removed from the Petri dish prior to fertilization. *In vitro* fertilization was achieved when the pre-prepared male testes were finely sliced using a razor blade to produce a thin slice that could be rubbed over the eggs. The testis section was then placed in a 2ml Eppendorf tube containing 1ml of 1XMMR and macerated. The resulting solution was deposited over the embryos using a 3ml Pasteur pipette and left for five minutes. The embryos were then flooded with 0.1XMMR and left for 20 minutes. Eggs can be collected in this manner a total of 6 times in one day, with a minimum of one hour between each squeeze.

2.1.1.3 Embryo dejellying

Immediately following *in vitro* fertilization the 0.1XMMR solution was removed from the embryos and replaced with 2% cysteine dissolved in 1XMMR. The embryos were left for 7 minutes and were subjected to occasional manual swirling until they could be seen to visibly touch each other. The embryos were then washed twice in 1XMMR, then twice in 0.1XMMR and placed into a BSA pre-coated 140mm Petri dish in 0.1XMMR. Embryos were left to develop at the

desired incubation temperature and checked regularly to dispose of dead or abnormal samples.

2.1.2 *X. tropicalis* egg generation and *in vitro* fertilisation

2.1.2.1 Testes isolation

A live *X. tropicalis* male was isolated and immersed in 0.5g of 1.6% ethyl 3-aminobenzoate methane sulfonate dissolved in 300ml reverse osmosis water in a 500ml beaker. The beaker was wrapped in tin foil and placed in the dark at RT for one hour. The testes were surgically removed and stored in *X. tropicalis* testes buffer at 4°C, remaining viable for a maximum of 1 week. The carcass was disposed of via incineration.

2.1.2.2 X. tropicalis egg generation and in vitro fertilization

Female frogs were primed 1 to 2 days prior to the experiment by injecting 10U HCG into one pericardial sac and placed into an isolated priming tank. The female *X. tropicalis* were not fed until the day of the experiment. Four hours prior to the experiment pre-primed female *X. tropicalis* were induced with 200U HCG by injecting into one pericardial sac and incubated at 25°C. Four hours later (or when eggs were visible in the tank) *X. tropicalis* eggs were collected by gently squeezing the animals with a massaging action ensuring eggs were deposited into a 25ml Petri dish. *In vitro* fertilization was achieved when the pre-prepared male testes was finely sliced using a razor blade to produce a slither that was then placed in a 2ml Eppendorf tube containing 1ml of *X. tropicalis* testes buffer and macerated. The resulting solution was deposited over the embryos using a

3ml Pasteur pipette and left for five minutes. The embryos were then flooded with 0.05XMMR and left for 20 minutes. Unlike with *X. laevis*, egg collection should typically only occur once per frog, per day.

2.1.2.3 Embryo dejellying

140mm petri dishes were pre-coated in BSA solution to prevent the embryos from sticking to the plate during their development. Immediately following *in vitro* fertilization the 0.05XMMR solution was removed from the embryos and replaced with 2% cysteine dissolved in 1XMMR. The embryos were left for 7 minutes and were subjected to occasional manual swirling until they could be seen to visibly touch each other. The embryos were then washed twice in 1XMMR, then twice in 0.05XMMR and placed into a BSA pre-coated Petri dish in 0.05XMMR. Embryos were left to develop at 25°C and checked regularly to dispose of dead or abnormal samples.

2.2 Chemical genetic screening

Imaging equipment and software – Q imaging 01-MP3.3-RTV-CLR-10 camera mounted on a Zeiss Stemi 5V6 microscope and processed with the Q capture software package.

2.2.1 Determining the optimal screening concentrations

The optimal screening concentrations for chemical genetic screening using *X. laevis* was previously determined in the lab to be 20µM and 40µM (Tomlinson et al., 2005). For consistency these concentrations were also used when screening

the *X. tropicalis*. These concentrations were chosen following a dose response screen (1 μ M - 100 μ M) using a range of randomly selected bioactive compounds to determine which concentrations ensured a satisfactory discovery rate with low overall toxicity (Tomlinson et al., 2005). Two concentrations were chosen to account for some compounds being toxic at higher concentrations versus compounds whose phenotypes were less pronounced at lower concentrations.

2.2.2 Chemical genetic screen using *X. laevis* or *X. tropicalis*

Embryos were grown in a 140mm Petri dish containing 10ml of 0.1XMMR at 18 $^{\circ}$ C until they reached stage 15. Compounds were arrayed into 48 or 96 well plates at double the desired final concentration in 500 μ l or 150 μ l respectively using a 12 channel Rannin multichannel pipette and an 8 well multichannel pipette. Embryos were then arrayed via pipette at 10 or 5 embryos per well into 48 or 96 well plates respectively. Embryos were transferred in 500 μ l or 150 μ l of 0.1XMMR (supplemented with gentamycin sulfate to 50mg/ml) making the final volume of each well 1000 μ l or 300 μ l in 48 or 96 well plates respectively. Plates were sealed using an O₂ permeable plate seal. Arrayed *X. laevis* and *X. tropicalis* embryos were grown at 18 $^{\circ}$ C and examined visually with a dissecting microscope at 1, 2 and 3 days post fertilisation (approximately stage 25, 32 and 38 respectively). Embryos were fixed at stage 38 in their respective wells by removing as much of the dosing solution as possible using a Pasteur pipette and fixed in 1000 μ l or 200 μ l of MEMFA in 48 or 96 well plates respectively. After 2 hours at RT the MEMFA was replaced with PBST (Tomlinson, 2012).

2.2.3 Observing embryos

Phenotypes were observed by transferring the desired embryos into a Petri dish coated with 2.5ml 1% agarose gel covered with PBS via Pasteur pipette. Embryos were observed using a Zeiss Stemi 5V6 microscope. Images were captured using a 01-MP3.3-RTV-CLR-10 camera mounted and processed with the Q capture software package. All images of embryos are orientated from left to right (anterior to posterior). To clarify the terminology used to describe the orientation of the *X. laevis* embryos in images taken, **Figure 12 A** Displays an annotated stage 38 Nieuwkoop and Faber embryo. This also indicates the positions of the lateral and dorsal pigmentation stripes that are referred to numerous times in this thesis. Also included are example images of a stage 38 wild type *X. laevis* embryos, accompanied by two commonly observed phenotypes in the form of total pigmentation loss and abnormal melanophore migration (**Figure 12 B i, ii and iii**).

2.2.4 Embryo Fixation

For long term storage embryos were removed from their wells using a Pasteur pipette and transferred to a 5ml glass vial and covered with a PBST/methanol (50/50) solution, and left on a rocker for 5 minutes. This wash step was repeated once again using PBST/methanol (50/50) solution and finally left in 100% methanol. Fixed embryos were stored at 4°C.

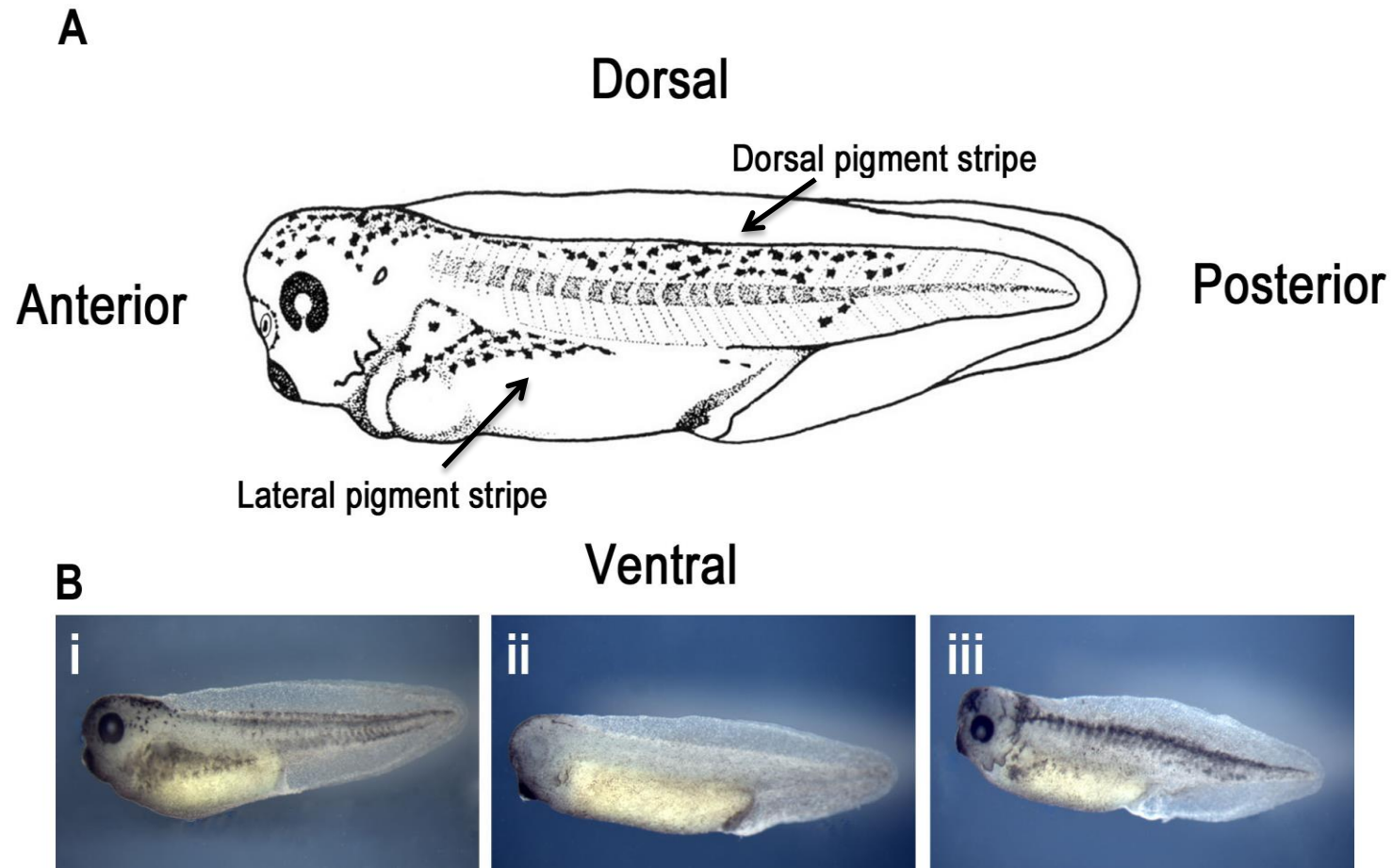


Figure 12. Example of *X. laevis* embryo image orientation. A. Typical stage 38 *X. laevis* embryo as defined by (Nieuwkoop, 1956). B. Example images of stage 38 *X. laevis* embryos displaying abnormal pigmentation phenotypes. i. Wild type embryo. ii. Embryo displaying a complete loss of pigmentation. iii. Embryo displaying abnormal melanophore morphology phenotype.

2.3 Small compounds used

The National Cancer Institute (NCI) Diversity set I and Diversity set II compound libraries, plus subsequent individual NCI compounds requested following identification during the initial chemical genetic screen, were all sourced from the Synthesis and Chemistry Branch, Developmental Therapeutics program, Division of Cancer Treatment and Diagnosis, National Cancer Institute, USA. The NCI Diversity set I and NCI Diversity set II compound libraries consisted of 1990 and 1363 compounds respectively and were supplied in a 96 well plate 10mM (dissolved in DMSO), 100µl per compound, per well format. All additional individual compounds were supplied as solids and were dissolved in DMSO to make 10mM stocks.

AstraZeneca organ specific toxic compounds were obtained from AstraZeneca, Alderley Park, Cheshire, UK. Compounds were obtained in a 96 well plate format in 10mM 100µl stock solutions (dissolved in DMSO). Compounds were selected and organised based on their specific organ toxicity (nephrotoxicity, hepatotoxicity, cardiotoxicity and non-toxic controls). AstraZeneca sourced compounds were chosen based on previously published information provided by (Lin and Will, 2012).

2.4 Dose response assays

Those compounds which were shown to give a repeatable phenotype were used in a dose response assay, Here compounds were added to stage 15 embryos (10 embryos per well, 1ml final volume) at either 0.1, 1, 10, 25, 50, 100µM.

Embryos were allowed to develop to stage 38 at which point they were fixed in MEMFA, and scored for abnormal phenotypes.

2.5 Cell culture assays

2.5.1 Cell lines used

The A375 (BRAF mutant) human melanoma cell line was obtained from the Ribas laboratory (University of California, USA). The RD1 human rhabdomyosarcoma line and the HEK293 Human epithelial kidney cell line were both obtained from the Biomedical Research Centre (University of East Anglia, UK). All cell lines were first used at passage 2 and finished with at passage 21. All cell lines were incubated at 38°C, 95% humidity and 5% CO₂ and were routinely tested for mycoplasma.

2.5.2 Cell viability assays

The Cell Titre Glo® (Promega) assay was used to determine cell viability in the cell lines used. First costar 96 well plates (Corning incorporated) were coated with poly-L-lysine (Sigma) (40µl per well) to aid cells in sticking to the plate. After rocking at RT for one hour poly-L-lysine was removed and cell lines were seeded into wells. A375, RD1 and HEK293 cell lines were seeded at 2000, 7500 and 15000 cells per well respectively in 100µl culture media.

After 24 hours media was removed from the wells and replaced with fresh media plus compounds at the desired concentrations. This also included a positive control (100nM Cytochalasin D) and vehicle control (0.1% DMSO). All chosen

NCI compounds were prepared as serial dilutions at 1.56, 3.13, 6.25, 12.5, 25, 50, 75 and 100 μ M. All concentrations (including controls) for all cell lines were run in triplicate within the same plate. Plates were then incubated at 37°C.

On day 5 the plates were removed from the incubator. 50 μ l of media was removed and replaced with 50 μ l CellTitre-Glo reagent. The plates were left to rock at RT for 10 minutes then immediately read using a Plate reader.

Cell viability was calculated using Microsoft Excel software, and was plotted as the average fluorescence of the three sample replicates as a percentage of the average fluorescence of the three DMSO control replicates found within the same plate. IC50's were generated using Prism Graphpad software and calculated using a nonlinear regression model.

2.6 Renal function toxicity assay

2.6.1 Salicylic acid assay detection of ammonia NH₃

The salicylic acid method of NH₃ detection was the first assay used first for the detection of ammonia in sample media. The JBL NH₄ Test kit is a commercially available assay that rapidly determines the amount of NH₄ / NH₃ in sample media. The kit was used with the protocol provided with some alterations to achieve a higher throughput format. Embryos were grown from stage 38-45 in a 96 deep well plate (five embryos per well, 2ml final volume, without experimental compounds). At stage 45, 1ml of media was removed from each well and placed in a fresh cuvette. Wells were only sampled once each as by removing media the final volume of the well would be changed, thereby altering the potential

concentration of ammonia present when sampling again at a later date. The assay protocol stipulates that 1ml of each sample is required per reaction. To this solution 33µl of JBL solution one, two and three (supplied with the assay kit) were added in sequence and mixed via inversion (with a 5 minute gap between each addition). Each sample was then left for 5 minutes at which point 300µl of each reaction solution was transferred to a 96 well plate and absorbance was subsequently read on a spectrophotometer at 695nm. A blank (media containing no embryos) was used as a negative control.

Experiments involving compounds followed the same assay protocol, but with a different dosing regimen. Embryos were incubated with compounds at the desired concentration from embryonic stage 38 to stage 41 (roughly three days) at 18°C, at which point the compound was removed and fresh media added. Embryos were then incubated until they reached embryonic stage 45 (roughly another 3 days) at 18°C, at which point their media was sampled according to above protocol. The reason for this dosing regime is that it was unclear whether the compound would have an immediate effect, therefore residual excreted ammonia may be present in the media when read at day 45 despite recent nephrotoxicity and thereby bias results. To avoid this, compounds were dosed for a period of time and then removed with fresh media added to effectively standardise the base level of ammonia present. This ensures that that ammonia concentrations detected reflect the effect of the compound after its potential effects have taken place.

The Tetra NH₄ Ammonia assay was used in exactly the same way as the JBL kit. The API NH₄ Ammonia assay contained two solutions instead of three, however the amount of each solution added remained the same.

It was not possible to continue to assess ammonia excretion in *X. laevis* embryos past embryonic stage 45. This is because UK law considers *X. laevis* embryos to be sentient past embryonic stage 45, requiring additional licensing not covered by our current agreement. It would significantly complicate the development of the assay if it were to progress past embryonic stage 45 due to the necessary government licensing involved and therefore any assay developed has to be sampled prior to this cut off.

2.6.2 Glutamate dehydrogenase assay detection of ammonia NH₃

The GDH assay protocol provided was used exactly as instructed in the provided protocol (including compound dosing regimens. 1000µl of the ammonia assay reagent was added to a cuvette followed by 100µl of sample media. A blank sample was also run alongside the test sample by adding 100µl H₂O to 1000µl of the ammonia assay reagent. The solution was inverted and incubated at RT for 5 minutes. The spectrophotometer was blanked using water as a reference. The absorbance of the solution was then read at 340nm. 10µl of L-glutamate dehydrogenase was then added to the solution which was inverted and then incubated at RT for 5 minutes. The solutions absorbance was then read every minute until it ceased decreasing. Using this data, the ΔA_{340} was calculated to determine the change in absorbance following the addition of the L-glutamate dehydrogenase enzyme. As the reaction is driven by the presence of ammonia, the larger the ΔA_{340} , the more ammonia present in the sample. A blank ΔA_{340} was then subtracted from the sample ΔA_{340} to generate the sample $\Delta(\Delta A_{340})$ so as to account for background levels of ammonia that may be present in the media.

$$\begin{aligned}\Delta A_{340} &= \\ &= A_{\text{initial}} - A_{\text{Final}} \\ \Delta(\Delta A_{340}) &= \\ &= \Delta A_{340}(\text{Test or Standard}) - \Delta A_{340}(\text{Blank})\end{aligned}$$

2.7 Chemoinformatical prediction of compound targets

All chemoinformatical analysis was performed by the Bender laboratory. For the full method of this analysis see (Liggi, 2013). The significant stages of the protocol are summarised below.

2.7.1 Chemoinformatical analysis of compounds identified from the NCI

Diversity set II chemical genetic screen

The aim of this experiment was to predict targets for those 72 compounds identified to give abnormal phenotypes in the *X. laevis* chemical genetic screen by using both the chemical structures of the compounds and the specific phenotypic class to which they were allotted (based on the phenotype they gave).

First the 72 identified compounds 2D structures were subjected to a pipeline (KNIME workflow) in which they were standardised (according to pre-set parameters) for consistency. Molprint 2D fingerprints (depth 3) were then generated and target prediction was run using the ChEMBL v10 training set (approximately 155,000 ligand pair covering 894 targets). A Laplacian-modified naïve Bayes classifier then calculated the relative class membership

probabilities for each compound and returned a ranked list of targets with scores. Several visualisation/clustering methods were then employed (Multi-Dimensional Scaling, network distance from k-nearest neighbour and hierarchical clustering) using Orange Canvas to assess bioactivity profile similarity amongst the different phenotypes. Inductive rules and classification trees (limited to depth = 5) were then generated to establish the best data splits for explaining each compounds relationship with its observed phenotype. Finally predicted targets were subjected to enrichment calculations in order to derive as much information as possible.

2.8 Statistical analysis

All statistical tests were carried out using Graph Pad Prism 6 software. Suitable statistical tests were chosen for each data set to suit the type of data analysed. Tests used in this thesis include Students T-test and IC50 generation.

Chapter III

3.0 *Xenopus laevis* and *Xenopus tropicalis* as reliable models for chemical genetic screening

3.1 Introduction

3.1.1 Assessment of *X. laevis* chemical genetic screening reliability

Previous research has already highlighted *X. laevis* as a robust model for chemical genetic screening capable of assessing a variety of end points (discussed in **Chapter I**) (Dush et al., 2011; Kalin et al., 2009; Tomlinson et al., 2009a; Tomlinson et al., 2009b; White et al., 2011). The primary aim of this thesis was to further assess the role of *X. laevis* as a chemical genetic screening model for drug discovery. It is appropriate to first assess the models reproducibility in such screens. The original Wheeler laboratory NCI diversity set I compound screen was amongst the first of its kind to assess the application of *X. laevis* towards chemical genetic screening (Brandli, 2004; Kalin et al., 2009; Tomlinson et al., 2005; Tomlinson et al., 2009b). It was successful in identifying 35 compounds that gave rise to a range of phenotypes (summarised in **Figure 13 A**). I aimed to assess the reproducibility of the *X. laevis* chemical genetic assay by rescreening each of the 35 original hit compounds and observing if a similar phenotype was elicited. To achieve this, fresh compound stocks were ordered for each compound from the National Cancer Institute (USA), and were prepared, screened and analysed using exactly the same method as described

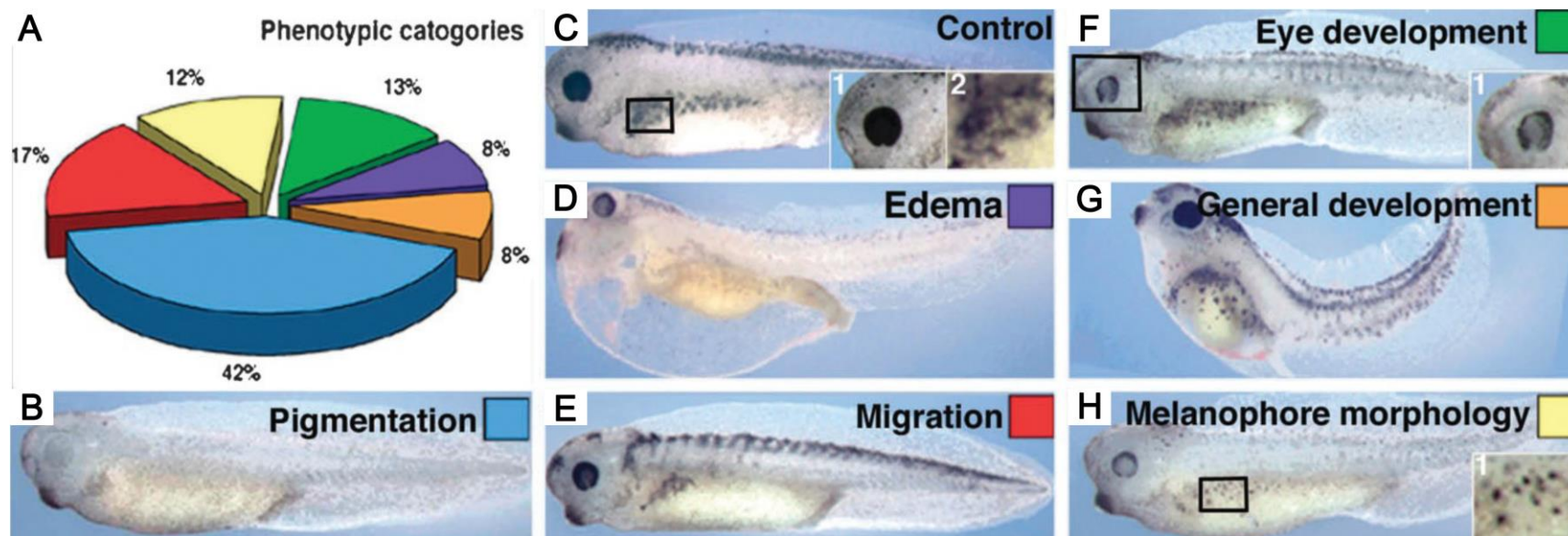


Figure 13. Phenotypic categories scored in the original Tomlinson et al., (2009) chemical genetic screen. A. Pie chart depicting the proportion of positive hits ($n=35$) in each category. B. Untreated control embryo, insert boxes show the eye (b1) and the melanophores on the lateral pigment stripe (b2). Categories include C. pigmentation, D. edema formation, E. melanophore migration, F. eye development (insert box shows disrupted eye development, black box shows magnified area f1), G. general development and H. melanophore morphology (insert box shows small melanophores on the lateral pigment stripe, h1). Coloured insert boxes relate to the coloured pie chart section. Embryos shown were screened at $40\mu\text{M}$. Figure taken from (Tomlinson et al., 2009b).

in (Tomlinson et al., 2009b). Should a phenotype similar to that previously described be observed, this would suggest the *X. laevis* chemical genetic model system is both reliable and robust in its ability to reproduce previous findings, further supporting its use as a model for drug discovery and development.

3.1.2 Assessment and comparison of X. tropicalis as a viable chemical genetic screening model

One negative towards using *X. laevis* as a model organism is that its paleopolyploidy genome complicates genetic experimentation and analysis. It is believed that the *X. laevis* polyploidy genome arose due to a hybridisation event of two parent species approximately 40 million years ago (Evans et al., 2004; Hellsten et al., 2007). This resulted in the formation of gene duplicates (known as homeologs) resulting in functional redundancy. These gene duplicates may retain overlapping functions and redundancies, complicating the generation and interpretation of mutant phenotypes.

All living *Xenopus* species possess a paleopolyploid genome with the exception of *X. tropicalis*, which possess a diploid genome. Retaining all of the practical advantages of the closely related species *X. laevis* (summarised in **Table 6**), *X. tropicalis* also has the advantage of being far more amenable towards genetic experimentation. In addition, *X. tropicalis* reaches sexual maturity in approximately four months whereas *X. laevis* takes approximately 12 to 24 months. This is significant as it permits the rapid generation of inbred mutant lines, which is comparatively much more difficult when using *X. laevis*. Such advantages explain the prominent rise in popularity of *X. tropicalis* as an experimental model over the past two decades. To date however, little literature

Table 6. Differences exhibited between the *X. laevis* and *X. tropicalis* animal models

	<i>X. laevis</i>	<i>X. tropicalis</i>
Ploidy	allotetraploid	diploid
Haploid	18 chromosomes	10 chromosomes
Genome size	3.1 x 10 ⁹ bp	1.7 x 10 ⁹ bp
Optimal temp	16-22°C	25-30°C
Adult size	10 cm	4-5 cm
Egg size	1-1.3 mm	0.7-0.8 mm
Brood size	300-1000	1000-3000
Generation time	24 months	4 months

exists as to whether *X. tropicalis* is amenable for chemical genetic screening. One exception is a study by Fort *et al.*, (2004), who aimed to assess the applicability of *X. tropicalis* as an alternative test species for use in the traditional Frog Embryo Tertogenesis assay – *Xenopus* (FETAX) assay. Results showed that *X. tropicalis* was not only equally amenable towards FETAX screening as *X. laevis*, but also produced similar phenotypes under the same conditions (Fort *et al.*, 2004).

Given the clear practical advantages exhibited by the *X. tropicalis* model, it appeared prudent to investigate as to whether it could also be applied to our chemical genetic screening system. It was important to assess not only whether they were practically amenable towards the existing protocol, but also whether

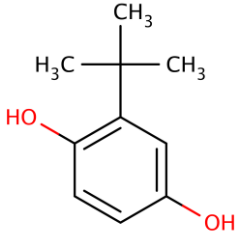
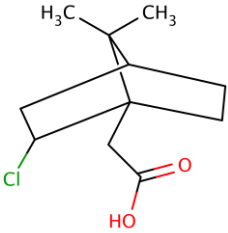
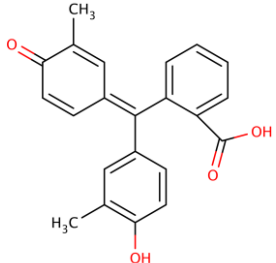
the phenotypes elicited were comparable to those previously identified in *X. laevis*. To determine this I screened the NCI diversity set I hit compounds identified in the previous Tomlinson *et al.*, (2005) screen using the same protocol described for *X. laevis*.

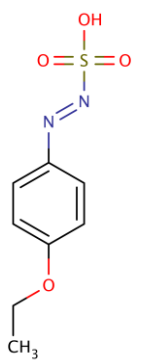
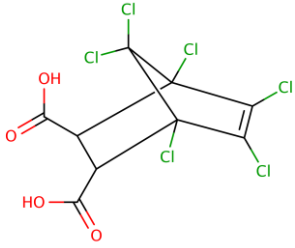
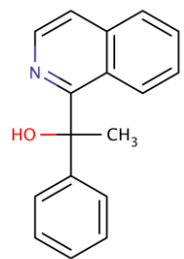
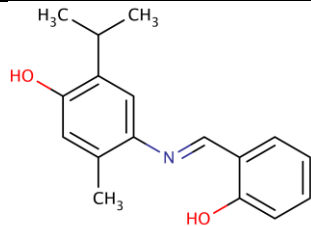
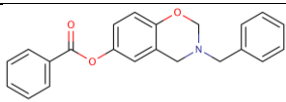
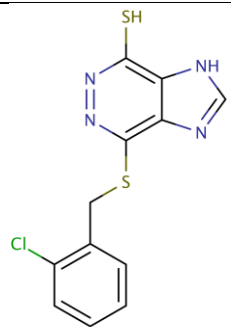
3.2 Results

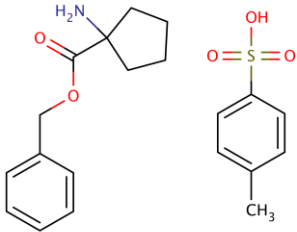
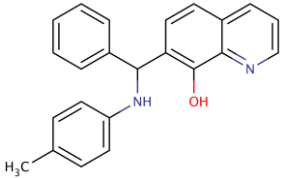
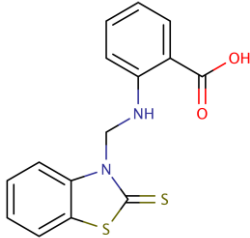
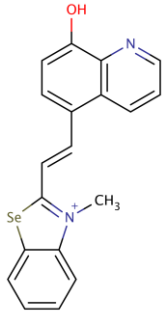
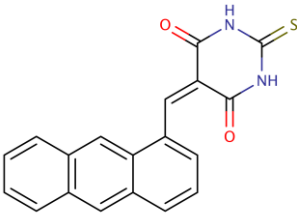
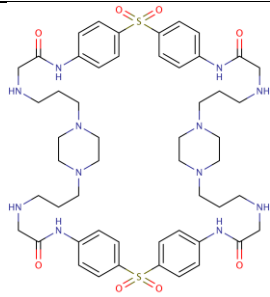
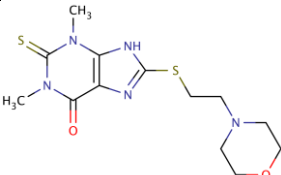
3.2.1 Rescreening of the original NCI diversity set I compound library

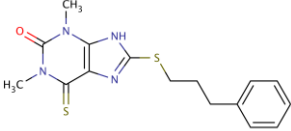
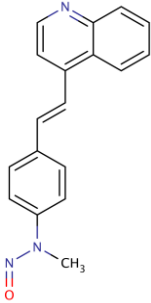
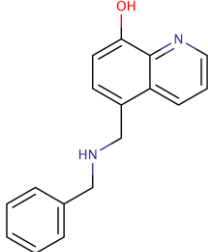
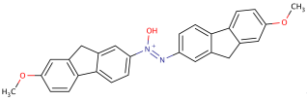
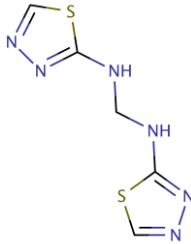
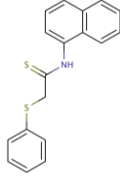
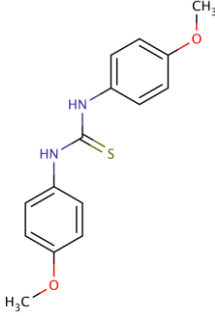
Fresh compound stocks for each of the 35 compounds identified in the Tomlinson *et al.*, (2005) screen were requested from the NCI repository. Of these, six were not obtainable due to lack of availability (as summarised in **Table 7**). To ensure consistency, all compounds were screened following the *X. laevis* chemical genetic screening protocol described in (Tomlinson *et al.*, 2009b). A representative example of each of the six commonly identified phenotypes (pigmentation, melanophore morphology, melanophore migration, edema, morphological and eye development phenotypes), identified in the original Tomlinson *et al.*, (2009) screen alongside the relative proportion of positive hits (n=35) for each phenotypic category are summarised in **Figure 13**. Of the 13 available abnormal pigmentation inducing phenotypic compounds rescreened, all reproduced their respective phenotypic effect in *X. laevis* (**Figure 14**). Notably, NCI 30712, NCI 47938, NCI 49762, NCI 62406, NCI 86153, NCI 99676, NCI 130830 and NCI 132230 (**Figure 14 C-G and I-K** respectively), showed a marked reduced pigmentation in both the lateral and dorsal stripe as well as in the head and eye. NCI 7734, NCI 158011 and NCI 164990 (**Figure 14 B, L and M** respectively) also showed markedly reduced pigmentation in the lateral and dorsal stripe, however the head and eye pigment still remain, albeit it

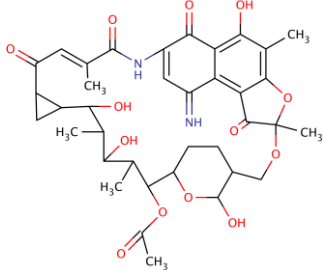
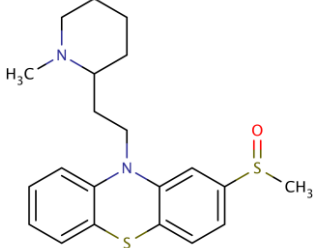
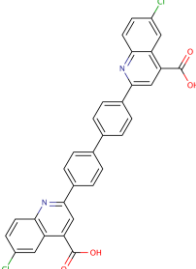
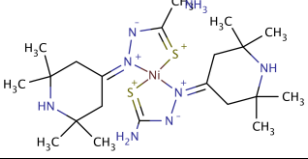
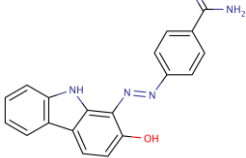
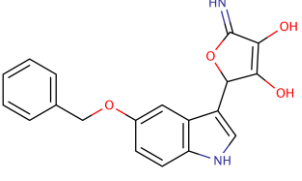
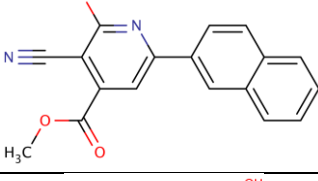
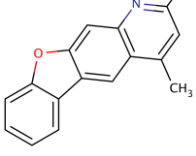
Table 7. Hit compounds identified in the Tomlinson *et al.*, (2005) NCI diversity set I chemical genetic screen, accompanied by their identified phenotype, molecular weight, formula, and structure. Also shown is their ability to be reliably replicated (n=3). E, (Edema phenotype). ED, (eye development phenotype). M, (abnormal morphology phenotype). Mg, (Abnormal melanophore migration phenotype). MM, (abnormal melanophore morphology phenotype). P, (abnormal pigmentation phenotype). *** Denotes those compounds for which new stocks were not available.

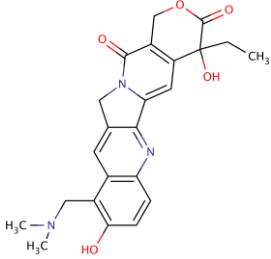
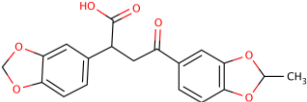
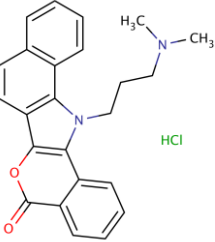
NCI Hit Compounds	Phenotype generated	MW	Formula	Structure	Phenotype replicated
4972	P	166	C ₁₀ H ₁₄ O ₂		✓
7734	P	216	C ₁₁ H ₁₇ ClO 2		✓
10470	E	346	C ₂₂ H ₁₈ O ₄		✓

17173	MM	230	$C_8H_{10}N_2O_4$ S		✓
22207	Mg	388	$C_9H_4Cl_6O_4$		✓
25431	Mg	249	$C_{17}H_{15}NO$		X
30712	P	269	$C_{17}H_{19}NO_2$		✓
47938	P	345	$C_{22}H_{19}NO_3$		✓
62406	P	308	$C_{12}H_9ClN_4$ S ₂		✓

80126	MM	391	$C_{20}H_{25}NO_5$ S		✓
84093	Mg	320	$C_{23}H_{20}N_2O$		✓
86153	P	316	$C_{15}H_{12}N_2O$ $2S_2$		✓
86374	P	493	$C_{19}H_{15}N_2O$ Se		***
90737	M	332	$C_{19}H_{12}N_2O$ $2S$		✓
95609	MM	1057	$C_{52}H_{72}N_{12}$ O_8S_2		✓
99667	P	341	$C_{13}H_{19}N_5O$ $2S_2$		✓

99676	P	346	$C_{16}H_{18}N_4O$ S_2		✓
101984	ED	289	$C_{18}H_{15}N_3O$		✓
130830	P	264	$C_{17}H_{16}N_2O$		✓
132230	P	434	$C_{28}H_{22}N_2O$ 3		✓
143019	ED	214	$C_5H_6N_6S_2$		✓
158011	P	309	$C_{18}H_{15}NS_2$		✓
164990	P	288	$C_{15}H_{16}N_2O$ $2S$		✓

177383	Mg	822	$C_{43}H_{54}N_2O$ 14		***
186066	P	386	$C_{21}H_{26}N_2O$ S_2		✓
210627	Mg	565	$C_{32}H_{18}Cl_2$ N_2O_4		✓
227147	MM	513	$C_{20}H_{38}N_8N$ iS_2		✓
357777	M	329	$C_{19}H_{15}N_5O$		✓
372074	Mg	336	$C_{19}H_{16}N_2O$ 4		✓
373070	P	304	$C_{18}H_{12}N_2O$ 3		***
375985	ED	249	$C_{16}H_{11}NO_2$		***

609699	MM	458	$C_{23}H_{24}ClN$ $3O_5$		***
627512	Mg	356	$C_{19}H_{16}O_7$		✓
638432	ED	407	$C_{24}H_{23}ClN$ $2O_2$		✓

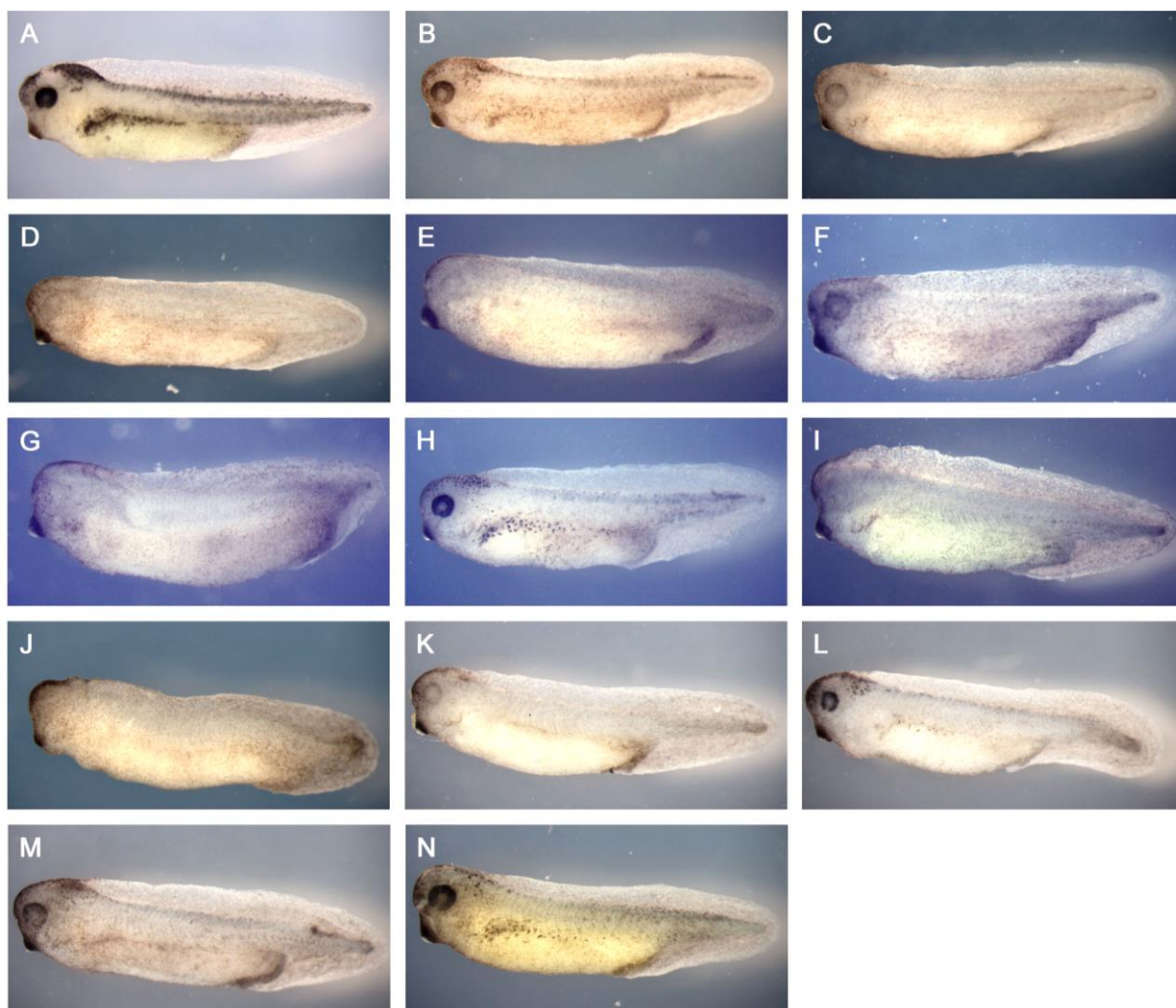


Figure 14. Abnormal pigmentation phenotypes replicated using compounds identified from the original Tomlinson NCI diversity set I compound screen. *X. laevis* embryos were assessed at stage 38 and compared to a corresponding DMSO vehicle control. Embryos shown were screened at 40 μ M. A. DMSO solvent control. B. NCI 7734. C. NCI 30712. D. NCI 47938. E. NCI 49762. F. NCI 62406. G. NCI 86153. H. NCI 99667. I. NCI 99676. J. NCI 130830. K. NCI 132230. L. NCI 158011. M. NCI 164990. N. NCI 186066.

at a reduced level when compared to the vehicle control. This is in fact still consistent with the phenotypes previously presented in the original Tomlinson *et al.*, (2009) screen. Both NCI 99667 (11H) and NCI 186066 (11N) showed reduced pigmentation, however melanocytes are clearly present in the head, eye and lateral / dorsal stripe regions. It would appear in each of these cases that the head and eye are unaffected as regards to pigmentation defects whereas the lateral and dorsal stripes indicate a reduced number of melanocytes that appear to have abnormal rounded morphology when compared to the dendritic morphology clearly exhibited in the vehicle control.

All five of the available melanophore morphology phenotype inducing compounds reproduced their previously prescribed phenotypic effect to varying degrees when compared to the vehicle control (**Figure 15**). NCI 17173, NCI 80126, NCI 95609, NCI 227147 and NCI 609699 (**Figure 15 B-F** respectively), all presented melanocytes in the lateral stripe with a rounded morphology that was far less dendritic than that displayed in the vehicle controls. NCI 17173 and NCI 609699 also showed a reduced number of melanocytes in the lateral and dorsal stripe when compared to the vehicle control. NCI 609699 also displayed abnormal morphology in the form of an undeveloped tail region when compared to the control.

Of the melanophore migration phenotype inducing compounds, all five reproduced their previously prescribed phenotypic effect to varying degrees when compared to the vehicle control (**Figure 16**). NCI 22207, NCI 84093, NCI 210627 and NCI 627512 all presented abnormal melanophore migration patterns down either the lateral or dorsal stripe (as highlighted in **Figure 16 B-D and F** respectively). NCI 372074 (**Figure 16 E**) showed some signs of abnormal

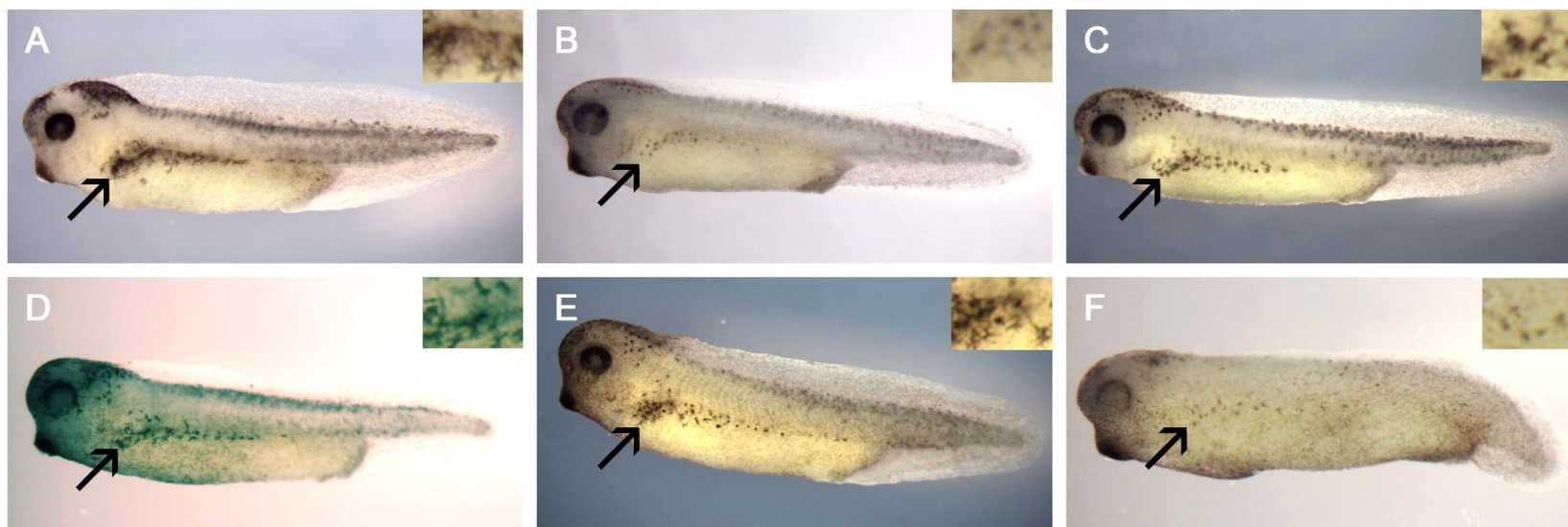


Figure 15. Abnormal melanophore morphology phenotypes replicated using compounds identified from the original Tomlinson NCI diversity set I compound screen. *X. laevis* embryos were assessed at stage 38 and compared to a corresponding DMSO vehicle control. Embryos shown were screened at 40 μ M. A. DMSO solvent control. B. NCI 17173. C. NCI 80126. D. NCI 95609. E. NCI 227147. F. NCI 609699

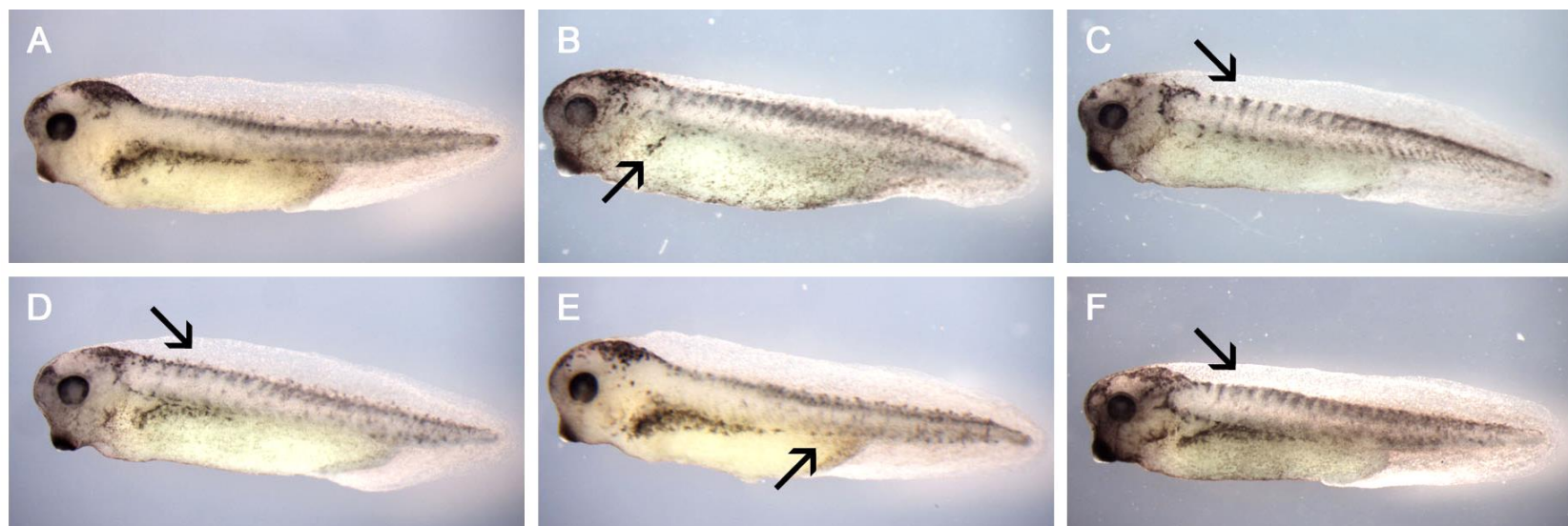


Figure 16. Abnormal melanophore migration phenotypes replicated using compounds identified from the original Tomlinson NCI diversity set I compound screen. *X. laevis* embryos were assessed at stage 38 and compared to a corresponding DMSO vehicle control. Embryos shown were screened at 40 μ M. A. DMSO solvent control. B. NCI 22207. C. NCI 84093. D. NCI 210627. E. NCI 372074. F. NCI 627512

melanophore migration with melanocytes unusually situated in the dorsal region of the lateral stripe, however this was not as prominent as other examples identified in the same phenotypic category. I was also able to reproduce the previously described edema phenotype (**Figure 17 B**). Likewise, both of the abnormal morphology inducing compounds induced phenotypes similar to that described in the original Tomlinson *et al.*, (2009) screen (**Figure 18 B and C**). For example, NCI 90737 presents an elongated trunk phenotype with a shortened tail exactly as described previously. Similarly, the enlarged forebrain displayed by NCI 357777 was also described in the original screen.

All three of the previously described abnormal eye development inducing compounds identified in the original Tomlinson *et al.*, (2009) screen induced abnormal eye development when rescreened to varying degrees (**Figure 19 B-D** respectively). NCI 101984 presented a malformed eye in which the size of the eye is not reduced when compared to the vehicle control as described in the Tomlinson *et al.*, (2009) screen but instead suggests possible abnormal development in the retinal pigment epithelial layer. NCI 143019 displays a complete loss of eye structure consistent with anophthalmia. The original phenotype was described as generating a small eye (microphthalmia) when compared to the vehicle control as well as a dislocation of the lens. NCI 638432 was previously described as having abnormal retinal epithelial layer, as indicated by a mottled pigmentation of the eye, which is also present in the replicate sample. The size of the eye presented in the replicated phenotype is smaller than that of the control, suggesting microphthalmia.

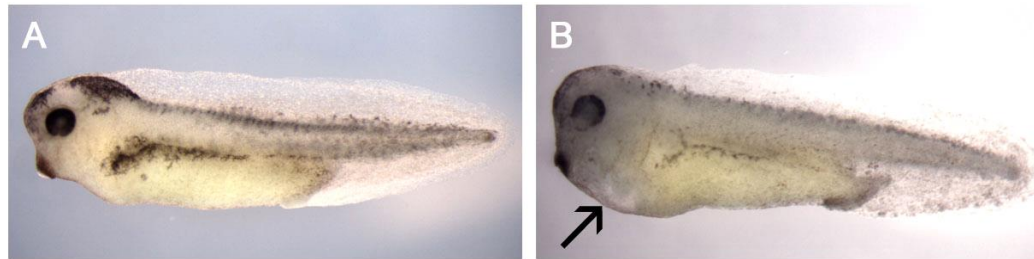


Figure 17. Abnormal edema phenotype replicated using compounds identified from the original Tomlinson NCI diversity set I compound screen. *X. laevis* embryos were assessed at stage 38 and compared to a corresponding DMSO vehicle control. Embryos shown were screened at 40 μ M. A. DMSO solvent control. B. NCI 10470.

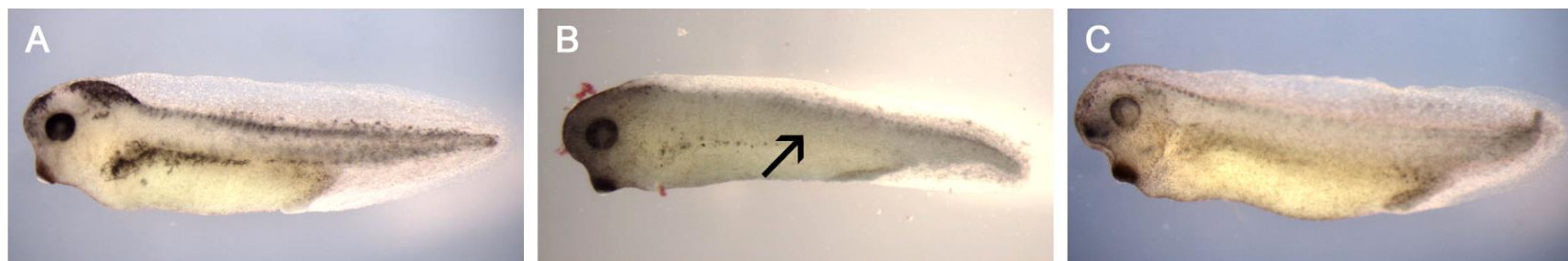


Figure 18. Abnormal morphology phenotypes replicated using compounds identified from the original Tomlinson NCI diversity set I compound screen. *X. laevis* embryos were assessed at stage 38 and compared to a corresponding DMSO vehicle control. Embryos shown were screened at 40 μ M. A. DMSO solvent control. B. NCI 90737. C. NCI 357777.

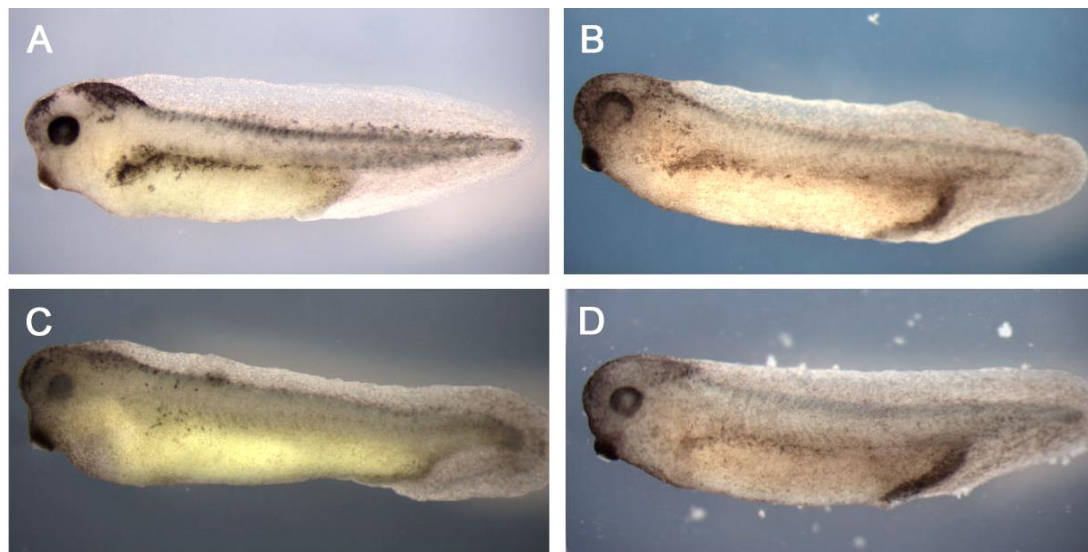


Figure 19. Abnormal eye development phenotypes replicated using compounds identified from the original Tomlinson NCI diversity set I compound screen. *X. laevis* embryos were assessed at stage 38 and compared to a corresponding DMSO vehicle control. Embryos shown were screened at 40 μ M. A. DMSO solvent control. B. NCI 101984. C. NCI 143019. D. NCI 638432.

3.2.2 Assessment of *X. tropicalis* as a chemical genetic screening model

To determine if the *X. tropicalis* model is amenable to chemical genetic screening, the same hit compounds identified by Tomlinson *et al.*, (2009) were screened upon *X. tropicalis* using the same method and concentrations (40µM) as described previously for the *X. laevis*. Due to limited stock availability, only 25 of the 29 original hit compounds in my possession were screened. This number was still a fair representation of all the six phenotypes identified, as the missing compounds (NCI 49762, NCI 99609, NCI 99676, NCI 372074 and NCI 627512) all came from phenotypic classes containing numerous alternative hit compounds. To allow for easy comparison of the similarities and differences exhibited between the phenotypes elicited in either the *X. laevis* or *X. tropicalis* models, all figures are presented with each compound induced phenotype side by side. As the majority of the compounds produced similar phenotypes in both models, the figures in this chapter have been condensed to show representative examples for each phenotypic class. For the complete collection of the phenotypes for all compounds in both models see to Appendix I.

Of the abnormal pigmentation compounds screened, all gave rise to a similar phenotype in *X. tropicalis* as was displayed in *X. laevis*. For example, NCI 47938 caused a significant loss in pigmentation in both the lateral and dorsal stripe in both the *X. laevis* and *X. tropicalis* embryos. Likewise NCI 62406 causes a global reduction of pigmentation in the lateral and dorsal stripe and the head and eye in both models. One notable difference between the models for some compounds is displayed highlighted by NCI 99676 (**Figure 20 Di and Dii**), in which there is global pigment loss in the *X. tropicalis* embryo, whereas the

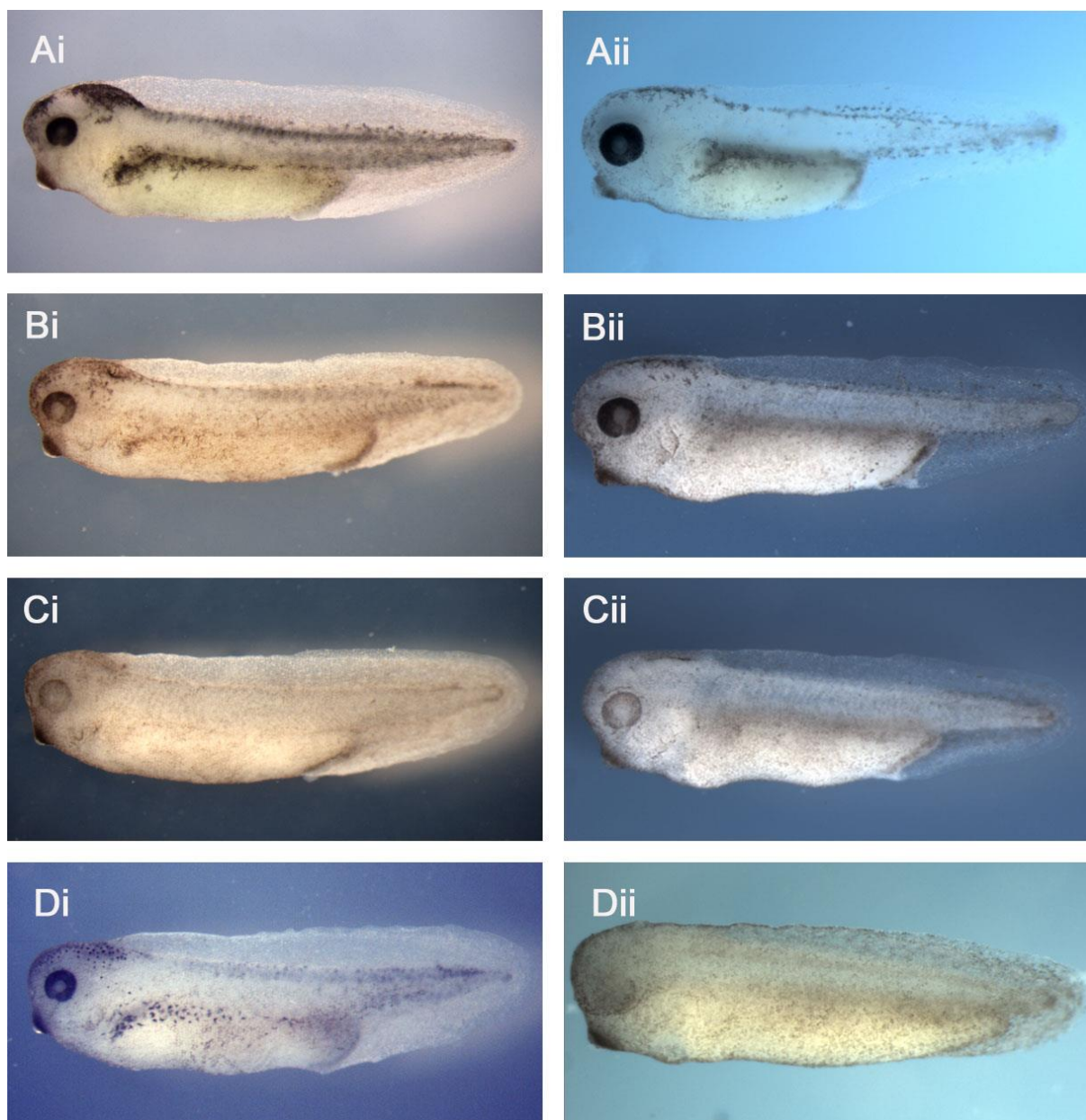


Figure 20. Side by side comparison of NCI compounds identified in the NCI diversity set I compound screen that gave rise to a similar prominent abnormal pigmentation phenotype when assessed at stage 38 (when compared to the DMSO vehicle control) in both *X. laevis* and *X. tropicalis*. Embryos shown were screened at 40 μ M. Ai. *X. laevis* DMSO solvent control. Aii. *X. tropicalis* DMSO solvent control. Bi. *X. laevis* NCI 7734. Bii. *X. tropicalis* NCI 7734. Ci. *X. laevis* NCI 30712. Cii. *X. tropicalis* NCI 30712. Di. *X. laevis* NCI 99676. Dii. *X. tropicalis* NCI 99676.

pigment is only lost in the dorsal and lateral stripe for the *X. laevis* embryo, but appears to still be present in the eye and head region.

A similar pattern was seen in those compounds that gave rise to a melanophore morphology phenotype in the *X. laevis* embryos. Two of the four compounds gave rise to similar phenotypes in both models, as seen with NCI 17173 (**Figure 21 Bi and Bii**). The remaining two compounds however, whilst presenting clear evidence of abnormal melanophore morphology also showed a greatly reduced number of melanocytes in general when compared to their *X. laevis* equivalent, as shown by NCI 80126 (**Figure 21 Ci and Cii**). Similarly, *X. tropicalis* embryos screened with all three of the compounds known to induce an abnormal melanophore migration phenotype in *X. laevis* appeared to produce an exaggerated phenotype in the *X. tropicalis*. For example NCI 22207 and NCI 84093 both produced notable abnormal melanophore migration phenotypes in the *X. tropicalis* but also markedly reduced pigmentation in the lateral and dorsal stripe (**Figure 22 Bi, Bii, Ci, and Cii**).

The one edema producing compound did appear to reproduce a phenotype in the *X. tropicalis* similar to the described in the *X. laevis* (**Figure 23 Bi and Bii**), although also presented a global reduction in pigmentation when compared to the *X. laevis* equivalent. Of the two abnormal morphology generating compounds screened, NCI 90737 produced a similar abnormally elongated trunk phenotype to that described in the *X. laevis* counterpart (**Figure 24 Bi and Bii**). NCI 357777 however produced an abnormal phenotype that was dissimilar to that induced in *X. laevis* (**Figure 24 Ci and Cii**). The *X. tropicalis* embryo presented a total lack of pigmentation accompanied by global developmental delay and embryos would typically not survive long past the stage presented

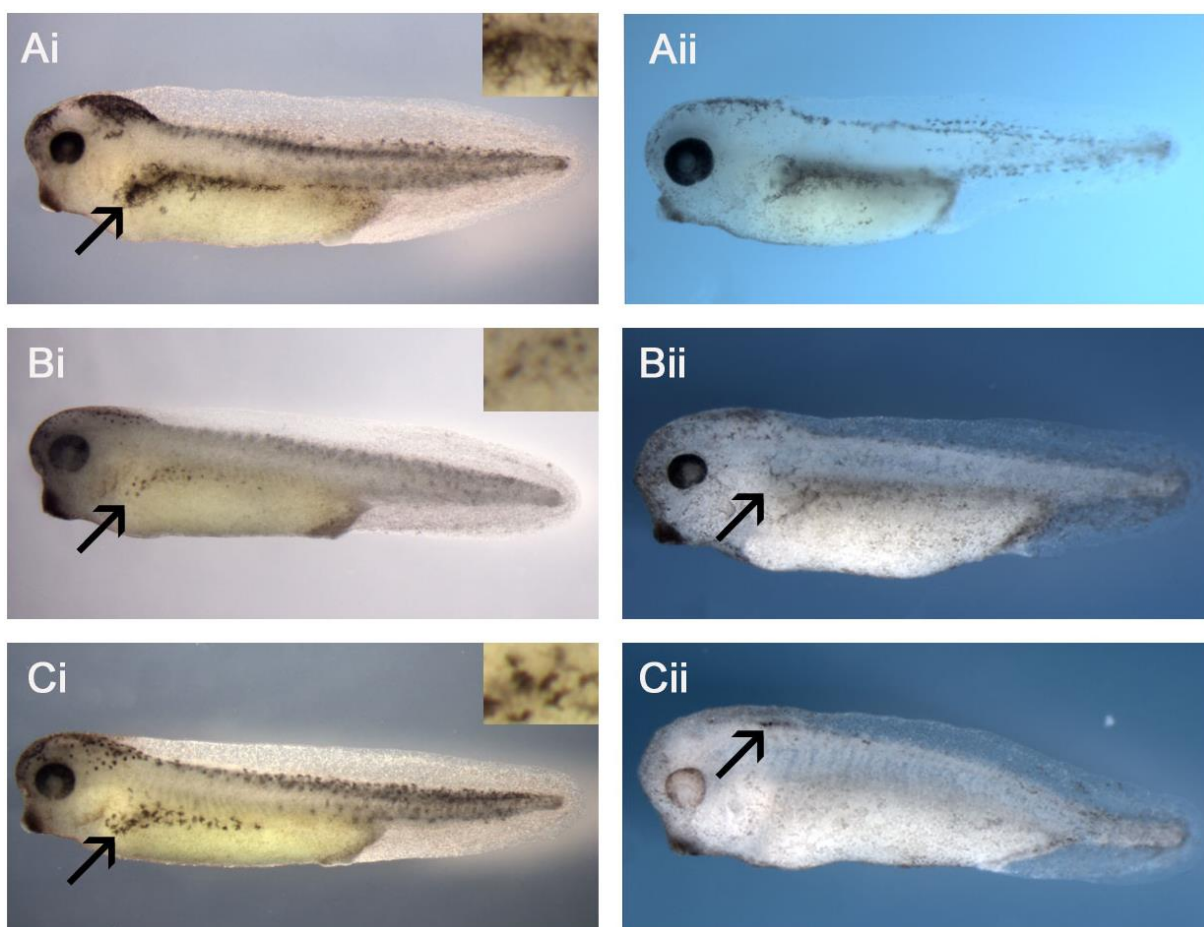


Figure 21. Side by side comparison of NCI compounds identified in the NCI diversity set I compound screen that gave rise to a similar prominent melanophore morphology phenotype when assessed at stage 38 (when compared to the DMSO vehicle control) in both *X. laevis* and *X. tropicalis*. Embryos shown were screened at 40 μ M. Ai. *X. laevis* DMSO solvent control. Aii. *X. tropicalis* DMSO solvent control. Bi. *X. laevis* NCI 17173. Bii. *X. tropicalis* NCI 17173. Ci. *X. laevis* NCI 80126. Cii. *X. tropicalis* NCI 80126.

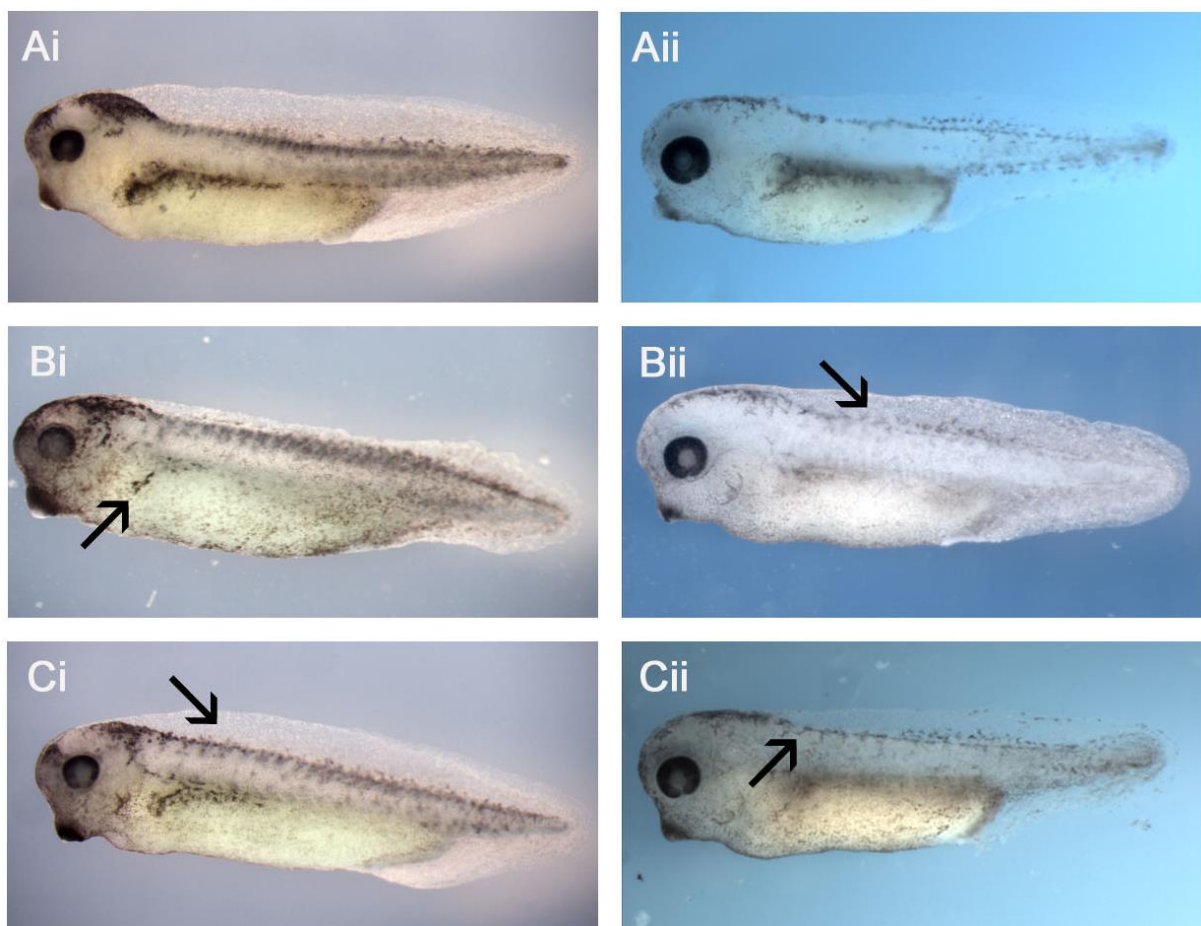


Figure 22. Side by side comparison of NCI compounds identified in the NCI diversity set I compound screen that gave rise to a similar prominent melanophore migration phenotype when assessed at stage 38 (when compared to the DMSO vehicle control) in both *X. laevis* and *X. tropicalis*. Embryos shown were screened at 40 μ M. Ai. *X. laevis* DMSO solvent control. Aii. *X. tropicalis* DMSO solvent control. Bi. *X. laevis* NCI 22207. Bii. *X. tropicalis* NCI 22207. Ci. *X. laevis* NCI 84093. Cii. *X. tropicalis* NCI 84093.

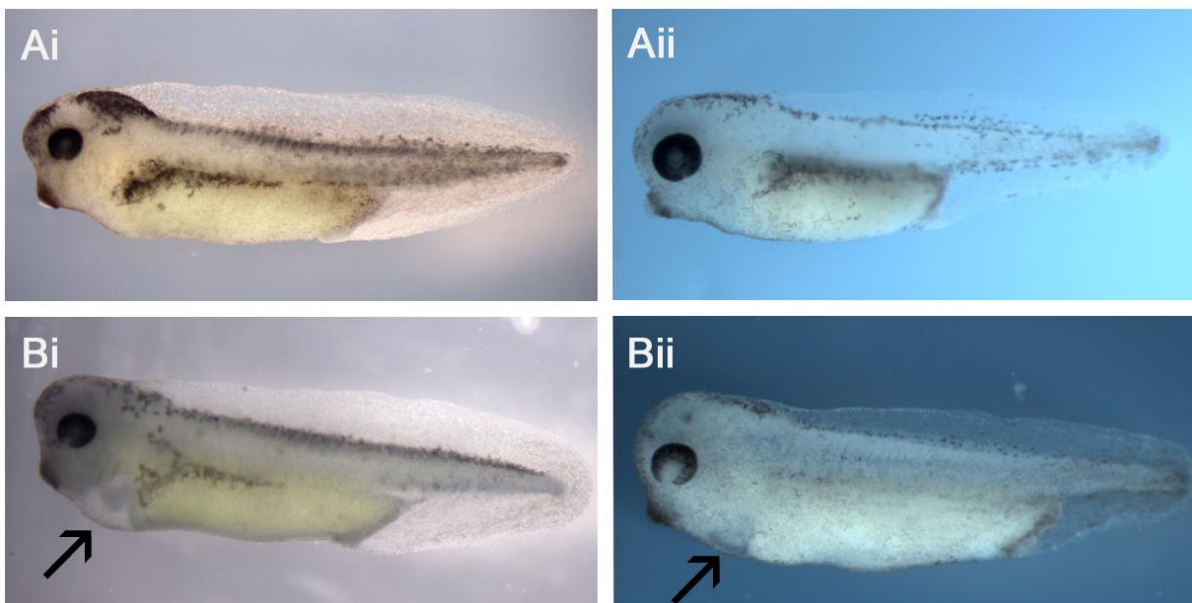


Figure 23. Side by side comparison of NCI compounds identified in the NCI diversity set I compound screen that gave rise to a similar prominent edema phenotype when assessed at stage 38 (when compared to the DMSO vehicle control) in both *X. laevis* and *X. tropicalis*. Embryos shown were screened at 40 μ M. Ai. *X. laevis* DMSO solvent control. Aii. *X. tropicalis* DMSO solvent control. Bi. *X. laevis* NCI 10470. Bii. *X. tropicalis* NCI 10470.

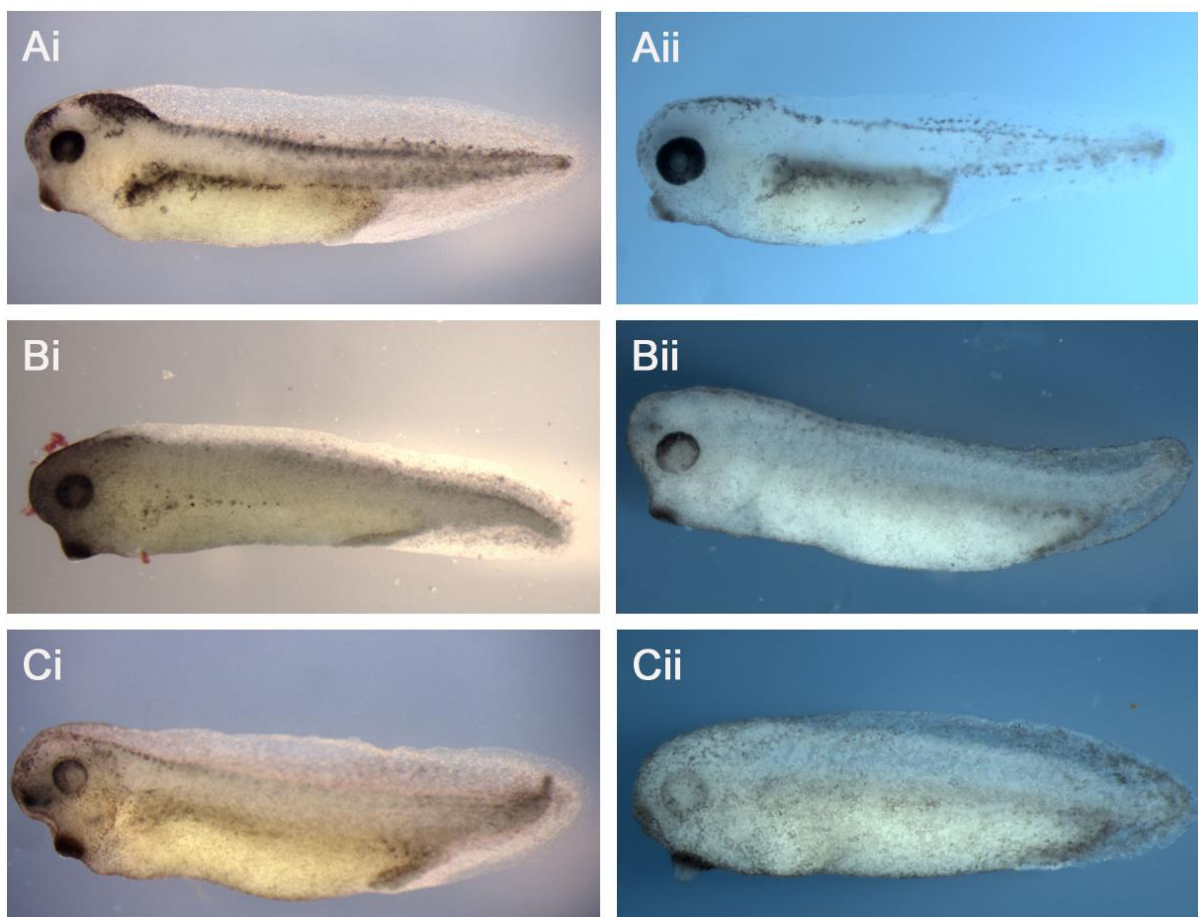


Figure 24. Side by side comparison of NCI compounds identified in the NCI diversity set 1 compound screen that gave rise to a similar prominent morphological phenotype when assessed at stage 38 (when compared to the DMSO vehicle control) in both *X. laevis* and *X. tropicalis*. Embryos shown were screened at 40 μ M. Ai. *X. laevis* DMSO solvent control. Aii. *X. tropicalis* DMSO solvent control. Bi. *X. laevis* NCI 90737. Bii. *X. tropicalis* NCI 90737. Ci. *X. laevis* NCI 357777. Cii. *X. tropicalis* NCI 357777.

here. The *X. laevis* embryo showed a loss of pigmentation in the lateral and dorsal stripe, but melanocytes were clearly present in the head and eye. It also had an enlarged fore brain which the *X. tropicalis* samples lacked. Of the three abnormal eye development compounds screened, only NCI 143019 produced a similar phenotype as described in *X. laevis* (**Figure 25 Bi, Bii, Ci and Cii**). NCI 143019 featured a very similar under developed eye in *X. tropicalis* as it did in *X. laevis*, with both also possessing a global lack of total pigment. NCI 101984 however shows little abnormality in the eye structure or development in the *X. tropicalis* when compared to the *X. laevis* equivalent, although it did present a more prominent decrease of pigmentation seen in the lateral and dorsal stripe.

3.3 Discussion

The first aim of this chapter was to assess the reproducibility of *X. laevis* as a chemical genetic screening tool by rescreening the original Tomlinson *et al.*, (2009) hit compounds. Using newly ordered stocks, this rescreening strategy resulted in the majority of the phenotypes previously described being replicated. For the edema, abnormal morphology, abnormal eye development, abnormal melanophore migration, abnormal melanophore morphology and the majority of the abnormal pigmentation phenotypes, the majority of compounds screened reproduced phenotypes that were very similar to those previously described. However, in a minority of cases it could be argued that whilst the phenotypic class allocated was clearly appropriate, the extent to which these phenotypes were expressed was not fully the same between the original and rescreened samples. For example both NCI 99667 and NCI 186066 showed reduced pigmentation, however the phenotype was not as clearly defined as it had been

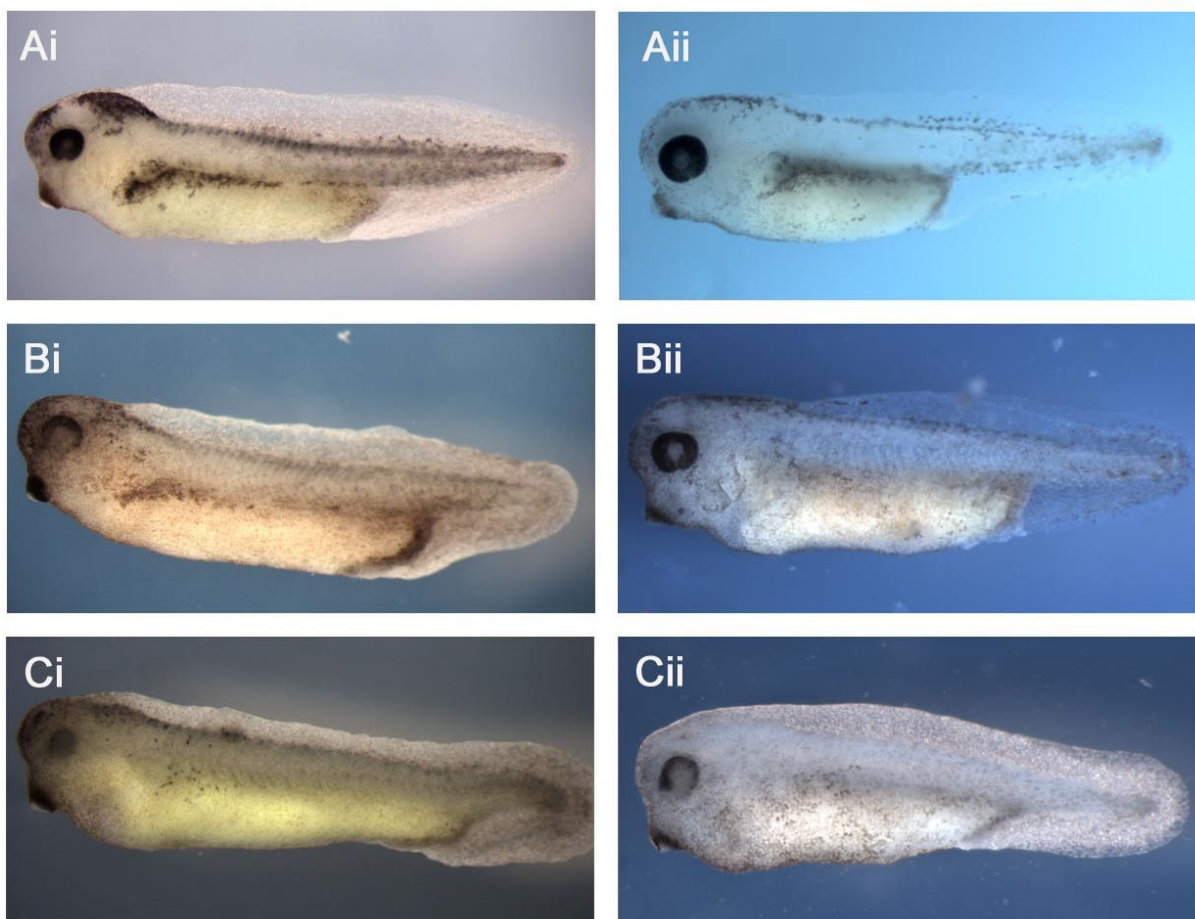


Figure 25. Side by side comparison of NCI compounds identified in the NCI diversity set I compound screen that gave rise to a similar prominent eye development phenotype when assessed at stage 38 (when compared to the DMSO vehicle control) in both *X. laevis* and *X. tropicalis*. Embryos shown were screened at 40 μ M. Ai. *X. laevis* DMSO solvent control. Aii. *X. tropicalis* DMSO solvent control. Bi. *X. laevis* NCI 101984. Bii. *X. tropicalis* NCI 101984. Ci. *X. laevis* NCI 143019. Cii. *X. tropicalis* NCI 143019.

when compared to other phenotypes in the same category. Indeed it is reasonable to suggest that in the case of these compounds, based on the number of melanocytes present and their rounded morphology, a more appropriate phenotypic class for both compounds might have been abnormal melanophore morphology. Despite this small discrepancy the majority of the phenotypes were successfully reproduced, implying that the assay is reproducible and therefore reinforces the position of *X. laevis* as a robust model for chemical genetic screening.

The second aim of this chapter was to assess the applicability of *X. tropicalis* towards chemical genetic screening. To determine this, the same hit compounds identified in the Tomlinson *et al.*, (2005) were screened upon *X. tropicalis* embryos, utilising the same method and concentrations (40µM) as described previously for *X. laevis*.

Of the 25 compounds screened, all gave a phenotype that resemble the phenotypic class ascribed previously to *X. laevis*. The extent to which some of these phenotypes presented themselves however did vary. In a number of cases (for example 99676 (**Figure 20 Di and Dii**)) the extent to which pigmentation was reduced in the embryo was increased. This also occurred for some compounds in which abnormal pigmentation had not previously been present in their *X. laevis* counterpart, as shown for NCI 10470 (**Figure 23 Bi and Bii**). All compounds however displayed high similarity between *X. laevis* and *X. tropicalis* phenotypes with three notable exceptions.

Both NCI 357777 (**Figure 24 Ci and Cii**) and NCI 101984 (**Figure 20 Bi and Bii**) failed to reproduce the abnormal morphology and abnormal eye

development phenotypes described in their *X. laevis* counter parts respectively. NCI 101984 showed no indication of abnormal eye development although shared a similar abnormal pigmentation phenotype. As the phenotype was subtle in the *X. laevis* sample, this may simply not overtly present itself in the *X. tropicalis* model. NCI 357777 however led to the death of the embryos before they reached stage 38. This could suggest that the *X. tropicalis* model may in some cases be more sensitive than their *X. laevis* counter parts requiring a reduced concentration to allow the embryos to survive until they can be assessed.

NCI 80126 (**Figure 21 Ci and Cii**) presented a phenotype in *X. tropicalis* that would be far better categorised as abnormal pigmentation, due to the distinct global absence of melanocytes presented by the samples. This may in fact be a reflection of the noticeable heightened reduction in pigmentation displayed by other compounds in the *X. tropicalis* when compared to the *X. laevis*, suggesting that the *X. tropicalis* melanocytes are either more prone to cease producing melanin or may simply fail to differentiate during neural crest specification when antagonised by a compound inhibitor. It is possible that due to their smaller size, the compound may penetrate the *X. tropicalis* system more readily, making them more sensitive than their *X. laevis* counterpart. It has been shown previously (unpublished data) that increasing the concentration of compounds that give rise to a melanophore morphology or migration in *X. laevis* can generate phenotypes that might more readily be categorised as abnormal pigmentation. Likewise, decreasing the concentration of those compounds that give rise to an abnormal pigmentation can sometimes generate phenotypes that would be better categorised as abnormal melanophore morphology or abnormal melanophore migration. The increased sensitivity of the *X. tropicalis* embryos

may explain why in some cases, phenotypes previously identified as abnormal melanophore morphology or abnormal melanophore migration phenotypes in *X. laevis* might present themselves as abnormal pigmentation in *X. tropicalis*. A future study might investigate whether lowering the concentration of such compounds when screening in *X. tropicalis*, reproduce the phenotypes described in *X. laevis*. This however does not explain why in some compounds that had no previous abnormal pigmentation phenotype pattern of any form when screened in *X. laevis* (such as the edema inducing compound NCI 10470 (**Figure 23 Bi and Bii**)) present themselves in *X. tropicalis*. This may suggest that the *X. tropicalis* model could generally be more sensitive. It is worth highlighting however that to increase the throughput of these typically medium throughput chemical genetic screens samples are tested at only a few concentrations to rapidly identify phenotypes of interest that might be worthy of further investigation. Whilst some of the *X. tropicalis* phenotypes may have differed in their intensity, interesting phenotypes were presented and therefore given the primary objective of the experiment the screen could be considered successful.

It is apparent that the *X. tropicalis* model has high potential in its practical application towards chemical genetic screens. There were no practical difficulties in either plating the embryos or their tolerance to equivalent concentrations of solvent. One significant and unavoidable difference between the two models was the difference in incubation temperature. Whilst *X. laevis* embryos were incubated at 18°C during the course of the assay (and can tolerate a range of temperatures between 12°C and 22°C that can be used to regulate speed of development), *X. tropicalis* can only be incubated at 22°C. This however did not seem to have any effect on the compounds in question

with no change in solubility observed (no precipitation was observed). The difference in temperature is also reflected by the *X. tropicalis* embryos' significantly faster development speed when compared to *X. laevis* (even when incubated at the same temperature). This allowed the *X. tropicalis* embryos to reach stage 38 a full day earlier than the *X. laevis*, thereby substantially reducing assay turnaround time. This is significant in the context of drug discovery where the reduction of protocol time by a full day would significantly increase throughput capacity.

Temperature differences between the two models may affect the binding of the compound to a particular target once absorbed. An increase in temperature would lead to an increase in kinetic energy, potentially therefore leading to more rapid binding in the *X. tropicalis* than the *X. laevis* and subsequently generating a phenotype more rapidly or to a greater extent. This may therefore skew observed IC50s when comparing the two models against the same compounds. It is not possible using the current data to speculate whether or not this may or may not have had an effect on the phenotypes generated by either model. As human core body temperature is around 37°C, the warmer incubation temperatures of the *X. tropicalis* may better represent a human model system.

A further practical consideration is the relatively smaller size of the *X. tropicalis* embryos, potentially suggesting they may be capable of being incubated in less media and are therefore more suited to a 96 well plate format. A future experiment could investigate reducing the media volume *X. tropicalis* embryos are incubated in to thereby reduce the amount of compound used per assay. This would again be of benefit to medium through-put screens by potentially reducing the cost of the assay.

One disadvantage of using the *X. tropicalis* model is the reduced number of eggs produced per female. The 300-1000 eggs produced per female in *X. tropicalis* is significantly lower than the 1000-3000 eggs produced per female in the *X. laevis*, thereby increasing the amount of husbandry required to perform a screen on a similar scale. A further disadvantage is the relatively low amount of genetic material recoverable per embryo due to their smaller size, requiring larger embryo pools depending on the amount of material required. However the significantly shorter generation time and genetically tractable genome enjoyed by the *X. tropicalis* model would permit the rapid generation of isolated mutant lines which could be used in conjunction with chemical genetic screening to identify molecules that could be used for the treatment of specific diseases. Such an advantage coupled with the practical capacity demonstrated in this experiment would suggest that *X. tropicalis* is highly suitable as a model towards chemical genetics screening and may potentially be a more viable option than *X. laevis*. It has yet to be determined whether *X. tropicalis* can be used for a full scale chemical genetic screen. A planned future preliminary experiment is to screen three to four plates from a library previously screened using *X. laevis* embryos to assess whether results across a broad range of compounds produced similar effects (such as death, abnormal phenotypes or no effect) comparable to that observed when using *X. laevis*.

To summarise this chapter I have shown that the use of *X. laevis* for chemical genetic screening is highly reproducible. This strengthens the value of the NCI diversity set II screen (which I outline in Chapter IV). Similarly, preliminary evidence would suggest that *X. tropicalis* is highly suited towards chemical genetic screening and the model's genetic advantages may one day lead to it

superseding *X. laevis* as the primary amphibian model for chemical genetic screening. However, further work is necessary to determine if the model is capable of a chemical genetic screen and further investigation is required as to the optimal screening concentrations required.

Chapter IV

4.0 NCI diversity set II *X. laevis* chemical genetic screen followed by cell viability assay screening

4.1 Introduction

4.1.1 *X. laevis* as a chemical genetic screening model

The practical utility of the *X. laevis* animal model towards forward chemical genetic screening has already been discussed in great length (see **Chapter I**), promoting its strengths as an ideal tool for medium throughput screening applications with a variety of potential endpoints at its disposal (Adams et al., 2006; Dush et al., 2011; Kalin et al., 2009). Tomlinson *et al.*, (2009) was one of the first to show this potential in *X. laevis* by screening the NCI diversity set I compound library on *X. laevis* embryos, focusing primarily on those compounds that gave rise to abnormal pigmentation phenotypes as a marker for interesting bioactivity of a screened molecule (Tomlinson et al., 2005; Tomlinson et al., 2009b). This led to the discovery of NCI 210627, a compound that gave rise to a subtle abnormal melanophore migration phenotype. This work was then continued in the Zon laboratory (Harvard, USA), where subsequent chemoinformatical analysis of NCI 210627 identified brequinar as a compound with a very similar structure to NCI 210627. Brequinar is a known inhibitor of the enzyme dihydroorotate dehydrogenase (DHODH) and when screened upon *X. laevis* embryos (under the same conditions as used in the identification of NCI 210627), produced a very similar phenotype. This suggested that the

mechanism of action of NCI 210627 in eliciting the observed phenotype may well also be through antagonising DHODH. Subsequent analysis led the identification of the anti-arthritis drug Leflunomide, a structurally dissimilar compound to both NCI 210627 and brequinar that was also a known inhibitor of DHODH. Leflunomide has since been shown to reduce spontaneous tumour growth in the BRAF V600E mutant Zebrafish line, and was also shown to significantly reduce the cell viability of melanoma cell lines when compared to non-melanoma controls (White et al., 2011). They subsequently showed leflunomide (in combination with the MEK inhibitor PLX4032) to significantly reduce melanoma tumour size and metastasis in mouse xenograft models. Leflunomide (in combination with PLX4032) is now undergoing human clinical trialling in the US with the hope that its will soon become a new novel therapeutic option for the treatment of melanoma (White et al., 2011).

The discovery of leflunomide was only possible through the highly successful screen originally carried out by Tomlinson *et al.*, (2009) and White *et al.*, (2011), and highlights the potential of abnormal pigmentation phenotypes identified in *X. laevis* screens as potential indicators of either molecules with therapeutic potential towards the treatment of melanoma, or may lead to the discovery of novel therapeutic targets with similar therapeutic potential. We felt that the possibilities of the developed *X. laevis* screening system had not been saturated by the original screen and that the potential was there to find additional molecules with therapeutic potential. We therefore sought to replicate the success of this experiment by screening the NCI diversity set II compound library using a similar protocol to that utilised by Tomlinson *et al.*, (2009). We then aim to expand upon this previous work by using a cell viability assay to assess either the therapeutic potential of hit compounds identified towards the

treatment of melanoma in house. By combining the *X. laevis* screening protocol with carefully selected follow up experiments (such as the melanoma cell viability assay), we aim to demonstrate (via the rapid identification of novel therapeutic compounds and targets) how the *X. laevis* model could be of value towards pharmaceutical drug discovery.

4.1.2 *The NCI diversity set II compound library*

The NCI diversity set II compound library consisted of 1363 compounds (supplied in 96 well, 100µl 10mM stocks), and was obtained from the NCI developmental therapeutic program. Formed as part of the NIH cancer initiative, the NCI diversity series was developed as an initiative to aid in the discovery and development of new drugs for the treatment of cancer. To date (March 2014), the latest available version is the NCI diversity set IV. Whilst the previous libraries (including the NCI diversity set I and II used the Tomlinson *et al.*, (2009) and this screen) are no longer available as libraries, the individual compounds may still be obtained (stock availability permitting).

The NCI diversity series set II compound library was chosen for several reasons. The NCI diversity set compounds are selected from the far larger NCI complete library, which consists of over 140000 compounds. Compounds included in NCI Diversity libraries have been selected based on their previously demonstrated biochemical activity and structural information. Such information enables the prediction of those compounds that will likely prove to be bioactive, whilst possessing features that are frequently attributed to improving a compounds 'druggability' (i.e. they are not electrophilic, unstable, organometallic, polycyclic aromatic hydrocarbons, possess low molecular

weight, etc.). In addition, the compounds are also selected based upon their dissimilarity. As such all compounds in the NCI diversity set libraries should be structurally dissimilar, ensuring that a screen of any kind is sampling a larger area of chemical space with little redundancy and thereby increasing its efficiency. The structural diversity and predicted bioactivity of the NCI diversity series make it an extremely attractive option for a wide variety of screening experiments (Jorissen and Gilson, 2005; Kau et al., 2003; Li et al., 2004).

A second reason for selecting the NCI diversity set II compound library (which was the latest edition available at the time of ordering), is that it is the direct sequel to that used in the Tomlinson *et al.*, (2009) screen. The NCI diversity set II library contains only 10% of those represented in the NCI diversity set I library. This enables a direct comparison between screens in terms of the percentage hit rate of phenotypes identified and may potentially further assess the applicability of the NCI diversity series towards such screens. Any compounds that may have generated phenotypes in the original screen that appear in the both libraries could also be used as a positive control to assess our capacity to identify presented phenotypes.

4.1.3 Screening of the NCI diversity set II compound library

One of the primary aims of this thesis is to further investigate the benefits of using the *X. laevis* model as a tool in drug discovery, to the benefit of both industry and prospective patients. To help determine this, my colleague Kim Hanson and I both screened the NCI Diversity set II compound library using the *X. laevis* model. Of the 1363 compounds screened, 72 gave rise to repeatable phenotypes that could be categorised as 'abnormal'. Many of the identified

phenotypes were involved in pigment loss, reduction or abnormal migration or melanophore morphology. It was previously observed that phenotypes such as these may be indicative of compounds with the potential to inhibit melanoma growth (Tomlinson et al., 2009b; White et al., 2011). To further investigate this potential, all 72 compounds were subjected to cell viability assays in which their ability to reduce the A375 melanoma cell line cell viability was observed in relation to two non-melanoma cell line controls (HEK293 and RD1). Of the 72 compounds screened, for 13 compounds the IC50s of the A375 melanoma cell line were shown to be statistically significantly reduced when compared to the IC50s of their respective HEK293 and RD1 controls. The selective nature of these compounds against the A375 cell line, combined with the structural diversity inherent in the NCI diversity set II library suggests that each of these 13 compounds may lead to novel targets for the treatment of melanoma or indeed be used as novel drugs themselves. This simple yet effective chemical genetic screening method once again highlights the benefits of using the *X. laevis* model. It also displays how (in conjunction with carefully chosen relevant assays) *X. laevis* chemical genetic screening assay can be used to rapidly generate promising lead compounds for the treatment of melanoma, thereby emphasising their potential towards improving drug discovery.

4.2 Results

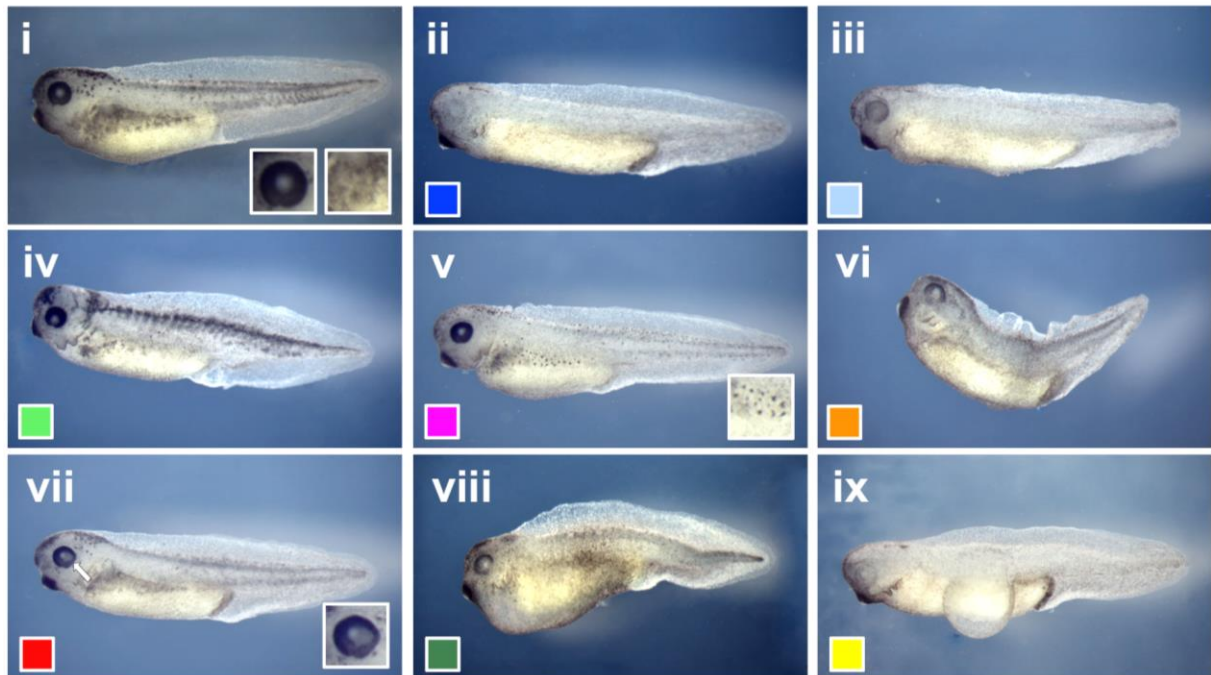
4.2.1 Phenotype scoring

This screen was primarily focused upon identifying phenotypes involving abnormal pigmentation defects (total or partial loss of pigmentation and/or abnormal melanophore migration or morphology). It also permitted easy

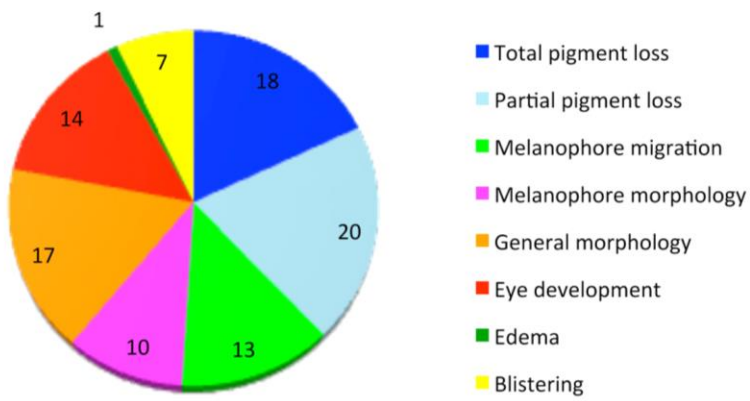
visualisation of other areas of *X. laevis* development, such as abnormal eye development, abnormal general morphology, edema and blistering (summarised in **Figure 26 A**). The criteria by which these phenotypic categories were defined is outlined below.

All compounds were screened at both 20 μ M and 40 μ M in 96 well plates and embryos were screened by eye for abnormal phenotypes at stage 38 using a light microscope. Each well consisted of 5 embryos, 80% of which must present a similar phenotype to be considered a phenotypic hit. To limit experimenter bias, all plates were screened blind by both my colleague Kim Hanson and myself. Many of the compounds elicited phenotypes that might fall into two or three separate categories (i.e. total pigmentation loss and abnormal morphology). During individual scoring of the plates we ranked the prominence of the phenotype observed on a scale of 1-3 (1 being clearly prominent, 3 implying a subtle effect). In cases where two phenotypic categories might be apparent for the same embryo, a consensus was reached based on the ranking of phenotypic prominence given by each experimenter. All identified hit compounds were repeated in larger volume (1ml) with a higher sample number (n=10 per well) and screened according to the same criteria outlined above to ensure they could be replicated. All hit compounds subsequently identified were then subjected to a dose response screen across a range of doses (0.1, 1, 10, 25, 50, 75 and 100 μ M, 20 embryos per well 1 ml final volume) to evaluate the phenotypes over a range of concentrations.

A



B



C

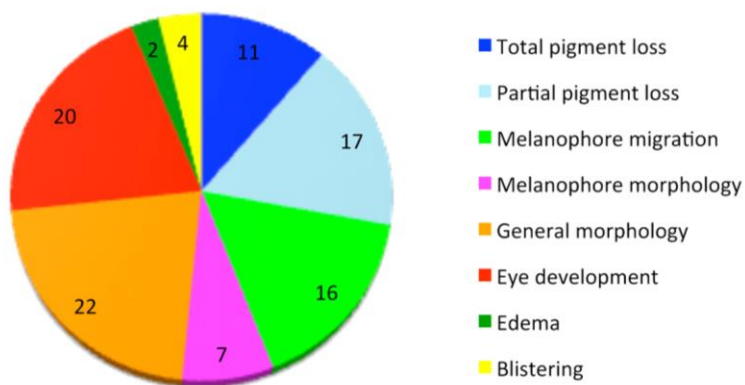


Figure 26. A. Example images for phenotypic categories to which identified phenotypes were allocated i. Vehicle DMSO control. ii. Total pigmentation loss. iii. Partial pigment loss. iv. Abnormal melanophore migration. v. Abnormal melanophore morphology. vi. Abnormal general morphology. vii. Abnormal eye development. viii. Edema. ix. Blistering. B. Chart displaying percentage of hit compounds allocated to each phenotypic category ($n = 72$). C. Chart displaying percentage of the total number of times a phenotype was identified ($n = 161$).

4.2.2 Summary of phenotypes observed from hit compounds identified in the NCI diversity set II X. laevis chemical genetic screen

The NCI diversity set II compound library was supplied as 100µl, 10mM stocks in 96 well plates that were transferred directly to the media upon plate set up. Phenotypes observed were broadly split into 8 phenotypic categories as summarised in **Figure 26 A ii** Total pigmentation loss (in which no or very little pigment is present in the entire embryo). iii. Partial pigment loss (in which obvious pigment loss has occurred (usually in the lateral and dorsal stripe) but some clearly remains (normally localised in the head and eye)). iv. Abnormal melanophore migration (in which melanocytes appear to present abnormal patterning (usually in the lateral and dorsal stripe)). v. Abnormal melanophore morphology (in which melanocytes fail to present the dendritic form that is consistent with healthy controls). vi. Abnormal general morphology (in which the embryo in any way appears to have a distinctive and consistent abnormal body shape or form not consistent with the corresponding control). vii. Abnormal eye development (in which the eye fails to form or where normal structures can be seen to have clear abnormal morphology). viii. Edema (in which the embryo presents an increase in fluid around the heart cavity). ix. Blistering (in which the embryo presents excessive fluid build-up beneath the skin that is irregularly located between samples subjected to the same conditions).

The total number of hit NCI compounds identified (n = 72) and the phenotypic class to which they were allocated (based on the strongest or most prominent phenotype presented) are represented in **Figure 26 B** Total and partial pigment loss account for 39% of all hit compounds identified, highlighting their prominence in this screen. Abnormal melanophore migration and melanophore

morphology phenotypes were also well represented (accounting for 13% and 10% of identified hits respectively), although they were less frequently observed than the total or partial pigment loss phenotypic categories. A high proportion of hits (17%) gave rise to phenotypes that could be characterised as having abnormal morphology. Similarly, abnormal eye development was also prominent and represented 14% of the hits. Both the blistering and edema phenotypic categories were less prominent, consisting of 7% and 1% of total hits identified respectively.

More often than not, embryos that presented a strong phenotype of any phenotypic class often possess attributes suggesting they could also belong to a second or third phenotypic category. For example **Figure 26 A ix** presents a clear blistering phenotype, however the embryo also significantly lacks pigmentation when compared to the vehicle control and therefore might also be considered to belong to the 'total pigmentation loss' phenotypic category. This is emphasised in **Figure 26 C** which represents the total number of compounds identified for each phenotypic category (irrespective of the strength of the phenotypes elicited) (n = 161). As such, an identified hit compound may well be represented more than once in this graph depending on the total number of phenotypes elicited in the embryo. For example, the blistering phenotype presented in **Figure 26 A ix** is represented here twice in both the blistering and total pigmentation loss phenotypic categories. In **Figure 26 C** the total and partial pigmentation represent only 28% of phenotypes identified, whereas abnormal morphology and eye development represent 42%. This reflects how despite often being only slight, abnormal morphology and abnormal eye development phenotypes were often present in embryos that were considered to have stronger alternative phenotypes (as demonstrated in the blistering example

exhibited in **Figure 26 A ix**). In total however, pigmentation phenotypes are still the dominantly observed phenotypic categories observed, with total and partial pigmentation loss combined with abnormal melanophore migration and morphology accounting for 51% of all phenotypes observed. Abnormal melanophore migration and morphology accounted for 23% of the total phenotypes identified. Both the edema and blistering phenotypes were still poorly represented, accounting for a total 6% of all phenotypes identified.

4.2.3 Summary of hit compounds identified in the NCI diversity set II X. laevis chemical genetic screen according to their allocated phenotypic categories

In total, the NCI diversity set II *X. laevis* chemical genetic screen was successful in identifying 72 compounds that gave rise to reproducible phenotypes. As outlined above previously, these phenotypes were broadly split into eight phenotypic categories. Those hit compounds that were categorised as presenting a phenotype consistent with total pigmentation loss are displayed in **Figure 27**. Of these compounds, NCI 9358, NCI 20618, NCI 20619, NCI 99657, NCI 99660, NCI 131982, NCI 131986, NCI 164965 and NCI 515893 **Figure 27 B, D-I, K and N**) all present a near total loss of pigmentation in the lateral and dorsal stripe as well as the head and eye when compared to their respective vehicle control. NCI 12588, NCI 135810, NCI 205913 and NCI 319034 (**Figure**



DMSO Control



NCI 12588 C7H14N2S MW: 158.26



NCI 20619 C13H14N4S MW: 258.34



NCI 99660 C14H21N5OS2 MW: 339.47



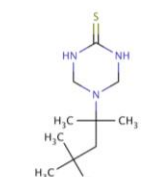
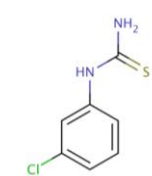
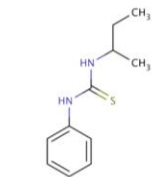
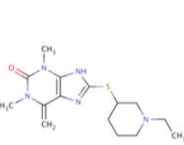
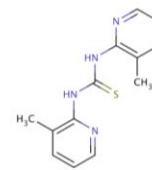
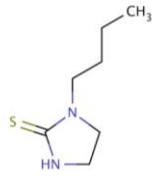
NCI 131986 C11H16N2S MW: 208.32



NCI 164965 C7H7ClN2S MW: 186.66



NCI 319034 C11H23N3S MW: 229.38



NCI 9358 C13H14N4 MW: 226.28



NCI20618 C13H14N4S MW: 258.34



NCI 99657 C13H19N5OS2 MW: 325.45



NCI 131982 C10H14N2S MW: 194.29



NCI 135810 C11H8N2S MW: 200.26



NCI 205913 C12H10N2O3S MW: 262.28



NCI 515893 C13H22N2S MW: 238.39

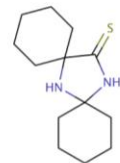
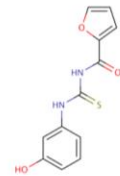
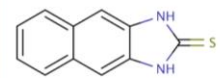
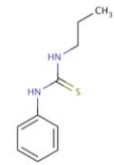
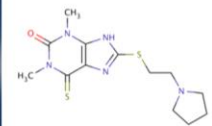
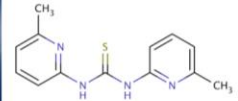
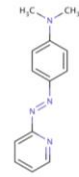


Figure 27. NCI compounds identified in the NCI diversity set II compound screen that gave rise to an abnormal pigmentation phenotype, in which no pigment is present in the whole embryo when assessed at stage 38 (when compared to the DMSO vehicle control). Phenotypes are shown alongside associated compound structure and chemical information (NCI ID, molecular formula and MW). Embryos shown were screened at 40 μ M. A. DMSO solvent control. B. NCI 9358. C. NCI 12588. D. NCI 20618. E. NCI 20619. F. NCI 99657. G. NCI 99660. H. NCI 131982. I. NCI 131986. J. NCI 135810. K. NCI 164965. L. NCI 205913. M. NCI 319034. N. NCI 515893. MW; Molecular weight.

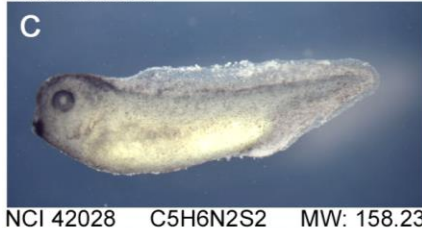
27 C, J, L and M) also show this phenotype however a very small amount of pigment remains in either the head or eye. Embryos determined to present a phenotype consistent with the partial loss of pigmentation phenotype were placed in the total loss of pigmentation phenotypic category as the amount of pigmentation remaining is relatively marginal.

Compounds categorised as presenting a phenotype consistent with partial pigmentation loss are displayed in **Figure 28**. NCI 30712, NCI 42028, NCI 45536, NCI 45545, NCI 59620, NCI 62609, NCI 62611, NCI 87084, NCI 104993, NCI 106581, NCI 111848, NCI 117741, NCI 153792, NCI 154718 and NCI 319471 all show a significant loss of pigmentation in either the lateral or dorsal stripe (or both), whilst still possessing pigmentation in the head and/or eye (**Figure 28 B-P**). Interestingly, NCI 30712 and NCI 45536 appear to also possess abnormal eye development phenotypes in which structures of the eye are consistent with anophthalmia. NCI 104993 and NCI 154718 also display slight abnormal eye development as presented by a partial lack of pigmentation in the eye which may suggest a disruption to the retinal pigment epithelial layer. Finally, NCI 319471 presents a slight abnormal eye phenotype in which the eye appears bigger when compared to the control, indicating myopia.

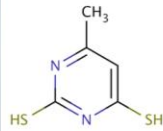
In total, seven hit compounds were categorised as presenting abnormal melanophore morphology in Stage 38 embryos (**Figure 29**). NCI4292, NCI 117987, NCI 133002, NCI 204262 and NCI 275971 (**Figure 29 B, D-E, G and H**), All possess melanocytes in the lateral stripe which appear round and compacted in morphology when compared to the dendritic shape exhibited in their relevant vehicle controls. NCI 34871 and NCI 138398 (**Figure 29 C and F**) present melanocytes which appear enlarged and disorganised when compared



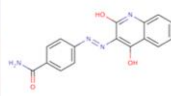
DMSO Control



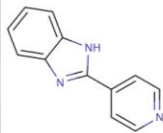
NCI 42028 C5H6N2S2 MW: 158.23



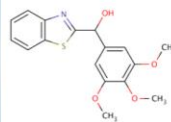
NCI 45545 C16H12N4O3 MW: 308.30



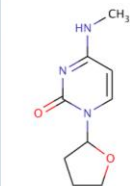
NCI 62609 C12H9N3 MW: 195.22



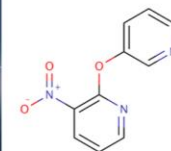
NCI 87084 C17H17NO4S MW: 331.39



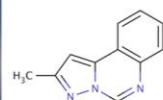
NCI 106581 C9H13N3O2 MW: 195.22



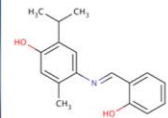
NCI 117741 C10H7N3O3 MW: 217.18



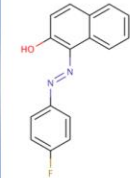
NCI 154718 C11H9N3 MW: 183.21



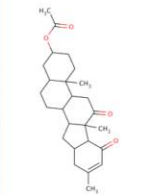
NCI 30712 C17H19NO2 MW: 269.34



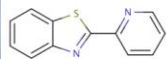
NCI 45536 C16H11FN2O MW: 266.27



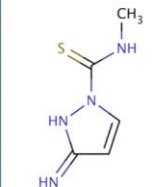
NCI 59620 C26H36O4 MW: 412.57



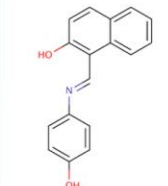
NCI 62611 C12H8N2S MW: 212.27



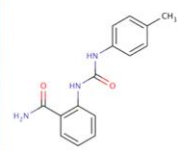
NCI 104993 C4H7N5S MW: 157.19



NCI 111848 C17H13NO2 MW: 263.30



NCI 153792 C15H15N3O2 MW: 269.30



NCI 319471 C12H16N2O2S MW: 252.33

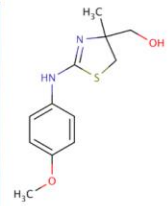


Figure 28. NCI compounds identified in the NCI diversity set II compound screen that gave rise to a partial abnormal pigmentation phenotype, in which patches of normal pigmentation were either absent or not prominent when assessed at stage 38 (when compared to the DMSO vehicle control). Phenotypes are shown alongside associated compound structure and chemical information (NCI ID, molecular formula and MW). Embryos shown were screened at 40 μ M. A. DMSO solvent control. B. NCI 30712. C. NCI 42028. D. NCI 45536. E. NCI 45545. F. NCI 59620. G. NCI 62609. H. NCI 62611. I. NCI 87084. J. NCI 104993. K. NCI 106581. L. NCI 111848. M. NCI 117741. N. NCI 153792. O. NCI 154718. P. NCI 319471. MW; Molecular weight.



DMSO Control



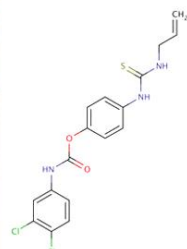
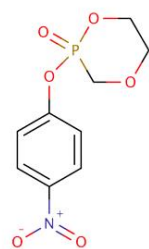
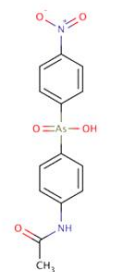
NCI 34871 C₁₄H₁₃AsN₂O₅ MW: 364.18



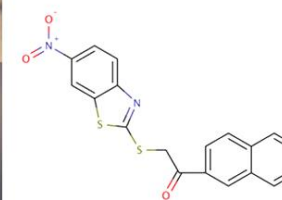
NCI 133002 C₉H₁₀NO₆P MW: 259.15



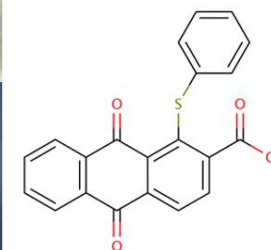
NCI 204262 C₁₇H₁₅Cl₂N₃O₂S MW: 396.29



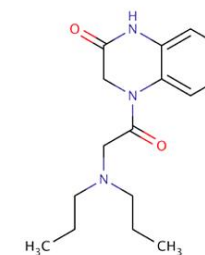
NCI 4292 C₁₉H₁₂N₂O₃S₂ MW: 380.44



NCI 117987 C₂₁H₁₂O₄S MW: 360.38



NCI 138398 C₁₆H₂₃N₃O₂ MW: 289.38



NCI 275971 C₁₆H₁₃ClN₂O₂S₂ MW: 364.86

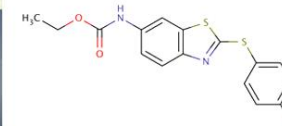


Figure 29. NCI compounds identified in the NCI diversity set II compound screen that gave rise to a prominent abnormal melanophore morphology phenotype when assessed at stage 38 (when compared to the DMSO vehicle control). Phenotypes are shown alongside associated compound structure and chemical information (NCI ID, molecular formula and MW). Embryos shown were screened at 40 μ M. A. DMSO solvent control. B. NCI 4292. C. NCI 34871. D. NCI 117987. E. NCI 133002. F. NCI 138398. G. NCI 204262. H. NCI 275971. MW; Molecular weight.

to the DMSO control. NCI 34871 and NCI 204262 appear to also present an abnormal eye development phenotype in which a distinct patch of pigmentation appears to be missing from the retinal epithelial layer. In addition, NCI 275971 also appears to present abnormal eye development in the form of a smaller eye than that of the vehicle control, suggesting microphthalmia.

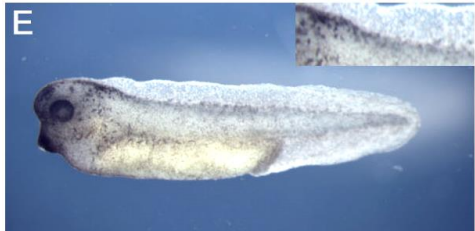
Of the 72 hit compounds identified, nine were categorised as presenting a phenotype constituent with abnormal melanophore migration (**Figure 30**). Of these compounds NCI 11624 and NCI 13156 (**Figure 30 B and C**) presented phenotypes in which the melanocytes appeared to be abnormally patterned in both the dorsal and lateral stripe (See **Figure 12**). In NCI 11624 the phenotype is slight but consistent between samples. NCI 13156 by far presents the most prominent example of abnormal melanophore migration whereby abnormal patterning down the lateral stripe can clearly be observed when compared to the vehicle control. It is also notable that melanocytes do not appear to be able to migrate down to the lateral stripe region suggesting this compound has severely interrupted normal melanocyte migration. NCI 13653, NCI 125197 and NCI 139021 all present abnormal melanophore migration phenotypes in which the condition is most prominent in the lateral stripe. In each example melanophores appear to have failed to migrate successfully in this specific region whereas the dorsal stripe remains relatively normal when compared to the vehicle control. In contrast however NCI 36525, NCI 92794, NCI 150982 and NCI 246415 (**Figure 30 E, F, I and J**) present abnormal melanophore migration phenotypes that appear primarily localised to the lateral stripe, whereas the dorsal stripe appears to be relatively normal. NCI 246415 appears to present several other phenotypes, with the relative lack of pigment in the head and eye indicative of



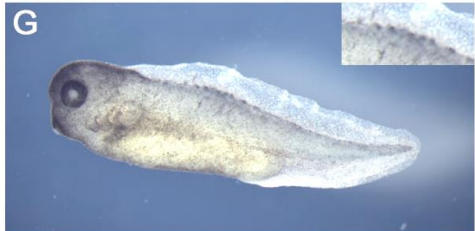
DMSO Control



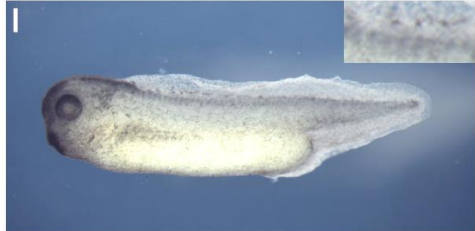
NCI 13156 C₁₅H₁₄N₄O₂S MW: 314.36



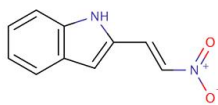
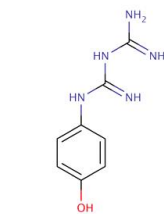
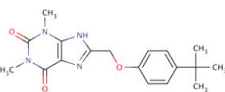
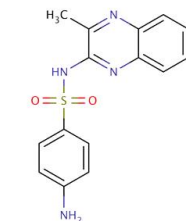
NCI 36525 C₁₈H₂₂N₄O₃ MW: 342.39



NCI 125197 C₈H₁₁N₅O MW: 193.21



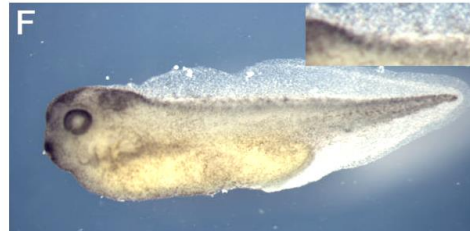
NCI 150982 C₁₀H₈N₂O₂ MW: 188.19



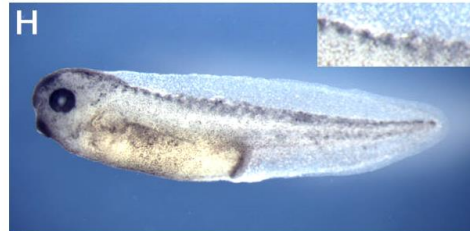
NCI 11624 C₁₂H₉CIN₄S MW: 276.74



NCI 13653 C₁₂H₁₀O₄ MW: 218.2086



NCI 92794 C₁₂H₁₁N₃O₃ MW: 245.24



NCI 139021 C₁₃H₉N₃O₃ MW: 255.29



NCI 246415 C₁₁H₈N₂S MW: 200.26

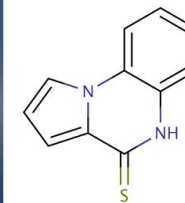
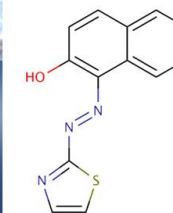
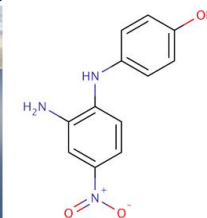
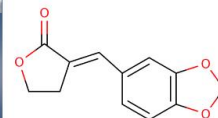
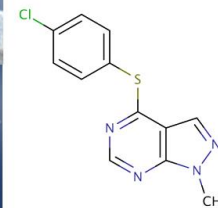


Figure 30. *NCI compounds identified in the NCI diversity set II compound screen that gave rise to a prominent abnormal melanophore migration phenotype, in which melanocytes have not progressed normally down either the lateral and/or dorsal stripe when assessed at stage 38 (when compared to the DMSO vehicle control). Phenotypes are shown alongside associated compound structure and chemical information (NCI ID, molecular formula and MW). Embryos shown were screened at 40 μ M. A. DMSO solvent control. B. NCI 11624. C. NCI 13156. D. NCI 13653. E. NCI 36525. F. NCI 92794. G. NCI 125197. H. NCI 139021. I. NCI150982. J. NCI246415. MW; Molecular weight.*

total pigment loss and the rounded morphology of the melanocytes present in the lateral stripe being consistent with abnormal melanophore morphology.

Only NCI 205832 presented a phenotype consistent with the edema phenotypic category (**Figure 31 B**). Five compounds in the form of NCI 14380, NCI 68971, NCI 246415, NCI 308847 and NCI 343557 (**Figure 32 B-F**), gave rise to phenotypes consistent with the blistering phenotypic category. NCI 14380 and NCI 343557 also gave rise to a stunted abnormal morphology phenotype, whereas NCI 246415 also gave rise to a phenotype consistent with that observed with a total loss of pigmentation.

Of the 72 hit compounds identified, 12 gave rise to a phenotype that could be considered to be abnormal morphology (**Figure 33**). NCI 21683, NCI 30390, NCI 31762, NCI 43013, NCI 79253, NCI 85326, NCI 88916, NCI 151262, NCI 377384, NCI 402590, NCI 645987 and NCI 667251 (**Figure 33 B-M**), all gave rise to phenotypes that presented consistent abnormal morphology when compared to the vehicle control. Of these compounds all generated an additional phenotype that could be attributed to either total or partial loss of pigmentation, with the exception of NCI 31762. NCI 21683, NCI 30390, NCI 79253, NCI 151262, NCI 377384, NCI 402590, NCI 645987 and NCI 667251 all additionally presented abnormal eye development phenotypes in the form of anophthalmia. NCI 31762, NCI 43013, NCI 85326 and NCI 88916 also present abnormal eye phenotypes that suggest abnormal development of the retinal pigment epithelial layer.

Of those NCI hit compounds identified 10 were recognised as giving an abnormal eye development phenotype (**Figure 34**). Of these compounds, NCI



DMSO Control



NCI 205832 C₁₈H₂₀ClNO₄ MW: 349.81

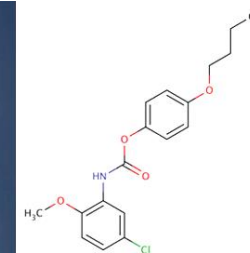


Figure 31. NCI compounds identified in the NCI diversity set II compound screen that gave rise to a prominent edema phenotype when assessed at stage 38 (when compared to the DMSO vehicle control). Phenotypes are shown alongside associated compound structure and chemical information (NCI ID, molecular formula and MW). Embryos shown were screened at 40 μ M. A. DMSO solvent control. B. NCI 205832. MW; Molecular weight.



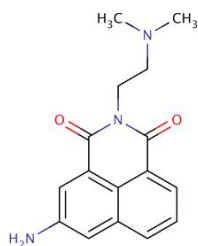
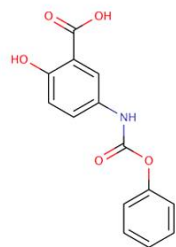
DMSO Control



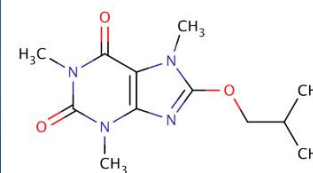
NCI 68971 C₁₄H₁₁NO₅ MW: 273.24



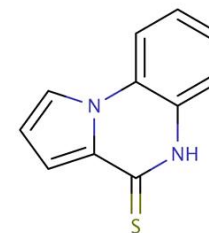
NCI 308847 C₁₆H₁₇N₃O₂ MW: 283.33



NCI 14380 C₁₂H₁₈N₄ MW: 266.29



NCI 246415 C₁₁H₈N₂S MW: 200.25



NCI 343557 C₁₃H₁₀Cl₂N₂O MW: 281.14

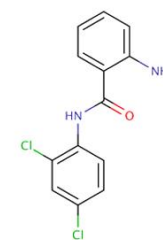


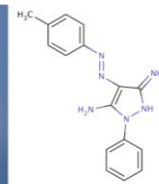
Figure 32. NCI compounds identified in the NCI diversity set II compound screen that gave rise to a prominent blistering phenotype when assessed at stage 38 (when compared to the DMSO vehicle control). Phenotypes are shown alongside associated compound structure and chemical information (NCI ID, molecular formula and MW). Embryos shown were screened at 40 μ M. A. DMSO solvent control. B. NCI 14380. C. NCI 68971. D. NCI 246415. E. NCI 308847. F. NCI 343557. MW; Molecular weight.



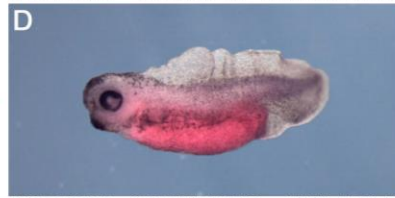
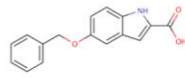
DMSO Control



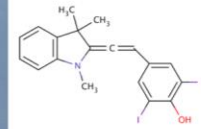
NCI 21683 C16H16N6 MW: 292.3426



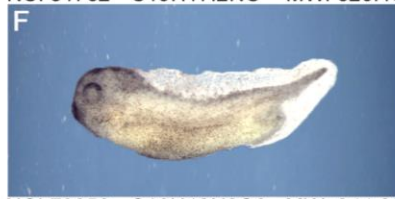
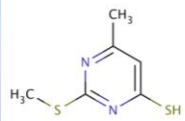
NCI 30930 C16H13NO3 MW: 267.28



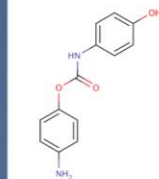
NCI 31762 C19H17I2NO MW: 529.16



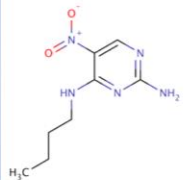
NCI 43013 C6H8N2S2 MW: 172.26



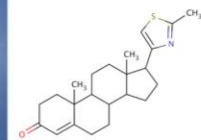
NCI 79253 C13H12N2O3 MW: 244.25



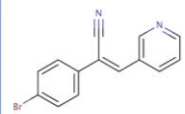
NCI 85326 C8H13N5O2 MW: 211.22



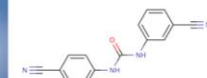
NCI 88916 C23H31NOS MW: 369.56



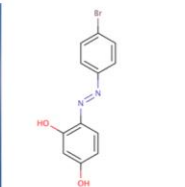
NCI 151262 C14H9BrN2 MW: 285.14



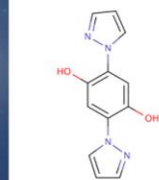
NCI 377384 C15H10N4O MW: 262.27



NCI 402590 C12H9BrN2O2 MW: 293.12



NCI 645987 C12H10N4O2 MW: 242.24



NCI 667251 C17H16N2 MW: 248.33

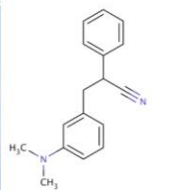


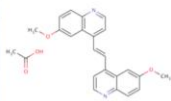
Figure 33. *NCI compounds identified in the NCI diversity set II compound screen that gave rise to a prominent abnormal morphological phenotype when assessed at stage 38 (when compared to the DMSO vehicle control). Phenotypes are shown alongside associated compound structure and chemical information (NCI ID, molecular formula and MW). Embryos shown were screened at 40µM. A. DMSO solvent control. B. NCI 21683. C. NCI 30390. D. NCI 31762. E. NCI 43013. F. NCI 79253. G. NCI 85326. H. NCI 88916. I. NCI 151262. J. NCI 377384. K. NCI 402590. L. NCI 645987. M. NCI 667251. MW; Molecular weight.*



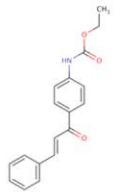
DMSO Control



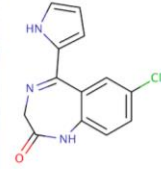
NCI 5907 C₂₄H₂₂N₂O₄ MW: 402.45



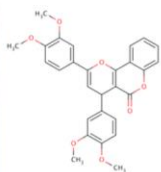
NCI 31703 C₁₈H₁₇NO₃ MW: 295.33



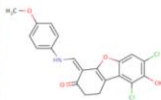
NCI 66020 C₁₃H₁₀ClN₃O MW: 259.69



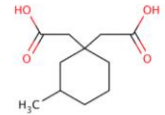
NCI 211490 C₂₈H₂₄O₇ MW: 472.49



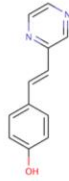
NCI 378719 C₂₀H₁₅Cl₂NO₄ MW: 404.25



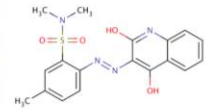
NCI 3001 C₁₁H₁₈O₄ MW: 214.26



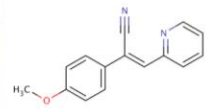
NCI 19219 C₁₂H₁₀N₂O MW: 198.22



NCI 45572 C₁₈H₁₈N₄O₄S MW: 386.42



NCI 130872 C₁₅H₁₂N₂O MW: 236.27



NCI 340852 C₂₈H₂₆ClN₃O MW: 455.99

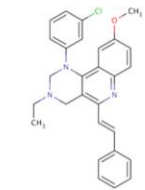


Figure 34. NCI compounds identified in the NCI diversity set II compound screen that gave rise to a prominent abnormal eye phenotype when assessed at stage 38 (when compared to the DMSO vehicle control). Phenotypes are shown alongside associated compound structure and chemical information (NCI ID, molecular formula and MW). Embryos shown were screened at 40 μ M. A. DMSO solvent control. B. NCI 3001. C. NCI 5907. D. NCI 19219. E. NCI 31703. F. NCI 45572. G. NCI 66020. H. NCI 130872. I. NCI 211490. J. NCI 340852. K. NCI 378719. MW; Molecular weight.

5907, NCI 19219, NCI 45572, NCI 66020, NCI 130872, NCI 211490, NCI 340852 and NCI 378719 (**Figure 34 C-D and F-K**) gave rise to abnormal eye development phenotypes that suggested abnormal development of the retinal pigment epithelial layer. NCI 3001 (**Figure 34 B**) appears to present a phenotype in which the lens is dislocated from its normal position, whereas NCI 31703 displays an eye phenotype in which the eye morphology is misshapen and larger than its vehicle control counterpart, possibly consistent with myopia. NCI 19219, NCI 31703 and NCI 340852 also present phenotypes consistent with that described for total or partial loss of pigmentation. NCI 340852 also appears to be exhibiting an abnormal morphology phenotype. NCI 130872 exhibits a slight abnormal melanophore migration phenotype in which melanophores do not appear to have migrated successfully along the lateral and dorsal stripe.

To further characterise the 72 phenotypes established, each compound was subject to a dose response assay (0.1, 1, 10, 25, 50, 75 and 100µM, 1ml final volume 20 embryos per well). **Table 8** provides an example of two compounds in which the phenotype that was previously recorded was replicated. For example NCI 4292 was recorded as producing a melanophore morphology phenotype which was replicated at high doses but appeared to not be apparent around lower concentrations. NCI 12588 also appears to replicate the described phenotype of abnormal pigmentation, whilst at lower concentration this phenotype is lost. Interestingly, there appears to be a transition period at 25 – 10µM in which the pigmentation loss phenotype is lost and an abnormal melanophore morphology/abnormal melanophore migration phenotype is presented. This may suggest in some cases at lower concentrations that those compounds that give rise to a total or partial loss of pigmentation may transitio

Table 8. Collated dose response data in which embryos were exposed to hit compounds identified over a range of concentrations. 20 embryos were initially plated in each well. Percentage of embryos that showed a prominent phenotype at each concentration are displayed as a percentage of total embryos alive when assessed at stage 38 (1 = 100%). B, (blistering). E, (Edema). ED, (eye development). P, (abnormal pigmentation). M, (abnormal morphology). Mg, (Abnormal melanophore migration). MM, (abnormal melanophore morphology). PD, (Percentage death). S, (stunted growth).

	Conc (μ M)	M	S	P	MM	MG	E	ED	B	PD
NCI 4292	0.1	0	0	0	0	0	0	0	0	0
	1	0	0	0	0	0	0	0	0	0
	10	0	0	0	1	0	0	0	0	0
	25	0	0	0	1	0	0	0	0	0
	50	0	0	0	1	0	0	0	0	0
	100	0	0	0	1	0	0	0	0	0
NCI 12588	0.1	0	0	0	0	0	0	0	0	0
	1	0	0	0	0	0	0	0	0	0
	10	0	0	0	0	1	0	0	0	0
	25	0	0	1	1	0	0	0	0	0
	50	0	0	1	0	0	0	0	0	0
	100	0	0	1	0	0	0	0	0	0

into other pigment related phenotypes as part of a spectrum. The majority of compounds however showed a consistent phenotype across the range of doses. A complete list of dose response results can be found in Appendix II.

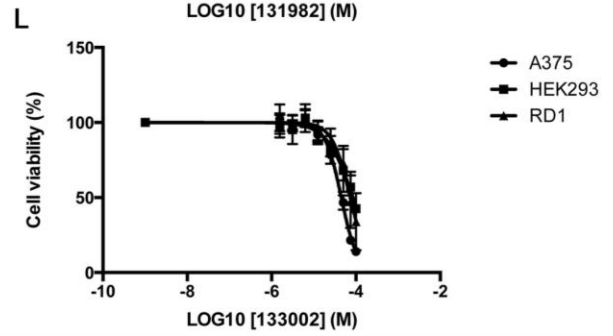
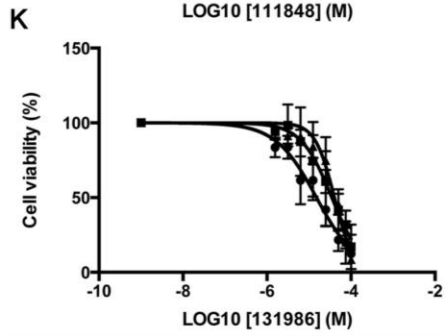
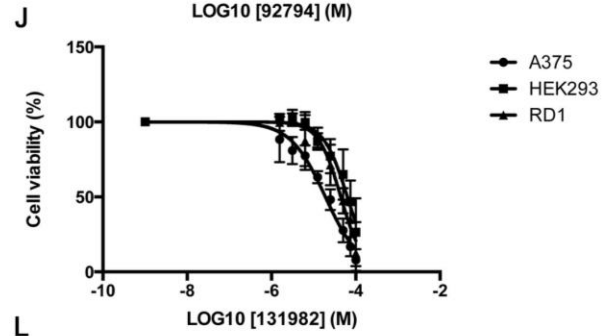
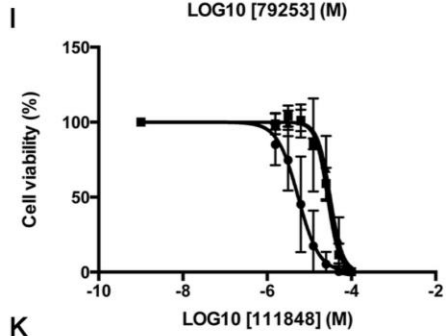
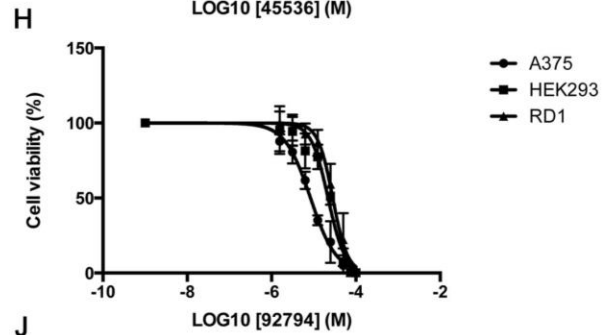
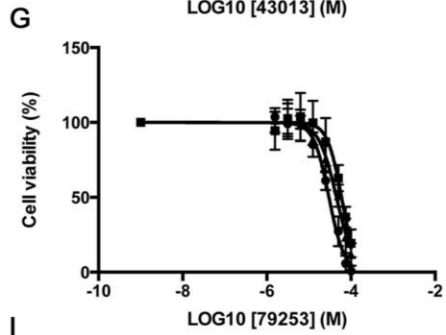
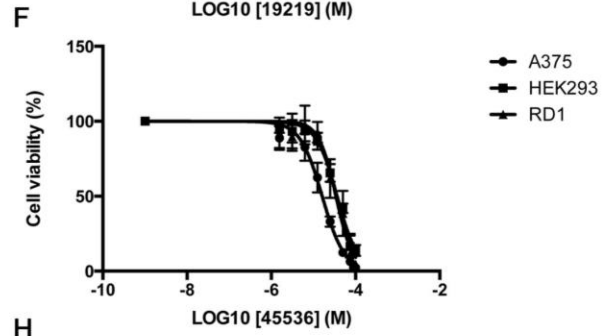
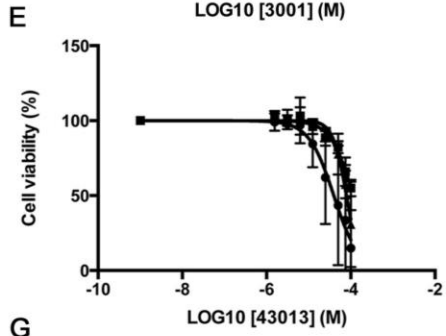
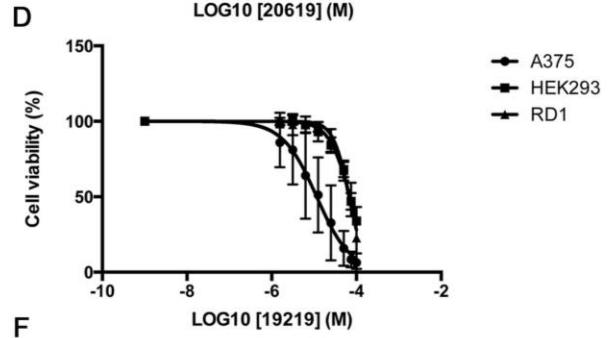
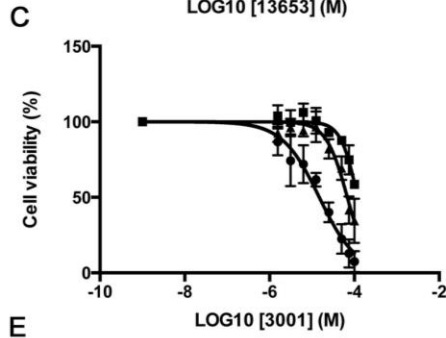
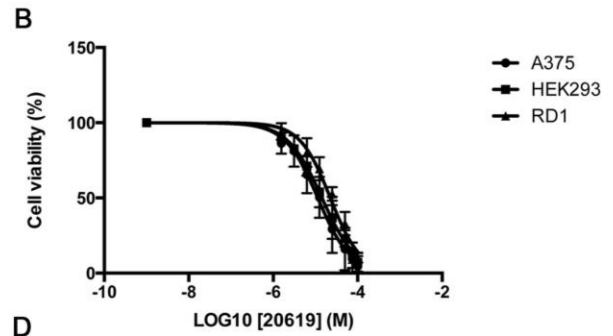
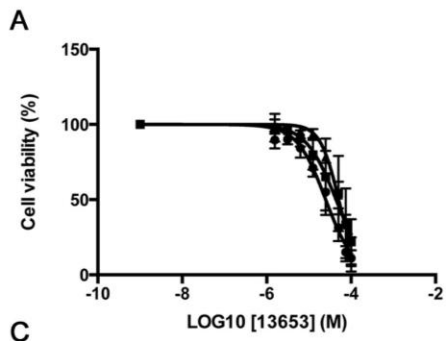
4.2.4 Melanoma cell viability screen in response to the 72 identified hit NCI diversity set II compounds

To identify those compounds with potential therapeutic applications towards the treatment of melanoma, the 72 hit compounds identified in the NCI diversity set II compound screen were subjected to cell viability screening using the A375 melanoma cell line and the HEK293 and RD1 non-melanoma control cell lines. Of the 72 hit compounds screened, preliminary experiments found that 40 compounds did not decrease A375 cell viability at 100µM and were subsequently disregarded (data not shown). The remaining 32 compounds which did preliminarily reduce A375 cell viability were screened 3 times each over a range of concentrations (from 1.56E-06 to 1.00E-04 M) on the A375, HEK293 and RD1 cell lines. The resultant data was used to generate growth inhibitory IC50s to compare the relevant ability of each NCI hit compound to reduce A375 cell viability in relation to the respective HEK293 and RD1 control. Of the 32 compounds screened, 13 gave rise to IC50s in the A375 cell lines that were statistically significantly lower than that displayed in their respective HEK293 and RD1 controls (**Table 9**). **Figure 35** displays dose response graphs in which the cell viability of the A375, HEK293 and RD1 cell line is displayed against an increasing concentration of each compound. NCI 13653 and NCI 20619 (**Figure 35 A and B**) are presented as examples of those compounds that did not give rise to IC50s that were statistically significantly lower in the A375 cell lines when compared to their respective HEK293 and RD1 controls.

Table 9. IC50s generated screening NCI hit compounds on the A375, HEK293 and RD1 cell lines. Highlighted cells indicate those compounds which gave rise to IC50s in the A375 melanoma lines that were statistically significantly lower than that produced when screened on the HEK293 and RD1 control.

NCI Compound	A375	HEK293	RD1
3001	1.487E-05	1.191E-04	6.828E-05
13653	2.504E-05	4.397E-05	5.074E-05
19219	1.152E-05	7.070E-05	6.685E-05
20619	1.137E-05	1.429E-05	2.258E-05
30712	4.397E-06	3.311E-06	9.185E-06
34871	2.724E-05	1.916E-05	1.081E-05
36525	9.710E-06	6.538E-06	2.646E-05
43013	3.947E-05	1.146E-04	7.887E-05
45536	1.616E-05	3.640E-05	3.423E-05
59620	3.975E-05	1.273E-05	2.881E-05
79253	2.996E-05	5.976E-05	4.509E-05
87084	1.115E-05	1.105E-05	2.895E-05
88916	3.630E-06	2.764E-06	1.248E-05
92794	8.391E-06	2.190E-05	2.829E-05
99660	4.357E-05	6.735E-05	3.860E-05
111848	5.431E-06	2.706E-05	3.128E-05
117987	1.911E-05	2.395E-05	1.703E-05
125197	7.423E-05	1.244E-04	7.737E-05
130872	2.788E-05	2.199E-05	3.402E-05

131982	1.904E-05	6.320E-05	4.424E-05
131986	1.505E-05	3.494E-05	4.020E-05
133002	4.502E-05	8.511E-05	7.336E-05
138398	2.738E-05	1.029E-04	8.174E-05
151262	2.340E-05	1.591E-05	3.512E-05
153792	2.365E-05	6.322E-05	6.194E-05
205832	1.533E-05	4.757E-05	2.506E-05
205913	3.791E-05	5.273E-05	5.731E-05
246415	2.588E-05	6.767E-05	3.826E-05
275971	4.539E-06	1.920E-05	7.897E-06
319471	2.958E-05	6.924E-05	6.866E-05
343557	1.855E-05	1.753E-05	2.952E-05
378719	3.652E-06	~1.238e-005	1.012E-05



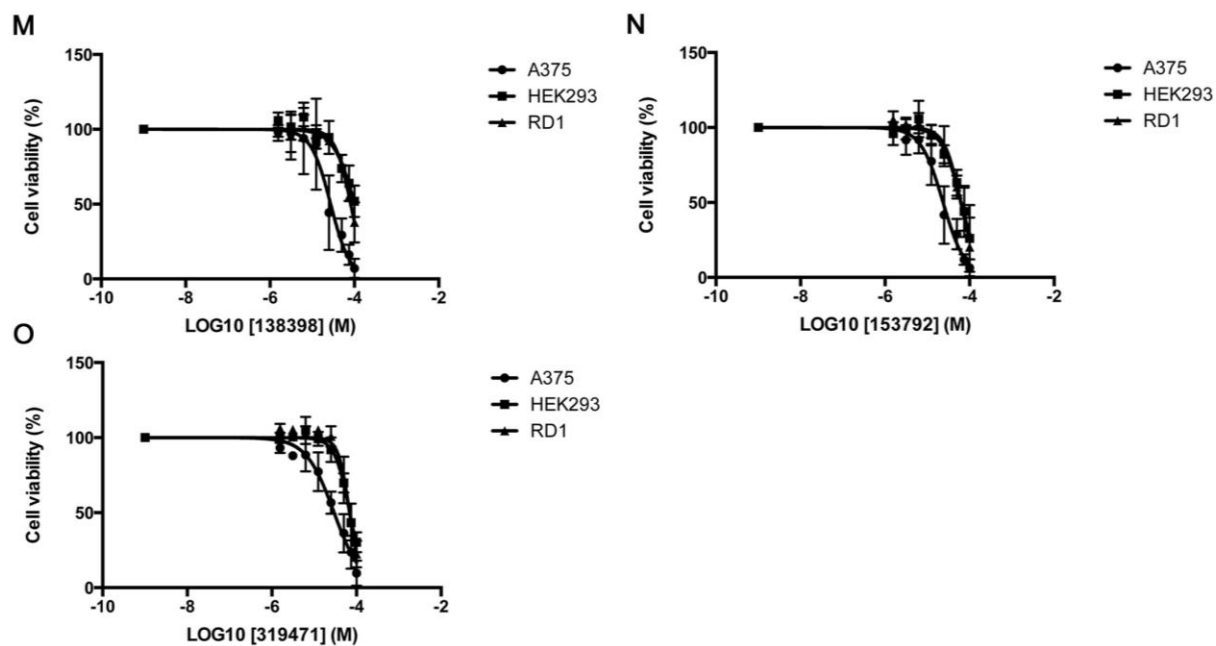
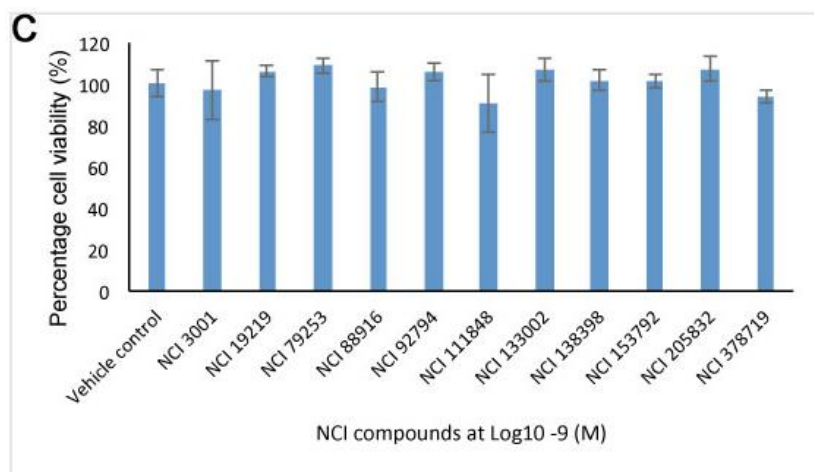
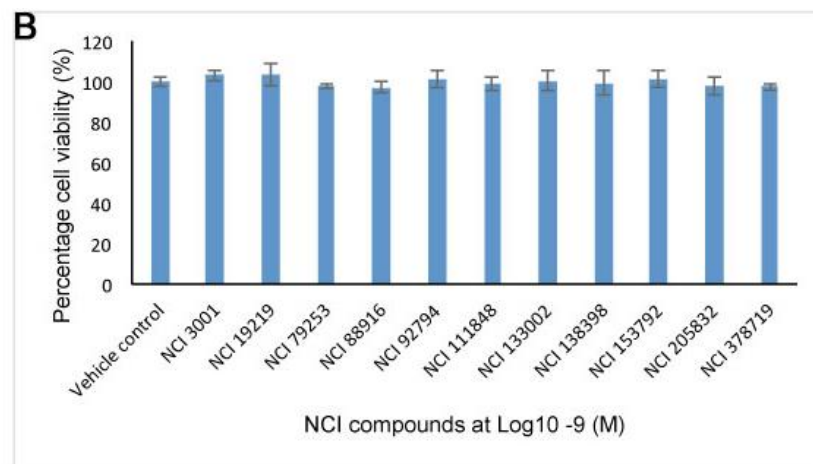
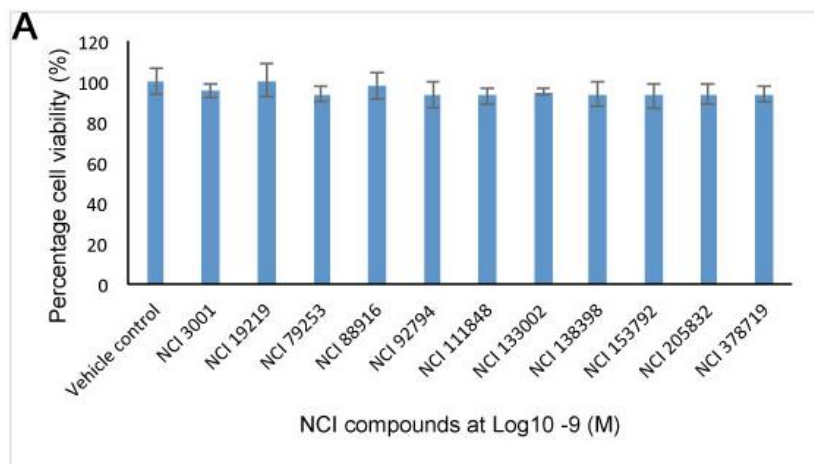


Figure 35. Dose response graphs displaying cell viability (%) of A375, HEK293 and RD1 cell lines in response to the designated NCI compound over an increasing concentration range (LOG10 M). Error bars represent standard error (n=3). All graphs shown (with the exception of NCI 13653 and NCI 20619 gave rise to IC50s in the A375 cell line which were statistically different to those obtained in both corresponding HEK293 and RD1 control cell lines. A. NCI 13653. B. NCI 20619. C. NCI 3001. D. NCI 19219. E. NCI 43013. F. NCI 45536. G. NCI 79253. H. NCI 92794. I. NCI 111848. J. NCI 131982. K. NCI 131986. L. NCI 133002. M. NCI 138398. N. NCI 153792. O. NCI 319471.

The remaining compounds (NCI 3001, NCI 19219, NCI 43013, NCI 45536, NCI 79253, NCI 92794, NCI 111848, NCI 131982, NCI 131986, NCI 133002, NCI 138398, NCI 153792 and NCI 319471 (**Figure 35 C-O**)), all presented IC50s that were statistically significantly lower in the A375 cell lines when compared to their respective HEK293 and RD1 controls. A complete figure summarising compiled dose response cell viability data for all 32 screened hit compounds can be found in Appendix III.

When the cell viability data was originally generated, we did not include a very low dose control. This made graphs difficult to interpret as in some cases it was hard to determine where the top of the graph plateaued, which also complicated IC50 generation. To correct for this a subset of the compounds assayed were rescreened at 1×10^{-9} M in the A375, HEK293 and RD1 cell lines to compare the cell viabilities detected between the 1×10^{-9} treated sample and the vehicle controls (**Figure 36**). For all compounds across all three cell lines the 1×10^{-9} treated samples were shown via T-test to have no significant difference in cell viability when compared to their respective vehicle control. As such a 1×10^{-9} data point was included on each graph (as shown in **Figure 35**) to aid in the interpretation of the data and IC50 generation.

It was not possible to calculate statistical differences between IC50s generated in the compiled graphs displayed in **Figure 35**. This is because for each cell viability assay, each concentration contained three replicates within each plate that were averaged when normalised to the in plate vehicle control (to calculate percentage cell viability). Each data point of the dose response compiled graphs shown in **Figure 35** is representative of three separate experimental repeats

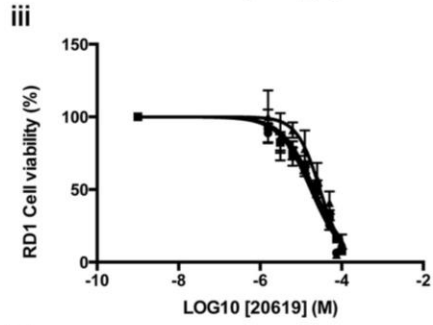
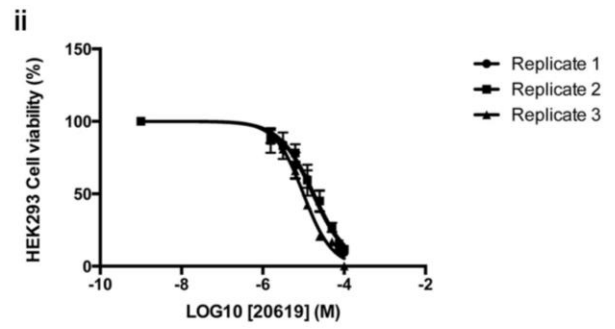
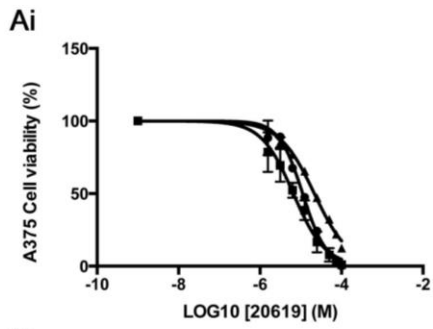


D

	p-value		
	A375	HEK293	RD1
NCI 3001	0.16	0.07	0.64
NCI 19219	0.89	0.22	0.06
NCI 79253	0.09	0.10	0.02
NCI 88916	0.57	0.10	0.68
NCI 92794	0.12	0.60	0.09
NCI 111848	0.06	0.45	0.18
NCI 133002	0.08	0.85	0.07
NCI 138398	0.11	0.75	0.56
NCI 153792	0.08	0.50	0.58
NCI 205832	0.08	0.32	0.08
NCI 378719	0.06	0.08	0.07

Figure 36. Summary of statistical difference of 11 hit NCI compounds cell viability when screened at \log_{10}^{-9} M using the A375, HEK293 and RD1 cell lines to their respective in plate vehicle DMSO controls. A. Percentage A375 cell viability of hit NCI compounds when compared to their respective vehicle DMSO control ($n = 6$). B. Percentage HEK293 cell viability of hit NCI compounds when compared to their respective vehicle DMSO control ($n = 6$). C. Percentage RD1 cell viability of hit NCI compounds when compared to their respective vehicle DMSO control ($n = 6$). D. Statistical student T-test comparison of each NCI compound towards its in plate vehicle DMSO control ($p = \leq 0.05$).

(each replicate having already been averaged to generate percentage cell viability). It is not possible to statistically analyse data that has been averaged twice and therefore the IC50s generated using these compiled graphs is not appropriate for this application. Instead it was necessary to generate IC50s for each of the cell line replicates (n=3) for each compound, which would enable the statistical comparison of each cell lines IC50s via T-test (**Figure 37**). For example **Figure 37 C** displays three dose response graphs for NCI 43013, each one representing each of the three replicates for each of the three cell lines screened (**Figure 37 C i, ii and iii**). For each replicate for each cell line, individual IC50s were generated (**Figure 37 C iv**). Using a student T-test it was then possible to statistically compare the IC50 values of each of the three replicates between two different cell lines (**Figure 37 C v**). In **Figure 37 C v** for example, the t-test p-value when comparing the A375 and HEK293 is 0.007, therefore stating the IC50s between these lines are statistically significantly different (this is also true when comparing the A375 and RD1 cell lines IC50s for this compound). Based on the previously obtained IC50s in the compiled graph (in which the A375 IC50 is lower than that of the HEK293 and RD1 IC50s), this data therefore states that the hit compound NCI 43013 generates an IC50 in the A375 cell line that is statistically significantly lower than that obtained in either the HEK293 or RD1 control cell line. Also included in this **Figure 37** is an example of a compound (NCI 20619) which did not give rise to a significant difference in the IC50 between the A375 cell line and either the HEK293 or RD1 cell line (**Figure 37 A**). Another example is provided for NCI 36525 in which the IC50 between the A375 cell line and either the HEK293 cell line was not significantly different, but was between the A375 and RD1 cell lines (**Figure 37**

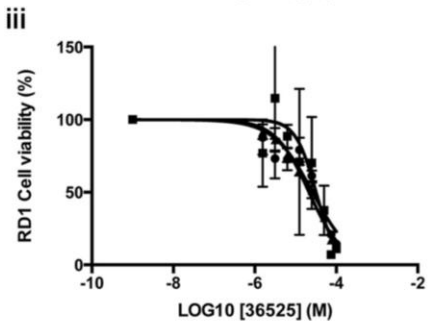
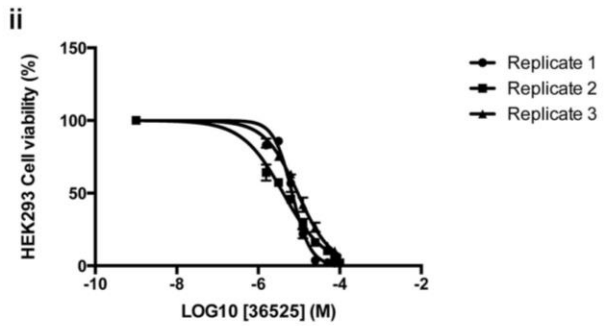
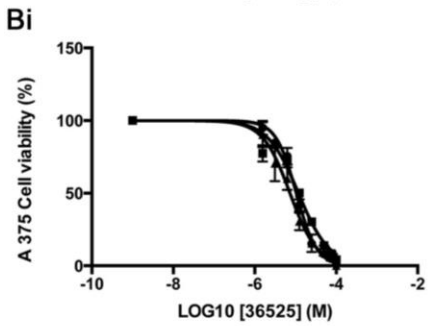


iv

NCI 20619	IC50		
	A375	HEK293	RD1
Replicate 1	1.11E-05	1.68E-05	1.76E-05
Replicate 2	6.57E-06	1.81E-05	2.15E-05
Replicate 3	2.15E-05	2.10E-05	2.94E-05

v

p-value	A375 VS HEK293	A375 VS RD1	HEK293 VS RD1
		0.294	0.158

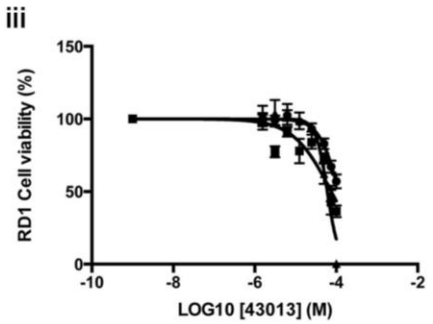
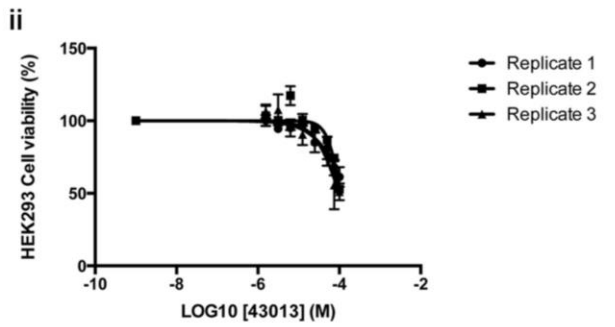
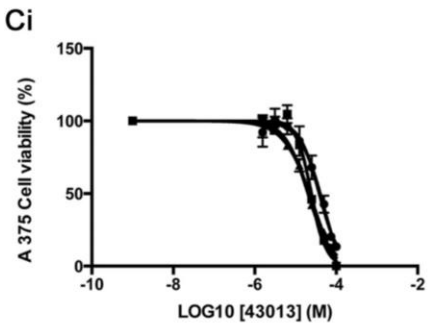


iv

NCI 36525	IC50		
	A375	HEK293	RD1
Replicate 1	1.05E-05	6.77E-06	2.61E-05
Replicate 2	1.18E-05	4.09E-06	3.19E-05
Replicate 3	7.32E-06	9.30E-06	2.15E-05

v

p-value	A375 VS HEK293	A375 VS RD1	HEK293 VS RD1
		0.192	0.007



iv

NCI 43013	IC50		
	A375	HEK293	RD1
Replicate 1	3.84E-05	1.57E-04	1.16E-04
Replicate 2	2.03E-05	1.07E-04	7.56E-05
Replicate 3	2.47E-05	1.00E-04	6.03E-05

v

p-value	A375 VS HEK293	A375 VS RD1	HEK293 VS RD1
		0.007	0.009

Figure 37. Data used to calculate statistical differences between IC50s generated for each of the 32 tested NCI 'hit' compounds screened upon three cell lines (A375, HEK293 and RD1). i. Graphs displaying A375 percentage cell viability (%) in response to the designated NCI compound over an increasing concentration range (LOG10 M), and were used to generate the IC50s for each of the 3 replicates (error bars represent standard error). ii. Graphs displaying HEK293 percentage cell viability (%) in response to the designated NCI compound over an increasing concentration range (LOG10 M), and were used to generate the IC50s for each of the 3 replicates (error bars represent standard error). iii. Graphs displaying RD1 percentage cell viability (%) in response to the designated NCI compound over an increasing concentration range (LOG10 M), and were used to generate the IC50s for each of the 3 replicates (error bars represent standard error). iv. IC50 values generated from the corresponding NCI 'hit' compound dose response graphs for each of the three replicates for the A375, HEK293 and RD1 cell lines respectively. v. P-values ($P\text{-value} = \leq 0.05$) generated using a student's T-test to statistically compare IC50 values generated using the corresponding NCI 'hit' compound dose response graphs for the A375, HEK293 and RD1 cell lines. Those p-values highlighted in bold indicate those cell lines whose IC50 values can be considered statistically different from one another. A. NCI 20619. B. NCI 36525. C. NCI 43013.

B). A complete figure summarising IC50 statistical analysis for all 32 screened hit compounds can be found in Appendix IV.

4.3 Discussion

The NCI diversity set II chemical genetic screen was a success. Of the 1363 compounds screened, 72 were identified as giving reproducible phenotypes. This suggests a hit rate of 5%, which represents a three percent increase from that exhibited in the previous Tomlinson *et al.*, (2005) NCI diversity set I compound screen (2%). This may reflect a refinement in the compound selection process employed by the NCI when designing the NCI diversity set II library when compared to the NCI diversity set I. It might also reflect the fact that the significant labour such screens require was split between a colleague and myself, whereas the original screen was carried out by a single person. This may have enabled us to be more stringent in our general experimental practice as phenotype screening is time consuming and tiring requiring focus over long periods of time, thereby potentially reducing errors we may have made screening alone. Interestingly, the only hit compound that was identified in the original Tomlinson screen that was also present in the NCI diversity set II library (NCI 30712) was also identified as giving an abnormal phenotype in our screen. This suggests that we were efficient in identifying abnormal phenotypes and gives us some confidence that the majority of possible phenotypes were identified. All identified hit compounds were replicated later to minimise the risk of false positives. However, there is a possibility that in some cases embryos may have died through natural causes which would have otherwise presented a phenotype. Such false negatives are difficult to account for giving the scale of the task at hand. However, all compounds were initially screened at two

separate concentrations and it is unlikely that in both instances the embryos were to have died of natural causes. Whilst this does not eliminate the possibility of false negatives, it does reduce the possibility to what we perceive to be an acceptable level given the high success rate of phenotypic hit identified.

It is clear that in many cases embryos presented phenotypes that could easily have been allocated into two or more separate phenotypic categories (the criteria for phenotypic classification and allocation is outlined above). For the purpose of this experiment it is not strictly important as to what phenotypic category they were assigned (this is covered in more detail in Chapter V), especially as all 72 of the compounds were preliminarily screened in the A375 cell viability assay. It is noticeable however that many phenotypes regardless of their category often present an additional abnormal eye or abnormal general morphology phenotype. Given the broad appearance of these phenotypes (which were often subtle) and the structural diversity inherent in the compounds screened, this was considered to be representative of general toxicity in the embryos. As such, as these additional phenotypes were often marginal, their importance with regards to the mechanism of action of the compound itself was considered less interesting than the mechanism of action responsible for generating the more interesting multiple abnormal pigmentation phenotypes.

As was the case in the original Tomlinson screen, the majority of phenotypes identified were pigmentation related. Total and partial pigment loss account for 39% of all hit compounds identified, highlighting their prominence in this screen. Abnormal melanophore migration and melanophore morphology phenotypes were also well represented (accounting for 13% and 10% of identified hits respectively). Melanocytes are the cells which give rise to melanoma in humans,

therefore any compound (such as those identified here) that can inhibit migration, inhibit growth or induce apoptosis in those cells could well have therapeutic potential (as was previously shown in the Tomlinson *et al.*, (2009) and White *et al.*, (2011) screen with the discovery of leflunomide). During early development, the migratory neural crest cells differentiate into the melanocytes which are present in the *X. laevis* embryo dorsal and lateral stripe. Interestingly, the pigment producing cells observed in the eye are not derived from these neural crest cells. This may suggest that of those compounds shown which generate a phenotype consistent with a total loss of pigment, some may in fact simply inhibit the synthesis of the melanin pigment as opposed specifically promoting apoptosis or abnormal migration of the cells themselves. To address this we aim to screen all such compounds using the mushroom tyrosinase assay. The tyrosinase enzyme is critical in the synthesis of the melanin pigment and therefore its interference would indicate a loss of melanin. As numerous tyrosinase inhibitors have already been characterised and their therapeutic potential is low, such an assay would aid in refining the 72 hits compounds identified by highlighting those that may be acting through a potential novel therapeutic target or pathway.

The cell viability assays have also been successful in identifying 13 compounds with significantly reduced the IC₅₀ of the A375 cell line when compared to the respective HEK293 and RD1 controls. Of these compounds, five gave rise to abnormal melanophore migration phenotypes, 7 abnormal total or partial pigmentation loss phenotypes and one abnormal melanophore morphology phenotype in the *X. laevis* screen. This provides further evidence that those phenotypes identified as giving abnormal pigmentation defects are indicative of compounds that may have therapeutic potential towards the treatment of

melanoma. The cell viability assay was chosen for its practical considerations (high-throughput potential, short run time and high reproducibility). It could be argued however that cell viability as an end point does not reliably inform as to whether the decrease in viability observed is due to apoptosis or a decrease in proliferation. Such information would aid in understanding the compounds mechanism of action. As such, in the future we aim to support the cell viability data with both migration assays (such as the scratch assay (Liang et al., 2007)) and apoptosis assays (such as the well documented TUNEL assay (Kasagi et al., 1994)) to further understand the mechanism of action of the compounds in question. However the cell viability assays in this instance have been successful in reducing the number of hit compounds from 72 to 13. An additional note is that due to the genetic variability inherent in cancers (especially melanoma), it will be necessary in the future to carry out these screens using additional melanoma and control cell lines so as to further support the extent to which these compounds might be considered to have therapeutic value.

The NCI diversity set II chemical genetic screen was a success. Of the 1363 compounds screened, 72 were identified as giving reproducible phenotypes. Of these, 13 were shown to statistically significantly reduce the IC₅₀ of the A375 melanoma cell line when compared to their HEK293 and RD1 controls, suggesting they may have therapeutic potential towards the treatment of melanoma. This strongly promotes the use of *X. laevis* as a forward chemical genetic screening model, which in combination with cell based assays has rapidly generated 13 structurally diverse lead compounds. This again highlights the potential of *X. laevis* as a tool for drug discovery. The benefit of a forward chemical genetic screening strategy is the rapid generation of hit compounds with potentially novel mechanisms of action. The traditional bottle neck of this

strategy however is the identification of the targets involved, particularly if little biological data is known about the compounds in question (as is the case with the NCI diversity set II compound library). This has led to the development of *in silico* chemoinformatical algorithms which are now used to predict potential binding targets. The application of chemoinformatics towards the identification of targets for compounds identified in this screen is discussed in Chapter V.

Chapter V

5.0 Chemoinformatical analysis of the *X. laevis* NCI diversity set II compound screen

5.1 Introduction

Forward chemical genetic screening excels in rapidly identifying compound bioactivity through the generation of interesting phenotypes. A critical bottleneck in forward chemical genetic screening arises when attempting to determine the identified compounds mechanism of action. Often compounds screened have ambiguous or no previous biological information, providing little help in identifying any potential target(s) involved. Chemoinformatical algorithms can be used to compare screened compound chemical information with known biological information from similar structural isoforms to predict potential targets. This provides a platform from which experimenters are able to begin investigating a compounds mechanism of action. Traditionally, mechanism of action has been predicted by comparing the screened libraries chemical information (such as two dimensional or three dimensional structures) with training sets consisting of compounds with known mechanism of action, which act as activity landmarks. This approach can be effective but is also limited, as it relies upon the availability of a relevant landmark compound that has a clear and specific mechanism of action, and often only accounts for the inhibition of a single target (whereas a phenotype may be produced by many). One approach to circumvent this issue is to integrate chemical similarity comparisons with

phenotypic data. Training statistical models (using compound structural information that are associated with known targets) can reveal new relationships between phenotypes and compounds. It is also possible to integrate relevant signalling pathways and disease information into the analysis.

5.2 Results

5.2.1 Bender laboratory chemoinformatical analysis of the NCI diversity set II chemical genetic screen

During my PhD we formed a collaboration with the Bender laboratory (Unilever, Cambridge), who specialise in chemoinformatical compound target prediction. The Bender laboratory utilised the data generated in my *X. laevis* chemical genetic screen (described in Chapter IV) to produce a list of targets for each phenotypic category, each of which being statistically strongly predicted to have not been associated by chance (Liggi, 2013). To achieve this, each of the compounds two dimensional structures from the NCI diversity set II compound library were pre-processed according to the Bender laboratories specific criteria (to enable consistent analysis). The compounds were then cross referenced with the ChEMBL v10 training set (approximately 155,000 ligand pair covering 894 targets) to predict potential targets for the entire NCI diversity set II compound library. The NCI diversity set II 72 identified hit compounds then isolated and processed using several visualisation and clustering methods so as their bioactivity profile similarity might be assessed. Similarities and dissimilarities between predicted targets for compounds belonging to each phenotypic category were then compared. Compounds were then further classified to establish the best data splits. This determined which predicted

targets were predicted to give rise to which phenotype. Predicted targets for each phenotypic category were then ranked statistically by calculating the probability that a particular prediction is relevant as opposed to occurring by chance. This was achieved by generating an estimation score for each target as a measure of the probability that a particular event (in this case: target predicted) might have occurred by chance (or is in fact actually relevant). Estimation scores were generated by first calculating the frequency of each predicted target (each of which having been predicted to generate a specific phenotype) in 10000 separate random control datasets. The "total frequency" of a target obtained in the NCI data set was then divided by the total frequency obtained by the same target in the random datasets, generating a value between 0 (enriched) and 1 (random). For example, let us consider the case of target A, which has a frequency of 3 in the NCI dataset, and is also found $^{150}/_{10000}$ times with a frequency smaller than 3 in the random datasets. Its estimation score would be $^{150}/_{10000} = 0.015$, and the target would be considered enriched - it is unlikely to obtain the same frequency by chance. Vice versa, target B has a frequency of 8, but its frequency is bigger in 7000 random datasets, having an estimation score of $^{7000}/_{10000} = 0.7$. Targets with an Estimation score less than 0.01 were considered to be enriched. The result of the Bender group analysis was the generation of predicted targets for each phenotypic category that were statistically highly unlikely to have occurred by chance (Liggi, 2013).

The generation of predicted targets for each phenotype gives us a platform from which to begin exploring the NCI hit compounds mechanism of action, however their involvement requires biological validation. To achieve this, compound antagonists for ten of the abnormal melanophore migration predicted targets

were obtained and screened on *X. laevis* embryos (under the same conditions and concentrations used in the NCI screen), to observe if the abnormal melanophore migration phenotypes could be replicated (**Table 10**). Abnormal melanophore migration predicted targets were chosen as the phenotype in *X. laevis* has been shown before to be indicative of compounds that might have therapeutic potential towards the treatment of melanoma (as was the case for leflunomide and is also supported by data presented in this thesis). Therefore these predicted targets if validated may have therapeutic potential as novel drug targets for the treatment of melanoma. Successful validation would also go some way towards providing confidence in such chemoinformatical predictions, thereby promoting this system as a potentially powerful tool for novel target discovery in forward chemical genetic screens.

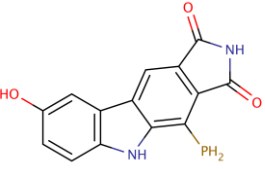
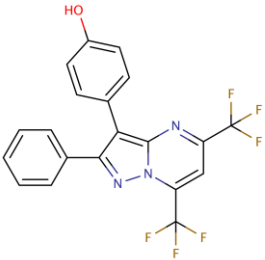
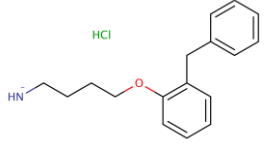
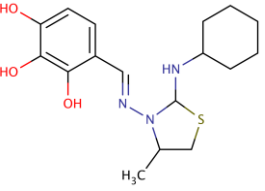
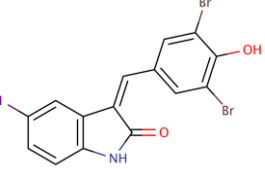
5.2.2 Summary of targets predicted to give rise to abnormal melanophore migration phenotypes when antagonised

The Bender report listed a number of targets predicted to give rise to each of the phenotypic categories listed previously. **Table 11** summarises those targets predicted to be involved in generating an abnormal melanophore migration phenotype. The targets are listed in order of p value significance, so that those targets with the lowest p-value (and therefore predicted to statistically have the highest probability of being involved in generating an abnormal melanophore migration phenotype) are listed at the top, and those with the highest estimation scores (and therefore are predicted to be less statistically significantly likely to be involved in generating an abnormal melanophore migration phenotype) are at the bottom. It should be noted that all targets shown are predicted to be

Table 10. Complete list of those compounds predicted to give rise to an abnormal melanophore migration phenotype ($p = \leq 0.01$).

Predicted target	Gene name	p-value
Urokinase-type plasminogen activator	PLAU	0
Serine/threonine-protein kinase WEE1	WEE1	0.0001
Estrogen-related receptor beta	ER- β	0.0002
3-phosphoinositide dependent protein kinase-1	PDK1	0.0004
MAP kinase-activated protein kinase 2	MAPKAPK2	0.0009
Monoamine oxidase A	MAO	0.0011
Estradiol 17-beta-dehydrogenase 2	HSD17B2	0.0027
Cytochrome P450 1A2	CYP1A1	0.0029
Protein-tyrosine phosphatase LC-PTP	PTPN7	0.0031
Induced myeloid leukemia cell differentiation protein	MCL-1	0.0033
Serine/threonine-protein kinase	c-RAF	0.0061
Vascular endothelial growth factor receptor 3	VEGF-C	0.008
cGMP-inhibited 3',5'-cyclic phosphodiesterase B	PDE3B	0.0091
Ribosomal protein S6 kinase 1	RSK3	0.0092
Tyrosine-protein kinase SRC	c-SRC	0.0093

Table 11. Summary of abnormal melanophore migration predicted targets, alongside their respective compound antagonists. The compound structure and source of the antagonists are also provided

Predicted target	Compound name	Source	Structure
Wee1	PD407824	Tocris Bioscience	
ER- β	PHTPP	Santa Cruz Biotechnology	
MAO	Bifemelane hydrochloride	Tocris Bioscience	
MCL-1	MIM1	Tocris Bioscience	
c-Raf1	GW 5074	Santa Cruz Biotechnology	

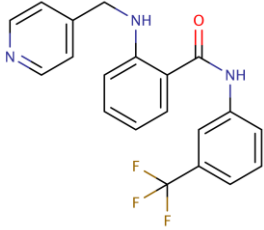
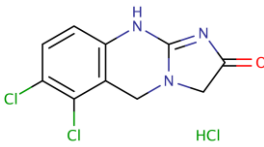
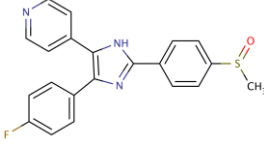
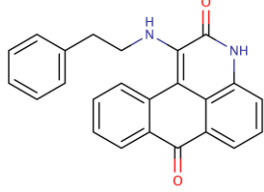
VEGF-C	AAL-993	Santa Cruz Biotechnology	
PDE3B	Anagrelide hydrochloride	Santa Cruz Biotechnology	
RSK2	SB203580	Santa Cruz Biotechnology	
RSK3	BRD 7389	Tocris Bioscience	

Table 12. NCI hit compounds shown to statistically significantly reduce the A357 melanoma line when compared to their respective non melanoma controls versus the abnormal melanophore migration predicted targets. X indicates those targets an NCI compound is directly predicted to bind to. NCI compounds are shown with there associated *X. laevis* phenotypes. Mg. Abnormal melanophore migration. P. Total or partial pigment loss

	19219	43013	45536	79253	92794	111848	133002	153792	319471
	Mg	P	P	P	Mg	P	Mg	P	P
ER-β	X	X	X		X	X			
MAO	X								
PLAU							X		
c-Raf1	X							X	
VEGF-C						X		X	X
RSK2	X								
RSK3	X								
Mcl-1		X		X	X			X	X
WEE1					X	X			
PDE3B			X			X		X	

statistically significantly likely to generate the abnormal melanophore migration phenotype, only the extent of this significance varies. Of those potential targets listed in **Table 8**, 10 were predicted to be targeted by nine of the 13 hit NCI compounds previously identified to generate a statistically lower IC50 in the A375 melanoma cell line when compared to its respective non-melanoma controls (**Table 9**). The remaining four NCI compounds previously identified to generate a statistically lower IC50 in the A375 melanoma cell line when compared to its respective non-melanoma controls were not predicted to interact with any of the abnormal melanophore migration predicted targets.

Of the nine NCI compounds that were predicted to interact with the abnormal melanophore migration predicted targets, three generated abnormal melanophore migration phenotypes in the *X. laevis* embryos whereas the remaining six generated phenotypes consistent with total or partial pigmentation loss (**Table 9**) when screened at 40µM. Of the nine NCI compounds listed, three (NCI 19219, NCI 92794 and NCI 153792) were predicted to interact with 4 or more of the abnormal melanophore morphology predicted targets. Only NCI 79253 and NCI 133002 were predicted to bind to a single target. Of the 10 predicted abnormal melanophore migration targets shown, MAO, PLAU, RSK2 and RSK3 were the only targets predicted to bind to a single NCI compound. NCI 133002 was the only example of an NCI compound to be predicted to interact with a single target, of which that single target (PLAU) was also only predicted to interact with that specific NCI compound.

As abnormal melanophore migration phenotypes in *X. laevis* may potentially be indicative of novel compounds or targets with possible therapeutic value towards the treatment of melanoma, each of the 10 predicted abnormal melanophore

migration targets predicted were looked at in more detail. It was determined as to whether these predicted targets had any previous evidence linking their involvement to the disease. **Table 13** provides a summary of this information. Of the 10 targets predicted, six (ER- β , PLAU, c_Raf1, VEGF-C, Mcl-1, MAO, RSK2 and WEE1) were found to have literature evidence linking them to being involved in melanoma. The remaining four (RSK3 and PDE3B) had no literature evidence linking their involvement towards melanoma.

5.2.3 Validation of abnormal melanophore migration predicted phenotypes

To validate the targets predicted to be involved in the generation of abnormal melanophore migration phenotypes, a compound antagonist was ordered for each of the 9 predicted targets **Table 10**. A compound antagonist for the predicted target PLAU has so far not been obtainable. Of the nine compounds ordered, six (GW5074, MIM1, Bifemelane hydrochloride, AAL993, BRD7389 and PHTPP).gave rise to abnormal pigmentation phenotypes in *X. laevis* embryos at stage 38 (40 μ M) (**Figure 38**). Embryos subjected to the remaining four compounds (PD407824, anagrelide hydrochloride, SB203580) at the same concentration did not survive. Due to time constraints, dose response assays analysing the effects of these antagonists have not yet been completed. All six phenotypes generated by the predicted target antagonists affected pigmentation in some way. The C-Raf1 antagonist GW5074 can be seen to give a clear loss of pigmentation in the lateral stripe and eye, and also presents what appears to be abnormal melanophore migration in the lateral and dorsal stripe (**Figure 39 B**). Of the hit NCI compounds listed above as being predicted to interact with C-

Table 13. Predicted abnormal melanophore migration targets are highlighted according to whether or not current literature has linked their involvement to melanoma. Example literature sources are provided for all positive examples.

Target	Involvement	Supporting literature
ER-β	Yes	(de Giorgi et al., 2011)
MAO	Yes	(Pietrangeli and Mondovi, 2004)
PLAU	Yes	(Besch et al., 2007; Marconi et al., 2008)
c-Raf1	Yes	(Karreth et al., 2009)
VEGF-C	Yes	(Peppicelli et al., 2013; Rinderknecht and Detmar, 2008)
RSK2	Yes	(Cho et al., 2012)
RSK3	No	
Mcl-1	Yes	(Jiang et al., 2008)
WEE1	Yes	(Magnussen et al., 2012)
PDE3B	No	

Raf1 (NCI 19219 and NCI 153792) (**Figure 39 C and D**), NCI 19219 would appear to present a phenotype that is very similar in appearance to that described for GW5074. The NCI 153792 phenotype is less similar in appearance, possessing near full normal pigmentation in the lateral stripe and eye when compared to GW5074, but is still similar in that it also presents a slight abnormal melanophore migration phenotype.

The Mcl-1 antagonist MIM1 appears to have generated a severely stunted embryonic phenotype that is devoid of pigment (**Figure 40 B**). Based on this image, it is not possible to determine whether the loss of pigment observed is due to a direct effect of the compound itself or the significantly delayed growth exhibited by the sample in question. Of the NCI compounds predicted to interact with Mcl-1 (NCI 43013, NCI 45536, NCI 79253, NCI 92794, NCI 111848, NCI 153792 and NCI 319472), all presented phenotypes that exhibit a similar loss of pigmentation to varying degrees (**Figure 40 C-I**). Of these, NCI 43013 and NCI 79253 appear to also display a similar stunted phenotype to that presented by MIM1.

The MAO antagonist bifemelane hydrochloride presented a phenotype in which rounded melanophores can be seen in the lateral, stripe suggesting abnormal melanophore morphology (**Figure 41 B**). In addition, slight abnormal patterning of melanocytes along the dorsal stripe can be observed suggesting abnormal melanophore migration. Also, an abnormal eye phenotype is visible as a loss of pigmentation in the retinal epithelial pigment layer. Only NCI 19219 was predicted to interact with MAO, and the phenotype exhibited is similar to that presented by bifemelane hydrochloride (**Figure 41 C**). The abnormal eye



Figure 38. Sourced compound antagonists for potential melanophore migration phenotype giving targets identified the chemoinformatics report that gave rise to prominent phenotypes when assessed at stage 38 (when compared to the DMSO vehicle control). Embryos shown were screened at 40 μ M. A. DMSO solvent control. B. GW5074. C. MIM1. D. Bifemelane hydrochloride. E. AAL993. F. BRD7389. G. PHTPP.

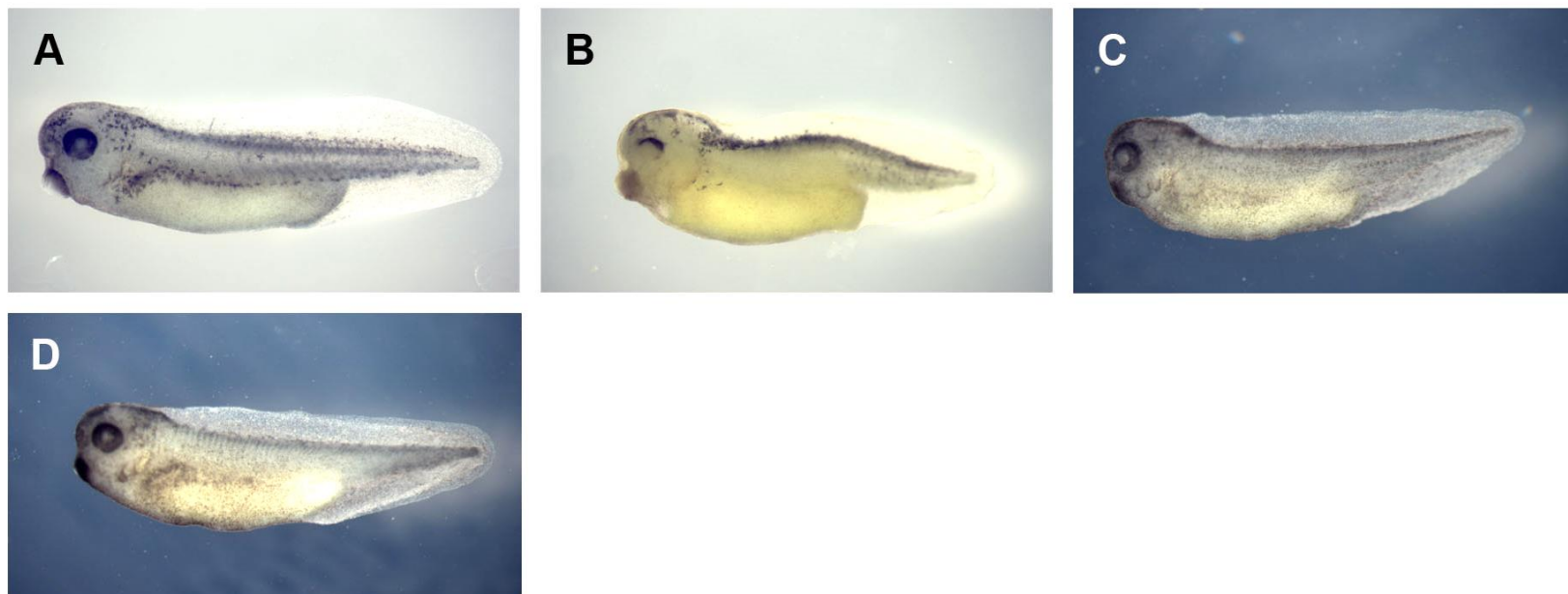


Figure 39. Stage 38 phenotype generated in response to GW5074 antagonist for predicted melanophore migration target c-Raf-1, alongside stage 38 hit NCI diversity set II compound phenotypes that were also predicted to antagonize the c-Raf-1 target. All NCI compounds shown have also previously been seen to give IC50s in the A375 melanoma cell line that were significantly different to their respective HEK293 and RD1 non-melanoma cell line controls. Embryos shown were screened at 40 μ M. A. DMSO solvent control. B. GW5074. C. NCI 19219. D. NCI 153792.



Figure 40. Stage 38 phenotype generated in response to MIM1 antagonist for predicted melanophore migration target Mcl-1, alongside stage 38 hit NCI diversity set II compound phenotypes that were also predicted to antagonize the Mcl-1 target. All NCI compounds shown have also previously been seen to give IC50s in the A375 melanoma cell line that were significantly different to their respective HEK293 and RD1 non-melanoma cell line controls. Embryos shown were screened at 40µM. A. DMSO solvent control. B. MIM1. C. NCI 43013. D. NCI 45536. E. NCI 79253. F. NCI 92794. G. NCI 111848. H. NCI 153792. I. NCI 319472.



Figure 41. Stage 38 phenotype generated in response to bifemelane hydrochloride antagonist for predicted melanophore migration target MAO, alongside stage 38 hit NCI diversity set II compound phenotypes that were also predicted to antagonize the MAO target. All NCI compounds shown have also previously been seen to give IC50s in the A375 melanoma cell line that were significantly different to their respective HEK293 and RD1 non-melanoma cell line controls. Embryos shown were screened at 40 μ M. A. DMSO solvent control. B. Bifemelane hydrochloride. C. NCI 19219.

development and abnormal melanophore morphology and migration can be observed as described for the bifemelane hydrochloride phenotype.

The VEGF-C antagonist AAL993 generated a clear melanophore migration phenotype in both the lateral and dorsal stripe of the embryo (**Figure 42 B**). Of the NCI compounds predicted to interact with VEGF-C (NCI 111848, NCI 153792 and NCI 319472), all presented phenotypes that exhibit a similar loss of pigmentation and abnormal melanophore migration to varying degrees (**Figure 42 C-E**), although none were as prominent as the phenotype displayed by AAL993.

The phenotype generated by BRD7389 (the RSK3 antagonist) was severely stunted, and presented a total lack of pigmentation, a complete lack of eye structure and blistering (**Figure 43 B**). As with MIM1 it is difficult to ascertain from this example the loss of pigment observed is due to a direct effect of the compound itself or the significantly delayed growth exhibited by the sample in question. The NCI compounds predicted to interact with RSK3 also present a loss of pigmentation in the lateral stripe (**Figure 43 C**).

The PHTPP (ER- β antagonist) phenotype presented a loss of pigmentation in the lateral stripe and eye, and also demonstrated abnormal slight melanophore migration in the dorsal and lateral stripe (**Figure 44 B**). Also, an abnormal eye phenotype is visible as a loss of pigmentation in the retinal epithelial pigment layer. Of the NCI compounds predicted to interact with ER- β (NCI 19219, NCI 43013, NCI 45536, NCI 92794 and NCI 111848), all demonstrated a loss of pigmentation similar to that generated by PHTPP to varying degrees (**Figure 44 C-G**). In particular, NCI 19219 presents a very similar loss of lateral stripe.

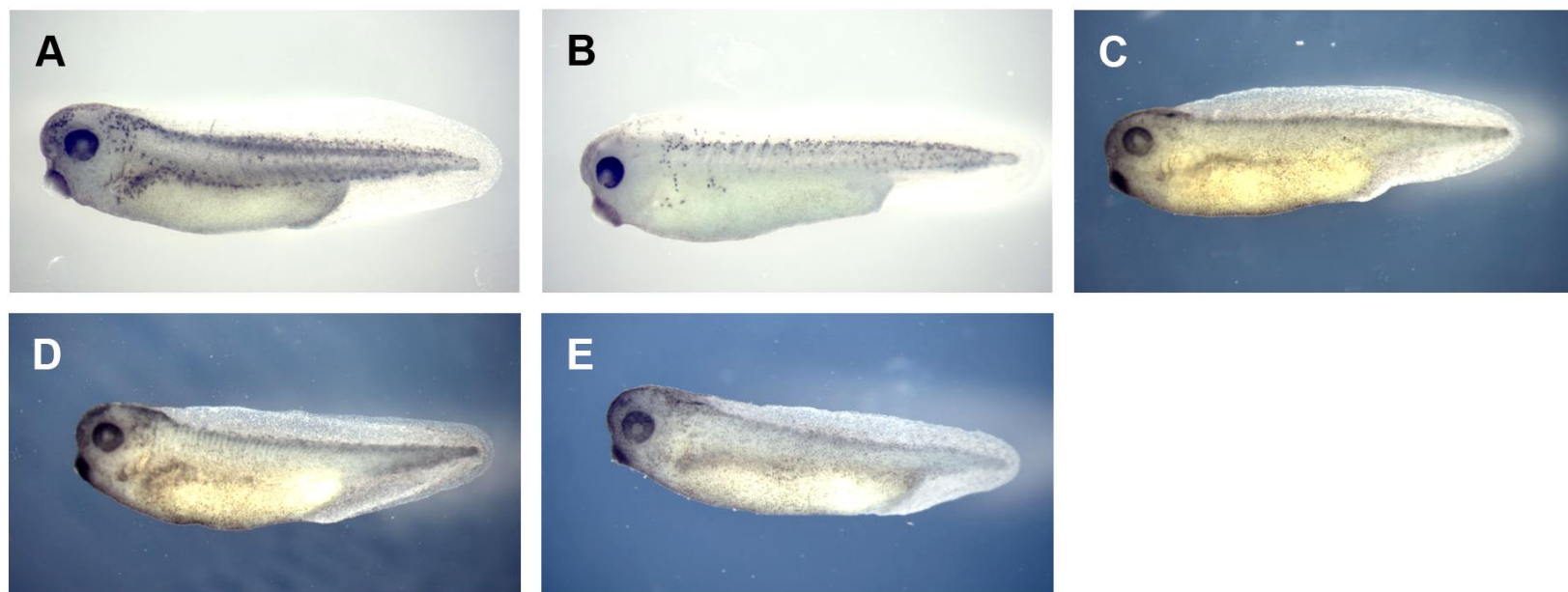


Figure 42. Stage 38 phenotype generated in response to AAL993 antagonist for predicted melanophore migration target VEGF-C, alongside stage 38 hit NCI diversity set II compound phenotypes that were also predicted to antagonize the VEGF-C target. All NCI compounds shown have also previously been seen to give IC50s in the A375 melanoma cell line that were significantly different to their respective HEK293 and RD1 non-melanoma cell line controls. Embryos shown were screened at 40 μ M. A. DMSO solvent control. B. AAL993. C. NCI 111848. D. NCI 153792. E. NCI 319472.



Figure 43. Stage 38 phenotype generated in response to BRD7389 antagonist for predicted melanophore migration target RSK, alongside stage 38 hit NCI diversity set II compound phenotypes that were also predicted to antagonize the RSK target. All NCI compounds shown have also previously been seen to give IC50s in the A375 melanoma cell line that were significantly different to their respective HEK293 and RD1 non-melanoma cell line controls. Embryos shown were screened at 40 μ M. A. DMSO solvent control. B. BRD7389. C. NCI 19219.



Figure 44. Stage 38 phenotype generated in response to PHTPP antagonist for predicted melanophore migration target ER- β , alongside stage 38 hit NCI diversity set II compound phenotypes that were also predicted to antagonize the ER- β target. All NCI compounds shown have also previously been seen to give IC50s in the A375 melanoma cell line that were significantly different to their respective HEK293 and RD1 non-melanoma cell line controls. Embryos shown were screened at 40 μ M. A. DMSO solvent control. B. PHTPP. C. NCI 19219. D. NCI 43013. E. NCI 45536. F. NCI 92794. G. NCI 111848.

pigmentation when compared to its PHTPP phenotypic counterpart. NCI 43013 is the only NCI compound to exhibit an abnormal eye phenotype similar to that observed in the PHTPP phenotype. NCI 45536 also exhibits an eye phenotype in which the eye lacks structure and is larger than its corresponding controls, however it is not similar in appearance to that observed in the PHTPP phenotype.

5.3 Discussion

Using the structural data of the NCI diversity set II compound library combined with the phenotypic data generated from the *X. laevis* chemical genetic screen (as described in Chapter IV), the Bender laboratory produced a report in which many targets were predicted for each phenotypic category described in our *X. laevis* chemical genetic screen. Each of these targets were predicted to give rise to a similar phenotype in *X. laevis* embryos to that presented by its allocated phenotypic category (i.e. a target predicted to be associated with generating a total loss of pigmentation should generate this phenotype when antagonised in *X. laevis* embryos). All of the identified protein targets shared greater than 70% homology between *Xenopus* and human. This would suggest a high degree of conservation and suggest that these targets would be relevant with regards to a human system.

Many of the abnormal melanophore migration predicted targets were also predicted to be targeted by nine out of 13 of the identified NCI compounds (shown previously to produce statistically significantly lower IC50 cell viabilities in the A375 melanoma cell line when compared to their respective non-melanoma controls). NCI 19219, NCI 92794, NCI 111848 and NCI 153792 were

predicted to bind to three or more of the targets predicted to give rise to abnormal melanophore migration. This may suggest that these compounds are more promiscuous. It may also indicate that some of the abnormal melanophore migration predicated targets may only elicit the described predicted phenotype in combination, however this cannot be said with certainty until each of the targets phenotype is assessed by inhibiting their expression individually. One point of note is that the structural diversity inherent in the NCI diversity set II compound library means that even if two or more of the hit NCI compounds do interact with the same target, it is likely they do so through different binding mechanisms. That is to say, the NCI hit compounds may potentially have the same predicted target(s) but almost certainly interact with them through very different mechanisms. MAO and PLAU were the only example whereby one target was predicted to bind to a single NCI compound (NCI 133002 and NCI 79253 respectively). Each of these NCI compounds are also both predicted to bind one single target. This may strongly suggest that the phenotypes elicited by NCI 133002 and NCI 79253 may well be acting through the inhibition of MAO and PLAU respectively, thereby potentially predicting their mechanism of action.

One benefit of using a chemoinformatical approach is that novel targets might be identified that were previously not associated with a disease or condition (in this case melanoma). Alternatively it may indicate that compounds screened might pose an alternative inhibitor of a target that is well characterised in its role within a disease. This is significant because alternative structures may bind more efficiently or present lower off target effects, and as such may potentially be a more preferable therapeutic option than alternative compounds already on the market. Two of the 10 predicted abnormal melanophore migration phenotype targets (RSK3 and PDE3B) had no literature as regards to their

involvement in melanoma, suggesting that they may prove to be novel and thus far unexplored targets for its treatment.

Of those predicted abnormal migration phenotype targets, the hormone ER- β has some evidence implicating its involvement towards melanoma progression. De Giorgi *et al.*, (2009) used qPCR to determine that thicker more invasive melanoma tumours are correlated with a decrease in expressed ER- β and ER- β when compared to controls and non-invasive melanoma tumours (de Giorgi *et al.*, 2009). As such, they go on to propose that the expression of ERs in melanoma tissue has the potential to be used as a prognostic indicator of invasive melanoma (de Giorgi *et al.*, 2009). More evidence is required to better understand the role of ER- β in melanoma progression, however it would appear to have potential as a therapeutic target. The ER- β antagonist (PHTPP) presents a phenotype that displays a clear loss of pigmentation in the lateral stripe and eye, as well abnormal melanophore migration in the dorsal stripe. The phenotype bears a strong resemblance to all five of the hit NCI compounds predicted to bind to it. Given the similarity between the phenotypes observed, this may possibly represent the mechanism of action through which they operate. However as not all of the phenotypes are identical, this may also suggest that other targets may also be involved.

Of those predicted abnormal migration phenotype targets, MAO was shown to have a link to melanoma. The primary function of the amine oxidase family is the deamination of oxidases, and are critical for the metabolism of amines. MAO is situated in the mitochondria and consists of two subtypes in the form of MAO-A and MAO-B. Only the MAO-A subtype has been implicated in melanoma progression (MacDonald and Lerer, 1994; Pietrangeli and Mondovi, 2004). The

MAO-A inhibitor clorgyline was shown to reduce apoptosis in A375 melanoma cells through a reduction in the production of free radicals (Pietrangeli and Mondovi, 2004). MAO-B has also been implicated to reduce the production of free radicals in cancerous cell lines, however its effects on melanoma survival have not yet been assessed (Mancocci et al., 2001). The target prediction does not appear to distinguish between the MAO subtypes and so a general inhibitor was obtained in order to observe if the predicted abnormal melanophore migration phenotype was replicated in *X. laevis*. Given that a slight melanophore migration/abnormal pigmentation phenotype was produced in the *X. laevis* embryo when exposed to the MAO antagonist (bifemelane hydrochloride) this suggests that the prediction was in fact accurate, in that compound interference with the MAO target produced the predicted phenotype. In the future it may be interesting to obtain inhibitors specific to each MAO subtype, so as to further assess their individual ability to produce an abnormal melanophore migration phenotype and begin to further evaluate their potential as targets for the treatment of melanoma.

PLAU was also linked to melanoma progression. PLAU is involved in a range of biological processes including adhesion, migration and inflammation. Its increase in expression has been associated with numerous forms of cancer (including melanoma) and is believed to be a promoter of metastasis. A study by Besch *et al.*, (2006) found that its inhibition in a range of melanoma cell lines induced apoptosis and mass death, implicating it as having strong potential as a therapeutic target towards the treatment of melanoma (Besch et al., 2007). A PLAU antagonist has been ordered but not yet screened on *X. laevis* embryos.

c-Raf1 has also already been well characterised in its role in melanoma. The b-Raf subtype is mutated in 41% of melanomas and has already been exploited as a promising target for the treatment of melanoma with several effective inhibitors on the market (e.g. Vermurafenib and Debrafenib). It is not uncommon for patients to rapidly develop resistance to these drugs, in which activation of c-Raf has been shown to play a critical role (Montagut et al., 2008). Activation of c-Raf has been shown to compensate for the inhibition of b-Raf in human melanoma cell lines by continuing to drive cell proliferation through the activation of the MAP kinase / ERK pathway (Karreth et al., 2009; Montagut et al., 2008). The c-Raf1 antagonist GW5074 produced a very pronounced melanophore migration phenotype in the *X. laevis* embryo, suggesting that the prediction of its role in generating an abnormal melanophore migration phenotype was accurate. Due to its role in b-Raf inhibitor resistance, c-Raf inhibition may well pose a potential route by which resistance can be avoided. As such the suggested NCI inhibitors of c-Raf shown here (NCI 19219 and NCI 153792) may have potential implications towards the treatment of melanoma.

Of those predicted abnormal migration phenotype targets, VEGF-C was also shown to be linked to melanoma in the literature. The VEGF family are well known for their role in promoting angiogenesis to increase oxygen levels in tissues suffering from an anoxic environment. Through promoting angiogenesis VEGF-C permits tumour growth allowing it to survive. VEGF-C has been implicated in melanoma by increasing tumour induced lymphangiogenesis and promoting metastasis by the A375 melanoma cell line (Papoutsi et al., 2000). However despite promising *in vivo* data of VEGF inhibitors in cancer mouse models, their ability to treat cancer has so far not been successfully replicated in humans (Bergers and Hanahan, 2008). The VEGF-C inhibitor (AAL993)

produced a pronounced abnormal melanophore migration phenotype thereby validating its prediction. The AAL993 generated phenotype would suggest VEGF-C to be a possible target of the NCI compounds predicted to interact with it (NCI 111848, NCI 153792 and NCI 319472). However, great effort has been made into developing VEGF inhibitors for the treatment of cancer with little success, suggesting that other identified targets may present a more attractive option to pursue.

The list of abnormal melanophore migration targets predicted two ribosomal s6 kinase subtypes in the form of RSK2 and RSK3. The ribosomal s6 kinase (RSK) family are well known for their role in signal transduction. RSK2 has been previously associated with melanoma. Phosphorylated RSK2 expression has been shown to be significantly enhanced in human cancer cell lines when compared to non-cancerous controls, and is hypothesised to play a role in tolerance to ultraviolet stress (a known cause of melanoma) (Cho et al., 2012). Preliminary experiments with the RSK2 compound antagonist has led to the death of the embryos, however further experimentation by reducing the concentration of the compound may reveal further information as to its ability to replicate its predicted phenotype. RSK3 currently has no known implication towards melanoma development or progression. Its predication in the chemoinformatical analysis followed by subsequent replication of predicted phenotype in *X. laevis* embryos suggest that NCI compounds which were effective in reducing A375 melanoma IC50s (in this case NCI 19219), may be operating through a mechanism that has as of yet not been explored. However, NCI 19219 also is predicted to interact with four other targets, and therefore each of these targets needs to be further characterised individually (potentially via individual knock down experiments), to further understand their role in

generating the abnormal melanophore migration phenotype, and therefore their potential role as a therapeutic target in melanoma.

Mcl-1 is well established in many cancers for promoting cell survival. Mcl-1 in melanoma has been previously shown to be critical for survival of human melanoma cell lines upon endoplasmic reticulum stress (Jiang et al., 2008), and its degradation has been shown to induce apoptosis in melanoma cells (Pandey et al., 2013). As such, it potentially poses an attractive target towards the treatment of melanoma. The phenotype generated by the Mcl-1 antagonist (MIM1) caused a severe delay in global development. It is hard to determine if the pigmentation phenotype observed is due to a direct effect of the compound antagonist or a result of the global toxicity observed. As such, it will be necessary in the future to screen using a lower concentration to see if the predicted abnormal phenotype can be validated *in vivo*. However, an abnormal pigmentation phenotype is still clearly visible, suggesting the chemoinformatical prediction may be correct. Another point of note is the large amount of hit NCI compounds predicted to interact with Mcl-1. This may suggest it represents a generic target and therefore possibly that all these NCI compounds may be acting through the same target. This would seem to be unlikely however as the original NCI phenotypes (for each of the hit compound predicted to bind to Mcl-1), do not all look the same in appearance thereby suggesting additional variables may be involved.

WEE1 has been strongly linked to melanoma and its expression is in fact a marker of prognosis (Magnussen et al., 2012). WEE1 plays a critical role in cell cycle regulation and has been implicated as a promoter of metastasis in melanoma (Magnussen et al., 2012). WEE1 therefore presents itself as an

attractive potential target towards the treatment of melanoma. The WEE1 antagonist (PD407824) has so far lead to the death of the embryos, and as such a phenotype has not been detectable to validate its chemoinformatical prediction of generating an abnormal melanophore morphology phenotype. By refining the concentration administered it may be possible to validate this particular target in the near future. Two hit NCI compounds (NCI 92794 and NCI 111848) were predicted to interact with WEE1, thereby suggesting that should WEE1 be successfully biologically validated they may potentially be novel inhibitors.

PDE3 enzymes are involved in the regulation of cardiac and vascular smooth muscle contractility. Whilst PDE3B has been implicated as having a genetic role in obesity, as of yet it has no known link towards the progression or promotion of melanoma. The PDE3B antagonist (anagrelide hydrochloride) led to the death of the embryos when screened. In the near future we aim to lower the concentration of the antagonist screened so as to assess whether a phenotype might be presented, or whether the compound is just generally toxic. PDE3B poses an interesting example of a compound which may potentially represent a novel target for the treatment of melanoma. However the prediction must be validated *in vivo* before we can hypothesise further.

Two of the predicted targets (RSK3 and PDE3B) are particularly interesting, in that neither of them have been previously linked directly to melanoma progression. This may suggest their role in melanoma development may either operate through an unknown pathway or through a known pathway via a novel mechanism. Additional chemotherapeutics targeting different targets offers additional lines of defence when treating aggressive cancers such as melanoma. As such the identification of two potentially novel targets for the

treatment of melanoma is significant and warrants further investigation. It remains to be shown whether these targets have abnormal expression in patient tumour samples.

The remaining eight compounds which were linked to melanoma can act as positive controls. It is to be expected that some compounds that generate abnormal melanophore migration phenotypes may well operate through targets known to be implicated in melanoma. Those predicted targets that were known to be associated with melanoma and also produced a pigmentation phenotype when antagonised in the *X. laevis* embryos go some way to supporting our belief that the *X. laevis* screening system is an excellent model for the identification of targets and/or compounds that have therapeutic potential towards the treatment of melanoma. That many of the hit NCI compounds identified reduce A375 cell viability were also predicted to interact with these predicted abnormal melanophore migration targets further strengthens our faith in the *X. laevis* screening assay we have developed but also in the predictive power of the chemoinformatical analysis itself. The six predicted target antagonists that produced an abnormal pigmentation phenotype support the predictive power of the assay. With adjustments to the dosing concentrations already discussed we hope to soon validate the remaining four predicted targets as well.

There is a chance that the small compound antagonists ordered may be eliciting their respective phenotypes (whether they produced their predicted phenotype or not) via additional targets. Whilst these antagonists were selected based on their strong affinity towards each of the identified abnormal melanophore migration targets predicted, it is not possible to guarantee that the phenotypes

observed occur only through that mechanism with no off target effects. To fully validate these target predictions it will be necessary in the future to knock down the expression of each target via morpholino injection so as to then assess the specific effects the predicted target has towards generating its predicted phenotype. For the time being however, the compound antagonists have served their purpose by giving promising signs that the chemoinformatical predictions are in fact accurate.

Through the combination of forward chemical genetic screening, appropriate cell based assays and chemoinformatical analysis we have developed an efficient and effective screening strategy for the rapid identification of numerous hit compounds that are likely to be acting through either well known or novel targets that may have possible implications towards the treatment of melanoma. As such, this strongly supports our argument that *X. laevis* screening systems such as this would be of great benefit to drug discovery.

Chapter VI

6.0 Development of the *X. laevis* renal function toxicity assay

6.1 Introduction

Work presented in this thesis so far has focused on the *X. laevis* model system towards its application as a tool for drug discovery. It is yet to be established if the model can match its potential in its application towards drug development, specifically as a toxicity assay for the early detection of toxic compounds. To address this, I have designed (in collaboration with AstraZeneca) an *X. laevis* renal toxicity assay. Renal toxicity is a serious concern for the pharmaceutical industry, being responsible for 7% of preclinical compound dropouts (Desrochers et al., 2013; Fuchs and Hewitt, 2011). In addition, 30-50% of reported kidney failure in patients is due to adverse drug reactions (Desrochers et al., 2013; Fuchs and Hewitt, 2011; Pannu and Nadim, 2008). As such, there is a clear demand for an improved capacity for renal toxicity detection, as our current capabilities are insufficient. This thesis has already outlined the significant practical advantages of utilising the *X. laevis* animal model towards drug discovery. Combined with the strong history of the FETAX assay, this suggests that if the assay development is successful the *X. laevis* model has the potential to contribute towards the prediction of renal toxicity to the benefit of industrial drug development.

Whilst *X. laevis* has already been successfully used for the study of renal development (Brennan et al., 1999; Osafune et al., 2002; Seufert et al., 1999), it has not yet been used as a model for renal function. It is known that the *X. laevis* pronephros is functional from as early as stage 38, actively excreting ammonia into the surrounding media. Using a simple biochemical assay we believe that it is possible to detect ammonia excreted into the media and use this as an indirect measure of active renal function. The hypothesis was that nephrotoxic compounds introduced into the *X. laevis* system would result in a significant change in the amount of ammonia excreted, thereby indicating abnormal renal function as a result of nephrotoxicity. To aid in the validation of the assay, AstraZeneca provided a library of compounds which were known to be either non-toxic or nephrotoxic in humans (**Table 14**). Many of these nephrotoxic compounds were known to act via different mechanisms, therefore if they were detected in this assay and gave rise to abnormal ammonia excretion this would have gone some way to validating the assay as a measure of renal function. Some of these mechanisms include

We have evaluated two possible assays for the detection of ammonia concentration in *X. laevis* media samples in the form of the salicylic acid assay and the glutamate dehydrogenase assay (outlined below).

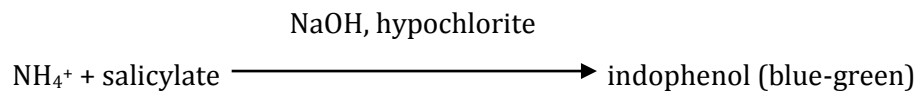
Table 14. List of AstraZeneca supplied nephrotoxic and non-toxic compounds.

Designated ID	Compound name	Known biological function
NT1	Beclomethasone dipropionate	Non-Toxic
NT2	Fluoxetine	Non-Toxic
NT3	Diphenhydramine hydrochloride	Non-Toxic
NT4	S(-)-Carbidopa	Non-Toxic
NT5	Gemfibrozil	Non-Toxic
NT6	Raloxifene hydrochloride	Non-Toxic
NT7	Zomepirac sodium salt	Non-Toxic
NT8	Loperamide hydrochloride	Non-Toxic
NT9	Rifapentine	Non-Toxic
NT10	Fexofenadine hydrochloride	Non-Toxic
NT11	Amiloride hydrochloride hydrate	Non-Toxic
NT12	Acarbose	Non-Toxic
Ne1	Vancomycin	Nephrotoxic
Ne2	Doxorubicin	Nephrotoxic
Ne3	Tobramycin	Nephrotoxic
Ne4	Leflunomide	Nephrotoxic
Ne5	Bithionol	Nephrotoxic
Ne6	Lisinopril	Nephrotoxic
Ne7	Amiodarone	Nephrotoxic
Ne8	Clindamycin hydrochloride	Nephrotoxic
Ne9	Zileuton	Nephrotoxic
Ne10	Rifabutin	Nephrotoxic
Ne11	Cefaclor	Nephrotoxic
Ne12	Idarubicin hydrochloride	Nephrotoxic

6.2 Results

6.2.1 Salicylic acid method of ammonia detection

The salicylic acid method of ammonia detection was originally selected due to its simplicity and potential capacity towards high-throughput screening. It represents a modified version of the original Berthelot reaction, in which ammonium ions and phenol react to form an indophenol dye which absorbs strongly between 630nm and 720nm. The salicylic acid method of ammonia detection occurs via a reaction between ammonium ions present with hypochlorous acid and salicylate ions in the presence of nitroferricyanide ions to form the salicylic acid analogue of indophenol blue (see reaction below).



The absorption maximum of salicylic acid is 665nm. The amount of salicylic acid produced is indicative of the amount of ammonia present, i.e. the higher the absorbance measured, the higher the concentration of ammonia present in the media. Initial experiments using the salicylic acid method of ammonia detection appeared to be promising. Initial optimisation experiments indicated that it was possible to detect an increase in detectable absorbance at 695nm with increasing concentration of ammonia, and that it was also possible to observe an increase in absorbance in incubated embryo media from stage 38 onwards (the stage at which the pronephros is believed to be functioning),

suggesting excreted ammonia was detectable with this assay. However, the DMSO solvent in which the AstraZeneca compounds were dissolved was later shown to inhibit the salicylic acid reaction from taking place (which was supported by (T. T. Ngo 1982))). As the majority of small molecules in compound libraries such as AstraZeneca's are dissolved in DMSO, this problem was found to be unavoidable and necessitated the evaluation of a different biochemical assay for the detection of ammonia that could function in the presence of DMSO.

6.2.2 Evaluation of the salicylic acid method of ammonia detection

Initial optimisation experiments using the salicylic acid method of ammonia detection presented positive results. Using the JBL salicylic acid ammonia detection kit, it was shown that media obtained from embryos incubated in 0.1 X MMR (five embryos per well) from developmental stage 15, showed absorbance that was similar to that displayed by the negative control (**Figure 45 A**). When the same embryos were allowed to continue to develop to stage 45, the media showed a large increase in absorbance detected. This supports published data suggesting the *X. laevis* pronephros is only functional post embryonic stage 38 and also suggests that little to no ammonia is excreted passively prior to this. In an attempt to standardise the JBL salicylic acid ammonia detection assay, standard curves were generated that showed a positive correlation between measured optical density at 695nm and increasing ammonia standard concentrations (6µM, 10µM, 20µM, 40µM, 60µM, 120µM, 160µM, 340µM and 560µM) (**Figure 45 B**). This suggests that the JBL ammonia assay kit is sensitive enough to detect varying levels of ammonia present in solution, which

is necessary to identify fluctuating ammonia excretion levels in embryos as a surrogate marker for renal function.

A time course assay was carried out to determine whether ammonia could be detected in the media of *X. laevis* embryos over increasing incubation time. *X. laevis* embryos were plated five embryos per well at stage 38 in 0.1 X MMR (2ml final volume). At each time point (12 hour intervals) *X. laevis* embryo media was sampled to measure absorbance at 695nm. In an attempt to refine the *X. laevis* ammonia assay protocol, this experiment was carried out using either a 1000µl or 200µl media sample protocol (**Figure 45 C**). For each time point recorded, the 1000µl protocol was carried out according to the same protocol outlined for the original *X. laevis* salicylic acid assay. The 200µl protocol sampled 200µl of media per well (the same well as each sample taken for the 1000µl protocol to ensure consistency) and deposited directly into a 96 well plate, to which 6.6µl of reagent one, two and three were added and mixed via multichannel pipette. Each solutions absorbance was subsequently read in a plate reader. Also included in the graph is a negative control (fresh media with no embryos) and a positive control (560µM NH₃ standard solution). Both the 1000µl and 200µl protocols showed a steady increase in absorbance over time. The 200µl protocol samples detected higher absorbance at each time point than the 1000µl protocol samples, although (with the exception of time point 72 hours) all of the time points between the 1000µl or 200µl media sample protocols have overlapping standard error. The negative and positive control show little change in adsorption over time, suggesting passive environmental ammonia diffusion was not occurring.

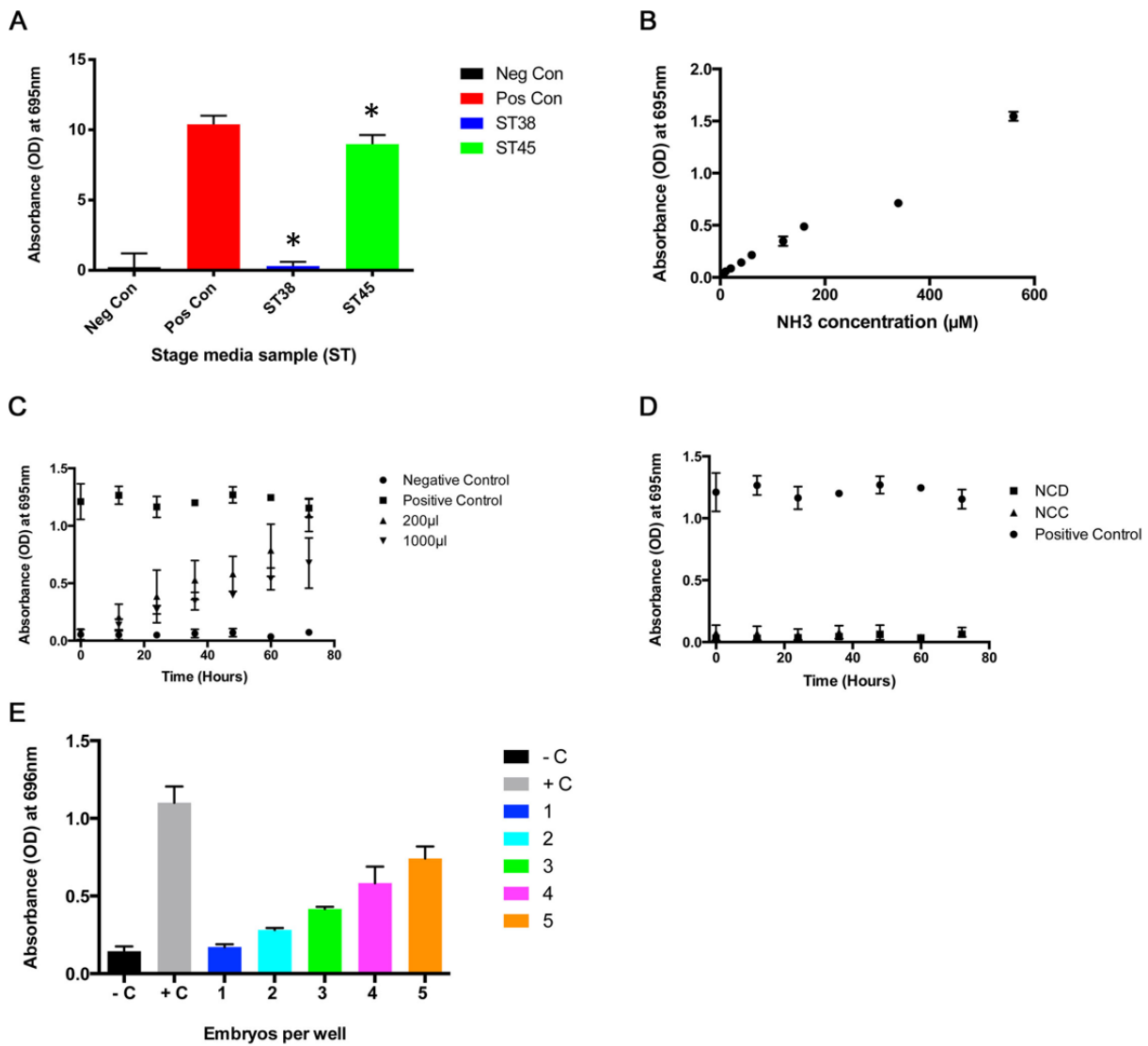


Figure 45. Optimization of the *X. laevis* salicylic acid ammonia detection assay.

A. Assessment of ammonia detectable in *X. laevis* media at different developmental stages (having been incubated in sample media from stage 15). The positive control represents a 560µM ammonium sulphate stock solution. The negative control represents fresh media containing no embryos. Error bars represent standard error ($n=3$). * denotes ST38 and ST45 significant difference ($P<0.01$).

B. Standard curve generated using increasing concentrations of ammonium sulphate solution. Error bars represent standard error ($n=3$).

C. Time course assay in which embryo media absorbance was read every 12 hours for 72 hours. The two protocols tested in this assay are represented as either the

200µl or 1000µl protocol. The positive control represents a 560µM ammonium sulphate stock solution. The negative control represents fresh media containing no embryos. Error bars represent standard error (n=3). D. Time course assay in which two types of negative control media absorbance were read every 12 hours for 72 hours. The two protocols tested in this assay are represented as either the NCC (Negative Control 'Clean') or NCD (Negative Control 'Dirty'). The positive control represents a 560µM ammonium sulphate stock solution. Error bars represent standard error (n=3). E. Absorption in response to number of embryos per well (1, 2, 3, 4 or 5 embryos per well, incubated at stage 38 and assayed at stage 45). – C, Negative Control (Fresh media containing no embryos). + C, Positive control (560µM ammonium sulphate stock solution). Error bars represent standard error (n=3)

In a separate time course experiment (**Figure 45 D**), two different negative controls were compared using the 1000µl media sample protocol in the form of 'dirty' and 'clean' controls. Both controls represent media in which no embryos have been incubated (and are both therefore negative controls). The 'clean' control indicates media that has come from a fresh stock of 0.1 X MMR whereas the 'dirty' control represents media that has come from incubated embryos before the pronephros was functional (prior to stage 38). The purpose of the 'dirty' control is to evaluate whether residual ammonia is being transferred to the sample wells during the experiment set up, and to see if this 'dirty' media has any effect on absorption over time. As the embryos have to be transferred in media, there is a possibility that ammonia in the incubated media may contaminate the experiment. The 'dirty' control can therefore be directly compared to the 'clean' control to assess this possibility. At no point during the time course assay did the 'dirty' negative control absorption appear to differ from the 'clean' control absorption.

The potential effect of number of embryos per well may have on detected absorption in the JBL ammonia assay was assessed by plating embryos as stipulated in the original protocol with either one, two, three, four or five embryos per well (**Figure 45 E**). Embryos were incubated for 72 hours (until embryonic stage 45) at which point their media absorbance was read. A positive correlation can be observed between number of embryos per well and absorbance detected at 695nm.

To assess the predictive capacity of the *X. laevis* salicylic acid ammonia renal function toxicity assay, embryos were incubated from ST38 with one of either 10 nephrotoxic or 5 nontoxic AstraZeneca compounds (40µM) (**Figure 46 A**).

Embryo media was then analysed according to the original protocol (outlined previously). For all 10 nephrotoxic and 5 nontoxic compounds screened, none presented an absorbance that was significantly different from the negative control. The positive control however recorded an absorbance consistent with that detected from previous experiments, suggesting that the lack of detectable absorbance in each test sample may be due to the addition of the AstraZeneca compounds to the assay. It is unlikely that 15 structurally diverse compounds would independently interfere with the salicylic acid assay reaction. The only common factor between these compounds is that they were all dissolved in the solvent DMSO. As such, the role of DMSO and its effect on the salicylic acid assay reaction was investigated.

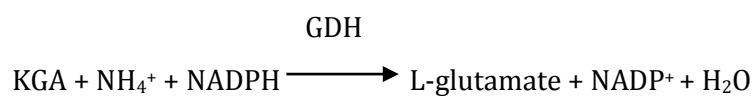
A literature search discovered that the salicylic acid reaction is inhibited by the presence of DMSO (T. T. Ngo 1982). This is supported by follow up studies using different salicylic acid ammonia detection assay brands (the API and TETRA ammonia detection kits) which also found in each case that the presence of DMSO at a variety of concentrations when using 560 μ M NH₃ standard solutions resulted in absorbance levels consistent with that of the negative control (across all three test kits) (**Figure 46 B**). The positive control (which contained no DMSO) gave absorption levels similar to those observed in previous assays for the same stock NH₃ concentration (560 μ M) and was consistent across all three test kits.

A final assay was conducted to determine if other solvents also inhibit the salicylic acid ammonia assay reaction (**Figure 46 C**). Of the solvents screened, DMF, EtOH and MeOH all appeared to have no effect on the absorbance detected when compared to the positive control. DMSO showed almost no

measurable absorbance detected (similar to that displayed by the negative control) suggesting that the reaction had been inhibited.

6.2.3 *Glutamate dehydrogenase assay method of detection*

The glutamate dehydrogenase assay was obtained in the form of an ammonia assay kit supplied by Sigma-Aldrich (AA0100). In this reaction, ammonia present in a sample solution (such as embryo media) reacts with α -ketoglutaric acid (KGA) and reduced nicotinamide adenine dinucleotide phosphate (NADPH) in the presence of L-glutamate dehydrogenase (GDH) to form L- glutamate and oxidised nicotinamide adenine dinucleotide phosphate (NADP⁺), as depicted in the reaction below.



The oxidation of NADPH to NADP⁺ results in a decrease in absorbance at 340nm that is directly proportional to the concentration of ammonia present in the sample. By subtracting initial absorbance (before addition of GDH enzyme) from final absorption (five minutes prior to GDH enzyme addition), the Delta A340 was calculated. The larger the Delta A340, the more ammonia is present in the sample solution.

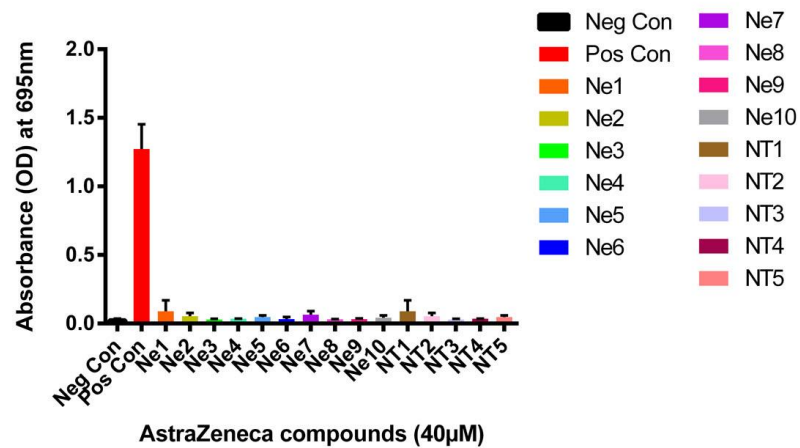
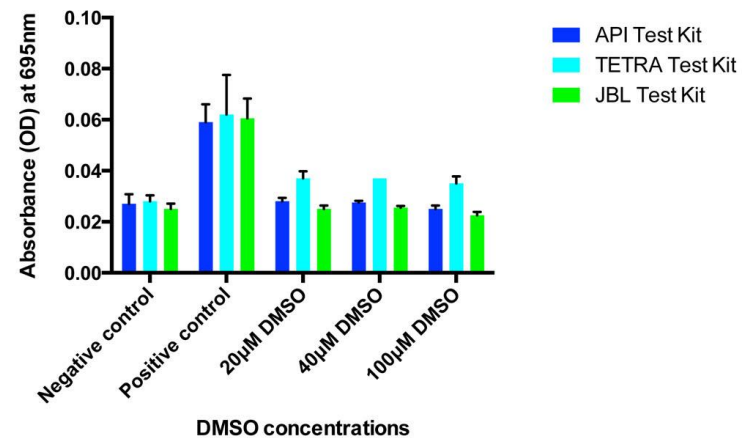
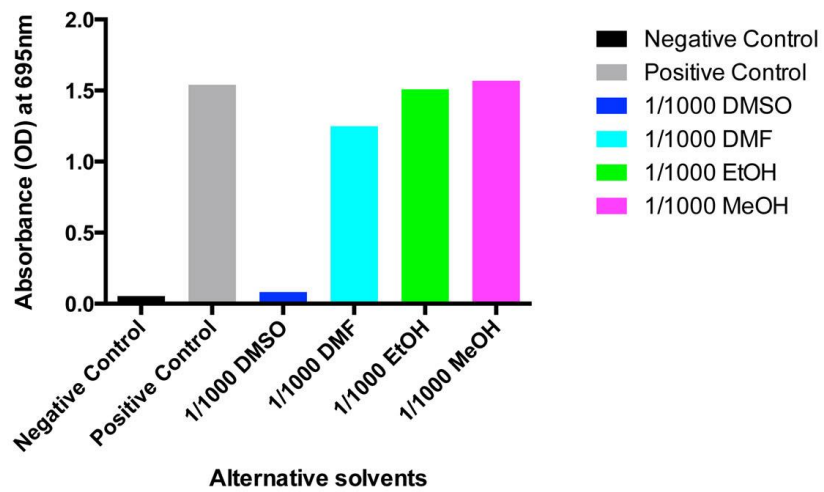
A**B****C**

Figure 46. Assessment of AstraZeneca compounds on *X. laevis* renal function using the *X. laevis* salicylic acid ammonia detection assay. A. Absorption detected following addition of 10 AstraZeneca nephrotoxic (Ne) compounds and five AstraZeneca non-toxic compounds (NT) (40 μ M final concentration). Positive control represents absorption of media containing five embryos with no compound present. Negative control represents absorption of fresh media containing no embryos. Error bars represent standard error (n=3). B. Assessment of differing concentrations of DMSO effect upon absorption detected from media containing 560 μ M ammonium sulphate using three different salicylic acid ammonia detection assay kits (represented as the API, TETRA and JBL test kits). The positive control represents absorption of media contain 560 μ M ammonium sulphate with no DMSO present. The Negative control represents absorption of fresh media containing no embryos. Error bars represent standard error (n=3). C. Assessment of different solvents and their effects on detectable absorbance when using the salicylic acid ammonia detection assay. Each solvent sample contained (1/1000) solvent concentration in a 560 μ M ammonium sulphate stock solution. The positive control represents absorption of media containing 560 μ M ammonium sulfate with no solvent present. The Negative control represents absorption of fresh media containing no embryos. (N=1).

6.2.4 Evaluation of the glutamate dehydrogenase assay method of ammonia detection

Due to the unavoidable DMSO inhibition of the salicylic acid reaction, the glutamate dehydrogenase assay was adopted as a potential alternative biochemical assay. Data for the GDH assay had to be generated using a spectrophotometer, as plate reader samples generated uninterpretable results (data not shown). A standard curve was created to ensure that the assay was sensitive to a range of ammonia concentrations (**Figure 47 A**). A preliminary range of ammonia concentrations were trialed using this method with DMSO which showed no sign of interference as experienced when using the salicylic acid assay method of ammonia detection (data not shown). Due to time constraints, it was necessary to begin testing AstraZeneca compounds as soon as possible to assess their effect upon *X. laevis* renal function.

To assess the predictive capacity of the *X. laevis* GDH ammonia renal function toxicity assay (and to ensure the assay functioned in the presence of DMSO), embryos were incubated from St38 with one of either 12 nephrotoxic or 12 nontoxic AstraZeneca compounds (100µM) (**Figure 47 B**). Embryo media was then analysed according to the outlined protocol. A vehicle control was also included alongside a positive control (embryo media without DMSO) to ensure the DMSO solvent was having no effect on the assay. For all 12 nephrotoxic and 12 nontoxic compounds screened, none generated a Delta(A430) that appeared significantly different to the vehicle control (**Table 15**). One possible exception is for the non-toxic compounds NT1 and NT7, which give rise to a significantly higher Delta(A430) suggesting an increase in ammonia excretion compared to the positive control. Nephrotoxic compounds NE5 and NE7 killed the embryos

Table 15. T-test comparison of AstraZeneca compound dosed embryo media generated Delta(A340) versus vehicle control Delta(A340). Significant values are highlighted in bold. Neg Con. Negative Control (P = 0.05) (n = 4).

AstraZeneca compound	P Value
Pos Con	0.131
Ne1	0.142
Ne2	0.493
Ne3	0.561
Ne4	0.626
Ne6	0.635
Ne8	0.885
Ne9	0.501
Ne10	0.711
Ne11	0.239
Ne12	0.641
NT1	0.028
NT2	0.289
NT3	0.406
NT4	0.602
NT5	0.958
NT6	0.492
NT7	0.019
NT8	0.886
NT9	0.738
NT10	0.237
NT11	0.859
NT12	1

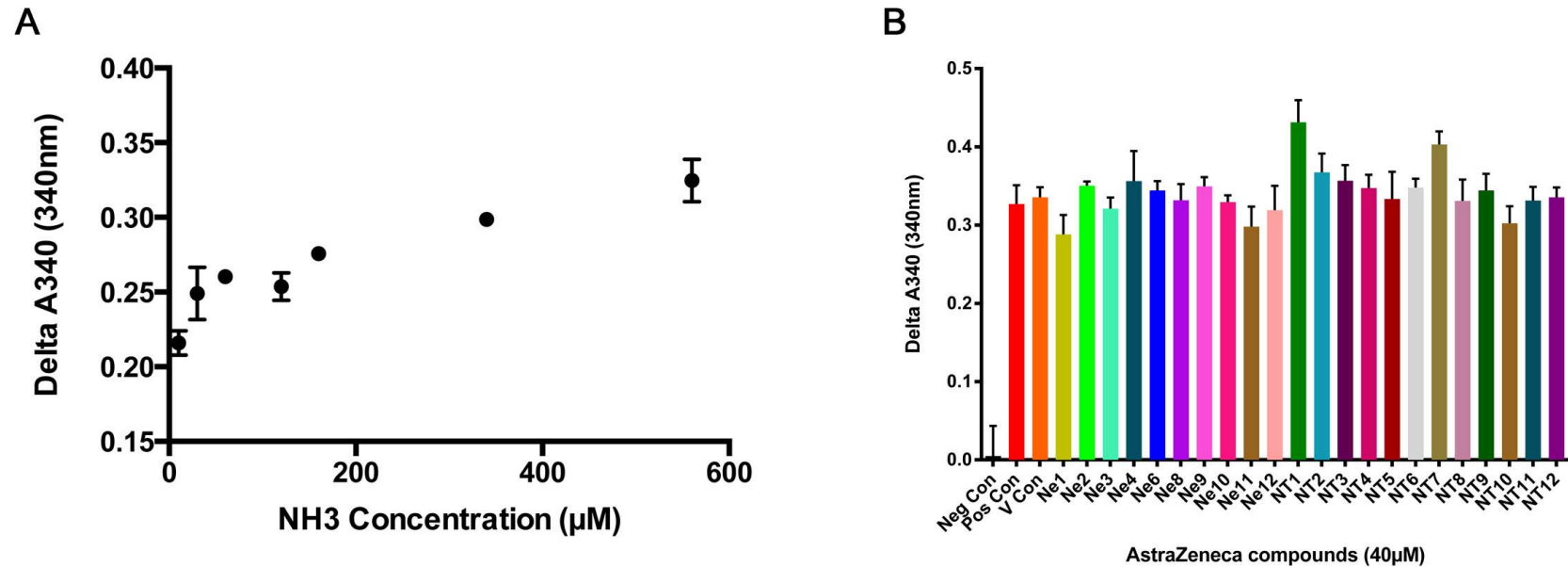


Figure 47. Assessment of the *X. laevis* GDH ammonia detection assay. A. Standard curve generated using increasing concentrations of ammonium sulphate solution. Error bars represent standard error (n=3). B. Delta A340 detected following addition of 10 AstraZeneca nephrotoxic (Ne) compounds and five AstraZeneca non-toxic compounds (NT) (100µM final concentration). Vehicle control (V Con) represents absorption of media containing five embryos with no compound present. Negative control represents absorption of fresh media containing no embryos. Pos Con represents embryo media without DMSO present. Error bars represent standard error (n=3).

before their media could be sampled. Phenotypes exhibited before death displayed no visible signs associated with *X. laevis* renal toxicity (such as edema formation). No significant difference was recorded between the vehicle and positive controls. The lack of identifiable change in Delta(A340) between the test samples and the positive control suggests either the assay is not sensitive enough to detect a change in ammonia excretion (and therefore renal function), or that the AstraZeneca compounds are not toxic in the *X. laevis* system.

6.3 Discussion

Our initial aim was to develop a renal function assay using the *X. laevis* animal model to rapidly and accurately identify nephrotoxic compounds during preclinical drug development. Results suggest that neither the salicylic acid nor the GDH biochemical detection of ammonia assays were capable of determining abnormal renal function in the *X. laevis* model. Despite promising preliminary data from the initial assessment of the salicylic acid method of ammonia detection, its application towards drug development is not feasible due to its inhibition in the presence of DMSO. Many compounds are dissolved as standard in the DMSO solvent (including the majority of the compounds stocked and supplied by our AstraZeneca collaborators), severely diminishing the value of the assay. This is unfortunate as optimisation assays showed it to be consistent and sensitive. Importantly, initial experiments using the salicylic acid method of ammonia detection suggested that it is indeed possible to detect excreted ammonia as absorbance increased in incubated media samples when compared to negative controls. Embryos incubated from embryonic stages 15 to 38 also showed no indication of ammonia present when compared to embryos

incubated from embryonic stages 15 to 45. This supports the literature which stipulates that the *X. laevis* pronephros is non-functional until after stage 38 (Jones, 2005).

The comparison between the original 1000µl and altered 200µl media sample salicylic acid assay methods suggested that the protocol could also be refined to improve throughput, another important concern in assay design. Another reason for comparing these two protocols was to assess whether or not the assay could be developed to reduce the quantity of reagents required (thereby making the assay more cost effective per reaction). Preliminary experiments suggest that utilising the 200µl protocol had potential, and thereby both the amount of reagents used and the assay throughput time could be reduced. This would have been worth investigating further had the assay not failed due to inhibition by DMSO. The increase in absorbance shown in the 200µl protocol may be due to it being transferred and mixed directly in the 96 well plates allowing each sample to be read in the plate reader faster than is possible in the 1000µl.

Standard curves generated for both the salicylic assay and GDH assay could have been used to calculate the concentration of the ammonia in the solution of other samples. This was not done for the preliminary assays as it was only of concern that the absorbance in test samples was higher to that of the negative controls. Had the assays progressed further this would have been implemented as standard practice for each experiment to enable accurate calculation of sample ammonia concentration. Whilst this could have been easily implemented for the salicylic acid assay, the significant increase in samples per experiment would be problematic for the GDH assay which would only function in the spectrophotometer at this stage. This significant increase in throughput time

would have been unacceptable, and therefore a future experiment would have been to investigate how the GDH assay could be adapted into a plate reader format.

The GDH assay was selected as the only remaining viable option for the biochemical detection of ammonia in solution. The original Berthelot reaction biochemical method of ammonia detection (from which the salicylic acid reaction is adapted), has also been shown to be inhibited by DMSO (Searle, 1984). Another alternative was the Nessler reaction, which functions through an entirely different reaction pathway (and therefore may not be inhibited by DMSO). However this was avoided as it produced large quantities of hot mercury as a side product and was considered unsuitable for use in a large scale industrial context. Ammonia electrochemical probes were also considered, however none could be sourced that would fit into the individual 96 wells in which the embryos were incubated. Further investigation would have required significant time and financial investment, leaving the GDH assay as the only viable remaining option.

The GDH original protocol (despite numerous attempts) could not be successfully adapted towards a 96 well plate to plate reader format. Data generated was consistently uninterpretable and was not consistent with the standard curves that could be generated using the original protocol (data not shown). Here the major issue was most likely a failure to mix the reagents thoroughly in the smaller volumes necessary when working with 96 well plates. The original protocol necessitates that the reagents be mixed and their absorbance read quickly and in unison, presenting a challenge when faced with large samples numbers (96 compounds per plate) which are to be expected when developing assays based on industrial throughput expectations. One

suggestion might be to dialyse the GDH enzyme from the glycerol in which it is stored and reconstitute it in water. The reduction in viscosity would enable for easier and rapid mixing. Additionally, it may be possible to increase the volume of GDH added to enable easier pipette mixing.

Addition of AstraZeneca compounds suggest that ammonia excreted by embryos is detectable by the GDH assay (in the form of elevated Delta(A340) measurements when compared to negative controls) and therefore DMSO was not inhibiting the reaction. However, Delta(A340) levels were not significantly different from that displayed by the vehicle control (with the exception of NT1 and NT7). The lack of identifiable change in Delta(A340) between the test samples and the positive control suggests either the assay is not sensitive enough to detect a change in ammonia excretion (and therefore renal function), or that the AstraZeneca compounds are not toxic in the *X. laevis* system. NT1 and NT7 did give significantly different Delta(A340) readings when compared with vehicle controls, despite these compounds having been shown to be previously non-toxic in humans (hence there should be no change in renal function). Also, in both cases the Delta(A340) of NT1 and NT7 are significantly higher than the vehicle control, suggesting an increase in ammonia excretion and therefore an increase in renal function. These findings suggest that the AstraZeneca compounds may not be eliciting the same effect in the embryos as they are known to elicit in humans.

One possible future experiment is to further investigate the AstraZeneca nephrotoxic compounds Ne5 and Ne7, which lead to the death of the embryos before they could be sampled at embryonic stage 45. The phenotypes elicited before death displayed no visible signs of renal failure (such as edema) however

they may still have possibly arisen through nephrotoxicity. Screening these compounds on embryos at lower concentrations should improve survivability and potentially give rise to a detectable change in renal function. Unfortunately however even if this were shown to be the case failure to identify any change in renal function for 10 out of the 12 known nephrotoxic compounds is unacceptable for an assay of this nature, as it would imply the assays specificity is insufficient and would lead to the generation of numerous false negatives. The detection of the two non-toxic compound that were significantly different to the vehicle control also suggests that the assay also has the potential to generate false positive results. In summary, the *X. laevis* GDH ammonia detection renal function assay in its current form is not capable of detecting abnormal changes in renal function.

A possible reason for the failure to detect a change in renal function may be due to a fault in the model itself. Cruz *et al.*, (2013) noted that *X. laevis* excrete around 50% of ammonia via the skin and that both the ventral and dorsal skin were capable of generating an ammonia efflux (Cruz *et al.*, 2013). This could lead to a situation whereby ammonia levels in the media are maintained by diffusion through the skin despite renal function impairment. This may potentially explain the observations in which there is no reduction in ammonia concentrations and consequently can claim no reduction in renal function regardless of the actual functionality of the embryo pronephros. However Cruz *et al.*, (2013) conducted this research using adult *X. laevis* post metamorphosis frogs and it is not known to what extent *X. laevis* embryos at stage 45 excrete ammonia through their skin (as used in the renal function assay). This may require further investigation to determine if there is indeed a difference between adult and juvenile ammonia excretion via the skin before a conclusion can be

drawn in regards to its contribution towards the inability of the renal function assay to detect significant difference in ammonia excretion in renal functionally impaired embryos.

Another possible flaw with the *X. laevis* model and its application towards prediction of renal toxicity is that the pronephros is essentially a single nephron, whereas the adult human kidney is comprised of millions of nephrons (Vize, 2003). This suggests that the chronic toxic effects often associated with human renal toxicity cannot necessarily be replicated in the *X. laevis* embryos, as any toxicity directed towards the *X. laevis* pronephros may immediately generate renal failure. As such, the *X. laevis* renal function assay would only have been able to identify nephrotoxic compounds as being acute renal function inhibitors and would not be able to predict the possible chronic effects that might be elicited in humans. However as this assay would have been implemented early in preclinical trialling in drug development, it could act as an early warning system identifying those compounds that are potentially nephrotoxic and highlighting them as necessary of further investigation. The assay would avoid false negatives (a significant problem in drug development) and allow potentially nephrotoxic compounds to be screened in other renal toxicity assay systems much sooner than they would have if the assay were not available, saving time and financial investment.

A novel toxicity assay must be proven to be both specific and efficient if it is to be successful. In being specific it must be able to determine its endpoint accurately with minimal false positives or false negatives. In being efficient it must be able to make such specific measurements in a timely manner with minimal labour. The extent to which these two factors can be achieved with

maximum effectiveness is dependent on factors such as the endpoint determined by the assay, the availability of other competing assays and the phase in development in which it is implemented. Evidence provided here suggests that the proposed *X. laevis* renal function assay cannot reliably achieve either of these goals. Whilst this may be disappointing, the assay was shown to be functional and ammonia excreted could be detected. Further investigation through other ammonia detection methods in the future (such as using an ammonium electrode) may yield better results.

Chapter VII

7.0 Final conclusions and future directions

7.1 Final Conclusions

One of the primary aims of this thesis was to assess the applicability of the *X. laevis* model towards pharmaceutical drug development. The *X. laevis* model has proven itself to be a reliable and robust chemical genetic screening model, capable of rapidly identifying numerous hit compounds with potentially novel mechanisms of action. The NCI diversity set II compound screen was a success. Of the 1363 compounds screened, 72 hit compounds were identified that gave rise to numerous phenotypes of which the majority involved pigmentation abnormalities. Compounds that generate abnormal phenotypes involving pigmentation in *X. laevis* embryos such as those presented in this thesis have previously been suggested to indicate potential therapeutic applications towards melanoma (Tomlinson et al., 2009b; White et al., 2011), either directly through the compound itself or the target or pathway through which it was acting. The NCI diversity set II screen would appear to support this as 13 compounds identified in the NCI diversity set II compound screen presented statistically significantly lower percentage cell viability IC50s in the A375 melanoma cell line when compared to the non-melanoma controls. These compounds strongly support the capability of our screening strategies to rapidly identify compounds with potentially novel therapeutic applications towards the treatment of melanoma. In addition, due to the structural diversity inherent in the NCI diversity set II compound library it is likely that all compounds identified

operate through different targets or pathways thereby further increasing the value of those compounds identified.

The addition of chemoinformatic analysis also significantly improved the value of the screen. Forward chemical genetic screens such as these typically stall when attempting to identify a hit compounds mechanism of action, particularly when the screened compounds have little or no known previous biological information. *In silico* predictions such as those generated by the Bender group (in collaboration with ourselves) have enabled us to rapidly identify both known and potentially novel predicted targets that may pose as novel therapeutic targets for the treatment of melanoma. Importantly these predictions do not only suggest targets for each of the individual hit compounds identified, but go further by predicting those targets which are commonly associated with a particular *X. laevis* phenotype generated. The replication of abnormal pigmentation and abnormal melanophore migration phenotypes (by screening alternative compound antagonists) validated 6 of the 10 abnormal melanophore migration phenotype predicted targets. This supports the accuracy of the chemoinformatic analysis and gives us encouragement that other predicted targets for both individual compounds and phenotypic categories have value and are worth exploring. The identification of two targets that have no known previous link to melanoma (RSK3 and PD3EB) suggest that this chemoinformatic prediction strategy is an effective method for identifying potentially novel targets with therapeutic applications towards the treatment of melanoma. Importantly, the majority of NCI compounds shown to give a statistically significantly lower IC₅₀ in the A375 melanoma cell line when compared to non-melanoma controls have also been predicted to interact with the abnormal melanophore migration predicted targets, suggesting that these

compounds may be eliciting their phenotypes through these same predicted targets. This suggests that not only have we predicted potentially novel targets with therapeutic application towards melanoma (which have already begun to be validated biologically), but also we have identified several structurally diverse compounds that have been shown to reduce melanoma cell viability that are likely to be acting through these same targets. By effectively developing both the prediction of targets and the assessment of hit compounds on melanoma cell viability simultaneously, we have rapidly generated nine structurally diverse compounds that reduce melanoma cell viability through potentially novel targets or have the potential to be acting through known targets with as of yet undefined efficacy (which may potentially be better than other inhibitors currently available).

In conclusion, the *X. laevis* chemical genetic screening model system we have implemented has proven itself to be capable of rapidly identifying numerous hit compounds, that in combination with appropriate cell based assays and chemoinformatics have generated several compounds and targets with potentially novel therapeutic applications towards the treatment of melanoma. As such the *X. laevis* chemical genetic system has proven itself to excel as a robust screening model, which in combination with appropriate supporting assays and chemoinformatical analysis has strong potential to contribute towards drug discovery.

The second primary aim of my thesis was to assess the applicability of the *X. laevis* model towards drug development by developing a renal function toxicity assay. Preliminary experiments with the renal function assay were initially promising. Unfortunately however recent data suggests that it is not capable of

detecting abnormal renal function in *X. laevis* embryos. Ammonia excreted from the embryos was detectable from embryonic stage 38 onwards and therefore supported the literature as being the stage in development at which the pronephros becomes functional (Jones, 2005). However significant setbacks such as the inhibition of the salicylic acid assay by DMSO and the failure to detect any change in renal function when exposed to nephrotoxic compounds in the GDH assay have severely stunted the development of this assay. It may be that the GDH was not sensitive enough to detect a significant change in renal function or that the compounds did not exhibit the same effects in the *X. laevis* model as they have been shown to in humans. The specific mechanism of action for each of the nephrotoxic compounds is not known, and so it is difficult to determine whether the lack of toxicity is due to specific inter-species differences.

Further work is required (as discussed previously) before the assay can progress further towards implementation in larger scale experiments. At this moment in time, whilst the assay remains an interesting and a potentially promising concept, it is not yet capable of contributing towards drug development.

7.2 Future considerations

The *X. laevis* screening strategy has proven itself to be highly amenable in its application towards drug discovery. However there are numerous areas in which further investigation would aid in validating the model as a chemical genetic screening organism. One particular concern when screening with aquatic organisms is that whilst it is convenient to simply add dosed compounds into the

embryos media as the primary route of exposure, it is not clear exactly what dose of the compound actually enters the *X. laevis* system. In adult organisms a primary route of exposure to xenobiotics is either orally or through uptake in the lungs or gut. The *X. laevis* embryos do not start feeding until embryonic stage 45 (at which point they are considered to be sentient) and therefore all uptake of xenobiotics must come through either passive diffusion or active uptake until the gills open at embryonic stage 40. It is unlikely that all compounds administered enter the *X. laevis* system at the same rate. Therefore it is difficult to say with certainty at what concentration a phenotype may be elicited. For the same reasons, penetration and distribution of the compounds around the *X. laevis* embryos system are equally unknown. A possible solution to this (if accurate embryonic system compound concentrations are required) may be to take embryo samples and analyse them using mass spectrometry. Further work into this may help in further understanding how capable different compounds are taken up by *X. laevis* embryos from the media, allowing us to make educated predictions based on compound structure as to whether a compound is likely to penetrate the embryo system or whether it will struggle to be taken up.

A further consideration with dosing embryos via media is that some compounds precipitate when administered. This is particularly relevant, as often some compounds in a library will precipitate and often this is unavoidable. Many of these compounds still elicit a phenotype, however it is not yet known what effect this has on *X. laevis* embryo uptake or what influences it might have on the phenotype presented. Personal observation suggests that precipitated compounds may lead to blistering in embryos. By developing the mass spectrometry technique suggested previously it may be possible to better understand the role precipitation has towards generating phenotypes.

In the future, visual scoring of the embryos phenotypes during the *Xenopus* screen may benefit from adopting approaches used during histopathology scoring. Terms used in the description of phenotypes during our screen included “mild, moderate and severe”. Such terms can reduce inter-observer repeatability over time, as their use is dependent on the observer’s opinion (Gibson-Corley et al., 2013). A better system would include a more quantitative approach. This could be achieved by described the percentage of pigmentation missing (when compared to a control) as a more specific measure of pigmentation loss. Such a process would increase throughput time of observing the embryos but would lead to more robust characterisation of phenotypes observed.

To improve the scoring system further we have begun to implement automated *X. laevis* phenotype recognition software. In collaboration with the Bender laboratory, we have developed a programme that is capable of detecting and categorising specific abnormal pigmentation phenotypes from images of *X. laevis* embryos (Drakakis, 2014) (see attached publication). The development of such an automated system enables the standardisation of identified phenotypes and removes any potential experimenter bias when screening by eye. Implementation of this programme may improve the hit rate of identified phenotypes in future screens.

Future work concerning those hit compounds from our screen that statistically significantly lowered IC50 cell viabilities in the A375 melanoma cell line when compared to controls will include the further assessment of their effect on different melanoma and control cell lines. This is important, as many cancers show large genetic variability (particularly melanoma) and as such it is important

that a potential therapeutic compound presents a desirable effect in several lines to predict its potential towards treating the wider population. As mentioned previously it will be necessary to assess these compounds using additional assays (such as the scratch or TUNEL assay) to better understand whether the decrease in observed cell viability is due to an increase in apoptosis or a decrease in proliferation.

Additional future characterisation of the identified compounds might include the use of three dimensional cell culture modelling. Such assays are more relevant towards *in vivo* systems as they attempt to replicate the three dimensional environment of a tissue or organ. For example, 3D invasion assays culture cancer cells on a layer of Matrigel in the presence of a compound. The ability of the compound to reduce metastasis is measured by the cells ability to migrate through the gel. This is particularly relevant to cancers such as melanoma given its aggressive metastatic nature. This assay would therefore help greatly in the characterisation of the identified hit compounds identified in the *Xenopus* screen and evaluate their therapeutic potential. Should the compounds give positive results in these additional assays, the next stage would be to assess the compounds using xenograft models (White et al., 2011). In these *in vivo* assays, immune compromised mice are transplanted with human melanoma cells. The mice subsequently grow humanised melanomas, and the ability of the identified lead compound to treat the tumours are assessed. Compounds are administered for a set number of doses at different concentrations. Success of the compound in treating the tumour is assessed by measuring the reduction of tumour size or inhibition of growth (White et al., 2011). If the compounds give promising results in both the *in vitro* and *in vivo* assays it would then be worth approaching a pharmaceutical company to continue the evaluation of the

compounds on an industrial scale and begin pushing the compounds towards clinical trials and ultimately regulatory approval.

It is notable that a large number of the phenotypes observed during the screen involve pigmentation. This may represent an inherent bias in the screen itself, whereby pigmentation is the most easily characterised and observed phenotype when embryos are scored visually. This may mean that less easily observed phenotypes (such as those involving specific organ function or development) may be missed under the current screening regime. As the primary focus of this screen has been directed towards identifying potential lead compounds for melanoma treatment, which derives from the melanocytes observed, this bias should not affect the assay in a detrimental way. As a screening system for identifying compounds for the treatment of melanoma, the current format has been shown to have a decent success rate (as shown by the discovery of leflunamide and potentially those compounds identified in this screen) (White et al., 2011).

It may be that the melanocytes themselves however are more sensitive to this screening assay system than other cell types. The neural crest cells begin specifying at around embryonic stage 15, the same stage at which the compounds are dosed. This may mean that they are at a more sensitive time during their development and compound exposure may make it more likely that they fail to differentiate into the melanocytes. This possibility could be investigated by whole mount *in situ* hybridisation. By staining for neural crest cell/melanocyte specific markers it will be possible to detect the presence of either the neural crest cell or the melanocytes, allowing us to comment further

on the likelihood that the neural crest cells are more sensitive to this form of screening assay.

The phenotypes described in this assay are developmental in nature. It could be asked as to whether a developmentally derived phenotype is translatable to a disease phenotype setting. Given the success of this screening strategy in the past with the discovery of Leflunomide, and the large number of pigmentation effecting compounds identified in this screen that were predicted to interact with therapeutic targets previously identified in melanoma, it would appear that our *Xenopus* screening system is relevant towards melanoma development.

Concerning the chemoinformatical predictions, experiments looking to further validate abnormal melanophore migration predicted targets by genetic knock down are currently being planned using a CRISPR/Cas9 system (Auer et al., 2014). If the same phenotype is observed in the *Xenopus* knockdowns as had been previously with the NCI compounds, this would suggest that the predicted target is correct. This will go some way to validating the original predictions and give us faith in the accuracy of other predictions in this analysis that have not yet been investigated. We also hope to investigate targets predicted for other phenotypic categories involving pigmentation, in the hope that they might also present promising novel targets for the treatment of melanoma.

The specificity of the compounds themselves may also be assessed by ectopically expressing their targets. This would be particularly useful for those compounds that are predicted to bind to multiple targets. For example, a compound is predicted to bind to targets A and B. If target A is ectopically expressed in the presence of the compound and the phenotype is present, this

would suggest that target A is not responsible for generating the phenotype and therefore imply target B is the correct target. If target B is then ectopically expressed in the presence of the compound and no phenotype is presented, this would further imply target B is responsible for the observed effect. It is likely however that some compounds may be eliciting their phenotype through several targets. In this instance, careful planning will be required to elucidate which targets in combination generate the observed effect (Dar et al., 2012).

There are few mutant lines available from which to explore the predicted target compounds identified. Interestingly, the MOA mutant zebrafish line (maco^{tt261/tt261}) has been shown to induce abnormal melanocyte development. As of yet, no *Xenopus* mutant lines are available from which to further explore any of the predicted targets.

A final future experiment concerning the *X. laevis* application towards drug discovery is to repeat the screen using different endpoints (i.e. not focusing on pigmentation), and see whether appropriate follow up assays and similar chemoinformatical analysis can identify promising lead compounds and targets in a similar manner to those discovered in this screen (Brandli, 2004; Kalin et al., 2009). Developing the *X. laevis* system to encompass different endpoints may require the generation of mutant lines to create specific disease models. Whilst *X. laevis* may not be easily amenable to genetic manipulation, the closely related model *X. tropicalis* already has numerous mutant lines readily available. As the application of *X. tropicalis* towards chemical genetic screening has been shown in this thesis to be promising, it may be prudent to begin evaluating their further use in drug discovery chemical genetic screens.

As discussed previously, the *X. laevis* renal function toxicity assay does not in its current form appear to be capable of accurately detecting change in renal function in response to nephrotoxic compounds. This is unfortunate as clearly ammonia excretion could be detected. It may be possible to use the assay however as a model for renal function outside of the context of drug development. For example, it has been shown through *in situ* hybridisation that megalin, LRP2 and cublin are highly expressed in the *Xenopus* proximal tubule. By genetic knock out it would be possible using the renal function toxicity assay to determine if any of these proteins impair renal function once removed (Christensen et al., 2008). If the assay can detect a change in renal function then its use as an assay for the detection of renal function impairment may have use in an academic setting.

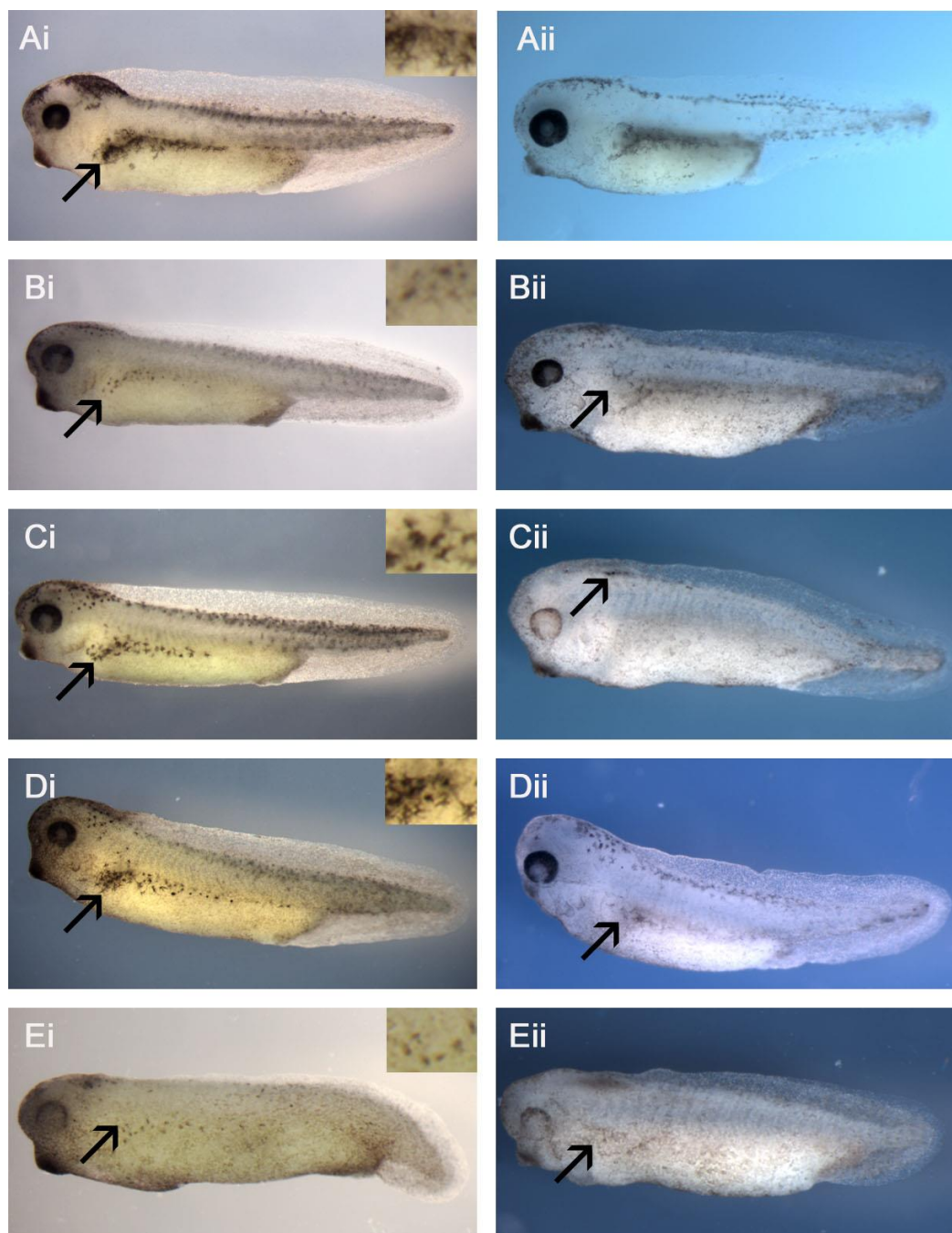
In the future it may be prudent to consider other toxicity assays using the *Xenopus* focusing on alternative organ systems. Other possible assays include exploring liver toxicity, structural cardio toxicity and macrophage infiltration. All of these suggestions would require the development of a system in the *X. laevis* whereby an endpoint could be measured as a marker of toxicity. The assay would have to be both reliable and high throughput and would require significant trialling and development time, but may one day potentially be of benefit towards drug development.

Appendix I



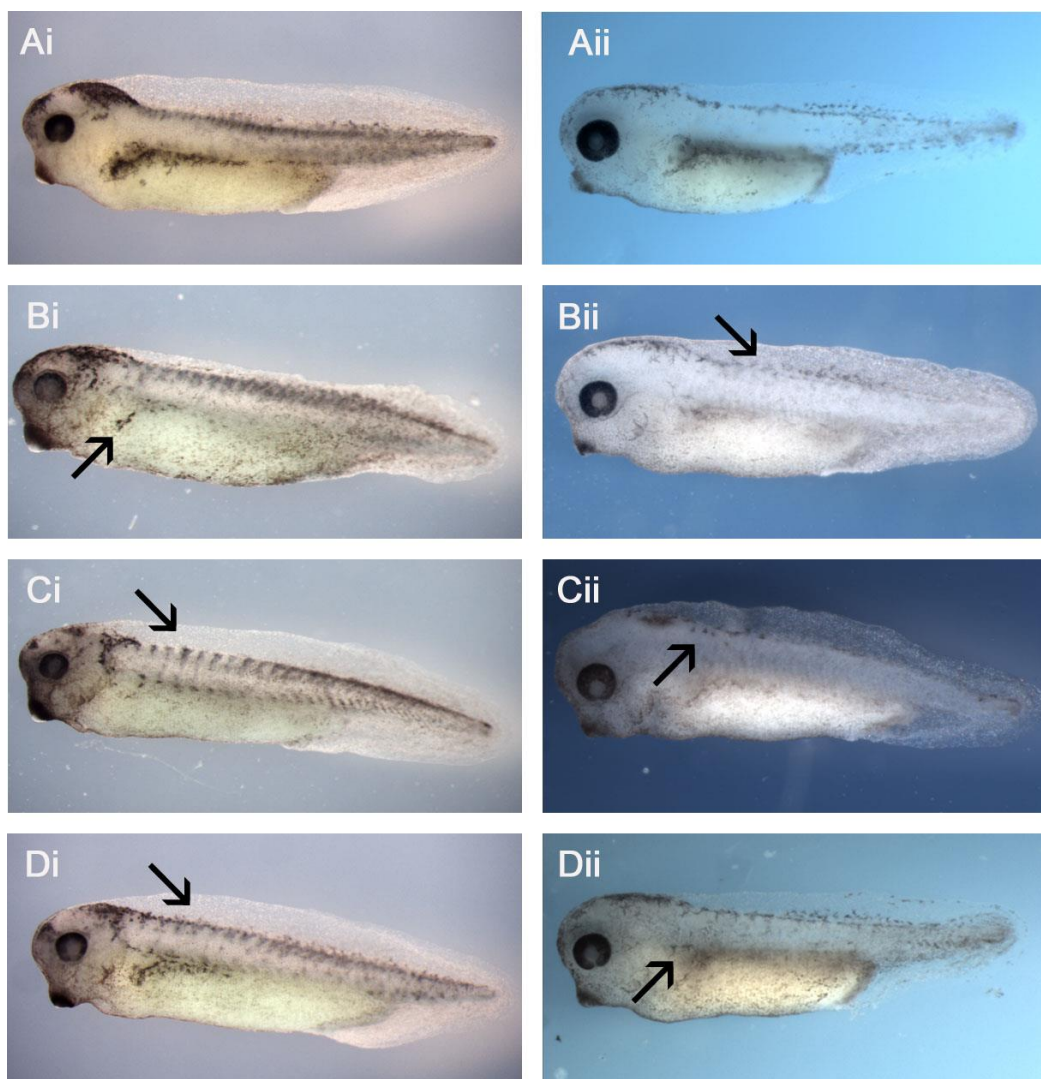


Appendix I Figure 1. Side by side comparison of NCI compounds identified in the NCI diversity set I compound screen that gave rise to a similar prominent abnormal pigmentation phenotype when assessed at stage 38 (when compared to the DMSO vehicle control) in both *X. laevis* and *X. tropicalis*. Ai. *X. laevis* DMSO solvent control. Aii. *X. tropicalis* DMSO solvent control. Bi. *X. laevis* NCI 7734. Bii. *X. tropicalis* NCI 7734. Ci. *X. laevis* NCI 30712. Cii. *X. tropicalis* NCI 30712. Di. *X. laevis* NCI 47938. Dii. *X. tropicalis* NCI 47938. Ei. *X. laevis* NCI 62406. Eii. *X. tropicalis* NCI 62406. Fi. *X. laevis* NCI 86153. Fii. *X. tropicalis* NCI 86153. Gi. *X. laevis* NCI 99676. Gii. *X. tropicalis* NCI 99676. Hi. *X. laevis* NCI 130830. Hii. *X. tropicalis* NCI 130830. Ii. *X. laevis* NCI 132230. Iii. *X. tropicalis* NCI 132230. Ji. *X. laevis* NCI 158011. Jii. *X. tropicalis* NCI 158011. Ki. *X. laevis* NCI 164990. Kii. *X. tropicalis* NCI 164990. Li. *X. laevis* NCI 186066. Lii. *X. tropicalis* NCI 186066.

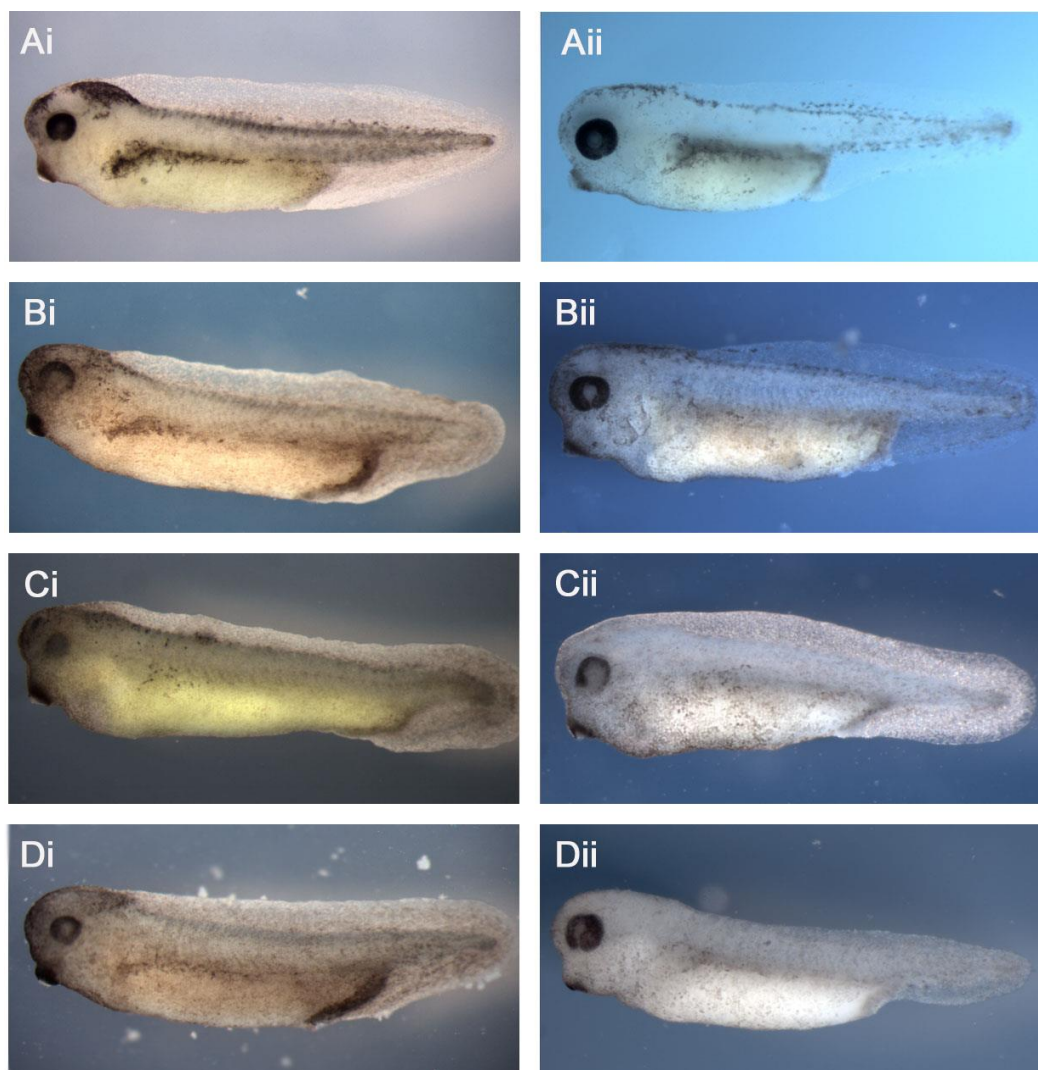


Appendix I Figure 2. Side by side comparison of NCI compounds identified in the NCI diversity set I compound screen that gave rise to a similar prominent melanophore morphology phenotype when assessed at stage 38 (when compared to the DMSO vehicle control) in both *X. laevis* and *X. tropicalis*. Ai. *X. laevis* DMSO solvent control. Aii. *X. tropicalis* DMSO solvent control. Bi. *X. laevis* DMSO solvent control. Bii. *X. tropicalis* DMSO solvent control. Ci. *X. laevis* DMSO solvent control. Cii. *X. tropicalis* DMSO solvent control. Di. *X. laevis* DMSO solvent control. Dii. *X. tropicalis* DMSO solvent control. Ei. *X. laevis* DMSO solvent control. Eii. *X. tropicalis* DMSO solvent control.

laevis NCI 17173. Bii. *X. tropicalis* NCI 17173. Ci. *X. laevis* NCI 80126. Cii. *X. tropicalis* NCI 80126. Di. *X. laevis* NCI 227147. Dii. *X. tropicalis* NCI 227147. Ei. *X. laevis* NCI 609699. Eii. *X. tropicalis* NCI 609699.



Appendix I Figure 3. Side by side comparison of NCI compounds identified in the NCI diversity set I compound screen that gave rise to a similar prominent melanophore migration phenotype when assessed at stage 38 (when compared to the DMSO vehicle control) in both *X. laevis* and *X. tropicalis*. Ai. *X. laevis* DMSO solvent control. Aii. *X. tropicalis* DMSO solvent control. Bi. *X. laevis* NCI 22207. Bii. *X. tropicalis* NCI 22207. Ci. *X. laevis* NCI 84093. Cii. *X. tropicalis* NCI 84093. Di. *X. laevis* NCI 210627. Dii. *X. tropicalis* NCI 210627.



Appendix I Figure 4. Side by side comparison of NCI compounds identified in the NCI diversity set I compound screen that gave rise to a similar prominent eye development phenotype when assessed at stage 38 (when compared to the DMSO vehicle control) in both *X. laevis* and *X. tropicalis*. Ai. *X. laevis* DMSO solvent control. Aii. *X. tropicalis* DMSO solvent control. Bi. *X. laevis* NCI 101984. Bii. *X. tropicalis* NCI 101984. Ci. *X. laevis* NCI 143019. Cii. *X. tropicalis* NCI 143019. Di. *X. laevis* NCI 638432. Dii. *X. tropicalis* NCI 638432.

Appendix II

Appendix II Table 1. Collated dose response data in which embryos were exposed to hit compounds identified in the NCI diversity set II compound screen over a range of concentrations. Amount of embryos per well ($n=20$) which displayed a prominent phenotype at each concentration are displayed as a percentage of total embryos alive when assessed at stage 38 (1 = 100%). B, (blistering phenotype). E, (Edema phenotype). ED, (eye development phenotype). P, (abnormal pigmentation phenotype). M, (abnormal morphology phenotype). Mg, (Abnormal melanophore migration phenotype). MM, (abnormal melanophore morphology phenotype). PD, (Percentage death). S, (stunted growth).

	Conc (μM)	M	S	P	MM	Mg	E	ED	B	PD
NCI 3001	0.1	0.05	0	0	0	0	0	0.05	0	0
	1	0.05	0	0	0	0	0	0.05	0	0
	10	0.05	0	0	0	0	0	0.05	0	0
	25	0.2	0	0	0	0	0	0.1	0	0
	50	0.15	0	0	0	0	0	0.1	0	0
	100	0	0	0	0	0	0	0.15	0	0
NCI 4292	0.1	0	0	0	0	0	0	0	0	0
	1	0	0	0	0	0	0	0	0	0
	10	0	0	0	1	0	0	0	0	0
	25	0	0	0	1	0	0	0	0	0

	50	0	0	0	1	0	0	0	0	0
	100	0	0	0	1	0	0	0	0	0
		<hr/>								
	0.1	0	0	0	0	0	0	0	0	0
	1	0	0	0	0	0	0	0	0	0
	10	0	0	0	0	0	0	0	0	0
NCI 5907	25	0	0	0	0	0	0	0	0	0
	50	0	0	0	0.25	0	0	0	0	0
	100	0	0	0	0	0	0	0	0	0
		<hr/>								
	0.1	0	0	0	0	0	0	0	0	0
	1	0	0	0	0	0	0	0	0	0
	10	0	0	1	0	0	0	0	0	0
NCI 9358	25	1	0	1	0	0	0	0	0	0
	50	1	0	1	0	0	0	0	0	0
	100	0	0	0	0	0	0	0	0	0
		<hr/>								
	0.1	0	0	0	0	0	0	0	0	0
	1	0	0	0	0	0	0	0	0	0
	10	0	0	1	0	0	0	0	0	0
NCI 11624	25	0	1	0	0	0	1	0	0	0
	50	0	1	0	0	0	1	0	0	0
	100	0	1	0	0	0	1	0	0	0
		<hr/>								
	0.1	0	0	0	0	0	0	0	0	0
	1	0	0	0	0	0	0	0	0	0

	10	0	0	0	0	1	0	0	0	0
NCI 12588	25	0	0	1	1	0	0	0	0	0
	50	0	0	1	0	0	0	0	0	0
	100	0	0	1	0	0	0	0	0	0
	<hr/>									
	0.1	0	0	0	0.85	0	0	0.85	0	0.15
	1	0.1	0	0	1	1	0	1	0	0
	10	0	0	0	1	1	0	1	0	0
NCI 13156	25	0	0	0	1	1	0	1	0	0
	50	0.2	0	0	1	1	0	1	0	0
	100	0	0	0	0	1	1	0	0	0
	<hr/>									
	0.1	0	0	0	1	0	0	0	0	0
	1	0	0	0	1	0	0	0	0	0
	10	1	0	0	1	0	0	0	0	0
NCI 13653	25	1	0	0	1	0	0	0	0	0
	50	1	0	1	1	0	0	1	0	0
	100	0	1	1	0	0	0	0	0	0
	<hr/>									
	0.1	0	0	0	1	0	0	0	0	0
	1	1	0	0	1	1	0	0	0	0
	10	1	0	0	1	0	1	0	0	0
NCI 14380	25	0	0	0	0	0	0	0	0	1
	50	0	0	0	0	0	0	0	0	1
	100	0	0	0	0	0	0	0	0	1
	<hr/>									

	0.1	0	0	0	0	0	0	0	0	0
	1	0	0	0	0	1	0	0	0	0
	10	0	0	0	0	1	0	0	0	0
NCI 19219	25	0	1	0	0	0	0	0	0	0
	50	0	1	0	0	0	0	0	0	0
	100	0	1	0	0	0	0	0	0	0

	0.1	0	0	0	0	0	0	0	0	0
	1	0	0	0	0	0	0	0	0	0
	10	0	0	1	0	0	0	0	0	0
NCI 20618	25	1	0	1	0	0	0	0	0	0
	50	1	0	1	0	0	0	0	0	0
	100	0	0	0.8	0	0	0	0	0	0.2

	0.1	0	0	0	0	0	0	0.05	0	0
	1	0	0	0	1	0	0	0	0	0
	10	0	0	0	1	0	0	0	0	0
NCI 20619	25	0	0	1	0	0	0	0	0	0
	50	0	0	0.95	0	0.05	0	0	0	0
	100	0	0	1	0	0	0	0	0	0

	0.1	0	0	0	0	0	0	0	0	0
	1	0	0	0	0	0	0	0	0	0
	10	1	0	0	0	0	0	0	1	0
NCI 21683	25	0	1	0	0	0	0	0	1	0
	50	0	1	0	0	0	0	0	1	0

	100	0	1	0	0	0	0	0	1	0
	0.1	0	0	0	0	0	0	0	0	0
	1	0	0	0	0	0	0	0	0	0
	10	0	0	0	0.7	0.5	0	0	0	0
NCI 30930	25	0	0	0	1	1	0	0.75	0	0
	50	0	0.3	0	0	0	0	0	0	0
	100	0	0	0	0	0	0	0	0	1
	0.1	0	0	0	0	0	0	0	0	0
	1	0	0	0	0	0	0	0	0	0
	10	0	0	0	1	1	0	0	0	0
NCI 31703	25	0	0	0	1	1	0	0	0	0
	50	0	0	0	1	1	0	0	0	0
	100	0	0	0	1	1	0	0	0	0
	0.1	0	0	1	0	0	0	0	0	0
	1	0	0	0	0	0	0	0	0	0
	10	0	0	0	0	0	0	0	0	0
NCI 31762	25	0	0	0	0	1	0	0	0	0
	50	0	0	0	0	0	0	0	0	0
	100	0	0	0	0	0	0	0	0	0
	0.1	0	0	0	0	0	0	0	0	0
	1	0	0	0	1	0	0	0	0	0
NCI 34871	10	0	0	0	0.5	0	0	0	0	0

	25	0	0	0	1	0	0	0	0	0
	50	0	0	0	1	0	0	0	0	0
	100	0	0	0	1	0	0	0	0	0
		<hr/>								
	0.1	0	0	0	1	1	1	0	0	0
	1	0	0	0	1	1	0	0	0	0
	10	1	0	1	0	0	0	1	0	0
NCI 36525	25	1	0	1	0	0	0	1	0	0
	50	1	0	1	0	0	0	1	0	0
	100	0	0	1	0	0	0	1	0	0
		<hr/>								
	0.1	0	0	0	0	0	0	0	0	0
	1	0.05	0	0	0	0	0	0	0	0
	10	0.05	0	0	0	0	0	0	0	0
NCI 42028	25	0	0	0	0	0	0	0	0	0
	50	0	0	0	0	0	0	0	0	0
	100	0	0	0	0	0	0	0	0	0
		<hr/>								
	0.1	0	0	1	0	0	0	0	0	0
	1	0	0	1	0	0	0	0	0	0
	10	0	0	1	0	0	0	0	0	0
NCI 43013	25	1	0	1	0	0	0	0	0	0
	50	1	0	1	0	0	0	0	0	0
	100	0	0	1	0	0	0	0	0	0
		<hr/>								
	0.1	0	0	0	0	0	0	0	0	0

	1	0	0	0	0	0	0	0	0	0
	10	0	0	0	0	0	0	0.05	0	0
NCI 45536	25	0	0	0	1	0	0	0	0	0
	50	0.05	0	0	1	0	0	0	0	0
	100	0	0	0	1	0	0	0	0	0

	0.1	0	0	0	0	0	0	0	0	0
	1	0	0	0	0	0	0	0	0	0
	10	0	0	0	0	0	0	0	0	0
NCI 45545	25	0	0	0	0	0	0	0	0	0
	50	0	0	0	0.3	0	0	0	0	0
	100	0	0	0	0.8	0	0	0	0	0

	0.1	0	0	0	0	1	0	0	0	0
	1	0	0	0	0	1	0	0	0	0
	10	0	0	0	0	1	0	0	0	0
NCI 45572	25	0	0	0	0	1	0	0	0	0
	50	0	0	0	0	1	0	0	0	0
	100	0	0	0	0	1	0	0	0	0

	0.1	0.1	0	0	0	0	0	0	0	0
	1	0.05	0	0.05	0	0	0	0	0	0
	10	0	0	0.05	0	0.05	0	0	0	0
NCI 59620	25	0	0	0	0	0	0	0	0	0
	50	0.1	0	0	0	0	0	0	0	0
	100	0	0	0	0	0	0	0	0	0

	0.1	1	0	0	0	0	1	0	0	0
	1	0.05	0	0	0	0	0	0	0	0
	10	0	0	0	0	0	0.05	0	0	0
NCI 62609	25	1	0	0	1	0	0.1	1	0	0
	50	1	0	0	1	0	1	1	1	0
	100	0	0	1	0	0	1	1	1	0
	0.1	0	0	0	0.1	0	0	0	0	0
	1	0	0	0	0	0	0	0	0	0
	10	0	0	0	0	0	0	0	0	0
NCI 62611	25	0	0	0	0.35	0	0	0	0	0
	50	0	0	0	1	0	0	0	0	0
	100	0	0	0	0.95	0	0	0	0	0
	0.1	0	0	0	0.85	0	0	0	0	0
	1	0	0	0	0	1	0	0	0	0
	10	1	0	0	0	1	0	1	0	0
NCI 66020	25	1	0	0	1	1	0	1	0	0
	50	1	0	0	1	1	0	1	0	0
	100	0	0	1	1	1	0	1	0	0
	0.1	0.05	0	0	0.05	0	0	0	0	0
	1	0	0	0	0	0	0	0	0	0
	10	0	0	0	0.05	0	0	0	0	0
NCI 68971	25	0	0	0	0.1	0	0	0	0	0

	50	1	0	0	0	0	0	0	0	0
	100	0	0	0	0	0	0	0	0	0
		<hr/>								
	0.1	0	0	1	0	0	0	0	0	0
	1	0	0	0	1	0	0	0	0	0
	10	0	0	0	1	0	0	0	0	0
NCI 79253	25	0	0	1	0	0	0	0	0	0
	50	0	0	1	0	0	0	0	0	0
	100	0	0	1	0	0	0	0	0	0
		<hr/>								
	0.1	0	0	0	0	0	0	0	0	0
	1	0	0	0	0	0	0	0	0	0
	10	0	0	0	0	0	0	0	0	0
NCI 85326	25	0	0	1	0	0	0	0	0	0
	50	0	0	1	0	0	0	0	0	0
	100	0	1	1	0	0	0	0	0	0
		<hr/>								
	0.1	0	0	0	0	0	0	0	0	0
	1	0	0	0	0	0	0	0	0	0
NCI 87084	10	0	0	0	0	0	0	0	0	0
	25	0	0	0	1	0	0	0	0	0
	50	0	0	0	1	1	0	0	0	0
	100	0	0	0	0	0	0	0	0	1
		<hr/>								
	0.1	0	0	0	0	0	0	0	0	0
	1	0	0	0	0	0	0	0	0	0

	10	0	0	0	0	0	0	0	0	0
NCI 88916	25	0	0	0	0	0	0	0	0	0
	50	0	0	0	0	1	0	0	0	0
	100	0	0	0	1	1	0	0	0	0

	0.1	0	0	0	0	0	0	0	0	0
	1	0	0	0	0	1	0	0	0	0
	10	0	0	0	0	1	0	0	0	0
NCI 92784	25	0	0	0	1	1	0	0	0	0
	50	1	0	1	0	0	0	0	0	0
	100	0	0	1	0	0	0	0	0	0

	0.1	0	0	0	0	0	0	0	0	0
	1	0	0	0	0	0	0	0	0	0
	10	0.05	0	1	0	0	0	0	0	0
NCI 99657	25	0.1	0	1	0	0	0	0	0	0
	50	0.1	0	1	0	0	0	0	0	0
	100	0	0	1	0	0	0	0	0	0

	0.1	0.1	0	0	0	0.2	0	0	0	0
	1	0	0	0.2	0	0	0	0	0	0
	10	0	0	0	0	1	0	0	0	0
NCI 99660	25	0	0	0.95	0.95	0.95	0	0	0	0.05
	50	0.1	0	1	0	0	0	0	0	0
	100	0	0	1	0	0	0	0	0	0

	0.1	0.05	0	0	0	0.7	0	0	0	0
	1	0	0	0	1	1	0	0	0	0
	10	0	0	0	1	1	0	0	0	0
NCI 104993	25	1	0	0	1	1	0	0	0	0
	50	1	0	1	0	0	0	0	0	0
	100	0	0	0	0	0	0	0	0	0

	0.1	0.05	0	0	0	0	0	0	0	0
	1	0.1	0	0	0	0	0	0	0	0
	10	0.05	0	0	0	0	0	0	0	0
NCI 106581	25	0.15	0	0	0	0	0	0	0	0
	50	0.1	0	0	0	0	0	0	0	0
	100	0	0	0	0	0	0	0	0	0

	0.1	0	0	1	1	1	0	0	0	0
	1	0	0	1	1	1	0	0	0	0
	10	0	0	1	1	1	0	0	0	0
NCI 111848	25	0	0	1	0	0	0	0	0	0
	50	0	0	1	0	0	0	0	0	0
	100	0	0	1	0	0	0	0	0	0

	0.1	0.15	0	0	0	0	0	0	0	0
	1	0	0	0	0	0	0	0	0	0
	10	0.1	0	0	0	0.2	0	0	0	0
NCI 117741	25	0.05	0	1	0	1	0	0	0	0
	50	0	0	1	1	1	0	0	0	0

	100	0	0	1	0	0	0	0	0	0
	0.1	0	0	0	0	0	0	0	0	0
	1	0	0	0	0	1	0	0	0	0
	10	0	0	0	0	1	0	0	0	0
NCI 130872	25	1	0	1	0	0	0	0	0	0
	50	1	0	1	1	1	0	0	0	0
	100	0	0	1	0	0	0	1	0	0
	0.1	0.05	0	0	0	0	0	0	0	0
	1	0.05	0	0	0	0	0	0	0	0
	10	0	0	1	1	0	0	0	0	0
NCI 131982	25	0	0	1	0	0	0	0	0	0
	50	0.15	0	1	0	0	0	0	0	0
	100	0	0	1	0	0	0	0	0	0
	0.1	0	0	0	0	0	0	0	0	0
	1	0	0	0	0	0	0	0	0	0
	10	0	0	1	1	0	0	0	0	0
NCI 131986	25	0.05	0	1	0	0	0	0	0	0
	50	0	0	1	0	0	0	0	0	0
	100	0	0	1	0	0	0	0	0	0
	0.1	0	0	0	0	0	0	0	0	0
	1	0	0	0	0	0	0	0	0	0
NCI 133002	10	0	0	0	0	0	0	0	0	0

	25	0	0	0	1	0	0	0	0	0
	50	0	0	0	1	0	0	0	0	0
	100	0	0	0	1	1	0	0	0	0
<hr/>										
	0.1	0	0	0	0	0	0	0	0	0
	1	0	0	0	0	0	0	0	0	0
	10	0	0	0	0	1	0	0	0	0
NCI 135810	25	0	0	1	0	0	0	0	0	0
	50	0	0	1	0	0	0	0	0	0
	100	0	0	1	0	0	0	0	0	0
<hr/>										
	0.1	0	0	0	0	1	0	0	0	0
	1	0	0	0	0	1	0	0	0	0
	10	0	0	0	0	0	0	0	0	0
NCI 138398	25	0	0	0	0	1	0	0	0	0
	50	0	0	0	0	0	0	0	0	0
	100	0	0	0	0	0	0	0	0	0
<hr/>										
	0.1	0	0	0	1	1	0	0	0	0
	1	0	0	0	1	1	0	0	0	0
	10	1	0	0	0	0	0	1	0	0
NCI 139021	25	1	0	1	0	0	0	0	0	0
	50	1	0	1	0	0	0	0	0	0
	100	0	0	1	0	0	0	0	0	0

	0.1	0	0	0	0	0	0	0	0	0
	1	0	0	0	1	1	0	0	0	0
	10	1	0	0	0	0	0	0	0	0
NCI 150982	25	1	0	0	0	0	0	0	0	0
	50	0	0	0	0	0	0	0	0	1
	100	0	0	0	0	0	0	0	0	1

	0.1	0	0	0	1	0	0	0	0	0
	1	0	0	0	1	0	0	0	0	0
	10	0	0	0	0	1	0	0	0	0
NCI 151262	25	0	1	0	0	0	0	0	0	0
	50	0	1	0	0	0	0	0	0	0
	100	0	1	0	0	0	0	0	0	0

	0.1	0.05	0	0.6	0	0	0	0	0	0
	1	0.3	0	0	0	0	0	0	0	0
	10	0.2	0	0	1	0	0	0	0	0
NCI 153792	25	0.15	0	0	1	0	0	0	0	0
	50	0	0	0	1	0	0.15	0	0	0
	100	0	0	0	1	0	0	0	0	0

	0.1	0	0	0	0	0	0	0	0	0
--	-----	---	---	---	---	---	---	---	---	---

	1	0	0	0	0	0	0	0	0	0
	10	0	0	0	0	0	0	0	0	0
NCI 154718	25	0	0	0	1	0	0	0	0	0
	50	1	0	0	1	1	0	0	0	0
	100	0	1	1	0	0	0	0	1	0

	0.1	0	0	1	1	0	0	0	0	0
	1	0	0	1	1	0	0	0	0	0
	10	0	0	1	0	0	0	0	0	0
NCI 164965	25	0	0	1	0	0	0	0	0	0
	50	0	0	1	0	0	0	0	0	0
	100	0	0	1	0	0	0	0	0	0

	0.1	0	0	0	0	0	0	0	0	0
	1	0	0	0	0	0	0	0	0	0
	10	0	0	0	0	0	0	0	0	0
NCI 204262	25	0	0	0	0	0	0	0	0	0
	50	0	0	1	1	1	0	0	0	0
	100	0	0	1	0	0	0	0	0	0

	0.1	0	0	0	0	0	0	0	0	0
	1	0	0	0	0	0	0	0	0	0
	10	0	0	0	0	0	0	0	0	0
NCI 205832	25	0	0	0	1	0	0	0	0	0

	50	1	0	0	0	0	0	0	0	0
	100	0	0	0	0	0	0	0	0	0
<hr/>										
	0.1	1	0	0.65	0	0	0	0	0	0
	1	1	0	0.45	0.35	0	0	0	0	0
	10	1	0	0.4	0.55	0.55	0	0	0	0
NCI 205913	25	1	0	1	1	1	0	0	0	0
	50	1	0	1	0	0	0	0	0	0
	100	0	0	1	0	0	0	0	0	0
<hr/>										
	0.1	0	0	0	0	0	0	0	0	0
	1	0	0	0	0	0	0	0	0	0
	10	0.05	0	0	0	0	0	0	0	0
NCI 308847	25	0	0	0	0	0	0	0	0	0
	50	0	0	0	0	0	0	0	0	0
	100	0	0	0	0	0	0	1	1	0
<hr/>										
	0.1	0.05	0	0	0.05	0	0	0	0	0
	1	0.1	0	0	0.25	0	0.05	0	0	0
	10	0	0	0.95	0.4	0	0	0	0	0
NCI 319034	25	0.05	0	0.35	0.05	0.15	0	0	0	0
	50	0	0	1	0	0	0	0.05	0	0
	100	0	0	1	0	0	0	0	0	0

	0.1	0	0	0	0	0	0	0	0	0
	1	0.05	0	0	0	0	0	0	0	0
	10	0	0	0	0	0.3	0.05	0	0	0
NCI 319741	25	0	0	0	0	0.2	0.05	0	0	0
	50	0	0	0	0	0	0	0.1	0	0
	100	0	0	0	0	0.1	0.05	0	0.05	0

	0.1	0	0	0	0	0	0	0	0	0
	1	0	0	0	0	0	0	0	0	0
	10	0	0	0	0	0	0	0	0	0
NCI 340852	25	0	0	0	1	1	0	0	0	0
	50	0	0	0	1	1	0	0	0	0
	100	0	0	0	1	1	0	0	0	0

	0.1	0.1	0	0	0	0.05	0	0	0	0
	1	0.05	0	0	0	0	0.05	0	0	0
	10	1	0	1	0	1	0	0	0	0
NCI 343557	25	1	0	1	0	1	0	0	0	0
	50	1	0	1	0	1	0	0	0	0
	100	0	0	1	0	1	0	0	0	0

	0.1	0	0	0	0.5	0	0	0	0	0
	1	0	0.2	0	1	0	0	0	0	0

	10	0	1	0	0	1	0	0	0	0
NCI 377384	25	0	1	1	0	0	0	0	0	0
	50	0	1	0	0	1	0	1	0	0
	100	0	0	0	0	0	0	0	0	1

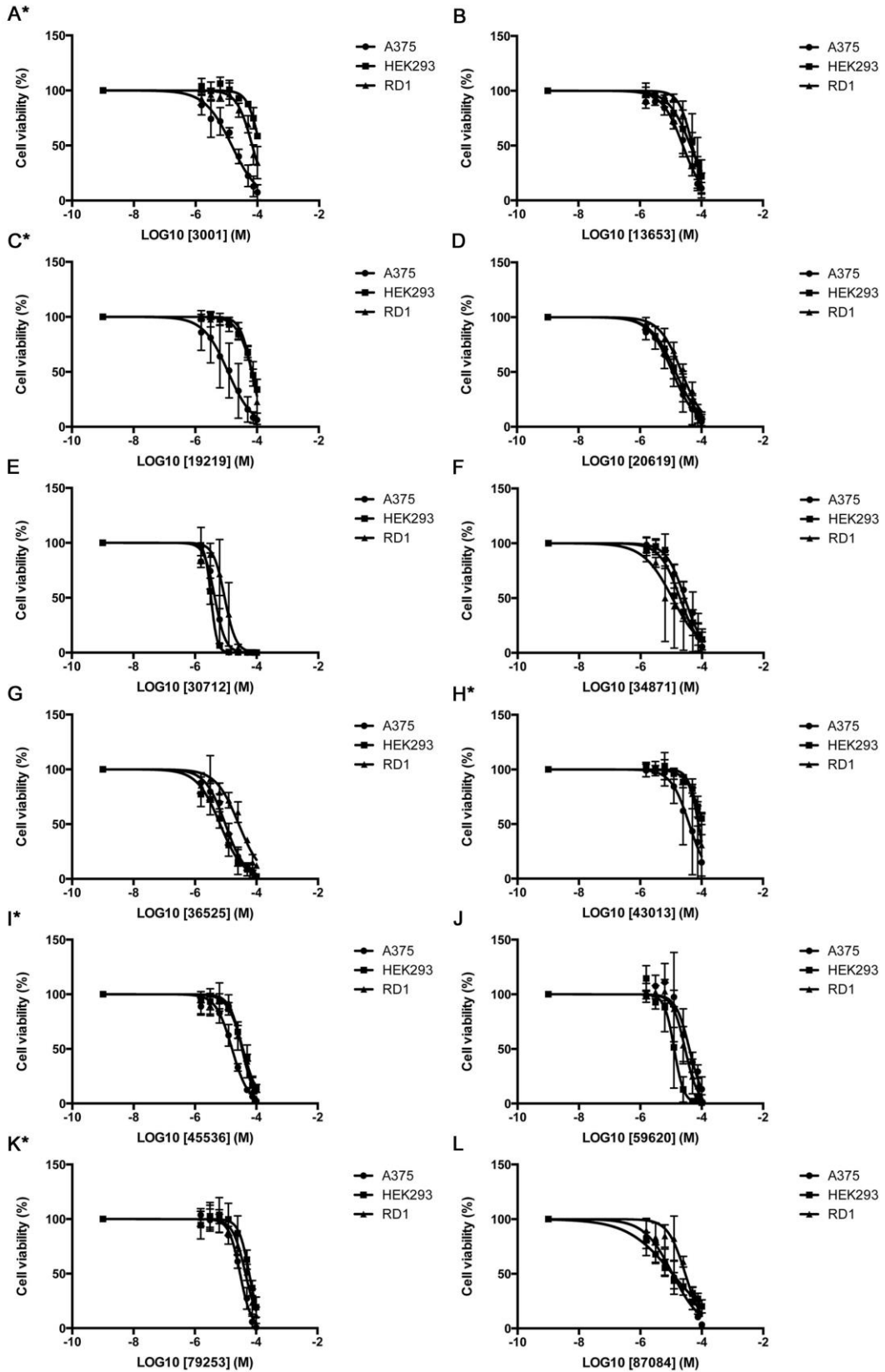
	0.1	0	0	0	1	1	0	0	0	0
	1	0	0	0	1	0	0	0	0	0
	10	0	0	0	1	0	0	0	0	0
NCI 378719	25	0	0	0	1	1	0	0	0	0
	50	0	0	0	1	1	0	0	0	0
	100	0	0	0	1	0	0	0	0	0

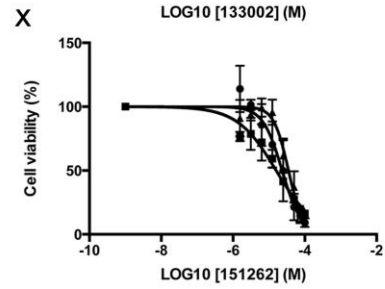
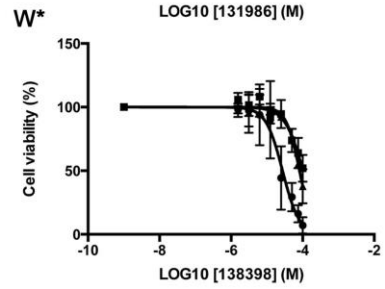
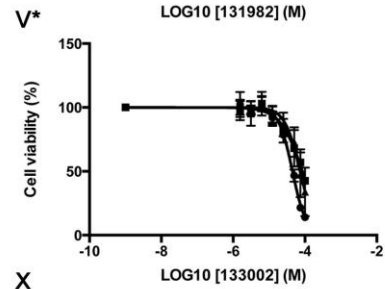
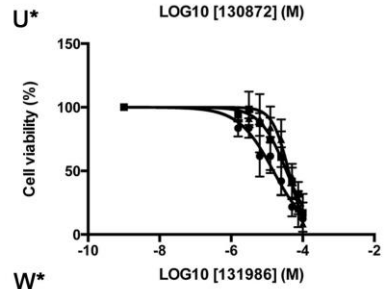
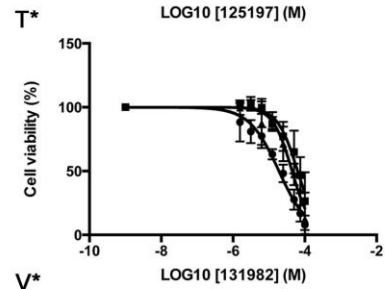
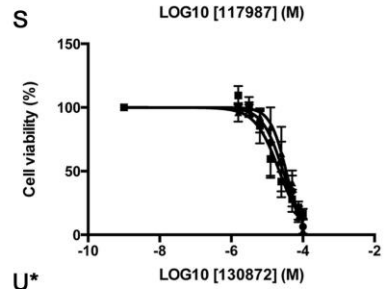
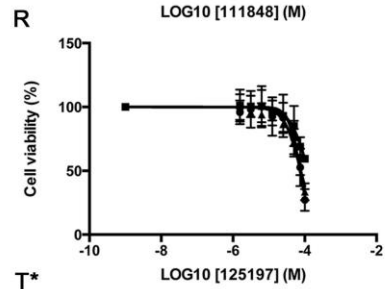
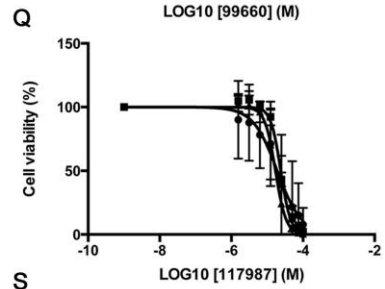
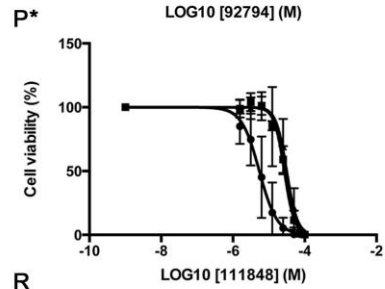
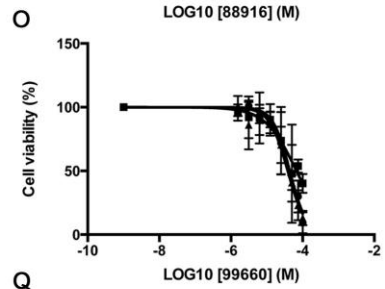
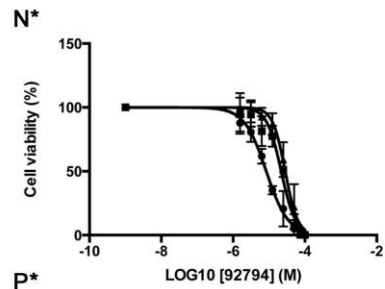
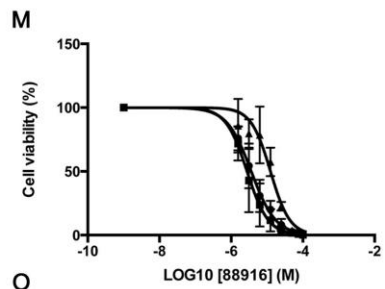
	0.1	0	0	0	0	0	0	0	0	0
	1	0	0	0	0	0	0	0	0	0
	10	0	1	0	0	1	0	0	0	0
NCI 402590	25	0	1	0	0	1	0	0	0	0
	50	0	1	0	0	1	0	0	0	0
	100	0	1	0	0	1	0	0	0	0

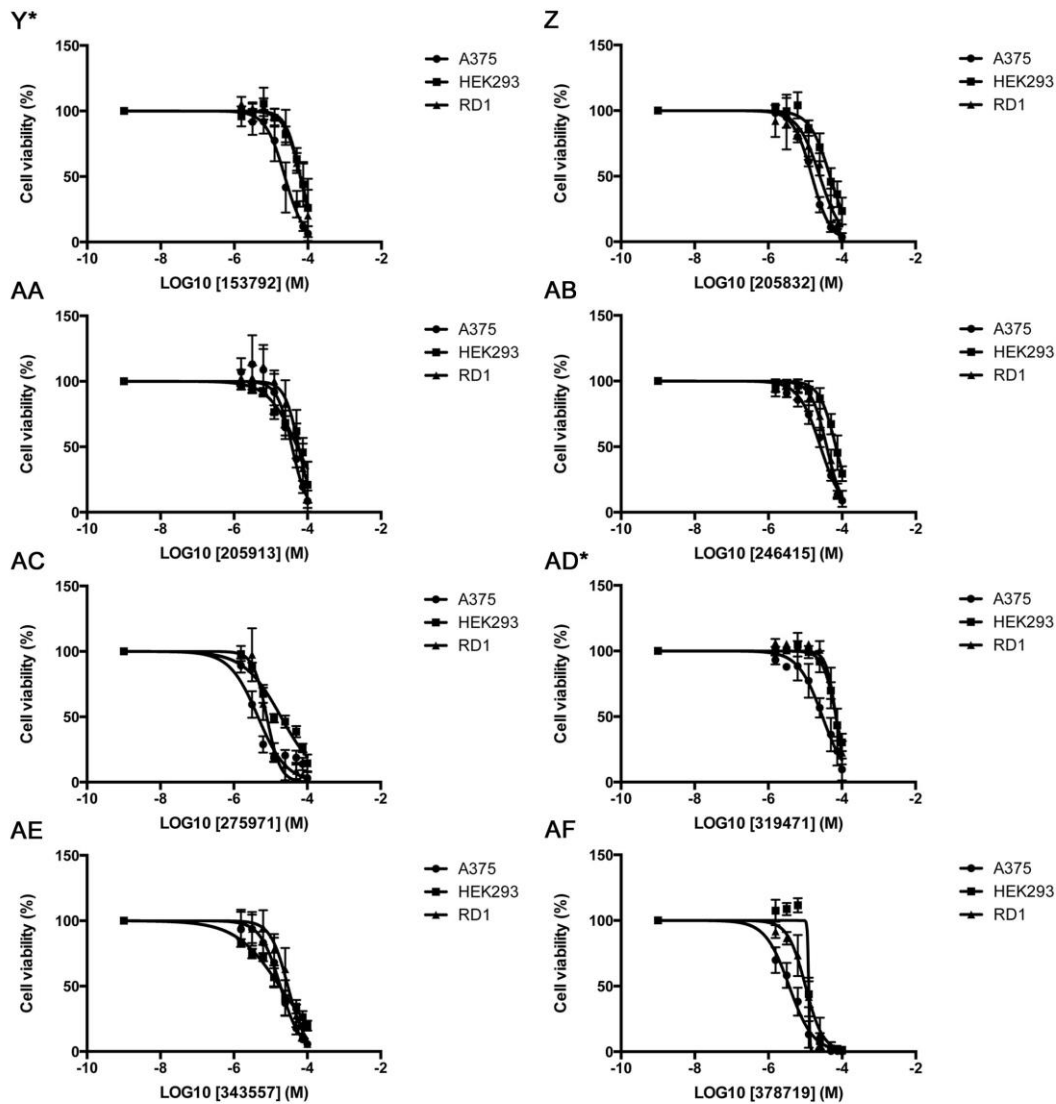
	0.1	0	0	0	0	0	0	0	0	0
	1	0	0	0	0	0	0	0	0	0
	10	1	0	1	0	0	1	0	0	0
NCI 515893	25	0	0	1	0	0	0	0	0	0
	50	0	0	1	0	0	0	0	0	0

	100	0	0	1	0	0	0	0	0	0
		<hr/>								
	0.1	0	0	0	0	0	0	0	0	0
	1	0	0	1	0	0	0	0	0	0
	10	0	0	1	0	0	0	0	0	0
NCI 645987	25	0	0	1	0	0	0	0	0	0
	50	0	0	1	0	0	0	0	0	0
	100	0	0	1	0	0	0	0	0	0
		<hr/>								
	0.1	0	0	0	0	0	0	0	0	0
	1	0	0	0	0	0	0	0	0	0
	10	0	1	0	1	1	0	0	0	0
NCI 667251	25	0	1	0	1	1	0	0	0	0
	50	0	1	0	1	1	0	0	0	0
	100	0	1	0	0	0	0	0	0	0
		<hr/>								

Appendix III



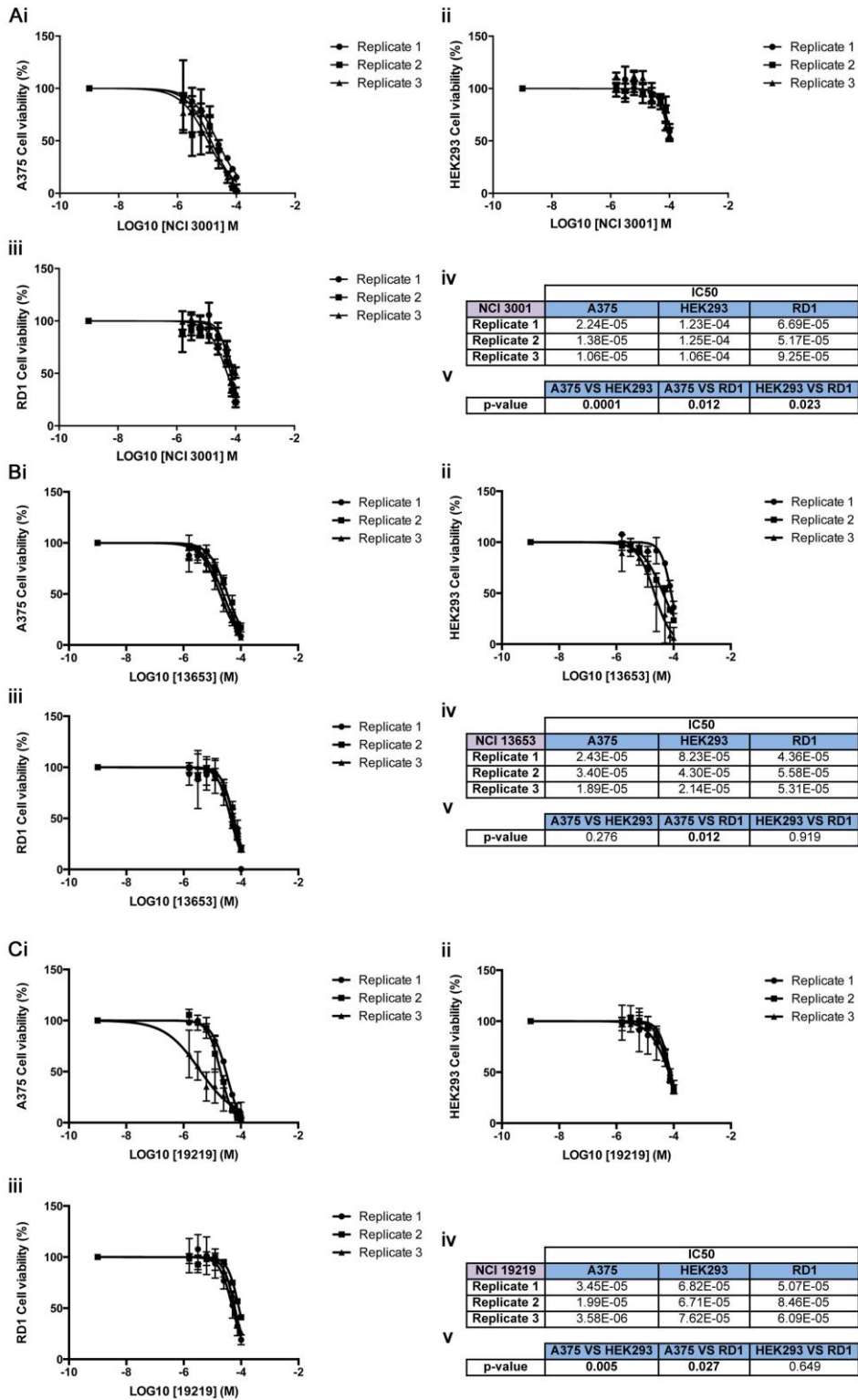


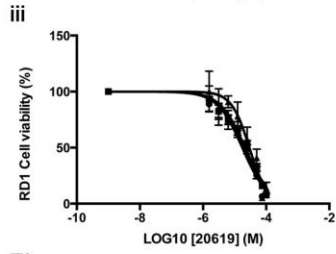
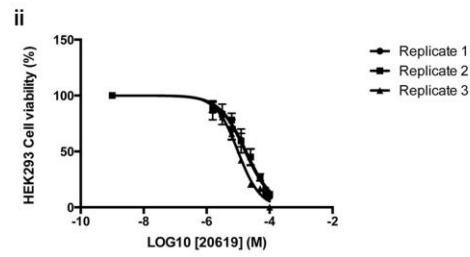
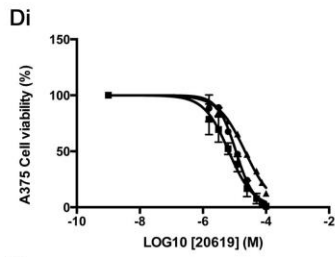


Appendix III Figure 1. Dose response graphs displaying cell viability (%) of A375, HEK293 and RD1 cell lines in response to the designated NCI compound over an increasing concentration range (LOG10 M). Error bars represent standard error (n=3). Asterisks (*) indicate those compounds which gave rise to IC50s in the A375 cell line which were statistically different to those obtained in both corresponding HEK293 and RD1 control cell lines. A. NCI 3001. B. NCI 13563. C. NCI 19219. D. NCI 20619. E. NCI 30712. F. NCI 34871. G. NCI

36525. H. NCI 43013. I. NCI 45536. J. NCI 59620. K. NCI 79253. L. NCI 87084.
M. NCI 88916. N. NCI 92794. O. NCI 99660. P. NCI 111848. Q. NCI 117987. R.
NCI 125197. S. NCI 130872. T. NCI 131982. U. NCI 131986. V. NCI 133002. W.
NCI 138398. X. NCI 151262. Y. NCI 153792. Z. NCI 205832. AA. NCI 205913.
AB. NCI 246415. AC. NCI 275971. AD. NCI 319471. AE. NCI 343557. AF. NCI
378719.

Appendix IV



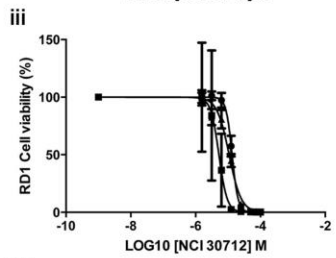
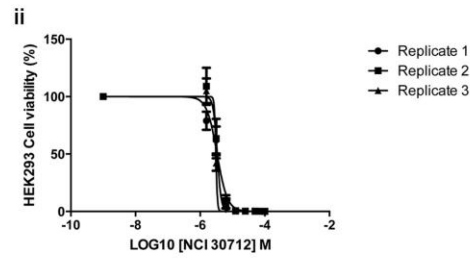
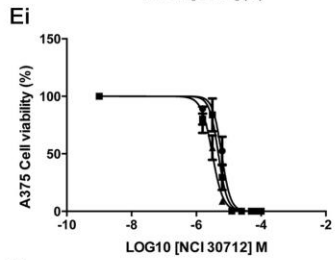


iv

NCI 20619	IC50		
	A375	HEK293	RD1
Replicate 1	1.11E-05	1.68E-05	1.76E-05
Replicate 2	6.57E-06	1.81E-05	2.15E-05
Replicate 3	2.15E-05	2.10E-05	2.94E-05

v

	A375 VS HEK293	A375 VS RD1	HEK293 VS RD1
p-value	0.294	0.158	0.320

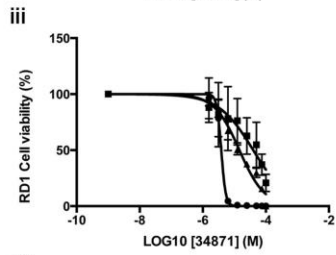
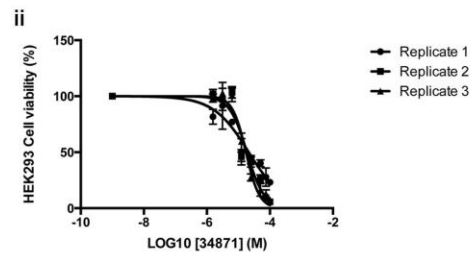
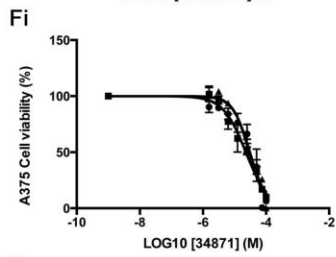


iv

NCI 30712	IC50		
	A375	HEK293	RD1
Replicate 1	6.03E-06	3.34E-06	1.33E-05
Replicate 2	4.78E-06	3.38E-06	5.24E-05
Replicate 3	3.10E-06	~ 3.072e-006	1.08E-05

v

	A375 VS HEK293	A375 VS RD1	HEK293 VS RD1
p-value	0.327	0.112	0.129

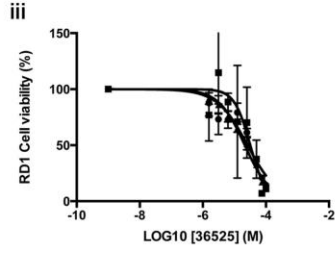
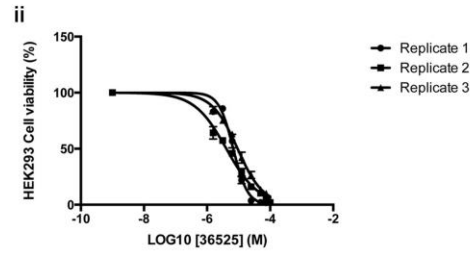
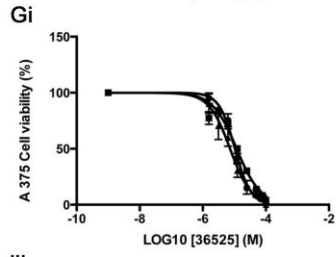


iv

NCI 34871	IC50		
	A375	HEK293	RD1
Replicate 1	2.90E-05	2.13E-05	3.85E-06
Replicate 2	2.29E-05	1.86E-05	3.98E-05
Replicate 3	3.07E-05	1.74E-05	1.45E-05

v

	A375 VS HEK293	A375 VS RD1	HEK293 VS RD1
p-value	0.033	0.308	0.794

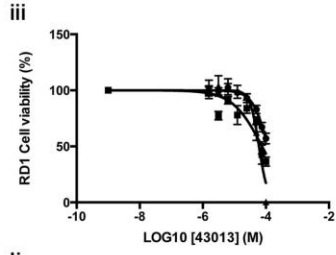
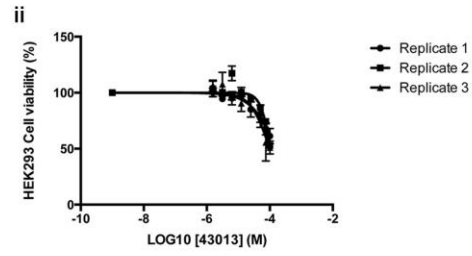
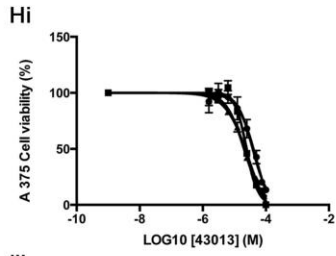


iv

NCI 36525	IC50		
	A375	HEK293	RD1
Replicate 1	1.05E-05	6.77E-06	2.61E-05
Replicate 2	1.18E-05	4.09E-06	3.19E-05
Replicate 3	7.32E-06	9.30E-06	2.15E-05

v

	A375 VS HEK293	A375 VS RD1	HEK293 VS RD1
p-value	0.192	0.007	0.004

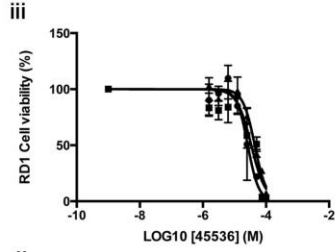
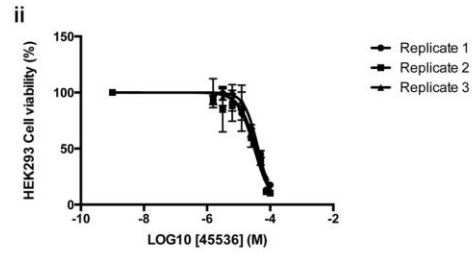
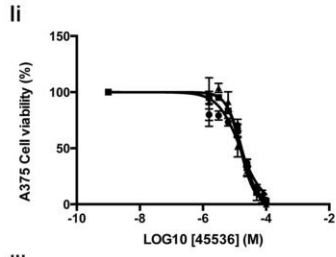


iv

NCI 43013	IC50		
	A375	HEK293	RD1
Replicate 1	3.84E-05	1.57E-04	1.16E-04
Replicate 2	2.03E-05	1.07E-04	7.56E-05
Replicate 3	2.47E-05	1.00E-04	6.03E-05

v

	A375 VS HEK293	A375 VS RD1	HEK293 VS RD1
p-value	0.007	0.009	0.290

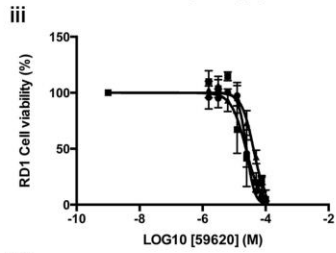
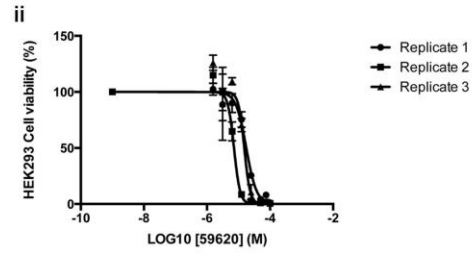
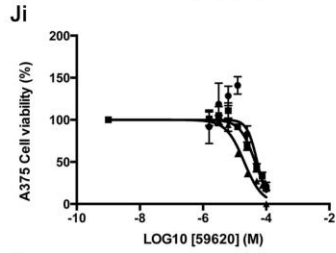


iv

NCI 45536	IC50		
	A375	HEK293	RD1
Replicate 1	1.52E-05	3.59E-05	2.64E-05
Replicate 2	1.68E-05	3.15E-05	3.40E-05
Replicate 3	1.52E-05	4.17E-05	4.40E-05

v

	A375 VS HEK293	A375 VS RD1	HEK293 VS RD1
p-value	0.002	0.020	0.806

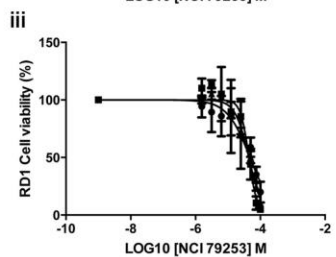
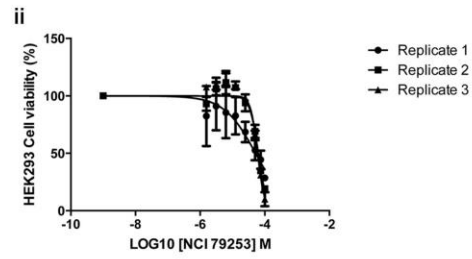
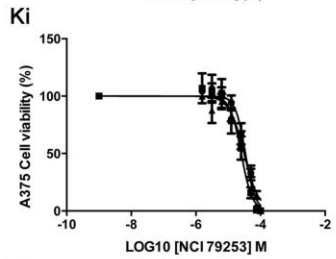


iv

NCI 59620	IC50		
	A375	HEK293	RD1
Replicate 1	5.19E-05	1.78E-05	2.48E-05
Replicate 2	4.45E-05	7.20E-06	2.37E-05
Replicate 3	2.00E-05	1.53E-05	4.10E-05

v

	A375 VS HEK293	A375 VS RD1	HEK293 VS RD1
p-value	0.066	0.465	0.062

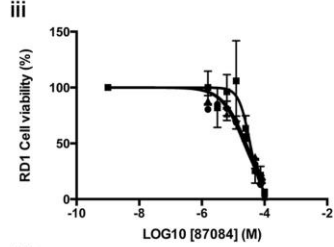
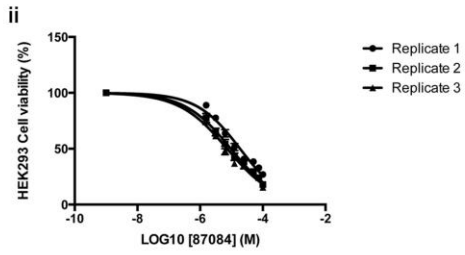
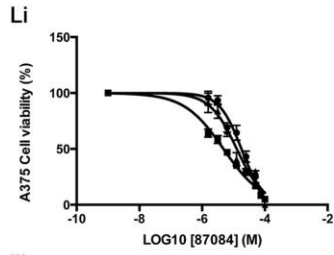


iv

NCI 79253	IC50		
	A375	HEK293	RD1
Replicate 1	3.41E-05	5.20E-05	4.79E-05
Replicate 2	2.53E-05	6.32E-05	4.45E-05
Replicate 3	3.09E-05	6.02E-05	4.42E-05

v

	A375 VS HEK293	A375 VS RD1	HEK293 VS RD1
p-value	0.0004	0.005	0.057

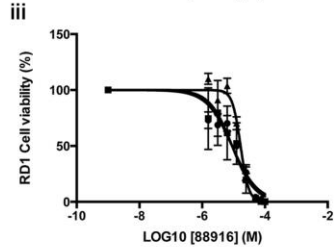
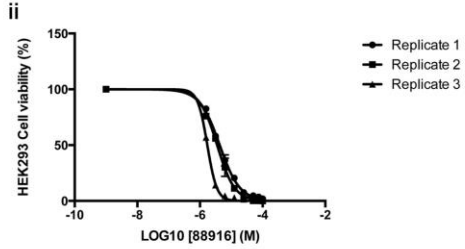
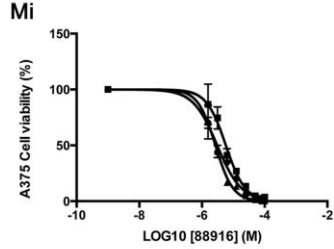


iv

NCI 87084	IC50		
	A375	HEK293	RD1
Replicate 1	1.79E-05	1.88E-05	2.22E-05
Replicate 2	4.78E-06	9.51E-06	3.45E-05
Replicate 3	1.27E-05	7.24E-06	2.59E-05

v

	A375 VS HEK293	A375 VS RD1	HEK293 VS RD1
p-value	0.992	0.041	0.037

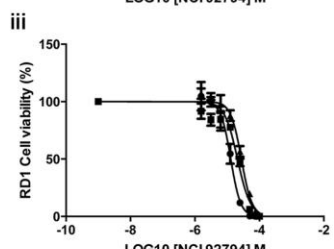
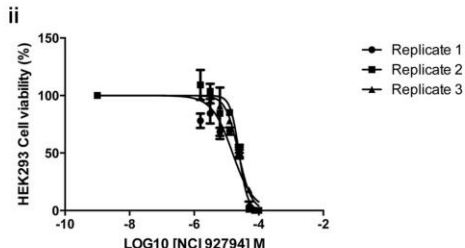
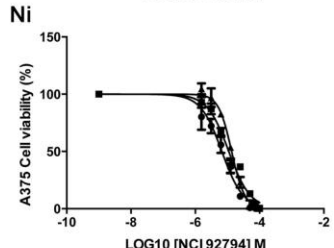


iv

NCI 87084	IC50		
	A375	HEK293	RD1
Replicate 1	1.79E-05	1.88E-05	2.22E-05
Replicate 2	4.78E-06	9.51E-06	3.45E-05
Replicate 3	1.27E-05	7.24E-06	2.59E-05

v

	A375 VS HEK293	A375 VS RD1	HEK293 VS RD1
p-value	0.992	0.041	0.037

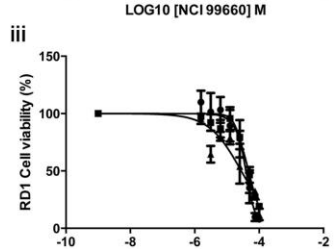
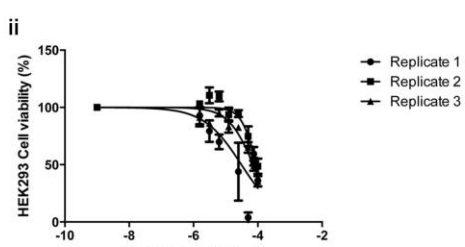
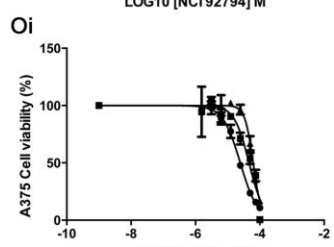


iv

NCI 92794	IC50		
	A375	HEK293	RD1
Replicate 1	6.71E-06	1.55E-05	1.30E-05
Replicate 2	1.10E-05	2.46E-05	2.09E-05
Replicate 3	1.35E-05	2.37E-05	2.77E-05

v

	A375 VS HEK293	A375 VS RD1	HEK293 VS RD1
p-value	0.013	0.036	0.604

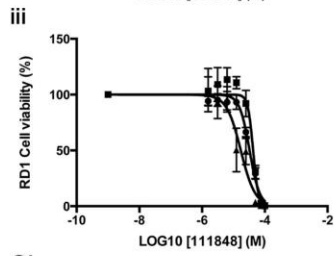
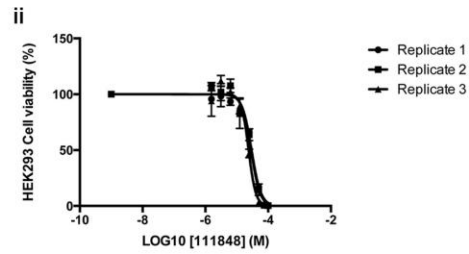
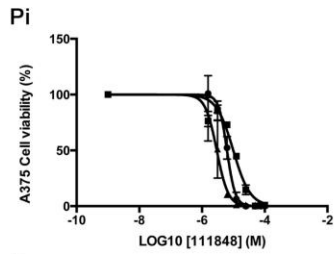


iv

NCI 99660	IC50		
	A375	HEK293	RD1
Replicate 1	2.48E-05	3.10E-05	3.88E-05
Replicate 2	4.63E-05	8.88E-05	4.68E-05
Replicate 3	6.23E-05	7.28E-05	2.78E-05

v

	A375 VS HEK293	A375 VS RD1	HEK293 VS RD1
p-value	0.388	0.614	0.219

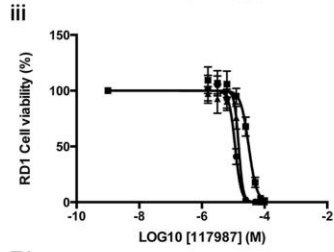
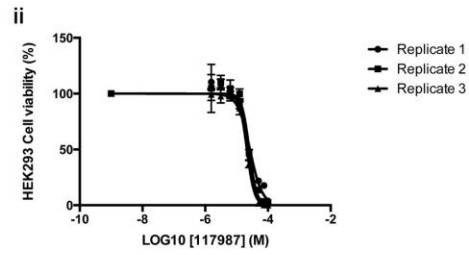
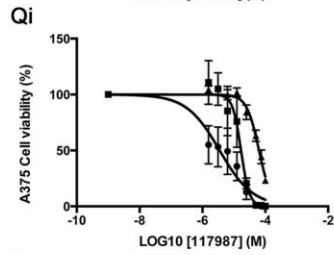


iv

NCI 111848	IC50		
	A375	HEK293	RD1
Replicate 1	6.26E-06	2.96E-05	3.28E-05
Replicate 2	9.92E-06	2.85E-05	4.24E-05
Replicate 3	2.95E-06	2.39E-05	1.72E-05

v

p-value	A375 VS HEK293	A375 VS RD1	HEK293 VS RD1
		0.001	0.033

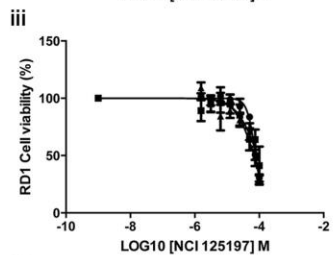
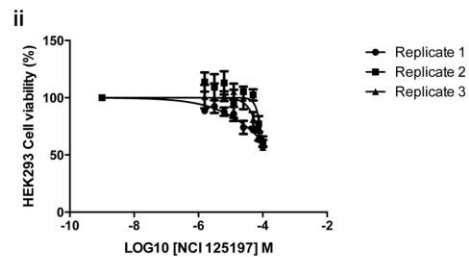
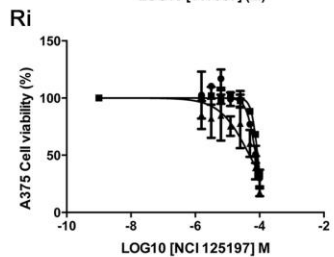


iv

NCI 117987	IC50		
	A375	HEK293	RD1
Replicate 1	3.52E-06	2.66E-05	1.15E-05
Replicate 2	1.69E-05	2.53E-05	3.13E-05
Replicate 3	6.32E-05	2.14E-05	1.50E-05

v

p-value	A375 VS HEK293	A375 VS RD1	HEK293 VS RD1
		0.859	0.674

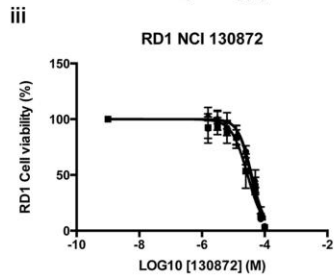
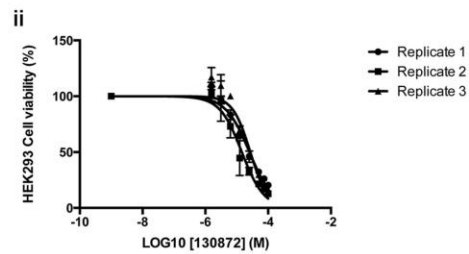
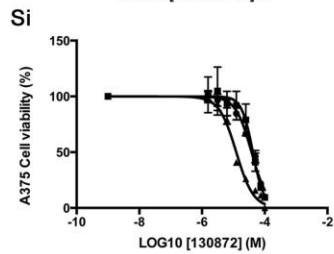


iv

NCI 125197	IC50		
	A375	HEK293	RD1
Replicate 1	7.56E-05	2.51E-04	7.73E-05
Replicate 2	8.71E-05	1.09E-04	8.95E-05
Replicate 3	4.86E-05	1.08E-04	6.97E-05

v

p-value	A375 VS HEK293	A375 VS RD1	HEK293 VS RD1
		0.155	0.548

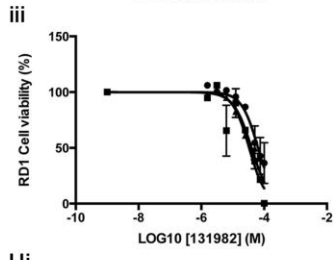
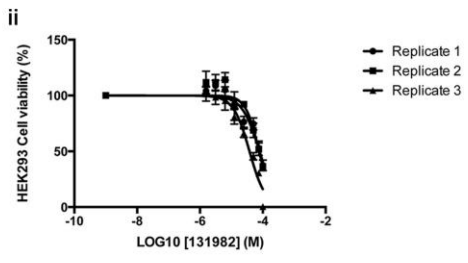
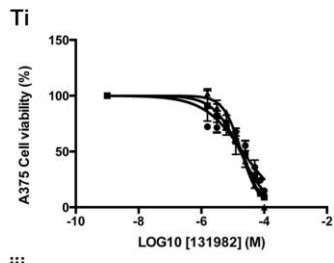


iv

NCI 130872	IC50		
	A375	HEK293	RD1
Replicate 1	3.81E-05	2.55E-05	3.60E-05
Replicate 2	4.20E-05	1.45E-05	2.84E-05
Replicate 3	1.24E-05	2.71E-05	3.84E-05

v

p-value	A375 VS HEK293	A375 VS RD1	HEK293 VS RD1
		0.449	0.740

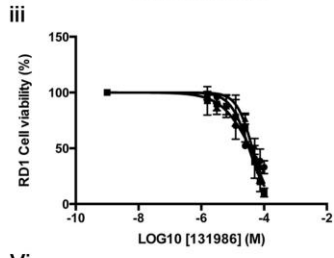
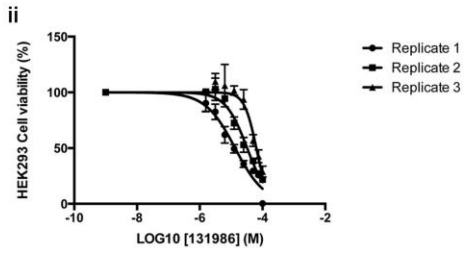
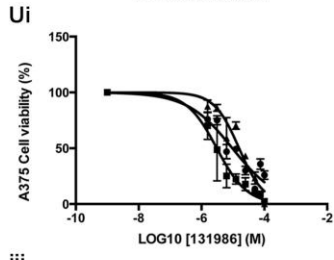


iv

NCI 131982	IC50		
	A375	HEK293	RD1
Replicate 1	2.06E-05	7.88E-05	6.39E-05
Replicate 2	1.73E-05	7.62E-05	3.34E-05
Replicate 3	1.88E-05	3.78E-05	3.97E-05

v

	A375 VS HEK293	A375 VS RD1	HEK293 VS RD1
p-value	0.005	0.031	0.403

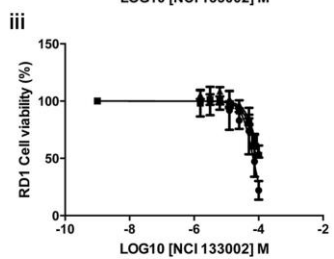
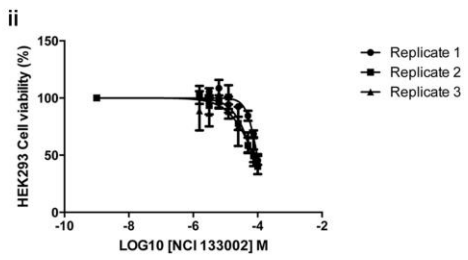
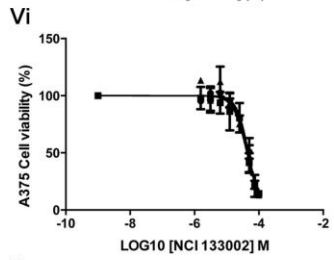


iv

NCI 131986	IC50		
	A375	HEK293	RD1
Replicate 1	1.57E-05	4.42E-05	3.74E-05
Replicate 2	9.58E-06	3.24E-05	3.31E-05
Replicate 3	3.06E-06	6.36E-05	4.26E-05

v

	A375 VS HEK293	A375 VS RD1	HEK293 VS RD1
p-value	0.019	0.003	0.395

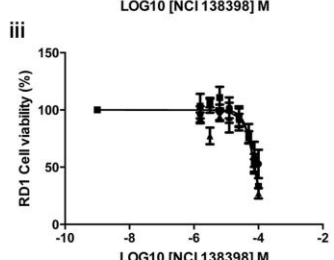
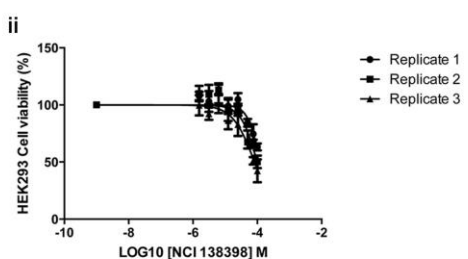
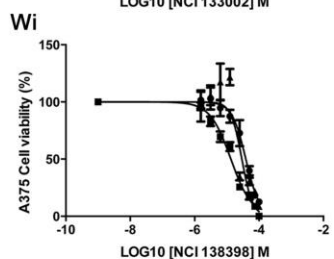


iv

NCI 133002	IC50		
	A375	HEK293	RD1
Replicate 1	4.75E-05	9.65E-05	6.81E-05
Replicate 2	4.28E-05	7.13E-05	1.08E-04
Replicate 3	4.47E-05	7.84E-05	1.07E-04

v

	A375 VS HEK293	A375 VS RD1	HEK293 VS RD1
p-value	0.008	0.020	0.461

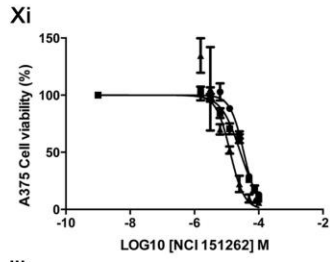


iv

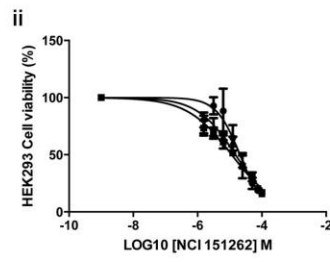
NCI 138398	IC50		
	A375	HEK293	RD1
Replicate 1	3.90E-05	1.24E-04	1.00E-04
Replicate 2	1.34E-05	9.94E-05	7.79E-05
Replicate 3	2.93E-05	8.19E-05	7.49E-05

v

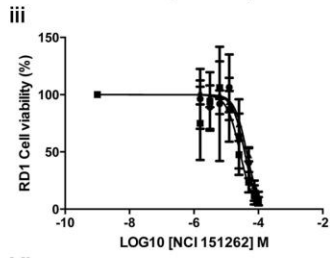
	A375 VS HEK293	A375 VS RD1	HEK293 VS RD1
p-value	0.007	0.006	0.297



● Replicate 1
■ Replicate 2
▲ Replicate 3



● Replicate 1
■ Replicate 2
▲ Replicate 3



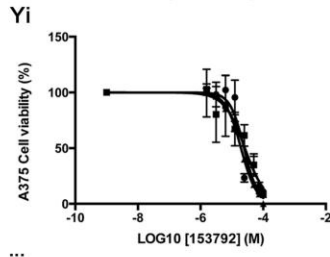
● Replicate 1
■ Replicate 2
▲ Replicate 3

iv

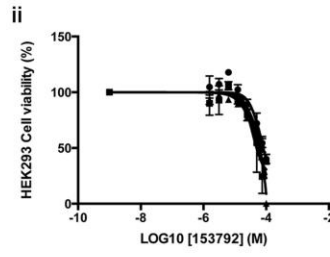
NCI 151262	IC50		
	A375	HEK293	RD1
Replicate 1	3.42E-05	2.08E-05	3.73E-05
Replicate 2	2.69E-05	1.15E-05	2.67E-05
Replicate 3	1.30E-05	1.51E-05	4.33E-05

v

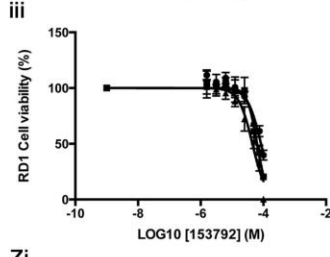
	A375 VS HEK293	A375 VS RD1	HEK293 VS RD1
p-value	0.260	0.232	0.023



● Replicate 1
■ Replicate 2
▲ Replicate 3



● Replicate 1
■ Replicate 2
▲ Replicate 3



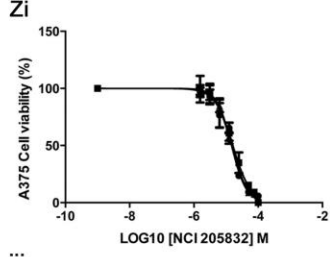
● Replicate 1
■ Replicate 2
▲ Replicate 3

iv

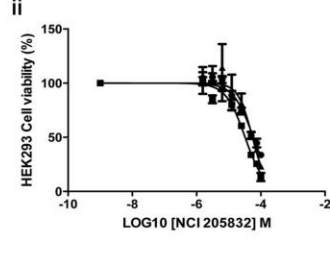
NCI 153792	IC50		
	A375	HEK293	RD1
Replicate 1	2.46E-05	8.12E-05	8.41E-05
Replicate 2	2.60E-05	5.44E-05	6.30E-05
Replicate 3	1.96E-05	5.75E-05	4.47E-05

v

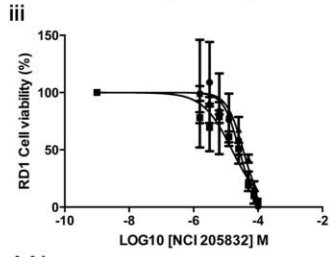
	A375 VS HEK293	A375 VS RD1	HEK293 VS RD1
p-value	0.014	0.028	0.978



● Replicate 1
■ Replicate 2
▲ Replicate 3



● Replicate 1
■ Replicate 2
▲ Replicate 3



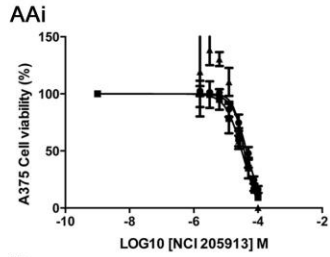
● Replicate 1
■ Replicate 2
▲ Replicate 3

iv

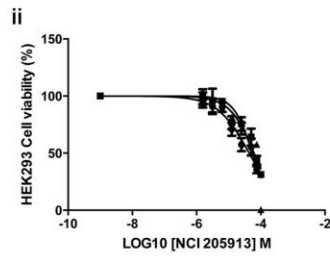
NCI 205832	IC50		
	A375	HEK293	RD1
Replicate 1	1.49E-05	5.87E-05	2.59E-05
Replicate 2	1.63E-05	3.25E-05	1.55E-05
Replicate 3	1.49E-05	5.49E-05	3.44E-05

v

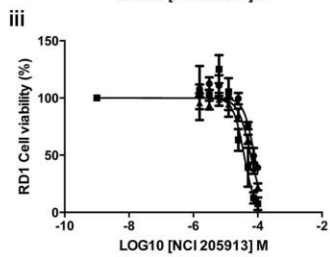
	A375 VS HEK293	A375 VS RD1	HEK293 VS RD1
p-value	0.015	0.144	0.076



● Replicate 1
■ Replicate 2
▲ Replicate 3



● Replicate 1
■ Replicate 2
▲ Replicate 3



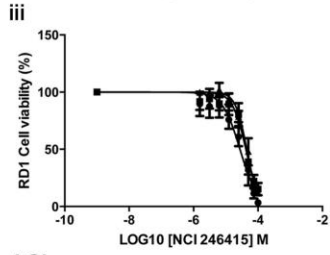
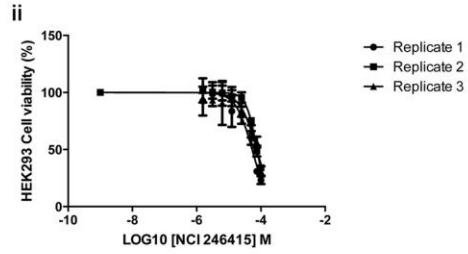
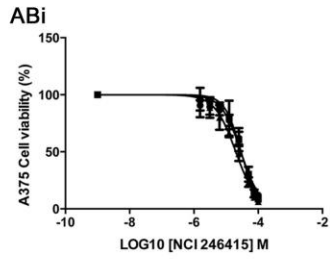
● Replicate 1
■ Replicate 2
▲ Replicate 3

iv

NCI 205913	IC50		
	A375	HEK293	RD1
Replicate 1	2.27E-05	5.49E-05	7.90E-05
Replicate 2	1.63E-05	4.34E-05	3.78E-05
Replicate 3	3.71E-05	6.17E-05	6.06E-05

v

	A375 VS HEK293	A375 VS RD1	HEK293 VS RD1
p-value	0.027	0.066	0.681

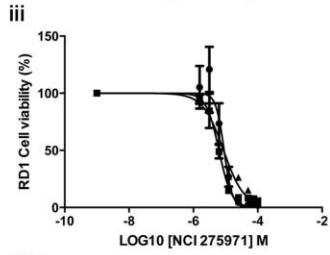
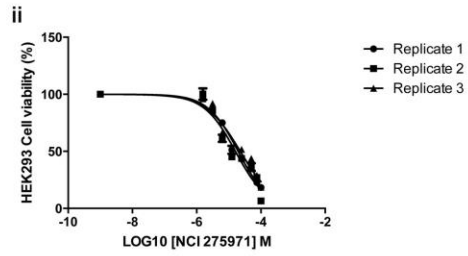
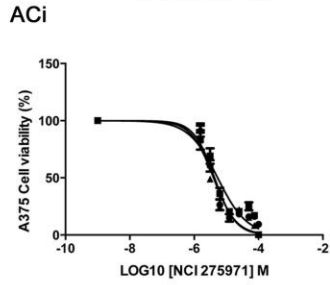


iv

NCI 246415	IC50		
	A375	HEK293	RD1
Replicate 1	2.89E-05	5.33E-05	2.76E-05
Replicate 2	2.94E-05	7.57E-05	4.22E-05
Replicate 3	2.01E-05	7.42E-05	4.48E-05

v

	A375 VS HEK293	A375 VS RD1	HEK293 VS RD1
p-value	0.006	0.176	0.344

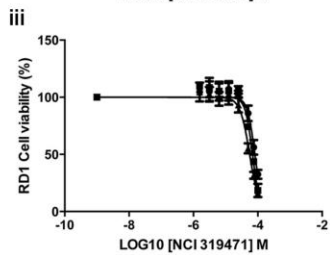
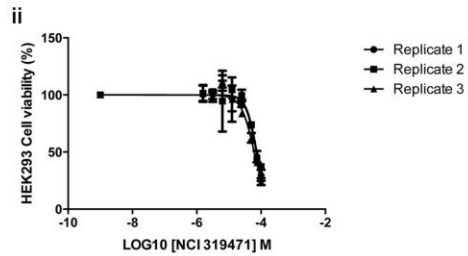
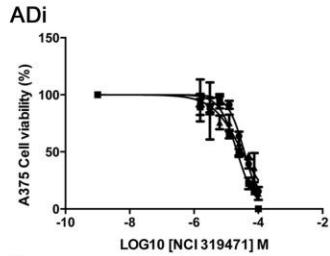


iv

NCI 275971	IC50		
	A375	HEK293	RD1
Replicate 1	4.30E-06	1.95E-05	8.99E-06
Replicate 2	5.38E-06	1.60E-05	6.23E-06
Replicate 3	4.00E-06	2.28E-05	8.64E-06

v

	A375 VS HEK293	A375 VS RD1	HEK293 VS RD1
p-value	0.009	0.107	0.053

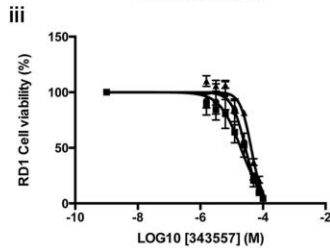
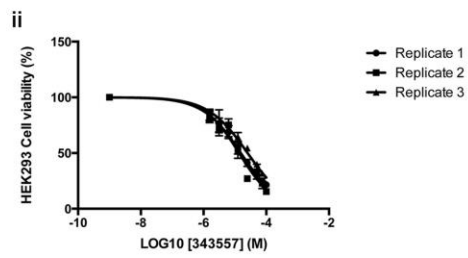
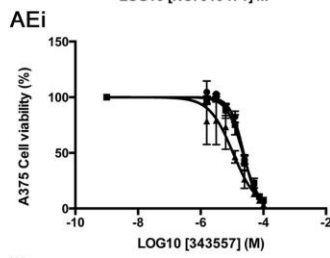


iv

NCI 319471	IC50		
	A375	HEK293	RD1
Replicate 1	3.67E-05	7.14E-05	8.12E-05
Replicate 2	2.20E-05	7.44E-05	6.88E-05
Replicate 3	3.16E-05	6.13E-05	5.59E-05

v

	A375 VS HEK293	A375 VS RD1	HEK293 VS RD1
p-value	0.003	0.010	0.965

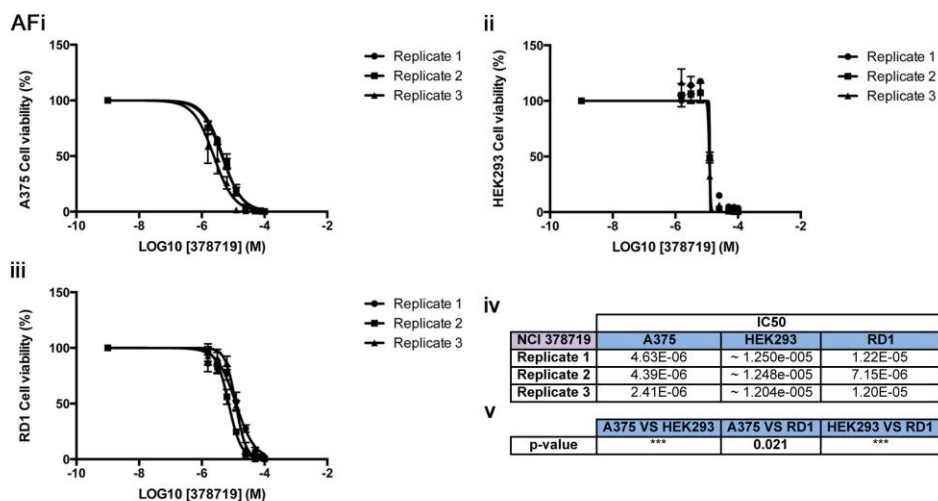


iv

NCI 343557	IC50		
	A375	HEK293	RD1
Replicate 1	2.34E-05	1.55E-05	2.74E-05
Replicate 2	2.21E-05	1.36E-05	1.94E-05
Replicate 3	1.07E-05	2.54E-05	4.19E-05

v

	A375 VS HEK293	A375 VS RD1	HEK293 VS RD1
p-value	0.908	0.232	0.173



Appendix IV Figure 1. Data used to calculate statistical differences between IC50s generated for each of the 32 tested NCI ‘hit’ compounds screened upon three cell lines (A375, HEK293 and RD1). i. Graphs displaying A375 percentage cell viability (%) in response to the designated NCI compound over an increasing concentration range (LOG10 M), and were used to generate the IC50s for each of the 3 replicates (error bars represent standard error). ii. Graphs displaying HEK293 percentage cell viability (%) in response to the designated NCI compound over an increasing concentration range (LOG10 M), and were used to generate the IC50s for each of the 3 replicates (error bars represent standard error). iii. Graphs displaying RD1 percentage cell viability (%) in response to the designated NCI compound over an increasing concentration range (LOG10 M), and were used to generate the IC50s for each of the 3 replicates (error bars represent standard error). iv. IC50 values generated from the corresponding NCI ‘hit’ compound dose response graphs for each of the three replicates for the A375, HEK293 and RD1 cell lines respectively. v. P-values ($P\text{-value} = \leq 0.05$) generated using a student’s T-test to statistically compare IC50 values generated using the corresponding NCI ‘hit’

compound dose response graphs for the A375, HEK293 and RD1 cell lines. Those *p*-values highlighted in bold indicate those cell lines whose IC50 values can be considered statistically different from one another. *** indicates those *p*-values that could not be generated due to ambiguous IC50 data. A. NCI 3001. B. NCI 13563. C. NCI 19219. D. NCI 20619. E. NCI 30712. F. NCI 34871. G. NCI 36525. H. NCI 43013. I. NCI 45536. J. NCI 59620. K. NCI 79253. L. NCI 87084. M. NCI 88916. N. NCI 92794. O. NCI 99660. P. NCI 111848. Q. NCI 117987. R. NCI 125197. S. NCI 130872. T. NCI 131982. U. NCI 131986. V. NCI 133002. W. NCI 138398. X. NCI 151262. Y. NCI 153792. Z. NCI 205832. AA. NCI 205913. AB. NCI 246415. AC. NCI 275971. AD. NCI 319471. AE. NCI 343557. AF. NCI 378719.

Abbreviations

2D: Two dimensional

3D: Three dimensional

ADME: Adsorption, distribution, metabolism and excretion

DMSO: Dimethyl sulphoxide

DNA: Deoxyribonucleic acid

DMF: Dimethylformamide

FBS: Foetal bovine serum

FCS: Foetal calf serum

FDA: USA Food and Drug Administration

GDH: Glutamate dehydrogenase

HCG: Human chorionic gonadotrophin

HTS: High throughput screening

μ: Micro

m: Milli

M: Molar

MEMFA: Fix (MEM salts + formaldehyde)

MOA: Mechanism of action

NA: Not applicable

NME: New molecular entity

P: Probability

PMSG: Serum gonadotrophin

RT: Room temperature

R&D: Research and development

SAR: Structure activity relationship

UV:ultraviolet

Reference

2011. Patent cliff. Billions to be saved--starting now. Lipitor led the way, and other blockbusters are following. *Managed care* 20, 65.
- Abdulla, M.H., Ruelas, D.S., Wolff, B., Snedecor, J., Lim, K.C., Xu, F., Renslo, A.R., Williams, J., McKerrow, J.H., Caffrey, C.R., 2009. Drug discovery for schistosomiasis: hit and lead compounds identified in a library of known drugs by medium-throughput phenotypic screening. *PLoS neglected tropical diseases* 3, e478.
- Adams, D.S., Robinson, K.R., Fukumoto, T., Yuan, S., Albertson, R.C., Yelick, P., Kuo, L., McSweeney, M., Levin, M., 2006. Early, H⁺-V-ATPase-dependent proton flux is necessary for consistent left-right patterning of non-mammalian vertebrates. *Development* 133, 1657-1671.
- Arias, A.M., 2008. *Drosophila melanogaster* and the development of biology in the 20th century. *Methods Mol Biol* 420, 1-25.
- Artal-Sanz, M., de Jong, L., Tavernarakis, N., 2006. *Caenorhabditis elegans*: a versatile platform for drug discovery. *Biotechnology journal* 1, 1405-1418.
- Auer, T.O., Duroure, K., De Cian, A., Concordet, J.P., Del Bene, F., 2014. Highly efficient CRISPR/Cas9-mediated knock-in in zebrafish by homology-independent DNA repair. *Genome Res* 24, 142-153.
- Austin, C.P., Battey, J.F., Bradley, A., Bucan, M., Capecchi, M., Collins, F.S., Dove, W.F., Duyk, G., Dymecki, S., Eppig, J.T., Grieder, F.B., Heintz, N., Hicks, G., Insel, T.R., Joyner, A., Koller, B.H., Lloyd, K.C., Magnuson, T., Moore, M.W., Nagy, A., Pollock, J.D., Roses, A.D., Sands, A.T., Seed, B., Skarnes, W.C., Snoddy, J., Soriano, P., Stewart, D.J., Stewart, F., Stillman, B., Varmus, H., Varticovski, L., Verma, I.M., Vogt, T.F., von Melchner, H., Witkowski, J., Woychik, R.P., Wurst, W., Yancopoulos, G.D., Young, S.G., Zambrowicz, B., 2004. The knockout mouse project. *Nature genetics* 36, 921-924.

Avdeef, A., 2001. Physicochemical profiling (solubility, permeability and charge state). *Curr Top Med Chem* 1, 277-351.

Balinsky, J.B.a.B., E., 1961. The mode of excretion of ammonia and urea in *Xenopus laevis*. *Journal of Experimental Biology* 38, 695-705.

Bender, A., 2010. How similar are those molecules after all? Use two descriptors and you will have three different answers. *Expert Opin Drug Dis* 5, 1141-1151.

Bender, A., Fergus, S., Galloway, W.R., Glansdorp, F.G., Marsden, D.M., Nicholson, R.L., Spandl, R.J., Thomas, G.L., Wyatt, E.E., Glen, R.C., Spring, D.R., 2006. Diversity oriented synthesis: a challenge for synthetic chemists. *Ernst Schering Res Found Workshop*, 47-60.

Bender, A., Jenkins, J.L., Scheiber, J., Sukuru, S.C., Glick, M., Davies, J.W., 2009. How similar are similarity searching methods? A principal component analysis of molecular descriptor space. *Journal of chemical information and modeling* 49, 108-119.

Benson, D.F., 1996. Neuropsychiatry and behavioral neurology: past, present, and future. *J Neuropsychiatry Clin Neurosci* 8, 351-357.

Beresford, A.P., Selick, H.E., Tarbit, M.H., 2002. The emerging importance of predictive ADME simulation in drug discovery. *Drug Discovery Today* 7, 109-116.

Berger, J., Currie, P., 2007. The role of zebrafish in chemical genetics. *Curr Med Chem* 14, 2413-2420.

Bergers, G., Hanahan, D., 2008. Modes of resistance to anti-angiogenic therapy. *Nature reviews. Cancer* 8, 592-603.

Bergstrom, C.A., Strafford, M., Lazorova, L., Avdeef, A., Luthman, K., Artursson, P., 2003. Absorption classification of oral drugs based on molecular surface properties. *J Med Chem* 46, 558-570.

Besch, R., Berking, C., Kammerbauer, C., Degitz, K., 2007. Inhibition of urokinase-type plasminogen activator receptor induces apoptosis in melanoma cells by activation of p53. *Cell Death Differ* 14, 818-829.

Bhadriraju, K., Chen, C.S., 2002. Engineering cellular microenvironments to improve cell-based drug testing. *Drug Discov Today* 7, 612-620.

Bier, E.a.M., W., 2004. Chapter 3. Model organisms in the study of development and disease, in: Epstein, R.P.E.C.J.a.W.-B., A. (Ed.), *Molecular Basis of Inborn Errors of Development*. Oxford University Press, New York, pp. 25-45.

Bis, S.a.T., H., 2013. Melanoma genetics: the other side. *Clinics in Dermatology* 31, 148-155.

Bleicher, K.H., Bohm, H.J., Muller, K., Alanine, A.I., 2003. Hit and lead generation: beyond high-throughput screening. *Nat Rev Drug Discov* 2, 369-378.

Bohacek, R.S., McMartin, C., Guida, W.C., 1996. The art and practice of structure-based drug design: a molecular modeling perspective. *Med Res Rev* 16, 3-50.

Boobis, A., Gundert-Remy, U., Kremers, P., Macheras, P., Pelkonen, O., 2002. In silico prediction of ADME and pharmacokinetics. Report of an expert meeting organised by COST B15. *Eur J Pharm Sci* 17, 183-193.

Bowes, J.B., Snyder, K.A., James-Zorn, C., Ponferrada, V.G., Jarabek, C.J., Burns, K.A., Bhattacharyya, B., Zorn, A.M., Vize, P.D., 2013. The Xenbase literature curation process. *Database : the journal of biological databases and curation* 2013, bas046.

Bowes, J.B., Snyder, K.A., Segerdell, E., Gibb, R., Jarabek, C., Noumen, E., Pollet, N., Vize, P.D., 2008. Xenbase: a Xenopus biology and genomics resource. *Nucleic Acids Res* 36, D761-767.

Bowes, J.B., Snyder, K.A., Segerdell, E., Jarabek, C.J., Azam, K., Zorn, A.M., Vize, P.D., 2010. Xenbase: gene expression and improved integration. *Nucleic Acids Res* 38, D607-612.

Boyd, W.A., McBride, S.J., Rice, J.R., Snyder, D.W., Freedman, J.H., 2010a. A high-throughput method for assessing chemical toxicity using a *Caenorhabditis elegans* reproduction assay. *Toxicol Appl Pharmacol* 245, 153-159.

Boyd, W.A., Smith, M.V., Kissling, G.E., Freedman, J.H., 2010b. Medium- and high-throughput screening of neurotoxicants using *C. elegans*. *Neurotoxicol Teratol* 32, 68-73.

Braeuer, R.R., Watson, I. R., Wu, C. J., Mobley, A. K., Kamiya, T., Shoshan, E., Bar-Eli, M., 2013. Why is melanoma so metastatic? *Pigment Cell Melanoma Res.* 27, 19-36.

Brandli, A.W., 2004. Prospects for the *Xenopus* Embryo Model in Therapeutics Technologies. *CHIMA International journal for Chemistry* 58.

Brennan, H.C., Nijjar, S., Jones, E.A., 1999. The specification and growth factor inducibility of the pronephric glomus in *Xenopus laevis*. *Development* 126, 5847-5856.

Brenner, S., 1974. The genetics of *Caenorhabditis elegans*. *Genetics* 77, 71-94.

Brown, F.K., 1998. Chemoinformatics: What is it and How does it Impact Drug Discovery, in: Bristol, J.A. (Ed.), *Annual Reports in Med. Chem.* . Academic Press, London.

Bucșa C, F.A., Cazacu I, Leucuta D, Achimas-Cadariu A, Mogosan C, Bojita M., 2013. How many potential drug-drug interactions cause adverse drug reactions in hospitalized patients? *Eur J Intern Med* 24, 27-33.

Bunnage, M.E., 2011. Getting pharmaceutical R&D back on target. *Nat Chem Biol* 7, 335-339.

Butcher, E.C., 2005. Can cell systems biology rescue drug discovery? *Nature Reviews Drug Discovery* 4, 461-467.

Cahn, L., 2012. Focus on the patent cliff to maximize generic savings. *Managed care* 21, 28-32.

Caldwell, G.W., Yan, Z.Y., Tang, W.M., Dasgupta, M., Hasting, B., 2009. ADME Optimization and Toxicity Assessment in Early- and Late-Phase Drug Discovery. *Curr Top Med Chem* 9, 965-980.

Carroll, P.M., Dougherty, B., Ross-Macdonald, P., Browman, K., FitzGerald, K., 2003. Model systems in drug discovery: chemical genetics meets genomics. *Pharmacol Therapeut* 99, 183-220.

Cha, E., Klinger, M., Hou, Y., Cummings, C., Ribas, A., Faham, M., Fong, L., 2014. Improved Survival with T Cell Clonotype Stability After Anti-CTLA-4 Treatment in Cancer Patients. *Science translational medicine* 6, 238ra270.

Chapman, P.B., Hauschild, A., Robert, C., Haanen, J.B., Ascierto, P., Larkin, J., Dummer, R., Garbe, C., Testori, A., Maio, M., Hogg, D., Lorigan, P., Lebbe, C., Jouary, T., Schadendorf, D., Ribas, A., O'Day, S.J., Sosman, J.A., Kirkwood, J.M., Eggermont, A.M., Dreno, B., Nolop, K., Li, J., Nelson, B., Hou, J., Lee, R.J., Flaherty, K.T., McArthur, G.A., Group, B.-S., 2011. Improved survival with vemurafenib in melanoma with BRAF V600E mutation. *The New England journal of medicine* 364, 2507-2516.

Chen, L., Morrow, J.K., Tran, H.T., Phatak, S.S., Du-Cuny, L., Zhang, S., 2012. From laptop to benchtop to bedside: structure-based drug design on protein targets. *Current pharmaceutical design* 18, 1217-1239.

Cheng, A.C., Coleman, R.G., Smyth, K.T., Cao, Q., Soulard, P., Caffrey, D.R., Salzberg, A.C., Huang, E.S., 2007. Structure-based maximal affinity model predicts small-molecule druggability. *Nat Biotechnol* 25, 71-75.

Cho, Y.Y., Lee, M.H., Lee, C.J., Yao, K., Lee, H.S., Bode, A.M., Dong, Z., 2012. RSK2 as a key regulator in human skin cancer. *Carcinogenesis* 33, 2529-2537.

Choudhury, D., Ahmed, Z., 2006. Drug-associated renal dysfunction and injury. *Nature clinical practice. Nephrology* 2, 80-91.

Christensen, E.I., Raciti, D., Reggiani, L., Verroust, P.J., Brandli, A.W., 2008. Gene expression analysis defines the proximal tubule as the compartment for endocytic receptor-mediated uptake in the *Xenopus* pronephric kidney. *Pflugers Arch* 456, 1163-1176.

Collazo, A., Bronner-Fraser, M., Fraser, S.E., 1993. Vital dye labelling of *Xenopus laevis* trunk neural crest reveals multipotency and novel pathways of migration. *Development* 118, 363-376.

Collins, F.S., 1999. The human genome project and the future of medicine. *Ann N Y Acad Sci* 882, 42-55; discussion 56-65.

Comanor, W.S., Scherer, F.M., 2013. Mergers and innovation in the pharmaceutical industry. *Journal of health economics* 32, 106-113.

Cong, F., Cheung, A.K., Huang, S.M., 2012. Chemical genetics-based target identification in drug discovery. *Annual review of pharmacology and toxicology* 52, 57-78.

Cortes-Ciriano, I., Koutsoukas, A., Abian, O., Bender, A. and Velazquez-Campoy, A., 2013. Experimental validation of in silico target predictions on synergistic protein targets. *Medchemcomm* 4, 278-288.

Cruciani, G., Pastor, M., Guba, W., 2000. VolSurf: a new tool for the pharmacokinetic optimization of lead compounds. *Eur J Pharm Sci* 11 Suppl 2, S29-39.

Cruz, M.J., Sourial, M.M., Treberg, J.R., Fehsenfeld, S., Adlimoghaddam, A., Weihrauch, D., 2013. Cutaneous nitrogen excretion in the African clawed frog *Xenopus laevis*: effects of high environmental ammonia (HEA). *Aquat Toxicol* 136-137, 1-12.

Dar, A.C., Das, T.K., Shokat, K.M., Cagan, R.L., 2012. Chemical genetic discovery of targets and anti-targets for cancer polypharmacology. *Nature* 486, 80-84.

Davies, M.A., 2012. The role of the PI3K-AKT pathway in melanoma. *Cancer journal* 18, 142-147.

Davies, W.J.a.F., S. J, 1995. Frog Embryo Teratogenesis Assay: *Xenopus* (FETAX), in: O'Hare, S.a.A., C. K. (Ed.), *In Vitro Toxicity Testing Protocols*. Humana Press Inc, Totowa, New Jersey, pp. 311-316.

de Giorgi, V., Gori, A., Grazzini, M., Rossari, S., Scarfi, F., Corciova, S., Verdelli, A., Lotti, T., Massi, D., 2011. Estrogens, estrogen receptors and melanoma. *Expert review of anticancer therapy* 11, 739-747.

de Giorgi, V., Mavilia, C., Massi, D., Gozzini, A., Aragona, P., Tanini, A., Sestini, S., Paglierani, M., Boddi, V., Brandi, M.L., Lotti, T., 2009. Estrogen receptor expression in cutaneous melanoma: a real-time reverse transcriptase-polymerase chain reaction and immunohistochemical study. *Arch Dermatol* 145, 30-36.

den Hertog, J., 2005. Chemical genetics: Drug screens in zebrafish. *Bioscience Rep* 25, 289-297.

Desrochers, T.M., Palma, E., Kaplan, D.L., 2013. Tissue-engineered kidney disease models. *Adv Drug Deliv Rev*.

Dobson, C.M., 2004. Chemical space and biology. *Nature* 432, 824-828.

Donato, M.T., Castell, J.V., 2003. Strategies and molecular probes to investigate the role of cytochrome P450 in drug metabolism: focus on in vitro studies. *Clin Pharmacokinet* 42, 153-178.

Drakakis, G., Hendry, A. E., Hanson, K. M., Brewerton, S. C., Bodkin, M. J., Evans, D. A., Wheeler, G. N. and Bender, A. , 2014. Bioactivity Profile Analysis from Automated Phenotype Detection in *Xenopus laevis* Using Image Processing. *Medchemcomm* 42.

Drews, J., 2003. Strategic trends in the drug industry. *Drug Discovery Today* 8, 411-420.

Dumont, J.N., Schultz, T.W., Buchanan, M. V., and Kao, G, L., 1983. Frog embryo teratogenesis assay *Xenopus*: FETAX - a short term assay applicable to complex environmental mixtures, in: Water, M.D., Sandhu, S. S., Lewtas, J., Claxton, L.,

Chernoff, N., and Nesnow, S. (Ed.), Symposium on the Application of Short-Term Bioassays in the Analysis of Complex Environmental Mixtures: III. Plenum, New York, pp. 393-405.

Dush, M.K., Mclver, A.L., Parr, M.A., Young, D.D., Fisher, J., Newman, D.R., Sannes, P.L., Hauck, M.L., Deiters, A., Nascone-Yoder, N., 2011. Heterotaxin: a TGF-beta signaling inhibitor identified in a multi-phenotype profiling screen in *Xenopus* embryos. *Chem Biol* 18, 252-263.

Eide, M.J., Weinstock, M.A., Clark, M.A., 2009. Demographic and socioeconomic predictors of melanoma prognosis in the United States. *J Health Care Poor Underserved* 20, 227-245.

Ertl, P., Rohde, B., Selzer, P., 2000. Fast calculation of molecular polar surface area as a sum of fragment-based contributions and its application to the prediction of drug transport properties. *J Med Chem* 43, 3714-3717.

Evans, B.J., Kelley, D.B., Tinsley, R.C., Melnick, D.J., Cannatella, D.C., 2004. A mitochondrial DNA phylogeny of African clawed frogs: phylogeography and implications for polyploid evolution. *Molecular phylogenetics and evolution* 33, 197-213.

Fedorenko, I.V., Paraiso, K.H., Smalley, K.S., 2011. Acquired and intrinsic BRAF inhibitor resistance in BRAF V600E mutant melanoma. *Biochem Pharmacol* 82, 201-209.

Feher, M., Schmidt, J.M., 2003. Property distributions: differences between drugs, natural products, and molecules from combinatorial chemistry. *J Chem Inf Comput Sci* 43, 218-227.

Feng, Y., Mitchison, T.J., Bender, A., Young, D.W., Tallarico, J.A., 2009. Multi-parameter phenotypic profiling: using cellular effects to characterize small-molecule compounds. *Nat Rev Drug Discov* 8, 567-578.

Fort, D.J., Rogers, R.L., Thomas, J.H., Buzzard, B.O., Noll, A.M., Spaulding, C.D., 2004. Comparative sensitivity of *Xenopus tropicalis* and *Xenopus laevis* as test species for the FETAX model. *J Appl Toxicol* 24, 443-457.

Fox, S., Farr-Jones, S., Sopchak, L., Boggs, A., Nicely, H.W., Khoury, R., Biros, M., 2006. High-throughput screening: update on practices and success. *J Biomol Screen* 11, 864-869.

Franks, M.E., Macpherson, G.R., Figg, W.D., 2004. Thalidomide. *Lancet* 363, 1802-1811.

Frantz, S., 2004. 2003 approvals: a year of innovation and upward trends. *Nat Rev Drug Discov* 3, 103-105.

Frye, S., Crosby, M., Edwards, T., Juliano, R., 2011. US academic drug discovery. *Nat Rev Drug Discov* 10, 409-410.

Frye, S.V., 2013. Drug discovery in academic institutions. Hematology / the Education Program of the American Society of Hematology. American Society of Hematology. Education Program 2013, 300-305.

Fuchs, T.C., Hewitt, P., 2011. Biomarkers for drug-induced renal damage and nephrotoxicity-an overview for applied toxicology. *The AAPS journal* 13, 615-631.

Gaggioli, C., Sahai, E., 2007. Melanoma invasion - current knowledge and future directions. *Pigment cell research / sponsored by the European Society for Pigment Cell Research and the International Pigment Cell Society* 20, 161-172.

Ganesan, A., 2008. The impact of natural products upon modern drug discovery. *Current opinion in chemical biology* 12, 306-317.

Garbe, C., Leiter, U., 2009. Melanoma epidemiology and trends. *Clin Dermatol* 27, 3-9.

Garraway, L.A., Widlund, H.R., Rubin, M.A., Getz, G., Berger, A.J., Ramaswamy, S., Beroukhim, R., Milner, D.A., Granter, S.R., Du, J., Lee, C., Wagner, S.N., Li, C., Golub, T.R., Rimm, D.L., Meyerson, M.L., Fisher, D.E., Sellers, W.R., 2005.

Integrative genomic analyses identify MITF as a lineage survival oncogene amplified in malignant melanoma. *Nature* 436, 117-122.

Gascoigne, K.E., Taylor, S.S., 2008. Cancer cells display profound intra- and interline variation following prolonged exposure to antimetabolic drugs. *Cancer cell* 14, 111-122.

Gaulton, A., Bellis, L.J., Bento, A.P., Chambers, J., Davies, M., Hersey, A., Light, Y., McGlinchey, S., Michalovich, D., Al-Lazikani, B., Overington, J.P., 2012. ChEMBL: a large-scale bioactivity database for drug discovery. *Nucleic Acids Res* 40, D1100-1107.

Gedeck, P., Rohde, B., Bartels, C., 2006. QSAR--how good is it in practice? Comparison of descriptor sets on an unbiased cross section of corporate data sets. *Journal of chemical information and modeling* 46, 1924-1936.

Geerts, T., Vander Heyden, Y., 2011. In silico predictions of ADME-Tox properties: drug absorption. *Combinatorial chemistry & high throughput screening* 14, 339-361.

Giacomotto, J., Segalat, L., 2010. High-throughput screening and small animal models, where are we? *British journal of pharmacology* 160, 204-216.

Giaever, G., Chu, A.M., Ni, L., Connelly, C., Riles, L., Veronneau, S., Dow, S., Lucau-Danila, A., Anderson, K., Andre, B., Arkin, A.P., Astromoff, A., El-Bakkoury, M., Bangham, R., Benito, R., Brachat, S., Campanaro, S., Curtiss, M., Davis, K., Deutschbauer, A., Entian, K.D., Flaherty, P., Foury, F., Garfinkel, D.J., Gerstein, M., Gotte, D., Guldener, U., Hegemann, J.H., Hempel, S., Herman, Z., Jaramillo, D.F., Kelly, D.E., Kelly, S.L., Kotter, P., LaBonte, D., Lamb, D.C., Lan, N., Liang, H., Liao, H., Liu, L., Luo, C., Lussier, M., Mao, R., Menard, P., Ooi, S.L., Revuelta, J.L., Roberts, C.J., Rose, M., Ross-Macdonald, P., Scherens, B., Schimmack, G., Shafer, B., Shoemaker, D.D., Sookhai-Mahadeo, S., Storms, R.K., Strathern, J.N., Valle, G., Voet, M., Volckaert, G., Wang, C.Y., Ward, T.R., Wilhelmy, J., Winzeler, E.A., Yang, Y., Yen, G., Youngman, E., Yu, K., Bussey, H., Boeke, J.D., Snyder, M., Philippsen,

P., Davis, R.W., Johnston, M., 2002. Functional profiling of the *Saccharomyces cerevisiae* genome. *Nature* 418, 387-391.

Gibson-Corley, K.N., Olivier, A.K., Meyerholz, D.K., 2013. Principles for valid histopathologic scoring in research. *Veterinary pathology* 50, 1007-1015.

Goodnow, R.A., Jr., Guba, W., Haap, W., 2003. Library design practices for success in lead generation with small molecule libraries. *Combinatorial chemistry & high throughput screening* 6, 649-660.

Granato, M., van Eeden, F.J., Schach, U., Trowe, T., Brand, M., Furutani-Seiki, M., Haffter, P., Hammerschmidt, M., Heisenberg, C.P., Jiang, Y.J., Kane, D.A., Kelsh, R.N., Mullins, M.C., Odenthal, J., Nusslein-Volhard, C., 1996. Genes controlling and mediating locomotion behavior of the zebrafish embryo and larva. *Development* 123, 399-413.

Greger, J.G., Eastman, S.D., Zhang, V., Bleam, M.R., Hughes, A.M., Smitheman, K.N., Dickerson, S.H., Laquerre, S.G., Liu, L., Gilmer, T.M., 2012. Combinations of BRAF, MEK, and PI3K/mTOR inhibitors overcome acquired resistance to the BRAF inhibitor GSK2118436 dabrafenib, mediated by NRAS or MEK mutations. *Molecular cancer therapeutics* 11, 909-920.

Grimaldi, A.M., Simeone, E., Ascierto, P.A., 2014. The role of MEK inhibitors in the treatment of metastatic melanoma. *Current opinion in oncology* 26, 196-203.

Hackshaw, A., 2009. *A Concise Guide to Clinical Trials*. BMJ Publishing Group Limited, Hoboken, New Jersey.

Han, C., Davies, C. B. and Wang, B., 2010. Evaluation of drug candidates for preclinical development : pharmacokinetics, metabolism, pharmaceutics, and toxicology. Wiley, Hoboken, N.J.

Hann, M.M., Leach, A.R., Harper, G., 2001. Molecular complexity and its impact on the probability of finding leads for drug discovery. *J Chem Inf Comput Sci* 41, 856-864.

Harvey, A.L., 2008. Natural products in drug discovery. *Drug Discov Today* 13, 894-901.

Hausheer, F.H., Kochat, H., Parker, A.R., Ding, D., Yao, S., Hamilton, S.E., Petluru, P.N., Leverett, B.D., Bain, S.H., Saxe, J.D., 2003. New approaches to drug discovery and development: a mechanism-based approach to pharmaceutical research and its application to BNP7787, a novel chemoprotective agent. *Cancer chemotherapy and pharmacology* 52 Suppl 1, S3-15.

Hellsten, U., Harland, R.M., Gilchrist, M.J., Hendrix, D., Jurka, J., Kapitonov, V., Ovcharenko, I., Putnam, N.H., Shu, S., Taher, L., Blitz, I.L., Blumberg, B., Dichmann, D.S., Dubchak, I., Amaya, E., Detter, J.C., Fletcher, R., Gerhard, D.S., Goodstein, D., Graves, T., Grigoriev, I.V., Grimwood, J., Kawashima, T., Lindquist, E., Lucas, S.M., Mead, P.E., Mitros, T., Ogino, H., Ohta, Y., Poliakov, A.V., Pollet, N., Robert, J., Salamov, A., Sater, A.K., Schmutz, J., Terry, A., Vize, P.D., Warren, W.C., Wells, D., Wills, A., Wilson, R.K., Zimmerman, L.B., Zorn, A.M., Grainger, R., Grammer, T., Khokha, M.K., Richardson, P.M., Rokhsar, D.S., 2010. The genome of the Western clawed frog *Xenopus tropicalis*. *Science* 328, 633-636.

Hellsten, U., Khokha, M.K., Grammer, T.C., Harland, R.M., Richardson, P., Rokhsar, D.S., 2007. Accelerated gene evolution and subfunctionalization in the pseudotetraploid frog *Xenopus laevis*. *BMC biology* 5, 31.

Helmcke, K.J., Avila, D.S., Aschner, M., 2010. Utility of *Caenorhabditis elegans* in high throughput neurotoxicological research. *Neurotoxicol Teratol* 32, 62-67.

Ho, R.L., Lieu, C.A., 2008. Systems biology: an evolving approach in drug discovery and development. *Drugs in R&D* 9, 203-216.

Hofmann, U.B., Westphal, J.R., Van Muijen, G.N., Ruitter, D.J., 2000. Matrix metalloproteinases in human melanoma. *J Invest Dermatol* 115, 337-344.

Hoke, R.A., Ankley, G.T., 2005. Application of frog embryo teratogenesis assay-*Xenopus* to ecological risk assessment. *Environ Toxicol Chem* 24, 2677-2690.

Hopkins, A.L., 2008. Network pharmacology: the next paradigm in drug discovery. *Nat Chem Biol* 4, 682-690.

Hopkins, A.L., Groom, C.R., 2002. The druggable genome. *Nat Rev Drug Discov* 1, 727-730.

Hornberg, J.J., Laursen, M., Brenden, N., Persson, M., Thougard, A.V., Toft, D.B., Mow, T., 2013. Exploratory toxicology as an integrated part of drug discovery. Part II: Screening strategies. *Drug Discov Today*.

Hughes, J.P., Rees, S., Kalindjian, S.B., Philpott, K.L., 2011. Principles of early drug discovery. *British journal of pharmacology* 162, 1239-1249.

Hurko, O., 2010. Future drug discovery and development. *Mol Genet Metab* 100 Suppl 1, S92-96.

James-Zorn, C., Ponferrada, V.G., Jarabek, C.J., Burns, K.A., Segerdell, E.J., Lee, J., Snyder, K., Bhattacharyya, B., Karpinka, J.B., Fortriede, J., Bowes, J.B., Zorn, A.M., Vize, P.D., 2013. Xenbase: expansion and updates of the *Xenopus* model organism database. *Nucleic Acids Res* 41, D865-870.

Jiang, C.C., Lucas, K., Avery-Kiejda, K.A., Wade, M., deBock, C.E., Thorne, R.F., Allen, J., Hersey, P., Zhang, X.D., 2008. Up-regulation of Mcl-1 is critical for survival of human melanoma cells upon endoplasmic reticulum stress. *Cancer Res* 68, 6708-6717.

Jones, E.A., 2005. *Xenopus*: a prince among models for pronephric kidney development. *Journal of the American Society of Nephrology : JASN* 16, 313-321.

Jorissen, R.N., Gilson, M.K., 2005. Virtual screening of molecular databases using a support vector machine. *Journal of chemical information and modeling* 45, 549-561.

Joyce, T., Oikonomou, E., Kosmidou, V., Makrodouli, E., Bantounas, I., Avlonitis, S., Zografos, G., Pintzas, A., 2012. A molecular signature for oncogenic BRAF in human colon cancer cells is revealed by microarray analysis. *Current cancer drug targets* 12, 873-898.

Kaitin, K.I., 2010. Deconstructing the drug development process: the new face of innovation. *Clin Pharmacol Ther* 87, 356-361.

Kalin, R.E., Banziger-Tobler, N.E., Detmar, M., Brandli, A.W., 2009. An in vivo chemical library screen in *Xenopus* tadpoles reveals novel pathways involved in angiogenesis and lymphangiogenesis. *Blood* 114, 1110-1122.

Karreth, F.A., DeNicola, G.M., Winter, S.P., Tuveson, D.A., 2009. C-Raf inhibits MAPK activation and transformation by B-Raf(V600E). *Molecular cell* 36, 477-486.

Kasagi, N., Gomyo, Y., Shirai, H., Tsujitani, S., Ito, H., 1994. Apoptotic cell death in human gastric carcinoma: analysis by terminal deoxynucleotidyl transferase-mediated dUTP-biotin nick end labeling. *Jpn J Cancer Res* 85, 939-945.

Kau, T.R., Schroeder, F., Ramaswamy, S., Wojciechowski, C.L., Zhao, J.J., Roberts, T.M., Clardy, J., Sellers, W.R., Silver, P.A., 2003. A chemical genetic screen identifies inhibitors of regulated nuclear export of a Forkhead transcription factor in PTEN-deficient tumor cells. *Cancer cell* 4, 463-476.

Kell, D.B., 2013. Finding novel pharmaceuticals in the systems biology era using multiple effective drug targets, phenotypic screening and knowledge of transporters: where drug discovery went wrong and how to fix it. *The FEBS journal* 280, 5957-5980.

King, S., 2013. The Best Selling Drug Since 1996 - Why AbbVie's Set to Eclipse Pfizer's Lipitor. *Forbes*, USA.

Kitano, H., 2007. Towards a theory of biological robustness. *Molecular systems biology* 3, 137.

Kneller, R., 2010. The importance of new companies for drug discovery: origins of a decade of new drugs. *Nat Rev Drug Discov* 9, 867-882.

Kodadek, T., 2011. The rise, fall and reinvention of combinatorial chemistry. *Chemical communications* 47, 9757-9763.

Kola, I., Landis, J., 2004. Can the pharmaceutical industry reduce attrition rates? *Nature Reviews Drug Discovery* 3, 711-715.

Kortagere, S., Lill, M., Kerrigan, J., 2012. Role of computational methods in pharmaceutical sciences. *Methods Mol Biol* 929, 21-48.

Kubinyi, H., 2003. Drug research: myths, hype and reality. *Nat Rev Drug Discov* 2, 665-668.

Kumar, S., Hedges, S.B., 1998. A molecular timescale for vertebrate evolution. *Nature* 392, 917-920.

Kumasaka, M., Sato, S., Yajima, I., Goding, C.R., Yamamoto, H., 2005. Regulation of melanoblast and retinal pigment epithelium development by *Xenopus laevis* Mitf. *Dev Dyn* 234, 523-534.

Kwong, L.N., Costello, J.C., Liu, H., Jiang, S., Helms, T.L., Langsdorf, A.E., Jakubosky, D., Genovese, G., Muller, F.L., Jeong, J.H., Bender, R.P., Chu, G.C., Flaherty, K.T., Wargo, J.A., Collins, J.J., Chin, L., 2012. Oncogenic NRAS signaling differentially regulates survival and proliferation in melanoma. *Nat Med* 18, 1503-1510.

Kwong, L.N., Davies, M.A., 2014. Targeted therapy for melanoma: rational combinatorial approaches. *Oncogene* 33, 1-9.

LaMattina, J.L., 2011. The impact of mergers on pharmaceutical R&D. *Nat Rev Drug Discov* 10, 559-560.

Lander, E.S., Linton, L.M., Birren, B., Nussbaum, C., Zody, M.C., Baldwin, J., Devon, K., Dewar, K., Doyle, M., FitzHugh, W., Funke, R., Gage, D., Harris, K., Heaford, A., Howland, J., Kann, L., Lehoczky, J., LeVine, R., McEwan, P., McKernan, K., Meldrim, J., Mesirov, J.P., Miranda, C., Morris, W., Naylor, J., Raymond, C., Rosetti, M., Santos, R., Sheridan, A., Sougnez, C., Stange-Thomann, N., Stojanovic, N., Subramanian, A., Wyman, D., Rogers, J., Sulston, J., Ainscough, R., Beck, S., Bentley, D., Burton, J., Clee, C., Carter, N., Coulson, A., Deadman, R., Deloukas, P.,

Dunham, A., Dunham, I., Durbin, R., French, L., Grafham, D., Gregory, S., Hubbard, T., Humphray, S., Hunt, A., Jones, M., Lloyd, C., McMurray, A., Matthews, L., Mercer, S., Milne, S., Mullikin, J.C., Mungall, A., Plumb, R., Ross, M., Shownkeen, R., Sims, S., Waterston, R.H., Wilson, R.K., Hillier, L.W., McPherson, J.D., Marra, M.A., Mardis, E.R., Fulton, L.A., Chinwalla, A.T., Pepin, K.H., Gish, W.R., Chissoe, S.L., Wendl, M.C., Delehaunty, K.D., Miner, T.L., Delehaunty, A., Kramer, J.B., Cook, L.L., Fulton, R.S., Johnson, D.L., Minx, P.J., Clifton, S.W., Hawkins, T., Branscomb, E., Predki, P., Richardson, P., Wenning, S., Slezak, T., Doggett, N., Cheng, J.F., Olsen, A., Lucas, S., Elkin, C., Uberbacher, E., Frazier, M., Gibbs, R.A., Muzny, D.M., Scherer, S.E., Bouck, J.B., Sodergren, E.J., Worley, K.C., Rives, C.M., Gorrell, J.H., Metzker, M.L., Naylor, S.L., Kucherlapati, R.S., Nelson, D.L., Weinstock, G.M., Sakaki, Y., Fujiyama, A., Hattori, M., Yada, T., Toyoda, A., Itoh, T., Kawagoe, C., Watanabe, H., Totoki, Y., Taylor, T., Weissenbach, J., Heilig, R., Saurin, W., Artiguenave, F., Brottier, P., Bruls, T., Pelletier, E., Robert, C., Wincker, P., Rosenthal, A., Platzer, M., Nyakatura, G., Taudien, S., Rump, A., Yang, H.M., Yu, J., Wang, J., Huang, G.Y., Gu, J., Hood, L., Rowen, L., Madan, A., Qin, S.Z., Davis, R.W., Federspiel, N.A., Abola, A.P., Proctor, M.J., Myers, R.M., Schmutz, J., Dickson, M., Grimwood, J., Cox, D.R., Olson, M.V., Kaul, R., Raymond, C., Shimizu, N., Kawasaki, K., Minoshima, S., Evans, G.A., Athanasiou, M., Schultz, R., Roe, B.A., Chen, F., Pan, H.Q., Ramser, J., Lehrach, H., Reinhardt, R., McCombie, W.R., de la Bastide, M., Dedhia, N., Blocker, H., Hornischer, K., Nordsiek, G., Agarwala, R., Aravind, L., Bailey, J.A., Bateman, A., Batzoglou, S., Birney, E., Bork, P., Brown, D.G., Burge, C.B., Cerutti, L., Chen, H.C., Church, D., Clamp, M., Copley, R.R., Doerks, T., Eddy, S.R., Eichler, E.E., Furey, T.S., Galagan, J., Gilbert, J.G.R., Harmon, C., Hayashizaki, Y., Haussler, D., Hermjakob, H., Hokamp, K., Jang, W.H., Johnson, L.S., Jones, T.A., Kasif, S., Kasprzyk, A., Kennedy, S., Kent, W.J., Kitts, P., Koonin, E.V., Korf, I., Kulp, D., Lancet, D., Lowe, T.M., McLysaght, A., Mikkelsen, T.,

Moran, J.V., Mulder, N., Pollara, V.J., Ponting, C.P., Schuler, G., Schultz, J.R., Slater, G., Smit, A.F.A., Stupka, E., Szustakowki, J., Thierry-Mieg, D., Thierry-Mieg, J., Wagner, L., Wallis, J., Wheeler, R., Williams, A., Wolf, Y.I., Wolfe, K.H., Yang, S.P., Yeh, R.F., Collins, F., Guyer, M.S., Peterson, J., Felsenfeld, A., Wetterstrand, K.A., Patrinos, A., Morgan, M.J., Conso, I.H.G.S., 2001. Initial sequencing and analysis of the human genome. *Nature* 409, 860-921.

Lash, L., 2009. Toxicology of the kidney, in: Bussiere, J. (Ed.), *Non-Clinical Testing for Toxicity of Pharmaceuticals: Regulatory and Practical Standards for Testing and Application*. The Biomedical and Life Sciences Collection, Henry Stuart Talks, London.

Lazarou, J., Pomeranz, B.H., Corey, P.N., 1998. Incidence of adverse drug reactions in hospitalized patients: a meta-analysis of prospective studies. *JAMA* 279, 1200-1205.

Lee, J.A., Uhlik, M.T., Moxham, C.M., Tomandl, D., Sall, D.J., 2012. Modern phenotypic drug discovery is a viable, neoclassic pharma strategy. *J Med Chem* 55, 4527-4538.

Lee, J.H., Choi, J. W. and Kim, Y. S., 2011. Frequencies of BRAF and NRAS mutations are different in histological types and sites of origin of cutaneous melanoma: a meta analysis. *Br J Dermatol* 164, 776-784.

Lemieux, G.A., Keiser, M.J., Sassano, M.F., Laggner, C., Mayer, F., Bainton, R.J., Werb, Z., Roth, B.L., Shoichet, B.K., Ashrafi, K., 2013. In silico molecular comparisons of *C. elegans* and mammalian pharmacology identify distinct targets that regulate feeding. *PLoS biology* 11, e1001712.

Li, C., Xu, L., Wolan, D.W., Wilson, I.A., Olson, A.J., 2004. Virtual screening of human 5-aminoimidazole-4-carboxamide ribonucleotide transformylase against the NCI diversity set by use of AutoDock to identify novel nonfolate inhibitors. *J Med Chem* 47, 6681-6690.

Li, L., Kang, Lan. and Gentela, Shilpa., 2008. 'China Versus India' - Reality check for pharma R&D. Korn/Ferry International, Los Angeles.

Liang, C.C., Park, A.Y., Guan, J.L., 2007. In vitro scratch assay: a convenient and inexpensive method for analysis of cell migration in vitro. *Nat Protoc* 2, 329-333.

Liggi, S., Drakakis, G., Hendry, A. E., Hanson, K. M., Brewerton, S. C., Wheeler, G. N., Bodkin, M. J., Evans, D. A. and Bender, A., 2013. Extensions to In Silico Bioactivity Predictions Using Pathway Annotations and Differential Pharmacology Analysis: Application to *Xenopus laevis* Phenotypic Readouts. *Mol. Inf.* 32, 1009-1024.

Lin, Z., Will, Y., 2012. Evaluation of drugs with specific organ toxicities in organ-specific cell lines. *Toxicol Sci* 126, 114-127.

Lipinski, C., Hopkins, A., 2004. Navigating chemical space for biology and medicine. *Nature* 432, 855-861.

Lipinski, C.A., Lombardo, F., Dominy, B.W., Feeney, P.J., 2001. Experimental and computational approaches to estimate solubility and permeability in drug discovery and development settings. *Adv Drug Deliv Rev* 46, 3-26.

Lopez-Vallejo, F., Caulfield, T., Martinez-Mayorga, K., Giulianotti, M.A., Nefzi, A., Houghten, R.A., Medina-Franco, J.L., 2011. Integrating virtual screening and combinatorial chemistry for accelerated drug discovery. *Combinatorial chemistry & high throughput screening* 14, 475-487.

Lorman, A.J., 2001. Clinical trials face heightened scrutiny as science and commerce appear to merge. *The journal of biolaw & business* 4, 23-32.

Lounkine, E., Keiser, M.J., Whitebread, S., Mikhailov, D., Hamon, J., Jenkins, J.L., Lavan, P., Weber, E., Doak, A.K., Cote, S., Shoichet, B.K., Urban, L., 2012. Large-scale prediction and testing of drug activity on side-effect targets. *Nature* 486, 361-367.

MacDonald, I.L., Lerer, L.B., 1994. A time-series analysis of trends in firearm-related homicide and suicide. *International journal of epidemiology* 23, 66-72.

Madureira, P., de Mello, R.A., 2014. BRAF and MEK Gene Rearrangements in Melanoma: Implications for Targeted Therapy. *Molecular diagnosis & therapy*.

Magnussen, G.I., Holm, R., Emilsen, E., Rosnes, A.K., Slipicevic, A., Florenes, V.A., 2012. High expression of Wee1 is associated with poor disease-free survival in malignant melanoma: potential for targeted therapy. *PLoS One* 7, e38254.

Maldonado, A.G., Doucet, J.P., Petitjean, M., Fan, B.T., 2006. Molecular similarity and diversity in chemoinformatics: from theory to applications. *Mol Divers* 10, 39-79.

Manev, H., Dimitrijevic, N., 2004. Drosophila model for in vivo pharmacological analgesia research. *Eur J Pharmacol* 491, 207-208.

Marcocci, L., De Marchi, U., Milella, Z.G., Agostinelli, E., Mondov, B., Toninello, A., 2001. Role of monoamine oxidases on rat liver mitochondrial function. *Inflammation research : official journal of the European Histamine Research Society ... [et al.]* 50 Suppl 2, S132-133.

Marconi, C., Bianchini, F., Mannini, A., Mugnai, G., Ruggieri, S., Calorini, L., 2008. Tumoral and macrophage uPAR and MMP-9 contribute to the invasiveness of B16 murine melanoma cells. *Clinical & experimental metastasis* 25, 225-231.

Meijer, A.J., Lamers, W.H., Chamuleau, R.A., 1990. Nitrogen metabolism and ornithine cycle function. *Physiological reviews* 70, 701-748.

Menzies, A.M., Long, G.V., 2013. New combinations and immunotherapies for melanoma: latest evidence and clinical utility. *Therapeutic advances in medical oncology* 5, 278-285.

Michelini, E., Cevenini, L., Mezzanotte, L., Coppa, A., Roda, A., 2010. Cell-based assays: fuelling drug discovery. *Analytical and Bioanalytical Chemistry* 398, 227-238.

Montagut, C., Sharma, S.V., Shioda, T., McDermott, U., Ulman, M., Ulkus, L.E., Dias-Santagata, D., Stubbs, H., Lee, D.Y., Singh, A., Drew, L., Haber, D.A.,

Settleman, J., 2008. Elevated CRAF as a potential mechanism of acquired resistance to BRAF inhibition in melanoma. *Cancer Res* 68, 4853-4861.

Moriya, N., Uchiyama, H. and Asashima, M., 1993. Induction of Pronephric Tubules by Activin and Retinoic Acid in Presumptive Ectoderm of *Xenopus laevis*. *Development, Growth and Differentiation* 35, 123-128.

Mouche, I., Malesic, L., Gillardeaux, O., 2011. FETAX assay for evaluation of developmental toxicity. *Methods Mol Biol* 691, 257-269.

Mullard, A., 2011. Partnering between pharma peers on the rise. *Nat Rev Drug Discov* 10, 561-562.

Munos, B., 2009. Lessons from 60 years of pharmaceutical innovation. *Nat Rev Drug Discov* 8, 959-968.

Murphy, P.J., 2001. Xenobiotic metabolism: a look from the past to the future. *Drug Metab Dispos* 29, 779-780.

Mushegian, A.R., Garey, J.R., Martin, J., Liu, L.X., 1998. Large-scale taxonomic profiling of eukaryotic model organisms: a comparison of orthologous proteins encoded by the human, fly, nematode, and yeast genomes. *Genome Res* 8, 590-598.

National Kidney, F., 2002. K/DOQI clinical practice guidelines for chronic kidney disease: evaluation, classification, and stratification. *Am J Kidney Dis* 39, S1-266.

Nichols, C.D., 2006. *Drosophila melanogaster* neurobiology, neuropharmacology, and how the fly can inform central nervous system drug discovery. *Pharmacol Ther* 112, 677-700.

Nieuwkoop, P.D.a.F., J, 1956. Normal table of *Xenopus laevis* (Daudin): a systematical and chronological survey of the development from the fertilized egg till the end of metamorphosis, North-Holland Publishing Company,. North-Holland Publishing Company, Amsterdam.

Osafune, K., Nishinakamura, R., Komazaki, S., Asashima, M., 2002. In vitro induction of the pronephric duct in *Xenopus* explants. *Development, growth & differentiation* 44, 161-167.

Pammolli, F., Magazzini, L., Riccaboni, M., 2011. The productivity crisis in pharmaceutical R&D. *Nat Rev Drug Discov* 10, 428-438.

Pandey, M.K., Gowda, K., Doi, K., Sharma, A.K., Wang, H.G., Amin, S., 2013. Proteasomal degradation of Mcl-1 by maritoclax induces apoptosis and enhances the efficacy of ABT-737 in melanoma cells. *PLoS One* 8, e78570.

Pannu, N., Nadim, M.K., 2008. An overview of drug-induced acute kidney injury. *Critical care medicine* 36, S216-223.

Papoutsis, M., Siemeister, G., Weindel, K., Tomarev, S.I., Kurz, H., Schachtele, C., Martiny-Baron, G., Christ, B., Marme, D., Wilting, J., 2000. Active interaction of human A375 melanoma cells with the lymphatics in vivo. *Histochemistry and cell biology* 114, 373-385.

Parker, C.N., Schreyer, S.K., 2004. Application of chemoinformatics to high-throughput screening: practical considerations. *Methods Mol Biol* 275, 85-110.

Paul, S.M., Mytelka, D.S., Dunwiddie, C.T., Persinger, C.C., Munos, B.H., Lindborg, S.R., Schacht, A.L., 2010. How to improve R&D productivity: the pharmaceutical industry's grand challenge. *Nat Rev Drug Discov* 9, 203-214.

Peppicelli, S., Bianchini, F., Contena, C., Tombaccini, D., Calorini, L., 2013. Acidic pH via NF-kappaB favours VEGF-C expression in human melanoma cells. *Clinical & experimental metastasis* 30, 957-967.

Peterson, R.T., Link, B.A., Dowling, J.E., Schreiber, S.L., 2000. Small molecule developmental screens reveal the logic and timing of vertebrate development. *Proc Natl Acad Sci U S A* 97, 12965-12969.

Pietrangeli, P., Mondovi, B., 2004. Amine oxidases and tumors. *Neurotoxicology* 25, 317-324.

Portilla, L.M., Alving, B., 2010. Reaping the benefits of biomedical research: partnerships required. *Science translational medicine* 2, 35cm17.

Proschak, E., 2013. Reconsidering the drug discovery pipeline for designed multitarget drugs. *Drug Discov Today* 18, 1129-1130.

Rautio, J., Kumpulainen, H., Heimbach, T., Oliyai, R., Oh, D., Jarvinen, T., Savolainen, J., 2008. Prodrugs: design and clinical applications. *Nat Rev Drug Discov* 7, 255-270.

Read, R.D., Goodfellow, P.J., Mardis, E.R., Novak, N., Armstrong, J.R., Cagan, R.L., 2005. A *Drosophila* model of multiple endocrine neoplasia type 2. *Genetics* 171, 1057-1081.

Reymond, J.L., van Deursen, R., Blum, L.C., Ruddigkeit, L., 2010. Chemical space as a source for new drugs. *Medchemcomm* 1, 30-38.

Rick, N.G., 2009. *Drugs: From Discovery to Approval*. John Wiley & Sons, Hoboken, New Jersey.

Rinderknecht, M., Detmar, M., 2008. Tumor lymphangiogenesis and melanoma metastasis. *Journal of cellular physiology* 216, 347-354.

Sabbatino, F., Wang, Y., Wang, X., Ferrone, S., Ferrone, C.R., 2013. Emerging BRAF inhibitors for melanoma. *Expert opinion on emerging drugs* 18, 431-443.

Scannell, J.W., Blanckley, A., Boldon, H., Warrington, B., 2012. Diagnosing the decline in pharmaceutical R&D efficiency. *Nat Rev Drug Discov* 11, 191-200.

Schrattenholz, A., Soskic, V., 2008. What does systems biology mean for drug development? *Curr Med Chem* 15, 1520-1528.

Schreiber, S., Kapoor, T. K., Wess, G., Olah, M., Rad, R., Ostopovici, L., Bora, A., Hadaruga, N., Hadaruga, D., Moldovan, R., Fuias, A., Mractc, M. and Oprea, T. I., 2008. WOMBAT and WOMBAT-PK: Bioactivity Databases for Lead and Drug Discovery. Wiley.

Searle, P.L., 1984. The berthelot or indophenol reaction and its use in the analytical chemistry of nitrogen. A review. *Analyst*, 549-568.

Segalat, L., 2007. Invertebrate animal models of diseases as screening tools in drug discovery. *ACS Chem Biol* 2, 231-236.

Seufert, D.W., Brennan, H.C., DeGuire, J., Jones, E.A., Vize, P.D., 1999. Developmental basis of pronephric defects in *Xenopus* body plan phenotypes. *Dev Biol* 215, 233-242.

Siddiqui, A.D., Piperdi, B., 2010. KRAS mutation in colon cancer: a marker of resistance to EGFR-I therapy. *Ann Surg Oncol* 17, 1168-1176.

Silber, B.M., 2010. Driving drug discovery: the fundamental role of academic labs. *Science translational medicine* 2, 30cm16.

Slusher, B.S., Conn, P.J., Frye, S., Glicksman, M., Arkin, M., 2013. Bringing together the academic drug discovery community. *Nat Rev Drug Discov* 12, 811-812.

Solomon, M.D., 1974. A study of codeine metabolism. *Clin Toxicol* 7, 255-257.

Song, Y., Chen, W., Kang, D., Zhan, P., Liu, X., 2014. "Old Friends in New Guise": Exploiting Privileged Structures for Scaffold Re-evolution/Refining. *Combinatorial chemistry & high throughput screening*.

Sorkin, A.R., and Duff, Wilson., 2009. Pfizer agrees to pay \$69 billion for rival drug maker Wyeth, *New York Times*. New York Times, New York, USA.

Spring, D.R., 2005. Chemical genetics to chemical genomics: small molecules offer big insights. *Chem Soc Rev* 34, 472-482.

Stevens, A.J., Jensen, J.J., Wyller, K., Kilgore, P.C., Chatterjee, S., Rohrbaugh, M.L., 2011. The role of public-sector research in the discovery of drugs and vaccines. *The New England journal of medicine* 364, 535-541.

Stevens, L.A., Coresh, J., Greene, T., Levey, A.S., 2006. Assessing kidney function--measured and estimated glomerular filtration rate. *The New England journal of medicine* 354, 2473-2483.

Stilwell, G.E., Saraswati, S., Littleton, J.T., Chouinard, S.W., 2006. Development of a *Drosophila* seizure model for in vivo high-throughput drug screening. *The European journal of neuroscience* 24, 2211-2222.

Swinney, D.C., Anthony, J., 2011. How were new medicines discovered? *Nat Rev Drug Discov* 10, 507-519.

Sykes, M.L., Avery, V.M., 2013. Approaches to protozoan drug discovery: phenotypic screening. *J Med Chem* 56, 7727-7740.

T. T. Ngo , A.P.H.P., C. F. Yam , H. M. Lenhoff, 1982. Interference in determination of ammonia with the hypochlorite-alkaline phenol method of Berthelot. *Anal Chem* 54, 46-49.

Tan, H., Ge, X., Xie, L., 2013. Structural systems pharmacology: a new frontier in discovering novel drug targets. *Current drug targets* 14, 952-958.

Tang, J., Aittokallio, T., 2014. Network pharmacology strategies toward multi-target anticancer therapies: from computational models to experimental design principles. *Current pharmaceutical design* 20, 23-36.

Taylor, K.L., Grant, N.J., Temperley, N.D., Patton, E.E., 2010. Small molecule screening in zebrafish: an in vivo approach to identifying new chemical tools and drug leads. *Cell communication and signaling : CCS* 8, 11.

Tian, S., Li, Y., Wang, J., Zhang, J., Hou, T., 2011. ADME evaluation in drug discovery. 9. Prediction of oral bioavailability in humans based on molecular properties and structural fingerprints. *Molecular pharmaceutics* 8, 841-851.

Tollman, P., Morieux, Y., Murphy, J.K., Schulze, U., 2011. Identifying R&D outliers. *Nat Rev Drug Discov* 10, 653-654.

Tomlinson, M.L., Field, R.A., Wheeler, G.N., 2005. *Xenopus* as a model organism in developmental chemical genetic screens. *Mol Biosyst* 1, 223-228.

Tomlinson, M.L., Guan, P.P., Morris, R.J., Fidock, M.D., Rejzek, M., Garcia-Morales, C., Field, R.A., Wheeler, G.N., 2009a. A Chemical Genomic Approach Identifies

Matrix Metalloproteinases as Playing an Essential and Specific Role in *Xenopus* Melanophore Migration. *Chemistry & Biology* 16, 93-104.

Tomlinson, M.L., Hendry, A, E. and Wheeler, G. W., 2012. Chemical Genetics and Drug Discovery in *Xenopus*, *Methods in Molecular Biology*.

Tomlinson, M.L., Rejzek, M., Fidock, M., Field, R.A., Wheeler, G.N., 2009b. Chemical genomics identifies compounds affecting *Xenopus laevis* pigment cell development. *Molecular Biosystems* 5, 376-384.

Tralau-Stewart, C., Low, C.M., Marlin, N., 2013. UK academic drug discovery. *Nat Rev Drug Discov* 13, 15-16.

Underhay, E., E. and Baldwin, E., 1955. Nitrogen excretion in the tadpoles of *Xenopus laevis* Daudin. *Biochem J* 61, 544-547.

Valerio, L.G., Jr., Choudhuri, S., 2012. Chemoinformatics and chemical genomics: potential utility of in silico methods. *J Appl Toxicol* 32, 880-889.

Vidal, M., Larson, D.E., Cagan, R.L., 2006. Csk-deficient boundary cells are eliminated from normal *Drosophila* epithelia by exclusion, migration, and apoptosis. *Developmental cell* 10, 33-44.

Villar, H.O., Hansen, M.R., 2009. Design of chemical libraries for screening. *Expert Opin Drug Discov* 4, 1215-1220.

Vize, P.D., Wolf, A. S. and Bard, J. B. L., 2003. *The Kidney*. Academic Press, London.

Vogt, M., Bajorath, J., 2012. Chemoinformatics: a view of the field and current trends in method development. *Bioorganic & medicinal chemistry* 20, 5317-5323.

Wan, P.T., Garnett, M.J., Roe, S.M., Lee, S., Niculescu-Duvaz, D., Good, V.M., Jones, C.M., Marshall, C.J., Springer, C.J., Barford, D., Marais, R., 2004. Mechanism of activation of the RAF-ERK signaling pathway by oncogenic mutations of B-RAF. *Cell* 116, 855-867.

Wang, X., Li, K.F., Adams, E., Van Schepdael, A., 2011. Matrix metalloproteinase inhibitors: a review on bioanalytical methods, pharmacokinetics and metabolism. *Curr Drug Metab* 12, 395-410.

Wang, Y., Xiao, J., Suzek, T.O., Zhang, J., Wang, J., Bryant, S.H., 2009. PubChem: a public information system for analyzing bioactivities of small molecules. *Nucleic Acids Res* 37, W623-633.

Waring, W.S., Moonie, A., 2011. Earlier recognition of nephrotoxicity using novel biomarkers of acute kidney injury. *Clinical toxicology* 49, 720-728.

Weigelt, J., 2009. The case for open-access chemical biology. A strategy for pre-competitive medicinal chemistry to promote drug discovery. *EMBO Rep* 10, 941-945.

Weir, A., 2009. General introduction to non-clinical toxicity testing of pharmaceuticals, in: Bussiere, J. (Ed.), *Non-Clinical Testing for Toxicity of Pharmaceuticals: Regulatory and Practical Standards for Testing and Application*. The Biomedical and Life Sciences Collection, Henry Stewart Talks, London.

West, D.B., Iakougova, O., Olsson, C., Ross, D., Ohmen, J., Chatterjee, A., 2000. Mouse genetics/genomics: an effective approach for drug target discovery and validation. *Med Res Rev* 20, 216-230.

Wheeler, G.N., Brandli, A.W., 2009. Simple vertebrate models for chemical genetics and drug discovery screens: lessons from zebrafish and *Xenopus*. *Dev Dyn* 238, 1287-1308.

Wheeler, G.N., Field, R. A. and Tomlinson, M. L., 2012. Chapter 10 - Phenotypic Screens wit Model Organisms. Cambridge university Press, UK.

White, R.M., Cech, J., Ratanasirintrawoot, S., Lin, C.Y., Rahl, P.B., Burke, C.J., Langdon, E., Tomlinson, M.L., Mosher, J., Kaufman, C., Chen, F., Long, H.K., Kramer, M., Datta, S., Neuberg, D., Granter, S., Young, R.A., Morrison, S., Wheeler, G.N., Zon, L.I., 2011. DHODH modulates transcriptional elongation in the neural crest and melanoma. *Nature* 471, 518-522.

Wienkers, L.C., Heath, T.G., 2005. Predicting in vivo drug interactions from in vitro drug discovery data. *Nat Rev Drug Discov* 4, 825-833.

Williams, M., 2003. Target validation. *Curr Opin Pharmacol* 3, 571-577.

Winzeler, E.A., Shoemaker, D.D., Astromoff, A., Liang, H., Anderson, K., Andre, B., Bangham, R., Benito, R., Boeke, J.D., Bussey, H., Chu, A.M., Connelly, C., Davis, K., Dietrich, F., Dow, S.W., El Bakkoury, M., Foury, F., Friend, S.H., Gentalen, E., Giaever, G., Hegemann, J.H., Jones, T., Laub, M., Liao, H., Liebundguth, N., Lockhart, D.J., Lucau-Danila, A., Lussier, M., M'Rabet, N., Menard, P., Mittmann, M., Pai, C., Rebischung, C., Revuelta, J.L., Riles, L., Roberts, C.J., Ross-MacDonald, P., Scherens, B., Snyder, M., Sookhai-Mahadeo, S., Storms, R.K., Veronneau, S., Voet, M., Volckaert, G., Ward, T.R., Wysocki, R., Yen, G.S., Yu, K., Zimmermann, K., Philippsen, P., Johnston, M., Davis, R.W., 1999. Functional characterization of the *S. cerevisiae* genome by gene deletion and parallel analysis. *Science* 285, 901-906.

Wood, J.S., 2012. Coming of age: Asia's evolving R&D landscape, in: Vadaketh, S. (Ed.), *Economist Intelligence Unit. The Economist, The Economist Intelligence Unit Limited*.

Wright, P.A., 1995. Nitrogen excretion: three end products, many physiological roles. *The Journal of experimental biology* 198, 273-281.

Xue, L., Bajorath, J., 2000. Molecular descriptors in chemoinformatics, computational combinatorial chemistry, and virtual screening. *Combinatorial chemistry & high throughput screening* 3, 363-372.

Zbinden, G., 1991. Predictive value of animal studies in toxicology. *Regulatory toxicology and pharmacology* : RTP 14, 167-177.

Zhao, S., Iyengar, R., 2012. Systems pharmacology: network analysis to identify multiscale mechanisms of drug action. *Annual review of pharmacology and toxicology* 52, 505-521.

Zimm, A.a.L., E., 2007. AstraZeneca to purchase MedImmune for \$15.2 Billion (Update 10), in: Elser, C.a.S., R. (Ed.). Bloomberg, US.

Zon, L.I., Peterson, R., 2010. The new age of chemical screening in zebrafish. *Zebrafish* 7, 1.

Zon, L.I., Peterson, R.T., 2005. In vivo drug discovery in the zebrafish. *Nat Rev Drug Discov* 4, 35-44.

Chemical Genetics and Drug Discovery in *Xenopus*

Matthew L. Tomlinson, Adam E. Hendry, and Grant N. Wheeler

Abstract

Chemical genetics uses small molecules to modulate protein function and has the potential to perturb any biochemical event in a complex cellular context. The application of chemical genetics to dissect biological processes has become an attractive alternative to mutagenesis screens due to its technical simplicity, inexpensive reagents, and low-startup costs. *Xenopus* embryos are particularly amenable to whole organism chemical genetic screens. Here we describe the basic protocols we have developed to screen small compound libraries on *Xenopus laevis* embryos. We score embryos either by observing phenotypic changes in the whole tadpole or by changes in gene expression pattern using automated wholemount in situ hybridization.

Key words: *Xenopus laevis*, Chemical genetics, Small molecule screens, Drug discovery, Embryo development, Tadpole, Wholemount in situ hybridization

1. Introduction

In recent years a great amount of effort has been focused upon the identification of novel molecular compounds with the capacity to modulate specific protein functions for drug development and new biological tools. The range of new drug targets needs to expand as it is getting harder to discover new novel drugs with conventional techniques. The recent discovery of a compound that can inhibit melanoma growth (1) is a good example of the power of chemical genetic approaches in *Xenopus* and zebrafish to discover new novel drug targets, unlikely to have been discovered with more conventional drug discovery approaches.

The advent of high-throughput chemical genetic screening has allowed researchers to quantitatively assess the phenotypic effects of hundreds of compounds in a short period of time. The benefits of screening in a whole organism such as *Xenopus* include being able to study cell to cell interactions, developmental processes,

toxicology, penetrance, and drug metabolism. In particular, assays such as the frog embryo teratogenesis assay—*Xenopus* (FETAX) are well-established methods for developmental toxicity hazard assessment (2, 3).

Xenopus laevis and *Xenopus tropicalis* are highly amenable to medium–high-throughput screening (4–8). Forward chemical genetic approaches using *X. laevis* can be used to identify and investigate specific developmental abnormalities (7, 9). There are more specific benefits to using *Xenopus* such as its well-characterized fate map, ability to regenerate, and the possibility to do high-throughput in situ screening. Using *X. tropicalis* will also allow the linking of genetics and small molecule screening as is currently done with zebrafish. For instance, to perform enhancer/suppressor screens and assist in molecular target identification.

Xenopus was first established as a chemical genetic model in a proof of principle study looking at its utility with a set of compounds used in an earlier zebrafish chemical genetic screen (5). In the past few years a number of screens using *Xenopus* have been published looking at the vasculature, lymphangiogenesis, left/right asymmetry, neural crest, and pigment cell development (1, 5, 9–11). A study conducted by Tomlinson et al. (6) was designed to screen 2,990 compounds to observe the developmental abnormalities the compounds may cause. The initial screen identified 41 compounds displaying various phenotypes affecting general development, edema, eye development, melanophore migration, melanophore morphology, and overall pigmentation (6). Using the chemoinformatic Discoverygate algorithm upon the pigmentation altering compound NSC210627 (originally identified in *Xenopus*) demonstrated strong structural similarities to the DHODH inhibitor brequinar. Further chemoinformatic analysis and testing compounds cross species with zebrafish and human melanoma cells (Xenografts) ultimately led to the discovery of leflunomide, an arthritic drug now shown to have great promise in reducing melanoma growth in vitro and in vivo (1). These studies highlight the potential for forward chemical genetics in *Xenopus* to identify new therapeutic compounds using readily available compound libraries (see Note 1).

Here we will describe in detail the methods used in our lab for screening large libraries of small molecules. We shall describe two methods. One is the visual screen used in Tomlinson et al. (6). The other involves using high-throughput wholemount in situ hybridization to look for phenotypes associated with changes in gene expression patterns or cellular behavior with cell specific markers.

2. Materials

2.1. Components Needed for Generating *Xenopus* Embryos

1. *1.6% Ethyl 3-aminobenzoate methane sulfonate (to euthanize male)*: 0.5 g dissolved in 300 mL 0.1× MMR in a 500 mL beaker.
2. *2% Cysteine (250 mL)*: This needs to be made fresh on the day of use. Keep at room temperature and discard at the end of the day. 5 g l-cysteine dissolved in 250 mL 1× MMR. Adjusted to pH 8 with NaOH.
3. *10× MEM salts (1 L)*: Add 209.3 g MOPS, 76.08 g 20 mM EGTA, and 2.46 g 10 mM MgSO₄ to a 2 L beaker and make up to 1 L with deionized H₂O. pH to 7.4 with NaOH and sterilize via autoclave. Store at 4 °C protected from light/wrapped in foil.
4. *MEMFA (10 mL)*: 1 mL of 10× MEM salts and 1 mL of 37% Formaldehyde dissolved in 8 mL H₂O (see Note 2).
5. *10× MMR (1 L)*: Add 58.45 g 1 M NaCl, 1.5 g 20 mM KCl, 2.0 g 10 mM MgCl₂, 2.7 g CaCl₂, and 11.9 g 50 mM HEPES to a 2 L beaker. Make up to 1 L with deionized H₂O. pH to 7.5 using NaOH (see Note 3) and sterilize via autoclave.

2.2. Wholemound In Situ Hybridization Components

1. *0.1% PBST*: Add 5 mL 10% Tween detergent to 495 mL DEPC PBS and mix well (see Note 4).
2. *Proteinase K*: Add 1 µL stock proteinase K to 1 mL of PBST (see Note 5). Stock Proteinase K at 10 mg/mL is stored at -20 °C.
3. *Hybridization buffer (Hyb Buffer)*: 50% formamide, 5× SSC, 1 mg/mL Torula RNA, 100 µg/mL Heparin, 1× Denharts solution, 0.1% Tween 20, 0.1% CHAPS, 10 mM EDTA.
4. *20× SSC*: 175.3 g NaCl, 88.2 g Sodium citrate. pH adjusted to 7.0 and volume to 1 L with DEPC H₂O.
5. *1× MAB (Maleic acid buffer)*: 100 mM Maleic acid; 150 mM NaCl (pH 7.5).
6. *10% BMB (Boehringer Mannheim blocking agent)*: 10% (w/v) Boehringer Mannheim blocking agent in preheated (50 °C) 1× MAB, stirred until dissolved and then autoclaved, aliquoted, and stored at -20 °C.
7. *Blocking solution*: 2% BMB in 1× MAB.
8. *Antibody solution*: 2% BMB, 20% goat serum, anti-DIG Fab fragment (Roche, 1:2,000 dilution) in 1× MAB. This can be reused, if stored at 4°C.
9. *Alkaline phosphatase buffer*: 100 mM Tris (pH 9.5), 50 mM MgCl₂, 100 mM NaCl, 0.1% Tween 20.

10. *NBT (nitro blue tetrazolium)*: 75 mg/mL in 70% dimethylformamide (DMF).
11. *BCIP (5-Bromo-4chloro-3-indolyl-phosphate)*: 50 mg/mL in 100% DMF.

2.3. Small Compounds Used

1. Synthetic compound libraries can be sourced from many different companies (see Note 6). The synthetic compounds were obtained either prealiquoted in microtiter plates at 20 mM in dimethyl sulfoxide (DMSO) for screening or in powdered form and subsequently prepared as 10 mg/mL stock solutions in DMSO (see Note 7).

3. Methods

3.1. Determining Optimal Screening Concentrations

Carry out all procedures at room temperature unless otherwise specified.

1. Before beginning a chemical genetic screen the optimal screening concentration needs to be determined, to ensure a good discovery rate and low toxicity. This is achieved by randomly selecting a plate from the library, then assaying at serial dilutions, e.g., from 1 to 50 μ M.
2. Each well is assayed and scored for the following effects on the five developing embryos: lethality, stunted growth and development, toxicity, and positive hits (effecting normal development) (5). The concentration which gives low toxicity but a good discovery rate should be used.

3.2. Screening Compounds

1. Embryos were grown in a Petri dish containing 10 mL of 0.1 \times MMR (supplemented with gentamycin sulfate to 50 mg/mL) at 18 $^{\circ}$ C until they reached stage 15 (see Notes 8 and 9).
2. Embryos were then arrayed by Pasteur pipette at 5 embryos per well (see Note 10) into 48 or 96 well plates, containing the compound in 1,000 or 200 μ L of 0.1 \times MMR (supplemented with gentamycin sulfate to 100 mg/mL) respectively (see Note 11). Figure 1 shows a schematic plan of our screening strategy.
3. Arrayed embryos were grown at 18 $^{\circ}$ C (see Note 12) and examined visually with a dissecting microscope at 1, 2, and 3 days post fertilization (approximately stage 25, 32, and 38 respectively) (see Note 13 and Fig. 2, e.g., how the embryos might look).
4. Embryos were fixed at stage 38 (see Note 14) in their respective wells by removing as much of the dosing solution as possible using a Pasteur pipette and replacing with 1,000 or 200 μ L MEMFA in 48 or 96 well plates respectively.

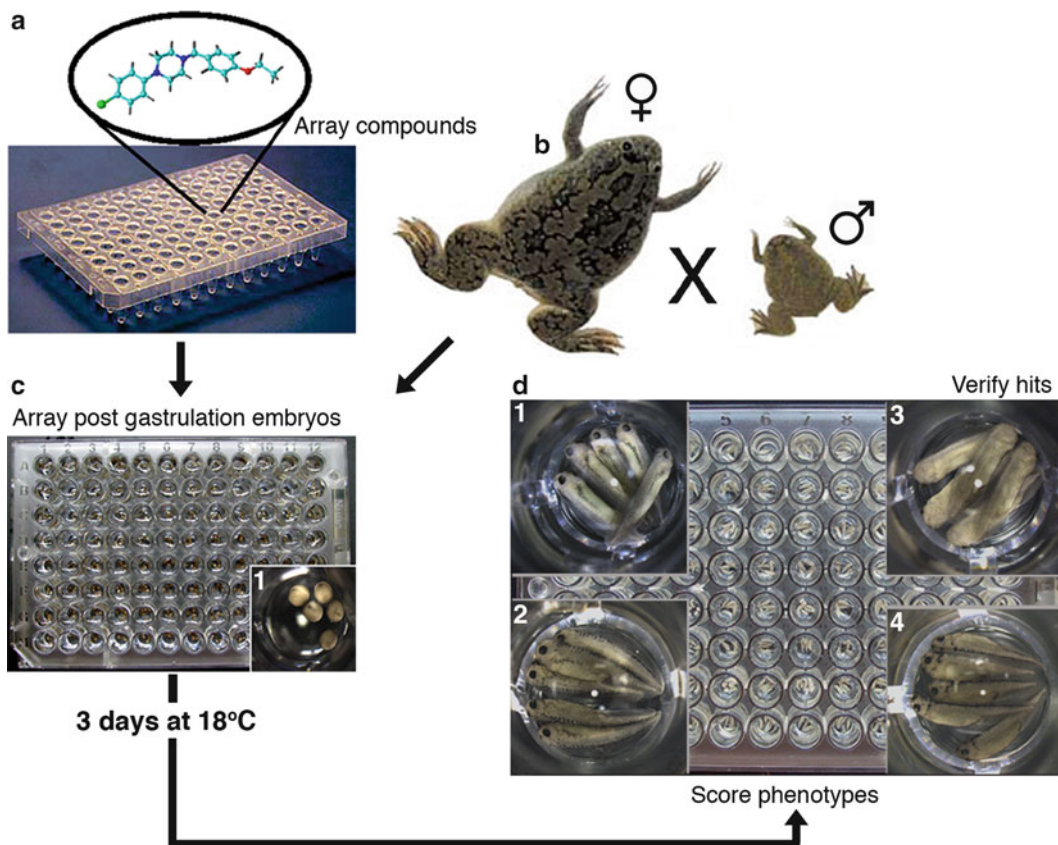


Fig. 1. Chemical genetic screening strategy with developing *Xenopus* embryos. Compound libraries are arrayed in 96 well format at 20 and 40 μM (**a**). Embryos are generated by in vitro fertilization (**b**) then arrayed post gastrulation at stage 15, 5 per well (**c** + **c1**). Plates are left to develop for 3 days at 18 °C. Once the embryos are post melanophore migration (stage 38) they are then visually scored (**d** 1–4) (Tomlinson et al. (6), Reproduced by permission of The Royal Society of Chemistry).

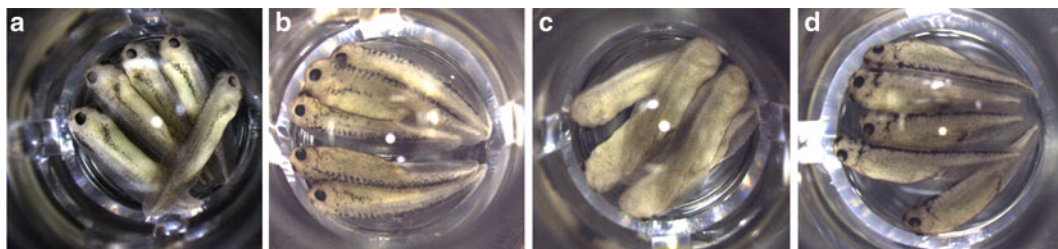


Fig. 2. Closer view of a range of pigmentation phenotypes. Embryos are shown in the screening plates, as they would be scored by the observer. (**a**) shows wild type embryos and typical pigmentation patterns. (**b**) shows a partial disruption (stripes) to the dorsal pigment stripe. (**c**) shows a complete loss of pigmentation. (**d**) shows a complete loss of pigment cell migration. All are at stage 38.

5. After fixation for a minimum of 2 h at room temperature the solution was replaced with PBST (see Note 15).
6. All positive hits need to be screened again in 5 cm Petri dishes with 20 embryos and 10 mL of 0.1× MMR with a serial dilution of the compound of interest. This will give statistical confidence and a dose response, revealing compound toxicity and efficacy.

3.3. Observing Embryos

1. Phenotypes were observed directly in the microtitre plate or by transferring the embryos identified in the primary screen (see Subheading 3.2, step 3) into a Petri dish containing a 2.5 mL 1% agar solution covered with PBS via Pasteur pipette (see Note 16).
2. Embryos were observed using a Q imaging 01-MP3.3-RTV-CLR-10 camera mounted on a Zeiss Stemi 5V6 microscope and processed with the Q capture software package (see Note 17).

3.4. Embryo Fixation

1. For long term storage, embryos in wells had as much PBST solution removed as possible using a Pasteur pipette and transferred to a 5 mL glass vial and covered with a PBST/methanol (50/50) solution, and left on a rocker for 5 min.
2. This wash step was repeated once again and twice using 100% methanol. Fixed embryos are labeled and stored at 4 °C (see Note 18).

3.5. High Throughput Combined In Situ Hybridization and Chemical Genetic Screen

The wholemount in situ hybridization technique (WISH) for localizing gene expression can be successfully coupled with chemical genetics to specifically identify compounds targeting individual cells or specific organs. An overview of the protocol is given in Fig. 3. We have developed a combined chemical genetic WISH screen to test small molecule compound libraries for their potential effects on embryonic macrophage migration with the aid of an automated in situ machine.

1. Developing embryos were applied to compounds at stage 15, as previously described and allowed to develop to the stage required for the WISH (in this case stage 25).
2. The embryos were then transferred to 96 well nylon net well plates, by Pasteur pipette, and assayed by in situ hybridization with the Intavis Biolane HT1 automated in situ machine, using a shortened WISH protocol.
3. The following steps were omitted from the standard WISH protocol used in the lab (see Note 19). The 0.1 M triethanolamine washing steps were removed. A 4-h incubation at room temperature with antibody solution may be sufficient to give a reproducible strong signal depending on the probe used.

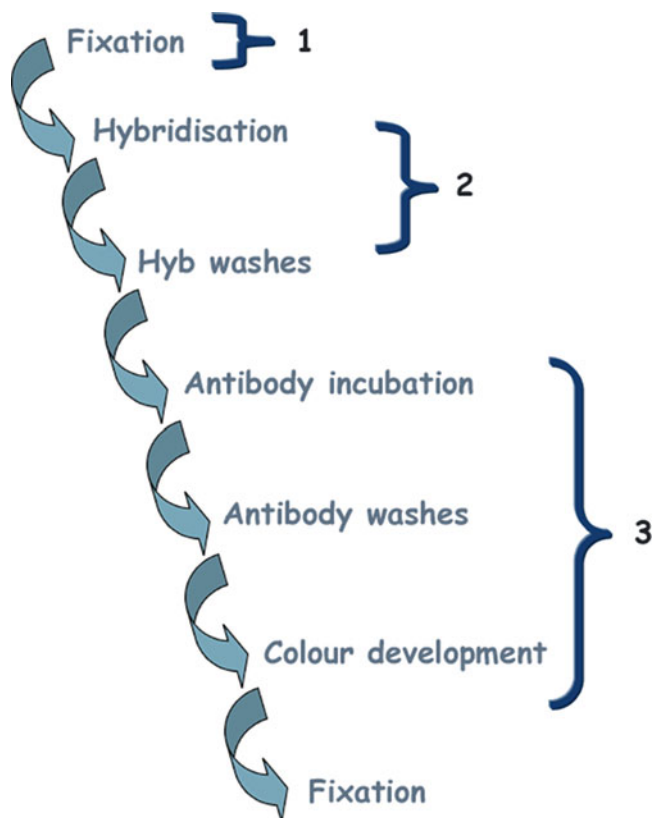


Fig. 3. Schematic overview of our automated in situ protocol. The different WISH stages are shown. *Numbers* indicate the days on which these stages are performed.

A last MAB wash (4 °C overnight) was omitted to increase the throughput of the screen. Typically four 96 well plates every 5 days were routinely assayed. A representative result is shown in Fig. 4 (12) and Tomlinson and Wheeler (unpublished results).

4. Fixation process—Day 1. Add MEMFA for 1 h with agitation at 20 °C. EtOH wash for 5 min with agitation at 20 °C, repeat three times. EtOH for 1 h with no agitation at 4 °C. Plates left at 4 °C to next day.
5. Rehydration and hybridization process—Day 2 (Start at mid-day) Initial Drain step. Wash with 100% MeOH for 5 min with agitation at 20 °C. The following steps are all for 5 min, 75% MeOH/25% H₂O with agitation at 20 °C. 50% MeOH/50% H₂O with agitation at 20 °C. 25% MeOH/75% PBST with agitation at 20 °C. PBST with agitation for 5 min at 20 °C, repeat again. Proteinase K/PBST for 10 min with agitation at 20 °C (see Note 20). PBST with agitation for 5 min at 20 °C, repeat twice more. 3.7% formaldehyde/PBST with agitation for 5 min at 20 °C. PBST with agitation for 5 min at 20 °C, repeat twice



Fig. 4. A chemical genetic screen using the Biolane HTI in situ machine and the macrophage marker *mpo*. Five stage 25 embryos can be seen with stained macrophages migrating away from the ventral blood island. Insert shows a closer view of an embryo, *white arrows* highlight individual macrophages.

more. Hyb buffer with agitation for 5 min at 20 °C. Hyb/probe step at 60 °C with agitation for 2 h, then in hyb buffer for 17 h at 4 °C (will finish at 10 a.m. next day).

6. Washing process and antibody incubation stage—Day 3 initial drain step. Hyb Buffer for 10 min with agitation at 60°C. 2× SSC for 20 min with agitation at 60°C, repeat twice. 0.2× SSC for 30 min with agitation at 60°C, repeat once. MAB for 5 min with agitation at 20°C, repeat twice. Blocking with blocking solution was then done for 60 min with agitation at 20°C. Add Antibody solution for 22 h with agitation at 4°C or 4 h at room temperature.
7. Antibody washing process—Day 3 Initial drain step. Wash with MAB for 30 min with agitation at 20°C, repeat three times more. Final MAB wash with agitation at 4°C until ready for color development. Color development (with NBT and BCIP) should be done manually, in microtitre plates (nylon mesh can cause precipitation), and tracked carefully by the observer (see Note 21). Wash several times in PBST then visually score (see Note 22). Embryos can be fixed again and stored in ethanol as previously described

4. Notes

1. The two critical factors in performing a successful forward chemical genetic screen are selecting an appropriate compound library to source from and the biological question posed. This problem is illustrated by the vastness of chemical space (a representation of all the possible organic molecules below 500 Da that are believed to be biologically relevant to drug discovery), which is estimated to contain at least 10^{60} molecules, and has generated difficult questions as to which compounds should be chosen for experimentation (12). The comparison of drug properties and descriptors has led to the emergent field of chemoinformatics, and there are many different established methods in place that use a variety of molecular descriptors to screen whole compound libraries to assess which compounds have the highest potential for successful screening. The unification of chemoinformatics and high-throughput chemical genetic screening has provided a powerful tool for identifying and screening hundreds of drug like compounds in a vertebrate model. Conversely the NCI diversity set library, used in our study, has been screened successfully many times using different cells/organisms and appears to have not yet reached saturation (6, 13). This suggests that not only is chemical diversity important but also the biological question being addressed. With a complex organism like *Xenopus* undergoing a wide range of developmental process a rich resource is there to be mined.
2. MEMFA should be made fresh each day and stored at 4 °C with light excluded by aluminum foil.
3. 10× MMR has a high buffering capacity, the use of 10 M NaOH will help speed up the pH process.
4. The use of DEPC is only necessary to eliminate RNase contamination from a solution where this could be a concern such as with WISH, elsewhere it is not necessary.
5. Only make up proteinase K solution just before it is needed and keep at 4 °C until then. Each new batch of proteinase K has to be optimized for its activity by varying the amount of time embryos are treated in a control WISH. This becomes more critical when netwells are used.
6. As mentioned in Note 1 there are numerous and extensive chemical libraries to obtain compounds from and it is likely that only a select few will be appropriate for an individual experiment. They can contain collections chosen for their diversity or for known biological activity, such as patent expired

drug compounds. It is therefore important to take careful consideration as to which compound libraries are selected for each individual experiment. The author refers you to Bender et al. (14) for a detailed review on choosing appropriate compound libraries (13) and to Wheeler and Brandli which contains an extensive list of libraries used to date in zebrafish and *X. laevis* screens (8).

7. *Xenopus* has been shown to have a DMSO EC₅₀ (malformation) of 1.92% (15). To improve solubility of some compounds either PBST or MeOH could be used instead of DMSO, these should be kept below 1% concentration when assaying embryos to avoid direct toxicity and use vehicle only controls as with DMSO.
8. Prior to stage 15 is the gastrulation phase of development. It is best to avoid screening during gastrulation as this stage of development is particularly sensitive to many compounds.
9. If by stage 15 more than 20% of embryos are dead or deformed than the screen should be abandoned as it is likely the embryos will not be robust enough to develop under the potential stress of a chemical genetic screen.
10. We find 5 embryos to be optimal in 96 well plates. In 48 well plates either 10 embryos can be cultured to stage 40 or 5 embryos to stage 44.
11. The Volume of 0.1% MMR transferred needs to be calculated and allowed for when determining compound concentration in the screen. Typically only 20 µL is transferred with the embryos.
12. *Xenopus* embryos will develop at different rates depending upon the incubation temperature. A *X. laevis* and *X. tropicalis* developmental timetable can be found in Xenbase (<http://www.xenbase.org/other/methods.do>). It is therefore particularly important to ensure that incubation temperatures remain consistent throughout the protocol.
13. Developmental effects can be noted at these stages which may be less obvious at later stages. Interesting effects can be re-assayed and returned to later.
14. The stage at which to fix is dependent on what the phenotype is that is being screened for, i.e., stage 38 for pigment and stage 42 for vasculogenesis. A smaller developmental window in the screen may give more specific phenotypes. For example in looking at pigment cell migration, applying compounds at stage 24 to stage 38 will decrease the chance of nonspecific binding to other proteins or the same molecular

target at different developmental stages (e.g., the matrix metalloproteinases) (7).

15. If required embryos can be stored in PBST at 4 °C for up to 1 week with the addition of 0.5% sodium azide as an antimicrobial.
16. We have found that embryos are much easier to orientate under the microscope when using a hair loop. A glass pipette (with a rubber bulb), which has been flamed smooth may be preferable to a plastic Pasteur pipette for transferring fragile treated embryos as it has a larger bore and a smoother surface. For viewing the fixed embryos in dorsal or ventral views a shallow indent can be made into the agar surface.
17. Pictures can be further processed using software such as Adobe Photoshop.
18. A reverse of this procedure will rehydrate the embryos for further manipulation.
19. Optimization may be needed for each in situ probe used as to which steps in the protocol can be omitted or reduced. The Macrophage specific marker mpo/XPOX2 probe gives a high signal to background and can be reused eight times before significant loss of signal (16).
20. Optimization and care will be needed in the length and temperature of the proteinase K permeabilization stage as the nylon netwells can be abrasive to the embryos.
21. NBT/BCIP color development solution can be added to plastic trays slightly bigger than a netwell microtiter plate, these are then immersed. The whole tray and lid covered in aluminum foil to exclude light and rocked gently.
22. False positive hits were detected in our macrophage chemical genetic screen due to a number of compounds developmentally stunting the embryos. The screen was stopped and assayed when the control vehicle only embryos were at stage 25. Positive hits then have to be rescreened when the treated embryos have also reached stage 25.

Acknowledgements

The authors would like to thank Rob Field and Andrea Munsterberg for helpful discussions. AH is funded by a UEA/JIC joint student-ship supported by AstraZeneca.

References

1. White RM, Cech J, Ratanasirintrao S, Lin CY, Rahl PB, Burke CJ, Langdon E, Tomlinson ML, Mosher J, Kaufman C, Chen F, Long HK, Kramer M, Datta S, Neuberger D, Granter S, Young RA, Morrison S, Wheeler GN, Zon LI (2011) DHODH modulates transcriptional elongation in the neural crest and melanoma. *Nature* 471:518–522
2. Song MO, Fort DJ, McLaughlin DL, Rogers RL, Thomas JH, Buzzard BO, Noll AM, Myers NK (2003) Evaluation of *Xenopus tropicalis* as an alternative test organism for frog embryo teratogenesis assay–*Xenopus* (FETAX). *Drug Chem Toxicol* 26:177–189
3. Longo M, Zanoncelli S, Della Torre P, Rosa F, Giusti A, Colombo P, Brughera M, Mazue G, Olliaro P (2008) Investigations of the effects of the antimalarial drug dihydroartemisinin (DHA) using the Frog Embryo Teratogenesis Assay–*Xenopus* (FETAX). *Reprod Toxicol* 25:433–441
4. Brandli AW (2004) Prospects for the *Xenopus* embryo model in therapeutics technologies. *Chimia* 58:694–702
5. Tomlinson ML, Field RA, Wheeler GN (2005) *Xenopus* as a model organism in developmental chemical genetic screens. *Mol Biosyst* 1:223–228
6. Tomlinson ML, Rejzek M, Fidock M, Field RA, Wheeler GN (2009) Chemical genomics identifies compounds affecting *Xenopus laevis* pigment cell development. *Mol Biosyst* 5:376–384
7. Tomlinson ML, Guan P, Morris RJ, Fidock MD, Rejzek M, Garcia-Morales C, Field RA, Wheeler GN (2009) A chemical genomic approach identifies matrix metalloproteinases as playing an essential and specific role in *Xenopus* melanophore migration. *Chem Biol* 16:93–104
8. Wheeler GN, Brandli AW (2009) Simple vertebrate models for chemical genetics and drug discovery screens: lessons from zebrafish and *Xenopus*. *Dev Dyn* 238:1287–1308
9. Kalin RE, Banziger-Tobler NE, Detmar M, Brandli AW (2009) An in vivo chemical library screen in *Xenopus* tadpoles reveals novel pathways involved in angiogenesis and lymphangiogenesis. *Blood* 114:1110–1122
10. Blackiston D, Adams DS, Lemire JM, Lobikin M, Levin M (2011) Transmembrane potential of GlyCl-expressing instructor cells induces a neoplastic-like conversion of melanocytes via a serotonergic pathway. *Dis Model Mech* 4:67–85
11. Dush MK, McIver AL, Parr MA, Young DD, Fisher J, Newman DR, Sannes PL, Hauck ML, Deiters A, Nascone-Yoder N (2011) Heterotaxin: a TGF-beta signaling inhibitor identified in a multi-phenotype profiling screen in *Xenopus* embryos. *Chem Biol* 18:252–263
12. Tomlinson ML, Garcia-Morales C, Abu-Elmagd M, Wheeler GN (2008) Three matrix metalloproteinases are required in vivo for macrophage migration during embryonic development. *Mech Dev* 125:1059–1070
13. Sierrecki E, Sinko W, McCammon JA, Newton AC (2010) Discovery of small molecule inhibitors of the PH domain leucine-rich repeat protein phosphatase (PHLPP) by chemical and virtual screening. *J Med Chem* 53:6899–6911
14. Bender A (2010) How similar are those molecules after all? Use two descriptors and you will have three different answers. *Expert Opin Drug Discov* 5:1141–1151
15. Dresser TH, Rivera ER, Hoffmann FJ, Finch RA (1992) Teratogenic assessment of four solvents using the Frog Embryo Teratogenesis Assay–*Xenopus* (FETAX). *J Appl Toxicol* 1:49–56.
16. Smith SJ, Kotecha S, Towers N, Latinkic BV, Mohun TJ (2002) XPOX2-peroxidase expression and the XLURP-1 promoter reveal the site of embryonic myeloid cell development in *Xenopus*. *Mech Dev* 117(1–2):173–86

DOI: 10.1002/minf.201300102

Extensions to In Silico Bioactivity Predictions Using Pathway Annotations and Differential Pharmacology Analysis: Application to *Xenopus laevis* Phenotypic Readouts

Sonia Liggi,^[a] Georgios Drakakis,^[a] Adam E. Hendry,^[b] Kimberley M. Hanson,^[b] Suzanne C. Brewerton,^[c] Grant N. Wheeler,^[b] Michael J. Bodkin,^[c] David A. Evans,^[c] and Andreas Bender^{*[a]}

Abstract: The simultaneous increase of computational power and the availability of chemical and biological data have contributed to the recent popularity of in silico bioactivity prediction algorithms. Such methods are commonly used to infer the 'Mechanism of Action' of small molecules and they can also be employed in cases where full bioactivity profiles have not been established experimentally. However, protein target predictions by themselves do not necessarily capture information about the effect of a compound on a biological system, and hence merging their output with a systems biology approach can help to better understand the complex network modulation which leads to a particular phenotype. In this work, we review approaches

and applications of target prediction, as well as their shortcomings, and demonstrate two extensions of this concept which are exemplified using phenotypic readouts from a chemical genetic screen in *Xenopus laevis*. In particular, the experimental observations are linked to their predicted bioactivity profiles. Predicted targets are annotated with pathways, which lead to further biological insight. Moreover, we subject the prediction to further machine learning algorithms, namely decision trees, to capture the differential pharmacology of ligand-target interactions in biological systems. Both methodologies hence provide new insight into understanding the Mechanism of Action of compound activities from phenotypic screens.

Keywords: In silico bioactivity prediction · Cheminformatics · Mechanism of action · *Xenopus laevis* · Pigmentation

1 Introduction

Computational methods play an important role in the drug discovery process, providing the expensive and time-consuming pharmaceutical research with established ways of support.^[1–4] In particular, with the increase of computational power and available small-molecule bioactivity data, ligand based computational methods such as in silico target prediction allow the identification of potential drug targets (relating to both efficacy and off-target effects) as well as discovery of new applications for known compounds.^[3,5–9] Their ability to rationalise the Mechanism of Action (MoA) and toxicity of a compound potentially reduces the number of compounds to subject to biological testing, making them a useful tool to support experimental techniques. Indeed, it has been shown that in silico methods can complement in vitro screening^[10] and therefore, with the information being stored in public databases (see Table 1), have become increasingly important in current drug discovery protocols.

Target prediction allows us to "fill in the gaps" between chemical and biological knowledge (shown in Figure 1), linking the 3 principal data components commonly analysed in work of this type, namely the chemical structure of compounds, the proteins they interact with, and the phe-

notype they modulate/cause on a cellular, tissue, or organism level.^[11,12] These three components are strongly interconnected, and hence cannot be considered in isolation. A drug indeed interacts with one or more proteins expressed in an elaborate biological pathways network, leading to a particular observed phenotype, which in turn also depends on factors such as cell state, compound concentration and time point. Thus, the final result of the administra-

[a] S. Liggi,⁺ G. Drakakis,⁺ A. Bender
Unilever Centre for Molecular Science Informatics, Department of
Chemistry, University of Cambridge
Lensfield Road, Cambridge CB2 1EW, UK
telephone: +44(0)1223 762983; fax: +44(0)1223 763076
*e-mail: ab454@cam.ac.uk

[b] A. E. Hendry, K. M. Hanson, G. N. Wheeler
School of Biological Sciences, University of East Anglia
Norwich Research Park, Norwich, NR4 7TJ, UK

[c] S. C. Brewerton, M. J. Bodkin, D. A. Evans
Eli Lilly U.K.
Erl Wood Manor, Windlesham, Surrey GU20 6PH, UK

[⁺] These authors contributed equally to this work


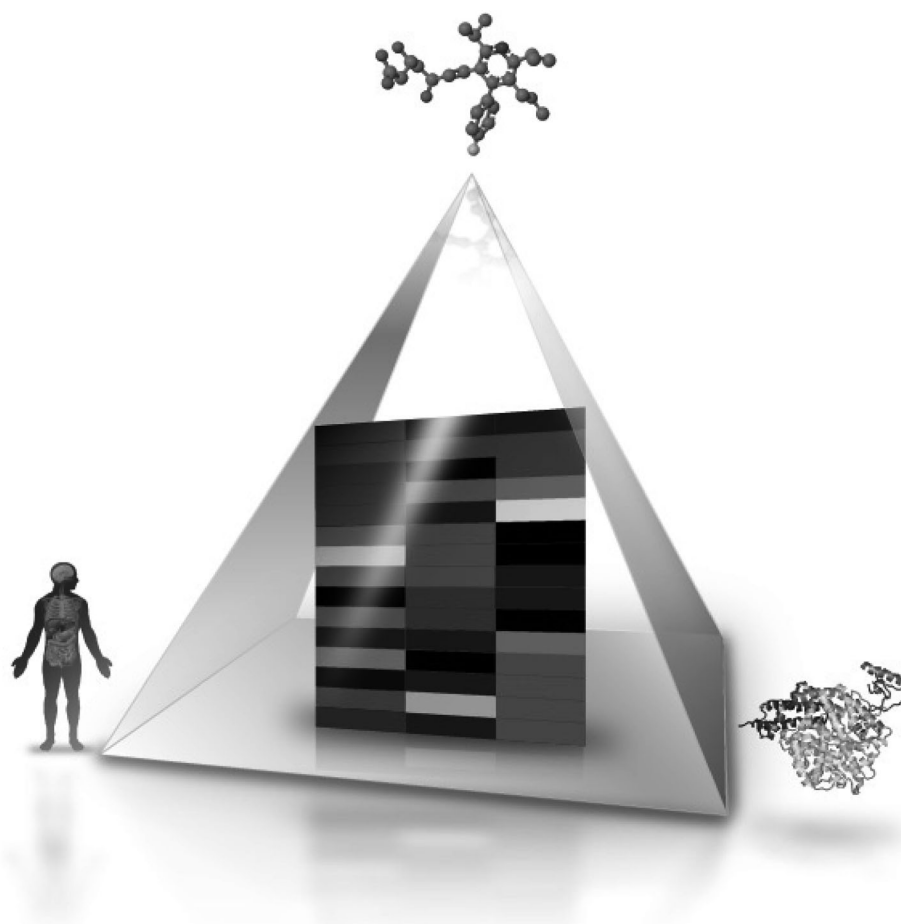
 Supporting information for this article is available on the WWW under <http://dx.doi.org/10.1002/minf.201300102>.

Table 1. List of main databases available, the data contained within them and their respective web addresses (data as of 25/03/2013).

Database	Content	Web address
ChEMBL ^[13]	9570 Targets; 1 434 432 compound records; 1 254 575 distinct compounds; 10 509 572 activities	https://www.ebi.ac.uk/chembl/
PubChem ^[14,15]	Pcsubstance contains about 93 million records; Pccompound contains nearly 33 million unique structures. PCBioAssay contains more than 621 000 BioAssays. Each BioAssay contains a various number of data points.	http://pubchem.ncbi.nlm.nih.gov/
DrugBank ^[16]	6712 drug entries, 4233 non-redundant protein	http://www.drugbank.ca/
Chemspider ^[17]	Over 28 million structures from hundreds of data sources.	http://www.chemspider.com/
ZINC ^[18]	Over 21 million purchasable compounds in ready-to-dock, 3D formats.	http://zinc.docking.org/
WOMBAT ^[19]	WOMBAT-PK 2010 contains 1260 entries (1260 unique SMILES), totaling over 9450 clinical pharmacokinetic measurements; it further includes 2316 physico-chemical properties; 932 toxicity endpoints, and 2186 annotated drug-target bioactivities.	http://www.sunsetmolecular.com/index.php?option=com_content&view=article&id=16&Itemid=11
Cerep BioPrint database ^[20]	2D and 3D descriptors, in vitro data and collected and curated in vivo data	http://www.cerep.fr/cerep/users/pages/ProductsServices/bioprintservices.asp
PDSP K _i Database ^[21]	55524 Published and internally derived affinity values for a large number of molecules on GPCRs, Ion channels, transporters and enzymes	http://pdsp.med.unc.edu/kidb.php

**Figure 1.** Visualisation of the links between compound, bioactivity and phenotypic data: the molecular structure of drugs, the biological target(s) they interact with and the organism where the protein is expressed are strongly interconnected between each other. Figure was obtained from Bender et al. 2007^[22] with permission.

tion of a compound is a rather complex system modulation, which needs to be properly understood in order to fully elucidate its effects related to both efficacy and potential toxicity. In the next section we will review the main fields where in silico target prediction approaches have been applied, and some essential applications will be described.

1.1 Applicability of In Silico Bioactivity Prediction

1.1.1 Polypharmacology

Target prediction algorithms can help the MoA analysis by understanding important targets responsible for an effect and their connection. One of the main areas where in silico techniques are increasingly being utilised in linking chemistry and biology is polypharmacology. The idea of "magic bullets" introduced by Ehrlich^[23,24] has been challenged in the case of complex diseases such as Central Nervous System (CNS) disorders, in which the therapeutic effect is exerted by modulating multiple targets.^[23,25,26] The limitations of the approach contribute (together with other factors such as Pharmacokinetic/Pharmacodynamic properties which are not discussed in detail in this paper) to the number of drugs failing late-stage clinical trials. According to a study conducted by the Centre for Medicines Research (CMR), the number of drugs that between 2008 and 2009 has been promoted from Phase II to Phase III has fallen by approximately 10% compared to the preceding two years, 2006–2007,^[27] while only ~50% of them succeed from Phase III to launch.^[28] The alternative solution of "magic shotguns" (selectively non-selective drugs)^[29] is also not without flaws since these drugs are often too promiscuous and exhibit undesired secondary activities.^[30–32] An example of such a drug is the atypical antipsychotic (and rather promiscuous compound) clozapine. Despite its high efficacy in the treatment of schizophrenia, it is infrequently administered because of the plethora of side effects associated with its use.^[33] The most important adverse reaction is the life-threatening agranulocytosis, which is most probably due to oxidoreductive stress/damage caused from the interaction of clozapine with proteins implicated in the antioxidant processes (such as NQO2, alpha-tocopherol transfer protein and glutathione-related enzymes). Ideally however, we can derive (or design) desired profiles for drugs based on existing knowledge between ligand-protein interactions, knowledge that can be derived from both experiments and target prediction.

1.1.2 Synergistic Effects of Compound Combinations

The modulation of multiple targets is not necessarily elicited by a single compound, but may in fact be due to the administration of multiple drugs in parallel. This can make MoA analysis more challenging, as additional parameters such as drug–drug interactions must also be taken into ac-

count. However, it has been suggested that the use of drug combinations can also help us understand the complexity of biological networks and signalling pathways in those systems.^[34] To this end, the effects of pairwise compound combinations were recently assessed with the use of a systematic high-throughput screening method.^[35] An interesting outcome of this study is the synergistic effect of the antipsychotic drug chlorpromazine and the antiprotozoal agent pentamidine. Both compounds showed mild antiproliferative activity on A549 lung carcinoma cells when separately tested, but the concentration required is too high to be considered clinically applicable on cancer treatment. They were later subjected to synergistic testing, where the combination performed better than the anti-cancer drug paclitaxel in inhibiting growth of A549 lung carcinoma cells in vitro and in vivo (human tumour xenograft assay in mice). Understanding the biological processes involved in the antiproliferative effect of the combination of the two drugs is not trivial, but literature support as well as the combination of the two compounds with other agents suggests that it might be elicited via DNA binding, calmoduline inhibition and regulation of polyamine levels.^[35] Hence, the unexpected phenotypes emerging from combinations of compounds can be attributed not only to interaction with the proteins involved, but also to their connectivity in biological pathways. Modulations of complex systems are thus possible via the interaction of multiple drugs with multiple targets, and computationally predicted bioactivity spectra could possibly facilitate in finding such synergistic drug combinations.

1.1.3 Repositioning

A practical application of multi-target bioactivity profiles of compounds is drug repositioning, which is the discovery of a new purpose for an already approved drug. This process can be driven by the same modulated target (and identifying another disease indication for the approved drug), or by taking advantage of secondary effects of a drug on the market. Drug repositioning is becoming increasingly popular due to the opportunity for pharmaceutical companies to expand their market by covering new disease areas with already marketed drugs in a fast and cost-effective manner, as these have already been subjected to clinical trials and have well-established safety profiles for humans.^[36,37] Therefore, an additional observation-based trial would (in theory) progress significantly faster than one for a novel compound with an unknown profile. Drug repositioning historically used to occur mainly by chance, by discovering unpredicted therapeutic effects in human. A classic example is the antipsychotic drug chlorpromazine: it was designed to have antihistaminic properties, but the strong sedative effect led to its use in psychosis,^[38,39] where it elicits its therapeutic effect thanks to the effect through multiple neurotransmitter receptors (most importantly dopaminergic and serotonergic). However, nowadays repositioning is also

being explored on a more rational and systematic level.^[40] When a drug has a desired multi-target profile (is known to modulate multiple targets of interest), it is suggested that it may elicit therapeutic effects on disease(s) different from the one for which it was originally intended, provided that the targets implicated are also relevant for the second pathology. The drug can therefore be proposed for repositioning and be tested in efficacy models in clinical trials straightaway, skipping the time consuming and expensive toxicological profiling tests. In silico target prediction can also be used to reposition drugs by predicting unknown biological targets, and it could be a viable solution for finding a therapeutic approach against neglected and orphan diseases.^[41]

1.1.4 Current Applications

Target prediction algorithms have been applied in a wide variety of applications. In a recent study, two machine learning algorithms were implemented and compared based on their performance in predicting activity, namely a Laplacian-modified Naïve Bayes classifier and a Parzen-Rosenblatt Window classifier.^[5] In particular, the predicted targets from the application of the Parzen-Rosenblatt Window method to a phospholipidosis dataset suggested that phospholipidosis can be instigated via two different mechanisms, namely inhibition of phospholipase activity and enhanced cholesterol biosynthesis, initiated by interaction of the compounds with several targets (Sphingomyelin phosphodiesterase, phospholipase A2 and lysosomal phospholipase A1 for the former, and lanosterol synthase for the latter).^[6] The aforementioned Bayesian classifier was used to predict protein targets on a cytotoxicity dataset.^[42] The predicted mechanism of action was tested and validated in vitro, whereas synergistic effects caused by combinations of compounds were also partially validated. A different implementation of the Laplacian-modified Naïve Bayesian method^[43] was used to derive predicted bioactivity profiles for a set of compounds sharing the same toxicity response.^[44] Predicted proteins were linked to their relevant pathways, and by comparing them to pathways annotated to non-toxic compounds it was possible to rationalise ADRs. On a larger scale, a recent application^[9] of in silico bioactivity profiles was carried out using the Similarity Ensemble Approach (SEA),^[45] which was used to predict drug-target interactions in 3665 approved and investigational drugs. 23 novel drug-target associations were uncovered, and 14 out of the 23 pairs were experimentally confirmed in binding assays. This is one of the few prospective validations of target prediction algorithms to date which shows how target prediction can be used in understanding poly-pharmacology and hence suggest new therapeutic application and propose off-target associations responsible for side effects. An extension to target prediction was attempted by shifting from structure-activity relationships to structure-selectivity relationships (SSR), with the use of “selectivi-

ty cliffs” instead of activity cliffs.^[46] Models built later however showed that SSR models currently work considerably worse for multi-target predictions relative to single target predictions^[47] and are therefore out of the scope of this work. Predicted bioactivity profiles can also be used as a measure of diversity, as target-based diverse compound selection has been shown to outperform conventional fingerprint diversity selection.^[48]

Hence, as this short overview illustrates, in silico methods play an important role in the drug discovery process as they are used to infer the MoA of compounds in toto, from therapeutic to off-targets. However, these methods are not without limitations, which are discussed in the next section.

1.2 Limitations of Target Prediction Methods

All computational methods have limitations and pitfalls,^[49] both on data and methodological levels. Only a deep understanding and critical analysis of these capabilities and deficiencies can lead to reliable results.^[50] Some of the most important aspects that have to be taken into consideration when applying in silico models in the area of chemical biology and drug design are discussed in the following sections, such as quality and reliability of data used.

1.2.1 Data Sources

Target prediction methods are based on databases which link small molecules (ligands) to bioactivity data (bioassays and target, see Table 1). These data are then used to extrapolate information about query molecules whose biological activity is unknown or incomplete. There is a considerable number of available biological and chemical data sources, both publicly available^[51] and commercial, however the essential limitations are shared between them. The main limitation for activity prediction tools is the lack of complete data matrices of a large number of compounds which have been experimentally measured against a broad panel of protein targets. Some bioactivity matrices have been made available, however the public ones are small in size and cover only specific subsets of pharmacological space (such as DrugMatrix,^[52] recently integrated into ChEMBL, containing toxicogenomics profiles for 638 compounds tested on rats and rat hepatocytes, and PDSP K_i Database, see Table 1), while more comprehensive ones are commercial (for instance the Cerep BioPrint database). Since models make predictions based on knowledge (similarity measures are used to assess relationships between molecules), such incomplete data matrices could introduce bias into the predictive models. This topic has also been discussed in more detail recently.^[2,53,54] One way to increase coverage of chemical space is to link all available non-overlapping data sources; however one of the limitations of this approach is the inconsistency between databases. In a recent study,^[55] several commercial and public sources (namely PubChem,^[14,15] WOMBAT,^[19] ChEMBL,^[13] Evolvus,^[56]

and PDSP K_i Database^[21]) were merged with the aim to create a joined relational database. In this process it was found that only 34% of the compounds were consistently annotated, with discrepancies spanning from UniProt names to doses for the remainder. Each source was found to contain unique molecules (from different bibliographic sources), the percentage of which varied considerably between databases – from 94.7% of unique molecules found in PubChem to 24.7% in PDSP K_i Database. Hence, this work highlighted the inconsistency between data sources already stated in previous studies,^[57–63] as well as their complementarities with respect to the information they contain.

Biological databases are affected by a number of limitations as well. A study attempting to connect small molecules acting on the Nuclear receptor family with biological pathways exposed the lack of data uniformity in these databases.^[64] 20 biological pathways involving 18 nuclear receptors were extracted from BioCarta,^[65] Cell Signalling Technology,^[66] ExPASy Biochemical Pathways Map,^[67] KEGG, Signal Transduction Knowledge Environment^[68] and Pathway Studio (PathwayAssist).^[69] The issues observed are due to both errors and literature information not yet integrated into the knowledge base, and span from the same process represented with different pathway schemes in different databases, to inconsistency in protein nomenclature. An example is the 'Estrogen receptor pathway' from BioCarta, which presents two inconsistencies. Firstly, the protein GRIP1 is linked to the Glutamate receptor interacting protein 1 instead of the glucocorticoid receptor interacting protein 1. Secondly, the nuclear receptor interacting protein 1 is defined as positive (instead of negative) regulator of ER- α . In a related study^[70] on transcription factors, poor correspondence between experimental data and pathway databases was also demonstrated. Seven transcription factors important in oncogenesis (MYC, NOTCH1, BCL6, TP53, AR, STAT1, and RELA) were associated with 84 pathways extracted from public (BioCarta,^[65] KEGG,^[71] WikiPathways^[72] and Cell Signalling Technology^[66]) and commercial (MetaCore,^[73] Ingenuity Pathway Analysis,^[74] BKL TRANSPATH^[75] and TRANSFAC,^[76] Pathway Studio^[69] and GeneSpring Pathways^[77]) pathways databases. Pairwise comparison between the different databases was estimated by calculation of the Jaccard index, which has an average grand value equal to 0.0533: only ~5% of targets were in common between 2 pathways. Hence, the coverage and reliability of life science data is often questionable, and this appears to apply to both the chemical and biological information domain.

The limitation of data sources just described has to be taken into consideration and properly addressed by data curation.^[78] Data curation is a task prone to human error in which information is extracted manually from literature. For this reason, it was recently proposed that journals impose formatting requirements regarding how data should be included in papers, meaning that all the important information would be provided in a easily accessible way, such as

a machine readable file in the Supplementary Information.^[51] This file would include all the key data, such as SMILES of the compounds, way of synthesis, list of protein targets, *in vitro/in vivo* tests, etc. and it would allow a comparison between, for instance, different molecules that share the same bioactivity, leaving "nothing open to interpretation".^[79] While currently few journals require submission of data in this consistent format, acceptance of this model is likely to increase database quality.

Moreover, users of these sources have to follow a standardisation process to (virtually) eliminate the consequences that an imprecise dataset can cause on their computational model. Ambiguities should be filtered using a cleaning/standardising pipeline^[80] in order to remove mixtures, inorganic and organometallic compounds (not all descriptors and cheminformatics programs are able to deal with them), convert structures from SMILES to 2D (easier visualisation and error checking), strip salt and neutralise, normalise mesomers, tautomers and aromatic rings, removal of duplicates, and last but not least manual checking. This cleaning procedure can be easily done with freely available programs (such as KNIME,^[81] Standardizer,^[82] etc.), and commercial ones (Sybyl,^[83] MOE,^[84] Pipeline Pilot,^[85] etc.)

1.2.2 Parameter Choice

A large number of machine learning algorithms are available,^[86] but only few of them have been extensively explored in the target prediction domain. Popular examples include the similarity-based SEA,^[45] the probabilistic (usually multi-class) Naive Bayes,^[5,43,87,88] the distance-based Parzen-Rosenblatt Window,^[5,6] and Support Vector Machines^[87,89] which use hyperplanes to separate data points. Apart from the choice of algorithm, the descriptors utilised to represent molecules significantly influence the outcome of the prediction. A number of molecular descriptors have been developed, but there is not one able to consistently outperform the others, as they are all able to capture different characteristics of molecules.^[90] Similar to the area of ligand-based virtual screening,^[91] it appears that 2D molecular descriptors outperform their 3D counterparts when it comes to target prediction.^[91,92]

1.2.3 Pharmacokinetic and Pharmacodynamic Properties

While ligand-target interactions are often responsible for an observed biological effect, this is not a one-to-one association and questions of dose, time, distribution, metabolism and associated properties often make the difference whether an effect is observed in practice or not. Hence, an evaluation of ADMET (Adsorption, Distribution, Metabolism, Excretion and Toxicity) properties of the compound under investigation needs to be coupled with its pure target interaction profile. It is indeed important to estimate in advance whether the compound will be absorbed by the organism and transported to the target organ/tissue in order to expli-

cate its therapeutic effect, its binding to plasma proteins, whether it accumulates in particular tissues, the kind of metabolic modification the molecule undergoes (and the potential production of active/toxic metabolites), etc. In silico ADMET prediction plays an important role in the drug discovery process, because it provides a (relatively) fast, cheap and efficient way to understand pharmacokinetics and pharmacodynamics properties,^[93–96] but it must be accompanied by experimental tests^[97] in a controlled and well organised workflow, in order to avoid misleading results.^[98] Current target prediction methods do not take ADMET into consideration explicitly (although they can be applied iteratively on the metabolites generated using e.g. other computational approaches, or those determined from experimental measurements), and in order to progress from qualitative to quantitative predictions this still remains to be addressed in the future.

1.3 Extensions to Bioactivity Prediction

A system biology approach provides the drug discovery field with a link between chemistry and biology, which is fundamental in assisting the development of tools to predict targets, and therefore side effects and efficacy of new drugs. A thorough understanding of biological conditions is possible only by integrating all the relevant data available.^[11,99,100] By providing researchers with – once unavailable or undecipherable – additional information via cheminformatics approaches, we can aid the polypharmacological paradigm in rationally developing drugs with increased efficacy.^[101] It is evident that the combination of network biology and polypharmacology can benefit from the use of target prediction algorithms. An example of bioactivity profiles network was constructed in a recent study,^[9] where in silico target prediction, in vitro tests, ADRs annotation and pharmacodynamics and pharmacokinetic properties were connected to build a drug-target-adverse effect network. 656 FDA approved drugs were screened in silico against 73 targets (belonging to the Novartis safety panel assays) using SEA.^[45] 48% of the of the predicted target-ligand pairs were confirmed by either databases search (~33%, found in ChEMBL, GeneGo Metabase, Thompson Reuters Integrity, Drugbank and GVKBio) or in vitro test, while only ~46% were confuted. The new predicted off targets were then annotated with the observed side effects, obtaining a total of 247 drug-target-side effect links. Calculation of enrichment factors for these triplets allowed the explanation of side effects via the new predicted targets. Finally, pharmacokinetic and pharmacodynamic properties were taken into consideration to understand if the link between drug, target and side effect was plausible, i.e. if the compound was able to reach an area under the curve (AUC) significant enough for the interaction with the target. A successful result of this study is, for example, the explanation of tremor for the drug diphenhydramine via interaction with the dopamine transporter. Networks can be also used for

the prediction itself, not only meta-analysis, as demonstrated by Yamanishi et al.^[102] In particular, new drug-target interactions were predicted by combining chemical, genomic and pharmacological data using supervised bipartite graph inference. Novel interactions for enzymes, ion channels, GPCRs and nuclear receptors were derived, suggesting that bioactivity similarity is more important than chemical similarity when predicting drug-target interaction.

In this work we will illustrate two extensions to in silico target prediction to phenotypic datasets, namely the utilization of pathway annotations and the differential pharmacology analysis of the resulting bioactivity spectra. With regard to the phenotypic nature of the datasets used, this screening paradigm has recently been highlighted as an important step in early drug discovery^[12,103,104] in order to uncover insights into small molecule MoA and possibly identify lead compounds more likely to show efficacy in the clinic.^[12,105] In particular, we present its application on a chemical genetic screen to identify small molecules that affect aspects of development of the *Xenopus laevis* tadpole.^[106,107] With respect to the extensions to in silico bioactivity prediction presented here, the resulting bioactivity profiles are annotated with the pathways they map to, leading to further biological insights into the system modulated. Furthermore, classification trees are generated on the aforementioned bioactivity profiles to establish the differences in compound MoA and thus explain different phenotypes. Both approaches are generally applicable to phenotypic datasets and we will illustrate their use for the first time in this work.

2 Materials and Methods

2.1 *Xenopus laevis* Phenotypic Screening Dataset

All experiments were performed in compliance with the relevant laws and institutional guidelines at the University of East Anglia. The research has been approved by the local ethical review committee according to UK Home Office regulations.

Compounds used in the study were obtained from the Diversity Set II compound library (comprised of 1394 compounds), provided by the Drug Synthesis and Chemistry Branch, Developmental Therapeutics Program, Division of Cancer Treatment and Diagnosis, National Cancer Institute.^[108] Compounds were prepared as 10 mM stock solutions in dimethyl sulfoxide. The library screens were carried out as previously described by Tomlinson et al.^[106,107] Compounds were defrosted overnight and arrayed into 96 well plates at either 40 μ M or 80 μ M in 150 μ L 0.1 X MMR solution. At stage 15, *Xenopus laevis* embryos were added to the plates (5 embryos per well in 150 μ L 0.1 X MMR, 300 μ L final volume, final respective concentrations 20 and 40 μ M), sealed with an oxygen permeable plate seal and incubated for 3 days (until stage 38) at 18 °C. Embryos were screened manually for the described phenotypes using a light micro-

scope. To reduce experimental bias each plate was screened separately by two individuals. Identified phenotypes were photographed using a light microscope mounted with a Micropublisher 3.3 RTV camera and processed using Qcapture and Adobe Photoshop.

2.2 Computational Methods

2.2.1 Compound Preprocessing

The 1364 compounds from the NCI Diversity Set Library II were subjected to a KNIME pipeline in which they were pre-processed (standardised) according to the following procedure: structures were converted to 2D, neutralised, salts are stripped and tautomers are normalised using MOE nodes. Molprint2D^[109] circular fingerprints of depth 3 were then generated using OpenBabel.^[110]

2.2.2 Target Prediction

A Laplacian-modified Naïve Bayes classifier^[5] was used for bioactivity profile prediction. The training set consists of approximately 190k ligand–protein pairs extracted from ChEMBL version 14 covering 477 targets. The criteria used for building the training set were similar to those described by Koutsoukas et al.^[5] with the exception of the binding affinity threshold (1 μ M) and the minimum number of instances per class (50). Information on agonism/antagonism is not retained, as only the ligand–protein interaction is considered. The model outputs a confidence score for each target on a per-compound basis. It is common in such analyses to use an empirical global score cut-off.^[111,112] However, the difference in score distribution among the target classes suggested our analysis could benefit from calculating class-specific confidence score cut-offs. The disparity in score distribution might be due to the different number of instances in each class, the diversity of molecules representing a particular class or the average number of features (fingerprints) used to describe these molecules. The class-specific thresholds were derived by calculating the optimal balanced accuracy (precision and recall trade-off) on a per target class basis, and were used to associate ligands with putative targets.

2.2.3 Pathway Annotations

Protein–pathway annotations were extracted from the KEGG^[71] (release 58.1) database and all predicted targets were annotated with the full set of pathway annotations from KEGG.

2.2.4 Enrichment Calculation

A background distribution was assembled in order to create a diverse library of compounds covering large chemical space. Approved drugs from DrugBank, drug-like mole-

cules from PubChem, human metabolites from HMDB, natural products from ZINC and computationally generated compounds from GDB13 were randomly extracted, yielding a dataset of 194 849 molecules with a molecular weight ranging from 100 to 900.

The background distribution was used in the enrichment calculations to randomly select 10 000 datasets having the same number of compounds of the test set. Several enrichment calculations were performed as outlined in the following, where the frequency of prediction/annotation was calculated as the number of times a given target/pathway was predicted/annotated in the test set.

The *Average Ratio* for a given target/pathway was calculated by comparing the frequency of prediction/annotation in each random dataset with the frequency of prediction/annotation in the test dataset:

$$\frac{\left(\frac{F_{\text{random set1}}}{F_{\text{test set}}} + \frac{F_{\text{random set2}}}{F_{\text{test set}}} + \dots + \frac{F_{\text{random set10000}}}{F_{\text{test set}}} \right)}{10000} \quad (1)$$

The *Estimation Score* was calculated by counting how many times the frequency of prediction/annotation for a given target/pathway in the random datasets is larger or equal to the one in the test dataset. The absolute frequency (*C* in Equation 2) obtained is then divided by the total number of random dataset, giving a value between 0 (enriched) and 1 (random).

Targets and pathways with Estimation Score = < 0.01 are considered enriched. In case of targets or pathways having the same Estimation Score, the Average Ratio value is used to further discriminate them: the lower the value, the more enriched the target is.

$$C/10000 \quad (2)$$

Where *C* = no. of times $F_{\text{random sets}} \geq F_{\text{test set}}$

2.2.5 Classification

The machine learning method chosen for establishing the differences in mechanism of action responsible for a particular phenotype was the WEKA^[113] implementation of Quinlan's C4.5 classification tree.^[114] In particular, active molecules (showing at least one phenotype) were separated into those altering Pigmentation and not. The predicted targets (bioactivity profile) for each active molecule were used as attributes (features) for the decision tree. The minimum number of instances in leaves was set to 3 and the criterion for determining the best splits was Information gain. Due to the small number of instances in the dataset, leave-one-out cross-validation was used to assess the performance of the decision tree. Furthermore, pruning (confidence factor 0.5, 10-fold) was used to shorten the length of the tree.

3 Results and Discussion

A chemical genetic screen was carried out on *Xenopus laevis* embryos as described previously.^[106,107] Phenotypes were scored for their effects on Pigmentation, Morphology (general), Edema, Melanophore morphology, Melanophore migration, Eye development and Blistering (Table 2). 72 of the 1364 NCI diversity set II compounds showed one or more of the phenotypes listed (Figure 2), 70 of which successfully made it through our computational pipeline (pre-processing as described in Materials and Methods, and at least one predicted target). A query of the ChEMBL data-

Table 2. Summary of phenotypes observed in *Xenopus* after treatment with compounds from the NCI Diversity Set II, along with their abbreviation and a brief description. In this work, we focused on the analysis of the Pigmentation (P) phenotype.

Phenotype	Abbreviation	Description
Pigmentation phenotype	P	Absence of common pigmentation
Morphology phenotype	M	Impaired tadpole physiological development
Edema phenotype	E	Significant swelling
Melanophore morphology phenotype	MM	Pigment cells appear rounded rather than dendritic
Melanophore migration phenotype	MG	Pigment cells have not migrated to their normal positions
Eye development phenotype	ED	Eye underdeveloped and altered retinal pigmentation
Blistering	B	Localised blistering

base revealed that only one of these compounds is annotated with a single target (2 measurements) according to the criteria used for the compilation of the in silico bioactivity method training file. This highlights the importance of bioactivity profile predictions in elucidating the MoA of compounds. It is interesting to observe that the majority (59/70) of the active compounds elicit more than one phenotype (Figure 3), suggesting the need to distinguish not only between the targets/pathways involved between actives and inactives but also amongst the individual phenotypes. In this work we will be focussing on the Pigmentation phenotype as it is the one most frequently observed in this screen, with 45 compounds causing it. These 45 compounds are associated with a total of 236 predicted targets, where each of these targets was predicted for at least one compound in the active subset.

3.1 Enrichment Calculation for Targets and Pathways

3.1.1 Enriched Targets

Out of the 236 predicted targets, 33 have been found to be enriched. The top ten enriched targets are shown in Table 3 (see Supporting Information Table S1 containing all enriched targets for further information). The only target with an Estimation Score = 0 is the Platelet-derived growth factor receptor alpha (PDGFR α) which is important in *Xenopus laevis* development^[115] since its impairment causes developmental defects^[116] such as alterations in pigmentation.^[117] The second most significantly enriched target is the Mast/stem cell growth factor receptor Kit, important in

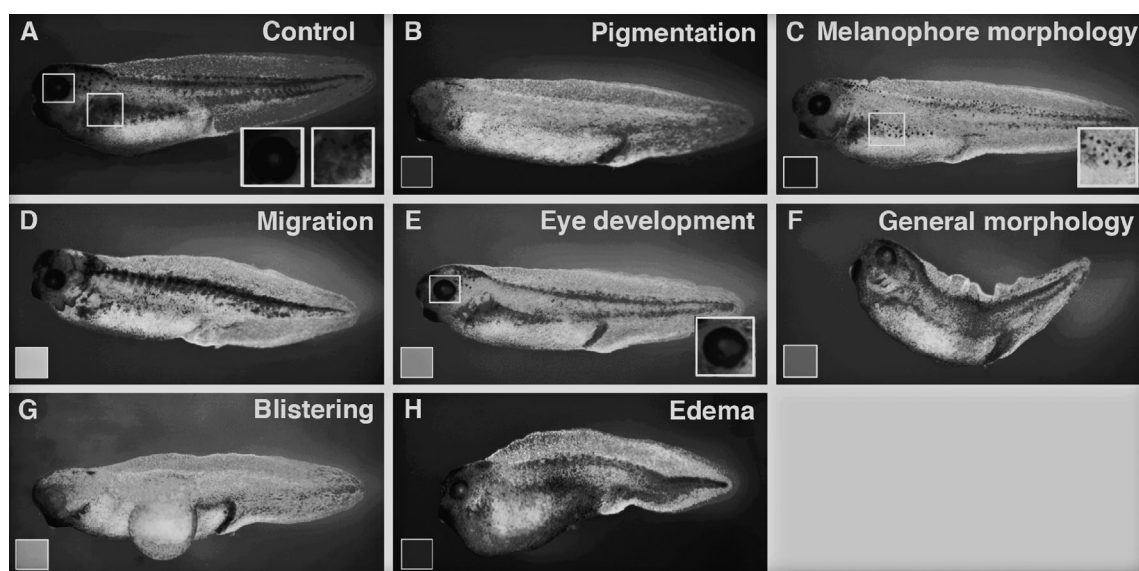


Figure 2. Summary of phenotypes observed in *Xenopus laevis* tadpoles against vehicle control (A). Categories include Pigmentation (B), Melanophore morphology (C), Melanophore migration (D), Eye development (E), General morphology (F), Blistering (G) and Edema (H). Colored insert boxes correspond with Figure 3. All embryos are shown in lateral view, with anterior to the left. In this work, we analysed compounds causing a Pigmentation phenotype, and to this end applied both pathway annotations and classification trees to further annotate in silico target predictions.

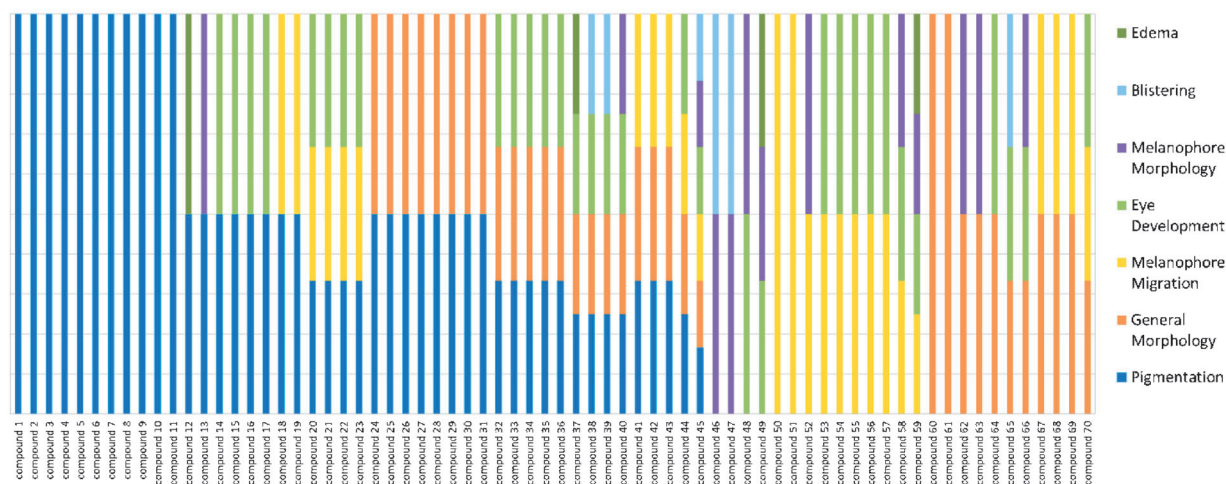


Figure 3. Distribution of phenotypes on a per-active-compound basis. The colour scale for each phenotype is shown on the right-hand side. Pigmentation is the most frequently observed phenotype in this dataset and also the only phenotype caused individually by 11 out of the 45 compounds in the set. Compound numbers do not correspond to library IDs.

Table 3. Top ten targets from the enrichment calculations against background distribution, along with Frequency of Prediction, Average Ratio and Estimation Score. Targets are ranked first by Estimation Score then by Average Ratio. The only target with an Estimation Score of zero is the Platelet-derived growth factor receptor alpha.

Target	Frequency of Prediction	Average Ratio	Estimation Score
Platelet-derived growth factor receptor alpha	7	0.0684	0
Mast/stem cell growth factor receptor Kit	5	0.0868	0.0001
Tyrosine-protein phosphatase non-receptor type 7	9	0.2105	0.0001
Induced myeloid leukemia cell differentiation protein Mcl-1	18	0.3803	0.0001
High affinity cAMP-specific 3',5'-cyclic phosphodiesterase 7A	2	0.0098	0.0002
Cyclin-dependent kinase 1	6	0.1220	0.0002
RAF proto-oncogene serine/threonine-protein kinase	6	0.1500	0.0002
Beta-2 adrenergic receptor	8	0.2232	0.0002
Glycogen synthase kinase-3 beta	12	0.3511	0.0002
Receptor-type tyrosine-protein kinase FLT3	4	0.1097	0.0004

melanocyte development, migration and survival.^[118] It is responsible for apoptosis of melanocytes in zebrafish,^[119] and its mutation has been reported to lead to abnormal pigmentation such as piebaldism in human^[120] which also links it to the phenotype observed here. A number of enriched targets are related to melanoma, confirming our analysis since proteins implicated in human melanoma are found to be important in *Xenopus* pigmentation (such as Dimerization co-factor of hepatocyte nuclear factor 1 (HNF1)/pterin-

4 α -carbinolamine dehydratase).^[121] These are the Induced myeloid leukemia cell differentiation protein Mcl-1,^[122] Cyclin-dependent kinases (CDKs)^[123,124] (moreover CDK-1 activation, along with JNK, triggers apoptosis in *Xenopus* unfertilised eggs^[125]), RAF proto-oncogene serine/threonine-protein kinase (RAF1)^[126] (whose defects are also responsible for hyperpigmentation in Noonan and Leopard syndrome,^[127,128] as well as altered pigmentation in *Xenopus*^[129]). A further enriched protein target is Glycogen synthase kinase-3 beta (GSK-3 β), implicated in energy metabolism, neuronal cell development, and body pattern formation in *Xenopus* and other vertebrates.^[130] Loss of GSK-3 β signalling is moreover associated with delayed pigmentation as observed in zebrafish treated with the lethal factor component of *Bacillus anthracis* lethal toxin.^[131] Overexpression of GSK-3 β also leads to alterations in neuroectodermal cell fates through activation of Xotx2 in *Xenopus*.^[132] Thus, this target is particularly relevant in both Pigmentation and development, in agreement with our analysis. Finally, enrichment of the β 2 adrenergic receptor is justified by its known involvement in pigmentation in humans,^[133] zebrafish^[134,135] and several other fish species.^[136] The remaining 3 targets in the top 10 positions in our analysis are High affinity cAMP-specific 3',5'-cyclic phosphodiesterase 7A, Tyrosine-protein phosphatase non-receptor type 7 (PTPN7) and Receptor-type tyrosine-protein kinase FLT3. No literature was found linking them to Pigmentation. However, PTPN7 is known to regulate a variety of cellular processes including cell growth, differentiation, mitotic cycle, and oncogenic transformation.^[137] Receptor-type tyrosine-protein kinase FLT3 also regulates differentiation and other processes such as, proliferation and survival of hematopoietic progenitor cells and of dendritic cells. implicated in hematopoietic malignancies.^[138] Overall the validity of our method in identifying targets implicated in either Pigmentation or develop-

ment is confirmed by the literature analysis, with the remaining targets enriched in our analysis being those where involvement in Pigmentation is implicated statistically, and where further mechanistic experimental studies would be warranted.

3.1.2 Enriched Pathways

In our analysis 44 out of 150 KEGG pathways have been found to be enriched. In Table 4 the top ten enriched pathways are shown (for further information giving the complete list of enriched pathways see Supporting Information Table S2). The enriched pathways can be classified in sever-

Table 4. Top ten pathways from the enrichment calculations against background distribution, along with Frequency of Annotation, Average Ratio and Estimation Score Pathways are ranked first by Estimation Score then by Average Ratio. We can observe that the top 10 enriched pathways have an Estimation Score equal to zero.

Pathway	Frequency of Annotation	Average Ratio	Estimation Score
hsa04060 Cytokine-cytokine receptor interaction	47	0.2715	0
hsa05221 Acute myeloid leukemia	41	0.2996	0
hsa04662 B cell receptor signalling pathway	41	0.3362	0
hsa04360 Axon guidance	40	0.3603	0
hsa04510 Focal adhesion	85	0.4407	0
hsa04144 Endocytosis	58	0.4444	0
hsa04110 Cell cycle	46	0.4573	0
hsa05218 Melanoma	50	0.4637	0
hsa05200 Pathways in cancer	128	0.5835	0
hsa04010 MAPK signalling pathway	87	0.5859	0

al clusters according to the biological function they modulate: development and cell migration ("Axon guidance", "Focal adhesion", "Adherens junction"), cancer ("Melanoma", "Acute myeloid leukemia", "Cell cycle", "MAPK cascade", "Basal cell carcinoma", "Pathways in cancer", etc.), cellular proliferation ("Neurotrophins", "Hematopoietic cell lineage", "Melanogenesis", etc.) and immune response/inflammation ("Cytokine-cytokine receptor interaction", "Chemokine signalling pathway", "T cell receptor signalling pathway", "B cell receptor signalling pathway", "Hepatitis", "Masles", etc.).

Amongst the most enriched pathways is "Axon guidance", fundamental in the CNS development,^[139] but implicated also in vascular system development,^[140] in retinal pigmentation in mouse^[141] and eye development in *Drosophila*,^[142] thus important for both the specific animal model (development) and the phenotype observed. Also interesting is the enrichment of the "Endocytosis" process, which is

implicated in the mechanism of melanosomes transfer into surrounding cells in *Xenopus*,^[143] in *Drosophila* wing pigmentation,^[144] and Loeys-Dietz syndrome (one of the symptoms is thin and translucent skin, caused by mutation on the TGF betareceptor gene,^[145] which is expressed in this pathway) and hence clearly related to our phenotype of interest. Several cancer-related pathways are enriched. Their enrichment is expected since pigment cells are derived embryonic neural crest cells which have many properties in common with cancer cells.^[146] An important enriched pathway in the cancer-related category is the "MAPK signalling pathway". Alterations of the MAPK cascade are responsible for several malignancies,^[147] skin abnormalities such as Noonan, Costello and Cardio-facio-cutaneous syndromes.^[148] Moreover, cAMP activation of the MAPK signalling pathway inhibits melanogenesis,^[149] suggesting a direct implication of this cascade in the observed phenotype. The next enriched pathway is "Cell cycle", where the microphthalmia-associated transcription factor Mitf can act as antiproliferative factor by inducing a G1 cell-cycle arrest in melanocytes-mutation of its genes, and thus impaired function of the protein, leading to melanoma.^[150] Overall, the enrichment of pathways implicated in tumour development could be mostly confirmed by literature. The enrichment of immune system pathways could be due not only due to their implication in cancer development. Cytokines are important in cell growth, immune response, angiogenesis, as well as neurodevelopment.^[151] They are implicated in several diseases whose symptomatology involves skin related problems, such as Familial progressive hyper- and hypopigmentation (caused by mutation of *KITLG* gene,^[152] expressed in the "Cytokine-cytokine receptor interaction"), Primary localized cutaneous amyloidosis (PLCA, caused by mutations of cytokine receptors^[153]) and Loeys-Dietz syndrome (where one of the symptoms is thin and translucent skin, caused by mutation on the TGF beta receptor gene,^[145] which is expressed in this pathway). This is evidence of a solid link to the phenotype studied. The next enriched pathway from the immunomodulation category is the "B cell receptor signalling pathway". The B cell receptor is an intramembrane protein complex whose activation is triggered by extracellular antigens and causes a cascade that leads to cellular response to stimulus, production of kinases, B cell proliferation and Immunoglobulin production. Its link to the phenotype studied is confirmed via its involvement in MAPKinase activation, (whose pathway is also enriched),^[154] as well as Incontinentia pigmenti, a disease characterised by several symptoms such as hyperpigmentation.^[155]

Hence, we conclude that overall, although at a first glance most of the pathways do not appear to be directly implicated in Pigmentation, a deeper literature analysis shows their link with the phenotype, confirming the validity of the pathways analysis in obtaining new insight into the biological mechanism of the studied phenotype. As with the enriched targets, the pathways not yet linked to the

phenotype under consideration warrant further mechanistic study. In this particular case though, most hypotheses could already be confirmed by literature analysis.

3.2 Classification of Differential Pharmacology for the Pigmentation Phenotype

So far, we have presented the analysis of enriched targets and pathways among compound causing the phenotype of interest, compared to a background distribution. However, many of the compounds found to be active in the current study cause multiple phenotypes (Figure 3) which may be due to similar MoA of the active compounds. From Table 5 (listing the targets with a higher raw frequency) we can observe that the former hypothesis is in accordance with our bioactivity predictions, namely that the most frequently predicted targets for the phenotype studied show considerable overlap for the remaining phenotypes. In particular, the targets most frequently predicted for the Pigmentation phenotype are the Induced myeloid leukemia cell differentiation protein Mcl-1 and the G-protein coupled receptor 55, which are also the two most predicted targets for the remaining phenotypes and therefore difficult to separate. Even from a polypharmacological point of view, simultaneous activity on both these targets is predicted 10 out of 45 times for the Pigmentation phenotype vs. 8 out of 25 times for the remainder of the compounds.

In the next step the C4.5 classification algorithm was employed to distinguish amongst the different phenotypes. Each node contains a target used to split the data based on whether a compound was predicted to be active ("1") or inactive ("0") against it, whereas leaves contain the final

Table 5. Top 10 ranked targets predicted for all active compounds, the number of times they were predicted globally and the number of times they were predicted for compounds showing the Pigmentation phenotype. We can see that there is significant overlap between bioactivity predictions for compounds showing the Pigmentation phenotype and total active compounds.

Top-10 targets predicted for active compounds	Times predicted in active compounds (70)	Times predicted for Pigmentation phenotype (45)
Induced myeloid leukemia cell differentiation protein Mcl-1	32	18
G-protein coupled receptor 55	32	19
Amine oxidase [flavin-containing] B	21	14
Glycogen synthase kinase-3 beta	19	12
E3 ubiquitin-protein ligase Mdm2	18	9
Cytochrome P450 1A2	16	12
Estrogen receptor beta	16	12
Amine oxidase [flavin-containing] A	16	7
Tyrosine-protein phosphatase non-receptor type 7	16	9
Carbonic anhydrase 5A, mitochondrial	16	12

classification. Figure 4 shows a classification tree for differentiating the active compounds causing the Pigmentation phenotype (Leaf Node outcome="Yes") from those causing any of the remaining phenotypes (Leaf Node outcome="No"). For this particular tree we can observe that each leaf node (outcome) is preceded by predicted activity on a single target, and inactivity on the remaining target-nodes leading up to it. From an initial observation, it becomes evident that distinguishing between the compounds

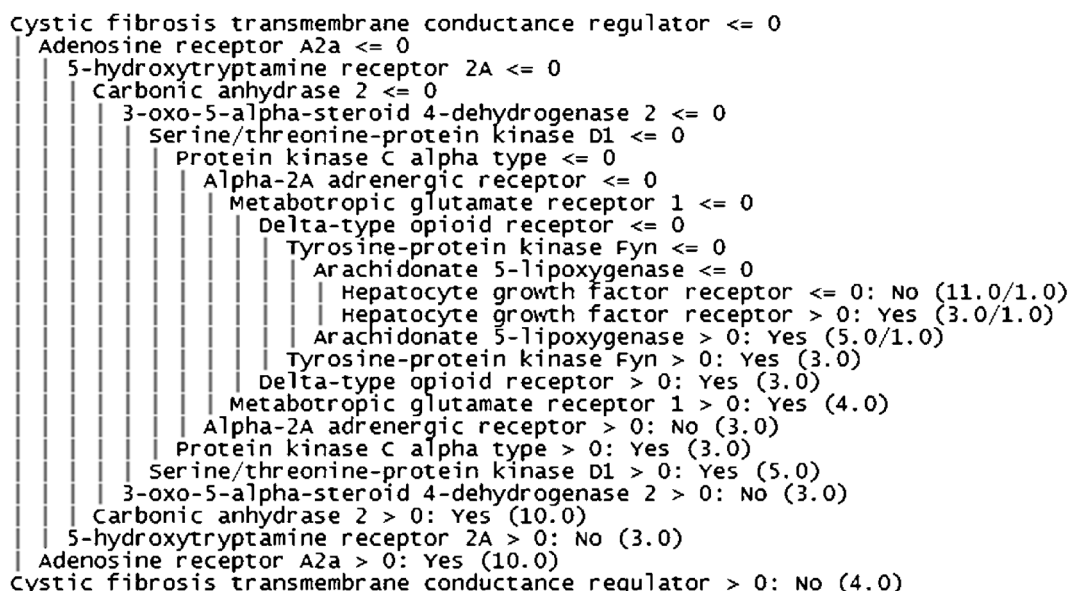


Figure 4. C4.5 classification tree for active compound set on Pigmentation phenotype against the 6 others. At each node activity ("1") on a protein target leads to phenotype classification, whereas inactivity ("0") proceeds deeper into the tree. In other words, starting from the root of the classification tree (top row), predicted activity on this target will lead to an outcome (indicated by the "pipes" leading down to the target name). On the other hand, inactivity will lead to the assessment of predicted activity on the next (indented) protein target.

that cause the Pigmentation phenotype from the others is difficult (indicated by the decision tree depth), as many of the molecules in our active dataset have very similar modes of action (the phenotype overlap has been highlighted in Figure 3). The difficulty is also reflected by the low classification accuracy (55.7% using leave-one-out cross-validation) obtained for the decision tree.

The targets of particular interest in the classification tree are the Carbonic Anhydrase 2 receptor and the Adenosine A2a receptor, as predicted activity on them points to the phenotype studied (Pigmentation = Yes) with the largest coverage (10 compounds). However, the predicted activity on these targets is not independent as each target depends on those preceding it. The tree is best read/interpreted in the form of predicted profiles. This means that activity/inactivity for all nodes are equally important from the root of the tree to each leaf. For example, we can observe that no activity on the Cystic fibrosis transmembrane conductance regulator (root of the tree) and activity on the Adenosine A2a receptor (leaf) is one complete predicted profile/path. Any compound that follows this rule is therefore predicted to show the Pigmentation phenotype.

Particularly in outer photoreceptor segments, CFTR activation helped with their elimination, whereas inhibition slowed lysosomal degradation. In this case study, predicted activity on CFTR was linked to *absence* of the phenotype, whereas inactivity would forward the compound being analysed to the next node in the classification tree, the Adenosine A2a receptor (A2a). A2a is also expressed in the RPE and is suggested to play a key role in sustaining its function.^[157] The A2a receptor (as well as its homologues, the A1, A2b and A3 receptors) is present in the human malignant melanoma A375 cell line.^[158]

Our classification indicates that 10 out of 45 compounds with predicted A2a activity (and simultaneous inactivity on CFTR) elicit the desired phenotype, suggesting this target is important for pigmentation modulation. The same number of compounds (10) is linked to activity on Carbonic anhydrase 2 (CA-II) and inactivity on the target-nodes leading to it. Yoshiura et al.^[159] have demonstrated that CA-II is a target antigen in various types of cancer including melanoma.^[159] CA-II has also been suggested to play a role in the regeneration of RPE,^[160] hence supporting the relevance of the target in the Pigmentation phenotype considered here. Next on the list of receptors expressed in the RPE (in this case in rat) is the 5-hydroxytryptamine 2A receptor (5HT2A),^[161] predicted activity against which is not meant to cause the Pigmentation phenotype according to our classification tree. Furthermore, the serotonin 2A receptor has been reported to interact with the Melanoma-associated antigen,^[162] therefore indicating a possible role in pigmentation. Activity on 3-oxo-5- α -steroid 4-dehydrogenase 2 (and inactivity on the target-nodes leading to it) is also classified as not altering pigmentation. 5- α reductase types 1 and 2 mRNA has been found in various ocular cells including RPE cells suggesting that they could be in-

involved in androgen action.^[163] However, predicted activity on Serine/threonine-protein kinase D1 (Protein kinase C μ -type) and Protein kinase C (PKC) α -type does modulate the phenotype. cAMP production in rat and chick RPE cells has been shown to be mediated by the activation of protein kinase C^[164,165]. Furthermore, melatonin-induced pigment aggregation was reversed by treating melanophores of *Xenopus laevis* with PKC activators,^[166] hence lending support to this rule derived in our analysis. The hepatocyte growth factor receptor (HGFR) was also confirmed to be expressed in RPE cells and is suggested to be involved in both RPE normal function and disease.^[167] For arachidonate 5-lipoxygenase however, Sakamoto et al.^[168] demonstrated that non-pigmented epithelial cells have the potential to synthesize 5-lipoxygenase 5-fold more than pigmented cells.

The remaining targets used for classification, namely the α -2a adrenergic receptor, delta-type opioid receptor metabotropic glutamate receptor 1 and tyrosine-protein kinase Fyn(p59Fyn) were found to have a more specific involvement in pigmentation and modulation of melanocyte function. Alpha-2 adrenergic receptors were suggested as mediators for melanophore pigment migration and later confirmed as melanosome aggregation mediators.^[169] In a recent patent, opioid receptor antagonists were suggested for the suppression of melanin formation on the human skin^[170] whereas the metabotropic glutamate receptor 1 has been linked to melanoma development^[171] in mice due to its abnormal expression in melanocytes.^[172] Finally, p59Fyn plays an important role in suppressing melanocyte differentiation by down-regulating mitogen-activated protein kinase 1 expression^[173] in agreement with our analysis.

The targets used in the classification tree along with the number of times they were predicted for the 45 compounds showing the Pigmentation phenotype are listed in Table 6. Interestingly, the predicted targets with a higher raw frequency (shown in Table 5) are *not* used in the tree. This is because the tree is designed to distinguish between Pigmentation and the other 6 observed phenotypes, meaning that targets predicted more frequently may indeed be relevant in causing a particular phenotype, but do not discriminate it from the other phenotypes observed in the study. Overall we can conclude that the targets used by the classification tree to separate the Pigmentation phenotype from the other phenotypes can give further insight into ligand-target-phenotype relationships, in addition to the pathway-based analysis presented above.

4 Conclusions

In silico target prediction is a commonly used approach to infer ligand-protein interactions for new small molecules,^[102] relating to both therapeutic target identification and also side-effect and "off-target" prediction.^[9] However, target annotations alone are not sufficient to observe bio-

Table 6. Ordered (from root to leaves) list of targets used in classification tree and the times they were predicted for compounds showing Pigmentation phenotype. These targets do not represent the MoA but may highlight the difference in MoA leading to different phenotypes.

Target Names used in classification tree (ordered)	Times predicted in pigmentation
Cystic fibrosis transmembrane conductance regulator	0
Adenosine A2a receptor	9
5-Hydroxytryptamine 2A receptor	2
Carbonic anhydrase 2	8
3-Oxo-5-alpha-steroid 4-dehydrogenase 2	2
Serine/threonine-protein kinase D1	6
Protein kinase C alpha type	5
Alpha-2A adrenergic receptor	2
Metabotropic glutamate receptor 1	8
Delta-type opioid receptor	2
Tyrosine-protein kinase Fyn	3
Arachidonate 5-lipoxygenase	3
Hepatocyte growth factor receptor	4

logical effects observed in a system, and hence in this work we extended previous approach both by pathway annotations, and subjecting the targets predicted to a classification tree analysis. For this purpose we used phenotypic screening data in *Xenopus laevis* and were able to show that the enrichment calculations for both targets and pathways indicated significant correlation with the phenotype studied, highlighting the underlying biological mechanism. While in most cases literature evidence could be found (in support of our analysis), the remaining cases form testable mode-of-action hypotheses which can be followed up experimentally in a protocol similar to the one described by Tomlinson et al.^[174] Furthermore, the classification analysis provided insight into differentiating amongst phenotypes with overlapping predicted bioactivity profiles, and therefore very similar modes of action. Hence we conclude that while in silico mode of action analysis has progressed a long way since its inception, system biology and polypharmacology extensions are likely to provide further insights into phenotypic screening data analyses in the future.

Conflict of interest

None declared.

Acknowledgements

This research was supported by *Unilever* (SL and AB), *Eli Lilly* (GD), *EPSRC* (GD), *University of East Anglia* (AH, KH), *John Innes Centre* (AH), *AstraZeneca* (AH), *John Jarrold Trust studentship* (KH).

References

- [1] M. Glick, E. Jacoby, *Curr. Opin. Chem. Biol.* **2011**, *15*, 540–546.
- [2] E. Jacoby, *Wiley Interdiscip. Rev.: Comput. Mol. Sci.* **2011**, *1*, 57–67.
- [3] A. Koutsoukas, B. Simms, J. Kirchmair, P. J. Bond, A. V. Whitmore, S. Zimmer, M. P. Young, J. L. Jenkins, M. Glick, R. C. Glen, et al., *J. Proteomics* **2011**, *74*, 2554–2574.
- [4] L. Mak, S. Liggi, L. Tan, K. Kusonmano, J. M. Rollinger, A. Koutsoukas, R. C. Glen, J. Kirchmair, *Curr. Pharm. Des.* **2013**, *19*, 532–577.
- [5] A. Koutsoukas, R. Lowe, Y. Kalantar-Motamedi, H. Y. Mussa, J. B. O. Mitchell, R. Glen, A. Bender, *J. Chem. Inf. Model.* **2013**, *53*, 1957–1966.
- [6] R. Lowe, H. Y. Mussa, F. Nigsch, R. C. Glen, J. B. Mitchell, *J. Cheminf.* **2012**, *4*, 2.
- [7] J. L. Jenkins, *Mol. Inf.* **2012**, *31*, 508–514.
- [8] M. J. Keiser, V. Setola, J. J. Irwin, C. Laggner, A. I. Abbas, S. J. Hufeisen, N. H. Jensen, M. B. Kuiser, R. C. Matos, T. B. Tran, et al., *Nature* **2009**, *462*, 175–181.
- [9] E. Lounkine, M. J. Keiser, S. Whitebread, D. Mikhailov, J. Hamon, J. L. Jenkins, P. Lavan, E. Weber, A. K. Doak, S. Côté, et al., *Nature* **2012**, *486*, 361–367.
- [10] D. Vidal, J. Mestres, *Mol. Inf.* **2010**, *29*, 543–551.
- [11] T. I. Oprea, A. Tropsha, *Drug Discov. Today: Technol.* **2006**, *3*, 357–365.
- [12] Y. Feng, T. J. Mitchison, A. Bender, D. W. Young, J. A. Tallarico, *Nat. Rev. Drug Discov.* **2009**, *8*, 567–578.
- [13] A. Gaulton, L. J. Bellis, A. P. Bento, J. Chambers, M. Davies, A. Hersey, Y. Light, S. McGlinchey, D. Michalovich, B. Al-Lazikani, et al., *Nucleic Acids Res.* **2011**, *44*, 1–8.
- [14] E. E. Bolton, Y. Wang, P. A. Thiessen, *Annu. Rep. Comput. Chem.* **2008**, *4*, 217–241.
- [15] Y. Wang, J. Xiao, T. O. Suzek, J. Zhang, J. Wang, Z. Zhou, L. Han, K. Karapetyan, S. Dracheva, B. A. Shoemaker, et al., *Nucleic Acids Res.* **2012**, *40*, D400–D412.
- [16] C. Knox, V. Law, T. Jewison, P. Liu, S. Ly, A. Frolkis, A. Pon, K. Banco, C. Mak, V. Neveu, et al., *Nucleic Acids Res.* **2011**, *39*, D1035–D1041.
- [17] H. Pence, A. Williams, *J. Chem. Edu.* **2010**, *87*, 1123–1124.
- [18] J. J. Irwin, T. Sterling, M. M. Mysinger, E. S. Bolstad, R. G. Coleman, *J. Chem. Inf. Model.* **2012**, *52*, 1757–1768.
- [19] M. Olah, R. Rad, L. Ostropovici, A. Bora, N. Hadaruga, D. Hadaruga, R. Moldovan, A. Fulas, M. Mractc, T. Oprea, "WOMBAT and WOMBAT-PK: Bioactivity Databases for Lead and Drug Discovery", in *Chemical Biology: From Small Molecules to Systems Biology and Drug Design*, Vol. 1–3 (Eds: S. Schreiber, T. Kapoor, G. Wess), Wiley-VCH, Weinheim, Germany, **2008**.
- [20] C. Krejsa, D. Horvath, S. Rogalski, J. Penzotti, B. Mao, F. Barbosa, J. Migeon, *Curr. Opin. Drug Discov. Dev.* **2003**, *6*, 470–480.
- [21] B. L. Roth, E. Lopez, S. Patel, W. K. Kroeze, *Neuroscientist* **2000**, *6*, 252–262.
- [22] A. Bender, J. Scheiber, M. Glick, *ChemMedChem* **2007**, *2*, 861–873.
- [23] J. Drews, *Nat. Rev. Drug Discov.* **2006**, *5*, 635–640.
- [24] J. Drews, *Science* **2000**, *287*, 1960–1964.
- [25] A. L. Hopkins, *Nat. Chem. Biol.* **2008**, *4*, 682–690.
- [26] M. T. Bianchi, E. J. Botzolakakis, *BMC Pharmacol.* **2010**, *10*, 3.
- [27] J. Arrowsmith, *Nat. Rev. Drug Discov.* **2011**, *10*, 328–329.
- [28] J. Arrowsmith, *Nat. Rev. Drug Discov.* **2011**, *10*, 87.
- [29] B. Roth, D. Sheffler, W. K. Kroeze, *Nat. Rev. Drug Discov.* **2004**, *3*, 353–359.
- [30] R. Morphy, Z. Rankovic, *J. Med. Chem.* **2005**, *48*, 6523–6543.

- [31] R. Morphy, Z. Rankovic, *J. Med. Chem.* **2006**, *49*, 4961–4970.
- [32] R. Morphy, C. Kay, Z. Rankovic, *Drug Discov. Today* **2004**, *9*, 641–651.
- [33] J. Tiihonen, J. Lönnqvist, K. Wahlbeck, T. Klaukka, L. Niskanen, A. Tanskanen, J. Haukka, *Lancet* **2009**, *374*, 620–627.
- [34] J. Lehár, A. Krueger, G. Zimmermann, A. Borisy, *Mol. Syst. Biol.* **2008**, *4*, 1–6.
- [35] A. A. Borisy, P. J. Elliott, N. W. Hurst, M. S. Lee, J. Lehar, E. R. Price, G. Serbedzija, G. R. Zimmermann, M. A. Foley, B. R. Stockwell, et al., *Proc. Natl. Acad. Sci. USA* **2003**, *100*, 7977–7982.
- [36] J. Aube, *ACS Med. Chem. Lett.* **2012**, *3*, 442–444.
- [37] T. T. Ashburn, K. B. Thor, *Nat. Rev. Drug Discov.* **2004**, *3*, 673–683.
- [38] F. López-Muñoz, C. Alamo, E. Cuenca, W. Shen, P. Clervoy, G. Rubio, *Ann. Clin. Psychiatry* **2005**, *17*, 113–135.
- [39] T. A. Ban, *Neuropsychiatric Disease and Treatment* **2007**, *3*, 495–500.
- [40] J. L. Medina-Franco, M. A. Giulianotti, G. S. Welmaker, R. A. Houghten, *Drug Discov. Today* **2013**, *18*, 495–501.
- [41] S. Ekins, A. J. Williams, M. D. Krasowski, J. S. Freundlich, *Drug Discov. Today* **2011**, *16*, 298–310.
- [42] I. Cortes-Ciriano, A. Koutsoukas, O. Abian, R. C. Glen, A. Velazquez-Campoy, A. Bender, *Med. Chem. Commun.* **2013**, *4*, 278–288.
- [43] Nidhi, M. Glick, J. W. Davies, J. L. Jenkins, *J. Chem. Inf. Model.* **2006**, *46*, 1124–1133.
- [44] J. Scheiber, B. Chen, M. Milik, S. C. K. Sukuru, A. Bender, D. Mikhailov, S. Whitebread, J. Hamon, K. Azzaoui, L. Urban, et al., *J. Chem. Inf. Model.* **2009**, *49*, 308–317.
- [45] M. J. Keiser, B. L. Roth, B. N. Armbruster, P. Ernsberger, J. J. Irwin, B. K. Shoichet, *Nat. Biotechnol.* **2007**, *25*, 197–206.
- [46] L. Peltason, Y. Hu, J. Bajorath, *ChemMedChem* **2009**, *4*, 1864–1873.
- [47] X. Ning, M. Walters, G. Karypis, G. Karypisxy, *J. Chem. Inf. Model.* **2012**, *52*, 38–50.
- [48] H. P. Nguyen, A. Koutsoukas, F. Mohd Fauzi, G. Drakakis, M. Maciejewski, R. C. Glen, A. Bender, *Chem. Biol. Drug Des.* **2013**, *82*, 252–266.
- [49] T. Scior, A. Bender, G. Tresadern, J. L. Medina-Franco, K. Martínez-Mayorga, T. Langer, K. Cuanalo-Contreras, D. K. Agrafiotis, *J. Chem. Inf. Model.* **2012**, *52*, 867–881.
- [50] S. Kortagere, S. Ekins, *J. Pharmacol. Toxicol. Meth.* **2010**, *61*, 67–75.
- [51] G. Nicola, T. Liu, M. K. Gilson, *J. Med. Chem.* **2012**, *55*, 6987–7002.
- [52] B. Ganter, R. D. Snyder, D. N. Halbert, D. M. Lee, *Pharmacogenomics* **2006**, *7*, 1025–1044.
- [53] F. López-Vallejo, M. A. Giulianotti, R. A. Houghten, J. L. Medina-Franco, *Drug Discov. Today* **2012**, *17*, 718–726.
- [54] J. Mestres, E. Gregori-Puigjané, S. Valverde, R. V. Solé, *Nat. Biotechnol.* **2008**, *26*, 983–984.
- [55] P. Tiikkainen, L. Franke, *J. Chem. Inf. Model.* **2012**, *52*, 319–326.
- [56] Evolus, *Discov. Informatics*, <http://www.evolus.com/>, (accessed 30/05/2013).
- [57] C. Southan, P. Várkonyi, S. Muresan, *J. Cheminf.* **2009**, *1*, 10.
- [58] Y. Zhou, B. Zhou, K. Chen, S. F. Yan, F. J. King, S. Jiang, E. A. Winzeler, *J. Chem. Inf. Model.* **2007**, *47*, 1386–94.
- [59] D. Stumpfe, J. Bajorath, *J. Chem. Inf. Model.* **2011**, *51*, 3131–3137.
- [60] P. Gedeck, C. Kramer, P. Ertl, *Prog. Med. Chem.* **2010**, *49*, 113–160.
- [61] M. Baker, *Nat. Rev. Drug Discov.* **2006**, *5*, 707–708.
- [62] G. Schneider, *Mol. Inf.* **2011**, *30*, 759–763.
- [63] A. J. Williams, S. Ekins, V. Tkachenko, *Drug Discov. Today* **2012**, *17*, 685–701.
- [64] K. Hettne, M. Cases, S. Boyer, J. Mestres, *Curr. Top. Med. Chem.* **2007**, *7*, 1530–1536.
- [65] D. Nishimura, *Biotech. Softw. Internet Rep.* **2001**, *2*, 117–120.
- [66] Cell Signaling Technology, <http://www.cellsignal.com>, (accessed 30/05/2013).
- [67] P. Artimo, M. Jonnalagedda, K. Arnold, D. Baratin, G. Csardi, E. de Castro, S. Duvaud, V. Flegel, A. Fortier, E. Gasteiger, et al., *Nucleic Acids Res.* **2012**, *40*, W597–W603.
- [68] N. R. Gough, *Ann. N.Y. Acad. Sci.* **2002**, *971*, 585–587.
- [69] A. Nikitin, S. Egorov, N. Daraselia, I. Mazo, *Bioinformatics* **2003**, *19*, 2155–2157.
- [70] E. Shmelkov, Z. Tang, I. Aifantis, A. Statnikov, *Biol. Direct* **2011**, *6*, 15.
- [71] M. Kanehisa, S. Goto, *Nucleic Acids Res.* **2000**, *28*, 27–30.
- [72] WikiPathways, <http://www.wikipathways.org>, (accessed 30/05/2013).
- [73] S. Ekins, Y. Nikolsky, A. Bugrim, E. Kirillov, T. Nikolskaya, *Methods Mol. Biol.* **2007**, *356*, 319–350.
- [74] *Ingenuity Pathway Analysis*, Ingenuity Systems Inc., www.ingenuity.com, (accessed 30/05/2013).
- [75] M. Krull, S. Pistor, N. Voss, A. Kel, I. Reuter, D. Kronenberg, H. Michael, K. Schwarzer, A. Potapov, C. Choi, et al., *Nucleic Acids Res.* **2006**, *34*, D546–D551.
- [76] V. Matys, O. V. Kel-Margoulis, E. Fricke, I. Liebich, S. Land, A. Barre-Dirrie, I. Reuter, D. Chekmenev, M. Krull, K. Hornischer, et al., *Nucleic Acids Res.* **2006**, *34*, D108–D110.
- [77] *GeneSpring*, Agilent Technologies, <http://www.genomics.agilent.com/CollectionSubpage.aspx?PageType=Product&SubPageType=ProductDetail&PageID=1675>, (accessed 30/05/2013).
- [78] A. J. Williams, S. Ekins, *Drug Discov. Today* **2011**, *16*, 747–750.
- [79] S. Orchard, B. Al-Lazikani, S. Bryant, D. Clark, E. Calder, I. Dix, O. Engkvist, M. Forster, A. Gaulton, M. Gilson, et al., *Nat. Rev. Drug Discov.* **2011**, *10*, 661–669.
- [80] D. Fourches, E. Muratov, A. Tropsha, *J. Chem. Inf. Model.* **2010**, *50*, 1189–1204.
- [81] M. R. Berthold, N. Cebron, F. Dill, T. R. Gabriel, “KNIME: The Konstanz information miner”, in *Studies in Classification, Data Analysis, and Knowledge Organization (GfKL 2007)*, Springer, Heidelberg, **2007**, pp. 319–326.
- [82] *Standardizer*, ChemAxon, <http://www.chemaxon.com>, (accessed 30/05/2013).
- [83] SYBYL, Tripos International, 1699 South Hanley Rd., St. Louis, Missouri, 63144, USA.
- [84] *Molecular Operating Environment (MOE)*, Chemical Computing Group, 1010 Sherbooke St. West, Suite #910, Montreal, QC, Canada, H3A 2R7.
- [85] *Pipeline Pilot*, Accelrys, 10188 Telesis Court, Suite 100, San Diego, CA 92121, USA.
- [86] A. Varnek, I. Baskin, *J. Chem. Inf. Model.* **2012**, *52*, 1413–1437.
- [87] M. Glick, J. L. Jenkins, J. H. Nettles, H. Hitchings, J. W. Davies, *J. Chem. Inf. Model.* **2006**, *46*, 193–200.
- [88] F. Nigsch, A. Bender, J. L. Jenkins, J. B. O. Mitchell, *J. Chem Inf Model* **2008**, *48*, 2313–25.
- [89] B.-H. Su, Y.-S. Tu, E. X. Esposito, Y. J. Tseng, *J. Chem. Inf. Model.* **2012**, *52*, 1660–1673.
- [90] A. Bender, J. L. Jenkins, J. Scheiber, S. C. K. Sukuru, M. Glick, J. W. Davies, *J. Chem. Inf. Model.* **2009**, *49*, 108–119.
- [91] G. Hu, G. Kuang, W. Xiao, W. Li, G. Liu, Y. Tang, *J. Chem. Inf. Model.* **2012**, *52*, 1103–1113.

- [92] J. H. Nettles, J. L. Jenkins, A. Bender, Z. Deng, J. W. Davies, M. Glick, *J. Med. Chem.* **2006**, *49*, 6802–6810.
- [93] J. Kirchmair, A. Howlett, J. E. Peironcelly, D. S. Murrell, M. J. Williamson, S. E. Adams, T. Hankemeier, L. van Buren, G. Duchateau, W. Klaffke, et al., *J. Chem. Inf. Model.* **2013**, *53*, 354–367.
- [94] P. Zhao, L. Zhang, J. A. Grillo, Q. Liu, J. M. Bullock, Y. J. Moon, P. Song, S. S. Brar, R. Madabushi, T. C. Wu, et al., *Clin. Pharmacol. Ther.* **2011**, *89*, 259–267.
- [95] D. F. Ortwine, I. Aliagas, *Mol. Pharmaceutics* **2013**, *10*, 1153–1161.
- [96] G. Moroy, V. Y. Martiny, P. Vayer, B. O. Villoutreix, M. A. Miteva, *Drug Discov. Today* **2012**, *17*, 44–55.
- [97] K. H. Grime, P. Barton, D. F. McGinnity, *Mol. Pharmaceutics* **2013**, *10*, 1191–1206.
- [98] D. A. Smith, *Mol. Pharmaceutics* **2013**, *10*, 1162–1170.
- [99] M. Iskar, G. Zeller, X.-M. Zhao, V. van Noort, P. Bork, *Curr. Opin. Biotechnol.* **2011**, *23*, 609–616.
- [100] T. I. Oprea, S. K. Nielsen, O. Ursu, J. J. Yang, O. Taboureau, S. L. Mathias, I. Kouskoumvekaki, L. A. Sklar, C. G. Bologna, *Mol. Inf.* **2011**, *30*, 100–111.
- [101] A. L. Hopkins, J. S. Mason, J. P. Overington, *Curr. Opin. Struct. Biol.* **2006**, *16*, 127–136.
- [102] Y. Yamanishi, M. Kotera, M. Kanehisa, S. Goto, *Bioinformatics* **2010**, *26*, 246–254.
- [103] M. Schenone, V. Dančák, B. K. Wagner, P. A. Clemons, *Nat. Chem. Biol.* **2013**, *9*, 232–240.
- [104] U. S. Eggert, *Nat. Chem. Biol.* **2013**, *9*, 206–209.
- [105] J. Besnard, G. F. Ruda, V. Setola, K. Abecassis, R. M. Rodriguiz, X.-P. Huang, S. Norval, M. F. Sassano, A. I. Shin, L. A. Webster, et al., *Nature* **2012**, *492*, 215–220.
- [106] M. L. Tomlinson, A. E. Hendry, G. N. Wheeler, *Meth. Mol. Biol.* **2012**, *917*, 155–166.
- [107] M. L. Tomlinson, M. Rejzek, M. Fidock, R. A. Field, G. N. Wheeler, *Mol. Biosyst.* **2009**, *5*, 376–384.
- [108] *Diversity Set Information*, NCI Repositories, http://dtp.nci.nih.gov/branches/dscbv/div2_explanation.html, (accessed 30/05/2013).
- [109] A. Bender, H. Y. Mussa, R. C. Glen, S. Reiling, *J. Chem. Inf. Comput. Sci.* **2004**, *44*, 1708–1718.
- [110] N. M. O'Boyle, M. Banck, C. A. James, C. Morley, T. Vandermeersch, G. R. Hutchison, *J. Cheminf.* **2011**, *3*, 33.
- [111] G. V. Paolini, R. H. B. Shapland, W. P. Van Hoorn, J. S. Mason, A. L. Hopkins, *Nat. Biotechnol.* **2006**, *24*, 805–815.
- [112] F. Mohd Fauzi, A. Koutsoukas, R. Lowe, K. Joshi, T.-P. Fan, R. C. Glen, A. Bender, *J. Chem. Inf. Model.* **2013**, *53*, 661–673.
- [113] M. Hall, E. Frank, G. Holmes, B. Pfahringer, P. Reutemann, I. Witten, *SIGKDD Explor. Newsl.* **2009**, *11*, 10–18.
- [114] J. R. Quinlan, *C4.5: Programs for Machine Learning*, Morgan Kaufmann, San Mateo CA, **1993**.
- [115] E. W. Damm, R. Winklbauer, *Development* **2011**, *138*, 565–575.
- [116] C. Betsholtz, L. Karlsson, P. Lindahl, *BioEssays* **2001**, *23*, 494–507.
- [117] P. Soriano, *Development* **1997**, *124*, 2691–2700.
- [118] A. Uong, L. I. Zon, *J. Cell. Physiol.* **2010**, *222*, 38–41.
- [119] D. M. Parichy, J. F. Rawls, S. J. Pratt, T. T. Whitfield, S. L. Johnson, *Development* **1999**, *126*, 3425–3436.
- [120] L. B. Giebel, R. A. Spritz, *Proc. Natl. Acad. Sci. USA* **1991**, *88*, 8696–8699.
- [121] E. P. v. Strandmann, S. Senkel, G. Ryffel, U. R. Hengge, *Am. J. Pathol.* **2001**, *158*, 2021–2029.
- [122] L. Zhuang, C. S. Lee, R. A. Scolyer, S. W. McCarthy, X. D. Zhang, J. F. Thompson, P. Hersey, *Mod. Pathol.* **2007**, *20*, 416–426.
- [123] J. Du, H. R. Widlund, M. A. Horstmann, S. Ramaswamy, K. Ross, W. E. Huber, E. K. Nishimura, T. R. Golub, D. E. Fisher, *Cancer Cell* **2004**, *6*, 565–576.
- [124] C. Abdullah, X. Wang, D. Becker, *Cell Cycle* **2011**, *10*, 977–988.
- [125] D. Du Pasquier, A. Dupré, C. Jessus, *PLoS One* **2011**, *6*, e23672.
- [126] G. Maurer, B. Tarkowski, M. Baccarini, *Oncogene* **2011**, *30*, 3477–3488.
- [127] M. Longoni, S. Moncini, M. Cisternino, I. M. Morella, S. Ferriaiuolo, S. Russo, S. Mannarino, V. Brazzelli, P. Coi, R. Zippel, et al., *Am. J. Med. Genet., Part A* **2010**, *152A*, 2176–2184.
- [128] B. Pandit, A. Sarkozy, L. A. Pennacchio, C. Carta, K. Oishi, S. Martinelli, E. A. Pogna, W. Schackwitz, A. Ustaszewska, A. Landstrom, et al., *Nat. Genet.* **2007**, *39*, 1007–1012.
- [129] S. Lebreton, L. Boissel, N. Iouzalén, J. Moreau, *Mech. Dev.* **2004**, *121*, 1481–1494.
- [130] I. Dominguez, J. Green, *Development* **2000**, *127*, 861–868.
- [131] A. E. Tucker, I. I. Salles, D. E. Voth, W. Ortiz-Leduc, H. Wang, I. Dozmorov, M. Centola, J. D. Ballard, *Cell. Microbiol.* **2003**, *5*, 523–532.
- [132] K. Itoh, T. L. Tang, B. G. Neel, S. Y. Sokol, *Development* **1995**, *121*, 3979–3988.
- [133] S. A. Grando, M. R. Pittelkow, K. U. Schallreuter, *J. Invest. Dermatol.* **2006**, *126*, 1948–1965.
- [134] Z. Wang, Y. Nishimura, Y. Shimada, N. Umemoto, M. Hirano, L. Zang, T. Oka, C. Sakamoto, J. Kuroyanagi, T. Tanaka, *Gene* **2009**, *446*, 18–27.
- [135] J. Xu, F. Xie, *Biochem. Biophys. Res. Commun.* **2011**, *405*, 250–255.
- [136] R. Fujii, *Pigm. Cell Res.* **2000**, *13*, 300–319.
- [137] E. Legius, C. Schrandner-Stumpel, E. Schollen, C. Pulles-Heintzberger, M. Gewillig, J.-P. Fryns, *J. Med. Genet.* **2002**, *39*, 571–574.
- [138] D. L. Stirewalt, J. P. Radich, *Nat. Rev. Cancer* **2003**, *3*, 650–655.
- [139] B. J. Dickson, *Science* **2002**, *298*, 1959–1964.
- [140] M. Klagsbrun, A. Eichmann, *Cytokine Growth Factor Rev.* **2005**, *16*, 535–548.
- [141] M. S. Deiner, T. E. Kennedy, A. Fazeli, T. Serafini, M. Tessier-Lavigne, D. W. Sretavan, *Neuron* **1997**, *19*, 575–589.
- [142] T. P. Newsome, B. Asling, B. J. Dickson, *Development* **2000**, *127*, 851–860.
- [143] S. Aspöngren, D. Hedberg, M. Wallin, *Pigm. Cell Res.* **2006**, *19*, 136–145.
- [144] F. Riedel, D. Vorkel, S. Eaton, *Development* **2011**, *138*, 149–158.
- [145] B. L. Loeys, J. Chen, E. R. Neptune, D. P. Judge, M. Podowski, T. Holm, J. Meyers, C. C. Leitch, N. Katsanis, N. Sharifi, et al., *Nat. Genet.* **2005**, *37*, 275–281.
- [146] R. M. White, J. Cech, S. Ratanasirintraoort, C. Y. Lin, P. B. Rahl, C. J. Burke, E. Langdon, M. L. Tomlinson, J. Mosher, C. Kaufman, et al., *Nature* **2011**, *471*, 518–522.
- [147] A. S. Dhillon, S. Hagan, O. Rath, W. Kolch, *Oncogene* **2007**, *26*, 3279–3290.
- [148] C. Nava, N. Hanna, C. Michot, S. Pereira, N. Pouvreau, T. Ni-hori, Y. Aoki, Y. Matsubara, B. Arveiler, D. Lacombe, et al., *J. Med. Genet.* **2007**, *44*, 763–771.
- [149] R. Buscà, R. Ballotti, *Pigm. Cell Res.* **2000**, *13*, 60–69.
- [150] S. Carreira, J. Goodall, I. Aksan, S. A. La Rocca, *Nature* **2005**, *433*, 764–769.
- [151] B. E. Deverman, P. H. Patterson, *Neuron* **2009**, *64*, 61–78.

- [152] M. Amyere, T. Vogt, J. Hoo, F. Brandrup, A. Bygum, L. Boon, M. Vikkula, *J. Invest. Dermatol.* **2011**, *131*, 1234–1239.
- [153] A. Tanaka, J. E. Lai-Cheong, P. C. van den Akker, N. Nagy, G. Millington, G. F. H. Diercks, P. C. van Voorst Vader, S. E. Clements, N. Almaani, T. Techanukul, et al., *Exp. Dermatol.* **2010**, *19*, 416–423.
- [154] J. M. Dal Porto, S. B. Gauld, K. T. Merrell, D. Mills, A. E. Pugh-Bernard, J. Cambier, *Mol. Immunol.* **2004**, *41*, 599–613.
- [155] A. L. Berlin, A. S. Paller, L. S. Chan, *J. Am. Acad. Dermatol.* **2002**, *47*, 169–190.
- [156] J. Liu, W. Lu, S. Guha, G. C. Baltazar, E. E. Coffey, A. M. Laties, R. C. Rubenstein, W. W. Reenstra, C. H. Mitchell, *Am. J. Physiol. Cell Physiol.* **2012**, *303*, C160–C169.
- [157] F. Dong, J. An, *Chin. J. Ophthalmol.* **2007**, *43*, 1110–1113.
- [158] S. Merighi, K. Varani, S. Gessi, E. Cattabriga, V. Iannotta, C. Ulouglu, E. Leung, P. A. Borea, *Br. J. Pharmacol.* **2001**, *134*, 1215–1226.
- [159] K. Yoshiura, T. Nakaoka, T. Nishishita, K. Sato, A. Yamamoto, S. Shimada, T. Saida, Y. Kawakami, T. A. Takahashi, H. Fukuda, et al., *Clin. Cancer Res.* **2005**, *11*, 8201–8207.
- [160] G. E. Korte, J. Smith, *Experientia* **1993**, *49*, 789–791.
- [161] M. Nash, T. Flanigan, R. Leslie, N. N. Osborne, *Ophthalmic Res.* **1999**, *31*, 1–4.
- [162] I. Raote, A. Bhattacharya, M. Panicker, "Serotonin 2A (5-HT_{2A}) Receptor Function: Ligand-Dependent Mechanisms and Pathways", in *Serotonin Receptors in Neurobiology* (Ed: A. Chattopadhyay), CRC Press, Boca Raton, FL, **2007**.
- [163] E. M. Rocha, L. A. Wickham, L. A. da Silveira, K. L. Krenzer, F. S. Yu, I. Toda, B. D. Sullivan, D. A. Sullivan, *Br. J. Ophthalmol.* **2000**, *84*, 76–84.
- [164] M. S. Nash, J. P. Wood, N. N. Osborne, *Exp. Eye Res.* **1997**, *64*, 249–255.
- [165] A. Hirota, *J. Jpn. Ophthalmol. Soc.* **1992**, *96*, 1412–1417.
- [166] D. Sudgen, *J. Cell. Biol.* **1992**, *119*, 1515–1521.
- [167] K. Lashkari, N. Rahimi, A. Kazlauskas, *Invest. Ophthalmol. Visual Sci.* **1999**, *40*, 149–156.
- [168] S. Sakamoto, H. Shichi, *J. Ocul. Pharmacol.* **1991**, *7*, 141–145.
- [169] J. O. Karlsson, R. G. Andersson, N. Grundström, *Br. J. Pharmacol.* **1989**, *97*, 222–228.
- [170] R. Beumer, J. Klock, "Use of Opioid Receptor Antagonists", *WO Patent 2007/039058 A2* **2007**.
- [171] Y. E. Marín, S. Chen, *J. Mol. Med.* **2004**, *82*, 735–749.
- [172] S.-S. Shin, B. A. Wall, J. S. Goydos, S. Chen, *Pigm. Cell Melanoma Res.* **2010**, *23*, 103–111.
- [173] C. Wellbrock, C. Weisser, E. Geissinger, J. Troppmair, M. Schartl, *J. Biol. Chem.* **2002**, *277*, 6443–6454.
- [174] M. L. Tomlinson, P. Guan, R. J. Morris, M. D. Fidock, M. Rejzek, C. Garcia-Morales, R. A. Field, G. N. Wheeler, *Chem. Biol.* **2009**, *16*, 93–104.

Received: May 31, 2013

Accepted: August 6, 2013

Published online: October 18, 2013

Comparative mode-of-action analysis following manual and automated phenotype detection in *Xenopus laevis*†

Cite this: *Med. Chem. Commun.*, 2014, 5, 386

Georgios Drakakis,^a Adam E. Hendry,^b Kimberley Hanson,^b Suzanne C. Brewerton,^c Michael J. Bodkin,^c David A. Evans,^c Grant N. Wheeler^b and Andreas Bender^{*a}

Given the increasing utilization of phenotypic screens in drug discovery also the subsequent mechanism-of-action analysis gains increased attention. Such analyses frequently use *in silico* methods, which have become significantly more popular in recent years. However, identifying phenotype-specific mechanisms of action depends heavily on suitable phenotype identification in the first place, many of which rely on human input and are therefore inconsistent. In this work, we aimed at analysing the impact that human phenotype classification has on subsequent *in silico* mechanism-of-action analysis. To this end, an image analysis application was implemented for the rapid identification of seven high-level phenotypes in *Xenopus laevis* tadpoles treated with compounds from the National Cancer Institute Diversity Set II. It was found that manual and automated phenotype classifications were in agreement with some of the phenotypes (e.g. 73.9% agreement observed for general morphology abnormality), while this was not the case in others (e.g. melanophore migration with 37.6% agreement between both annotations). Based on both annotations, protein targets of active compounds were predicted *in silico*, and decision trees were generated to understand mechanisms-of-action behind every phenotype while also taking polypharmacology (combinations of targets) into account. It was found that the automated phenotype categorisation greatly increased the accuracy of the results of the mechanism-of-action model, where it improved the classification accuracy by 9.4%, as well as reducing the tree size by eight nodes and the number of leaves and the depth by three levels. Overall we conclude that consistent phenotype annotations seem to be generally crucial for successful subsequent mechanism-of-action analysis, and this is what we have shown here in *Xenopus laevis* screens in combination with *in silico* mechanism-of-action analysis.

Received 23rd October 2013
Accepted 28th January 2014

DOI: 10.1039/c3md00313b

www.rsc.org/medchemcomm

Introduction

In recent years phenotypic screening has experienced a comeback,^{1–3} both due to technological advances and the realization that single-target based screens appear to oversimplify the drug discovery process in many cases. However, two questions that need to be addressed in this approach are a solid choice of phenotype definitions (many initiatives have recently been started^{4,5} to address this question), as well as the subsequent mode-of-action analysis^{6,7} to understand compound action also on a mechanistic level. In this work we attempt to resolve both

these issues by introducing an automated phenotype classification software application followed by an *in silico* bioactivity profile analysis.

Phenotype annotation is not always a straightforward process, especially when it relies heavily on human input and involves large datasets.^{8–11} For this reason and being heavily dependent on recent developments in IT data storage and processing abilities, automated image processing has recently been introduced for the analysis of high content screening (HCS) data, which also has been a major technology driver behind the recent trend towards phenotypic screening.¹² CellProfiler,¹³ one of the first open-source applications for detecting cell phenotypes, is able to process cell images for simple readouts such as cell count/size, as well as more complicated readouts such as protein staining. The CellProfiler image processing workflow includes image illumination correction and iterative object detection, before assessing the image for the desired measures. However, this is not easily transferable to the current work as the focus is whole-organism readouts and the resulting detection of very different features. The importance of

^aUnilever Centre for Molecular Science Informatics, Department of Chemistry, University of Cambridge, Lensfield Road, Cambridge CB2 1EW, UK. E-mail: ab454@cam.ac.uk; Fax: +44 (0)1223 763076; Tel: +44 (0)1223 762983

^bSchool of Biological Sciences, University of East Anglia, Norwich Research Park, Norwich, NR4 7TJ, UK

^cEli Lilly U.K., Erl Wood Manor, Windlesham, Surrey GU206PH, UK

† Electronic supplementary information (ESI) available. See DOI: 10.1039/c3md00313b

pre-processing and feature extraction was also highlighted by Bayraktar *et al.*,¹⁴ who proposed that the physiological state of cells could be analysed using moment invariants (image properties which remain unchanged after the application of a particular transformation such as rotation). This is because noisy images may compromise classification. In order to improve the detection quality also in cases of noisy images, recently an image segmentation methodology was introduced to aid object detection for improved classification of bipolar and monoaster cells using Laplacian of Gaussian edge detection on grayscale images, which sharpened important features.¹⁵ The sharpening and detection of objects in an image is commonly performed by assessing colour values of neighbouring pixels. For simpler/faster calculations images are usually converted to the greyscale, leaving the developer to have to deal with only one colour channel. This can, however, result in the loss of important information. An example of using different colour channels for object detection highlighted the potential of image analysis in siRNA screens,¹⁶ where by overlapping the same image using the values of two different colour channels (different cells were highlighted in each colour channel) the authors were able to successfully identify VSV-GFP infected cells. Given that biological effects often change as a function of time, temporal resolution also becomes important as shown by Neumann *et al.*,¹⁷ who used time-lapse in a high-throughput RNAi screen to detect phenotypes such as mitosis and apoptosis. A number of similar cellular readouts such as changes in morphology and cycle progression can be easily computed with KineticScan® HCS Reader BioApplications.¹² As one can see, different approaches for automated image processing and feature extraction exist, the correct selection of which depends on the nature of the readout and experiment conducted.

Related to the particular system considered in this study, *Xenopus laevis* phenotypic readouts and also several imaging studies have been reported recently. Time-lapse imaging has been employed for developmental readouts on a tissue level, as embryo cells are larger compared to other vertebrate models.¹⁸ Alternative approaches to exploring morphogenesis in *Xenopus laevis* include kymographs and 3D image projections which allow the in-depth investigation and monitoring of cell and tissue.¹⁹ Moving to higher dimensions, 3D imaging was used for the visualisation of the differences in cardiac microstructures in normal and abnormal *Xenopus laevis* tadpoles.²⁰ Higher-level phenotype identification aided with pinpointing heritable developmental abnormalities in *Xenopus tropicalis* screens with chemically induced mutations.²¹ Similarly, early stage *X. tropicalis* development phenotypes were studied by inhibiting the function of 202 different genes *via* the injection of morpholino oligonucleotides, and corresponding 'synphenotype groups' of genes which cause similar phenotypes were identified.²² This seems to be one of the few systematic and consistent classifications of phenotypes available today for *Xenopus*. However, no algorithms have been described as of yet for an automated and hence consistent feature extraction and hence phenotype classification in these studies.

Automated image analysis for phenotype detection has been employed in zebrafish though, which is one of the prototypic

model organisms employed for developmental analysis.²³ A comparison of two stages of zebrafish development was recently carried out using images derived from a Cellomics® ArrayScan® II high-content reader on fluorescent embryos.²⁴ A more flexible approach, ZebIAT, allows comparisons not only between individual zebrafish, but across different embryos under varying conditions by detecting regions of interest using reference landmarks,²⁵ similar to the IN Cell Investigator Zebrafish Analysis Plug-In for the commercially available IN Cell Analyzer System developed by GE Healthcare Life Sciences. (For further image processing methods in zebrafish the reader is referred to extensive recent reviews.^{26,27}) Hence it seems that automated high-level phenotype detection has been explored to a higher degree in zebrafish than *Xenopus*.

We believe that the introduction of human input into phenotype identification and annotation may incur inconsistencies similar to those which occur during compound assessment and prioritisation by medicinal chemists.^{28,29} This may arise from large datasets (image series), the quality of the images themselves, or merely the difficulty in pinpointing the subtle details in particular regions of interest. Therefore, the introduction of an algorithm with consistent phenotype definitions in *Xenopus* phenotypic screens would provide researchers with a classification method that is at the same time more objective, as well as faster. The results of such an application significantly depend on the quality of the images used as input and therefore the quality needs to be regulated on a systematic level in order to become consistent. Related open source quality control metrics have already been introduced into HCS applications by Bray *et al.*³⁰ for discarding low quality images which would have a negative effect on the output of an experiment. They proceeded to evaluate these metrics on a series of 2154 images of which 910 were manually considered blurry, yielding only 81 false positives and 28 false negatives with an overall F-score of 0.975 and the algorithm was hence found to be rather successful. Since software applications become error-prone when dealing with noisy images, we additionally aimed in our work to ensure that objective pre-processing metrics are incorporated into our analysis algorithms.

The reason why a solid phenotypic definition of readouts is crucial becomes even more evident in the next step, when the mode of action of compounds needs to be elucidated. This is true on a case-by-case basis, given that there are a limited number of mechanisms that can achieve the same phenotype, also when grouping compounds per phenotypic class and considering which targets are more frequently present in this class than others.^{31,32} (This principle is similar to 'Gene Set Enrichment Analysis', which has become commonplace when analyzing transcriptomics data.³³) In case phenotype definitions are inconsistent, the signal given by a shared mode-of-action by compounds causing a given phenotype will be weakened or, in the worst case, disappear completely. In our work, we will employ *in silico* target predictions to suggest possible modes of action related to particular phenotypes of interest.³⁴ The most commonly used methods in the field are the similarity ensemble approach (SEA),^{35,36} pharmacophores,^{37,38} support vector machines (SVM)³⁹ and the multinomial Naïve Bayes.⁴⁰⁻⁴²

It should be noted that different methods use different descriptors, such as 2D/3D or binding site descriptors. Validating *in silico* approaches due to incomplete data has been highlighted as a major problem in the field, at times leading to non-representative network analyses.⁴³ However, when dealing with complete data, *in silico* screening has been shown by Vidal *et al.*⁴⁴ to be a rather accurate alternative to *in vitro* screening, where an ensemble approach of three descriptors resulted in 70% affinity predictions on a complete ligand–protein interaction matrix for antipsychotic drugs. In a recent study we have demonstrated how such bioactivity predictions can be utilised to gain biological insights, namely by annotating predicted targets with pathways on the one hand, and by generating polypharmacological bioactivity profiles that differentiate between phenotypes on the other.³¹ However, what has not been paid attention to before – and this is the aim of the current study – is the impact that phenotype annotations have on subsequent mode-of-action analyses, here in the form of *in silico* activity profiles. In particular, we introduce a methodology for automated phenotype classification of *Xenopus laevis* tadpoles treated with compounds from the National Cancer Institute Diversity Set II.⁴⁵ Bioactivity profiles are then predicted *in silico* for the molecules in this dataset which show an effect *in vivo*, and these are used for training decision trees to identify underlying common modes of action. We will show that mode-

of-action analyses depend heavily on phenotype classifications, hence suggesting that an automated and consistent approach appears to be beneficial.

Materials and methods

Compound screening

Compounds from the NCI Diversity Set II⁴⁵ library were screened as described by Tomlinson *et al.*^{10,11} *Xenopus laevis* embryos (stage 15) were added to 96 well plates (5 embryos per well) at two different concentrations (20 and 40 μ M) for 3 days (until stage 38) at 18 °C. Images of the tadpoles were reproduced using a light microscope mounted with a Micropublisher 3.3 RTV camera. The original phenotype annotation was performed manually using the consensus observation from two individuals to decrease experimenter bias.

Automated phenotype analysis

An image analysis software application (the algorithm is described below; all steps are outlined in Fig. 1 and parameters summarized in Table 1) was developed in Microsoft® Visual C++ Express 2010 using the OpenCV⁴⁶ 2.45 library for *Xenopus* image processing named 'XePhIAS' (*Xenopus* Phenotypic Imaging Analysis Software). While the primary aim of the application is

1. For "environment control" image:
 - 1.1. Prompt user to set Canny⁴⁷ edge detection threshold. Show output dynamically
 - 1.2. Prompt user to set Dilation threshold. Show output dynamically
2. For All images:
 - 2.1. Perform Canny⁴⁷ edge detection using threshold set in Step 1.1
 - 2.2. Perform Dilation on image using threshold set in Step 1.2
 - 2.3. Detect objects using findcontours⁴⁹ function
 - 2.4. Select only the largest object using connected component analysis
 - 2.5. Perform Erode on image to return object to original size using threshold from Step 2
 - 2.6. Set 21 equally-spaced points (can segment image into 20 sub-images) on the X-axis
 - 2.7. Set Bounding points (minimum and maximum value on Y-axis from points in Step 2.6) and Average Y-axis points
 - 2.8. Get tadpole orientation. Head faces the largest <Ymax-Ymin> value (from Step 2.7) in first/last 3 points from Step 2.6 (both ends of tadpole)
 - 2.9. Set head region (<Ymax-Ymin> converges in neighbouring X-axis points)
 - 2.10. Set eye region (box with size 2/3 of head region in Step 2.10)
 - 2.11. Set upper/lower regions by using average Y values from Step 2.7 and by removing head region
 - 2.12. Create a blurred grayscale copy using GaussianBlur⁵⁰ function
 - 2.13. Create a binary (black and white) copy
 - 2.14. Derive regions of interest in the appropriate image copies of interest and check for phenotypes according to definitions (See Table 1)

Fig. 1 Workflow of the algorithm for automated phenotype categorisation in *Xenopus laevis* image series. Part 1 refers to the two thresholds set by the user on a single image assuming that the environment (lighting, background) will be similar throughout the series. Part 2 details the detection of regions of interest and phenotype annotation, based on the definitions given in Table 1.

Table 1 Definition of phenotypes in the automated image analysis software for chemical genetics *Xenopus laevis* screens. Fig. 2 gives examples of all phenotypes, and Fig. 1 the workflow of the algorithm

Phenotype	Description	Strict definitions for application	Method
Pigmentation	Absence of common pigmentation	Pigmented cells/all cells < 10%	Count number of black pixels in the binary image region of interest)
General morphology	Impaired physiological development	Tadpole length/height < 3	From global max ($X_{\max} - X_{\min}$) and largest ($Y_{\max} - Y_{\min}$) value (from the 21 points on the X-axis)
Melanophore morphology	Pigment cells rounded, not dendritic	Rounded pigmentation occurrences > 10	Locate circles in the blurred image with maximum radius of 3 pixels using HoughCircles ⁵¹⁻⁵³
Melanophore migration	Pigment cells have not migrated to normal positions	Pigmented cells in the top half excluding head/pigmented cells in the bottom half excluding head > 3/2 and reverse	Draw lines between all average Y-values and remove the head region. Count black cells
Eye development	Eye underdeveloped	Eye detectable (circle in the blurred image) in the tadpole head region	Locate the circle in the blurred image with a minimum radius = 1/10 head region using HoughCircles ⁵¹⁻⁵³
Blistering or edema (merged)	Localised blistering or significant swelling	Difference in height values in neighbouring X-axis values excluding the head region > 5/4 (sudden height increase)	Check ($Y_{\max} - Y_{\min}$) values in neighbouring X-axis points (from the 21 points on the X-axis)

the rapid and objective classification of consistently defined phenotypes, it at the same time needs to remain flexible for varying environmental parameters/circumstances such as lighting or background noise. For the latter reason we have inserted a pre-processing step into the application which requires minimal human input prompting for two thresholds to apply to a control image in the form of slide bars which dynamically show the outcome on the screen. These thresholds are for performing Canny⁴⁷ edge detection to locate the tadpole and for dilating (using the Dilate⁴⁸ function) the image so that all edges of the tadpole are connected. From this point onwards the application is able to automatically process the image series.

In the second step, all images are processed and the phenotypes detected are written to a text file. The images are

subjected to Canny⁴⁷ edge detection and are then dilated according to the user-defined thresholds. Objects are detected, retaining only the largest object (in this case the tadpole). Erosion (using the OpenCV Erode⁴⁸ function) transformed the object back to its original size. Bounding points were then set around the tadpole in our image, allowing the definition of regions of interest (eye location, for instance) as well as metrics such as the relative length of the tadpole. A binary copy of each image was used to search for pigmented cells and a blurred copy helped locate rounded pigmented cells without too many false positives. From the derived regions of interest in each image, the algorithm classified each tadpole according to the phenotype definitions. The phenotypes annotated are pigmentation, melanophore morphology, melanophore migration, eye

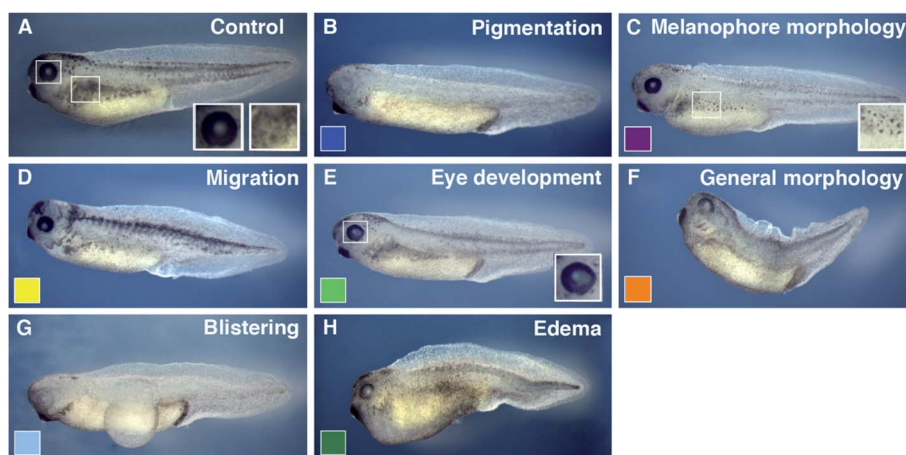


Fig. 2 Illustration of phenotypes derived from the *Xenopus laevis* chemical genetics screen using the NCI diversity set II. Control tadpole shown in image A. Phenotypes observed in order from image B to H: pigmentation, melanophore morphology, melanophore migration, eye development, general morphology, blistering, edema. We compare the impact of manual and automated annotations of images into those categories in our work, and the impact on the subsequent mode-of-action analysis. (Reproduced with permission from Liggi *et al.*³⁴)

development, general morphology, blistering and edema, which are visualised in Fig. 2 against a control tadpole. The phenotypes are described in detail in Table 1 both qualitatively and quantitatively, along with the method used by the software application for automated detection. Based on the definitions in Table 1, the algorithm follows the steps detailed in Fig. 1.

Data analysis

Active compounds (72 of 1398 in total) were pre-processed using a KNIME⁵⁴ pipeline as described in a recent study³¹ and then subjected to an *in silico* bioactivity prediction method (Laplacian-modified Naïve Bayes classifier) described by Koutsoukas *et al.*⁴⁰ The predictions were refined with the use of per-class confidence score thresholds.³¹ The 70 compounds with at least one bioactivity prediction were linked to both the manually and automatically annotated phenotypes (where only 69 readouts could be used; snapshots of inactive compounds were not provided and one image file was found to be corrupted). Predicted bioactivities proved key for this analysis as a ChEMBL⁵⁵ search for ligand–protein pairs based on the same criteria as the training set⁴⁰ resulted in a single datapoint. Finally, decision trees were built for mode-of-action analysis in the melanophore migration phenotype. We used WEKA⁵⁶ to derive unpruned C4.5 (ref. 57) classification trees with a minimum number of instances in each leaf equal to 20% of the instances of the smallest class (those causing and not causing the melanophore migration phenotype, respectively).

Results and discussion

The chemical genetic screening of *Xenopus laevis* embryos described in the Materials and methods section gave rise to 72 compounds manually annotated as belonging to the pigmentation, general morphology, melanophore morphology, melanophore migration, eye development, blistering or edema phenotypes (illustrated in Fig. 2), 70 of which had at least one predicted protein target (see Materials and methods for details; compounds were also allowed to have multiple phenotypic class labels). 69 of the 70 embryos had an accompanying image (one image failed to be parsed since the file was found to be corrupted), and those were also automatically annotated with their corresponding phenotypes.

We will now firstly explore the impact of parameter choice on the image analysis algorithm, followed by a detailed analysis of the consistency of manual and automated phenotype annotation methods, and the resulting impact on the mode-of-action analysis.

Impact of parameter choice on image analysis

One of the main goals set for the software was flexibility for application to similar image series in the future. For this reason, the software application prompts the user for two thresholds on a “control” image (untreated *Xenopus* tadpole), which should have a similar environment to the image series being analysed, and which are used for Canny⁴⁷ edge detection

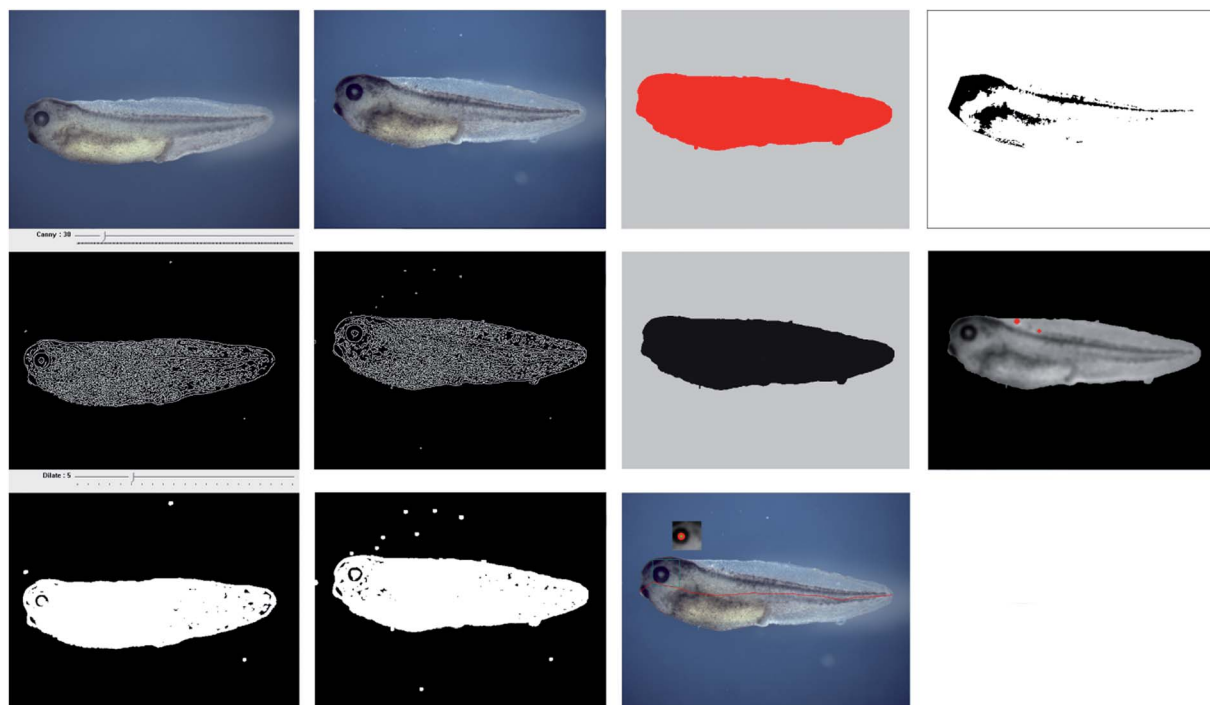


Fig. 3 Impact of parameter choice on the automated phenotype classification algorithm. Column 1 shows the raw image (top) used for deriving the 2 user-defined thresholds for the program, the resulting image after Canny⁴⁷ edge detection (middle) and the dilated image (bottom). Column 2 shows the same three resulting images on an image being automatically processed. Column 3 shows the image after selecting the largest object (top), eroding (middle) and selection of regions of interest along with eye detection (bottom). Finally, Column 4 shows the cells annotated as pigmented (top) and detection of those with rounded pigmented cells.

and object dilation for locating the tadpole in each image. The resulting images from applying these thresholds change dynamically on the screen and are shown in the first column (top: original image, middle: image after edge detection, bottom: image after dilation) in Fig. 3. Based on the steps outlined in Fig. 1, the algorithm applies the definitions from Table 1 to the 69 images in our dataset. In Column 2 of Fig. 3 the same thresholds and transformations are applied to one of the images in our series. In Column 3 the largest object (tadpole) is detected (top) and then eroded back to its normal shape (middle). This is the image from which the analogies are measured for detecting the general morphology and blistering/edema phenotypes. Regions of interest are then extracted such as the 'eye region' shown in Column 3 (bottom) of Fig. 3. Finally, Column 4 shows the regions on the tadpole detected as pigmented (top) and rounded pigmented cells (last screenshot). Overall, and given by the results shown below, we believe that this algorithm is sufficiently robust for the classification of the phenotypes described here. (In case phenotype definitions need to be changed it should be noted that those are entirely flexible, so the user can adjust any of the parameters employed, if so desired.)

Consistency of manually and automatically annotated phenotypes and impact on subsequent mode-of-action analysis

When comparing both annotations – the details of which are given in Table 2 (full table of annotations and smiles are provided in ESI Table 1†) – it was found that for five out of the six annotation comparisons the agreement achieved was higher than 50%. Manual and automated annotations were in better agreement for the phenotypes which are more straightforward to define such as general morphology (73.9%), where only the analogies (the length and height of the tadpole 2D projection) of the tadpole are assessed. For melanophore migration, however, the categorisation was in agreement for only 37.6% of the cases, which was the lowest of all values observed. We next investigated the reason underlying this low agreement between both annotations, and a typical example is displayed in Fig. 4, where the pictures on the left refer to



Fig. 4 Contradicting melanophore migration phenotype annotations between manual and automated classifications. Tadpoles on the left were annotated automatically to belong to this phenotype (but not manually), and those on the right were annotated manually (but not automatically). The two images at the top are an indicator of more subtle differences which may lead to classification differences (and where it is not clearly apparent whether automatic or manual annotation would be more appropriate to be used), while those on the bottom of the figure appear to be a case where manual annotation appeared to have missed the melanophore migration phenotype.

images annotated automatically (but not manually) to belong to the melanophore migration phenotype, while those on the right have a manual (but not automatic) class annotation. The two images at the top are an indicator of more subtle differences which may lead to classification differences (and where it is not clearly apparent whether automatic or manual annotation would be more appropriate to be used), while those on the bottom of the figure appear to be a case where manual annotation appeared to have missed the melanophore migration phenotype.

Given the low agreement between phenotype annotations we hence in the next step subjected this phenotype subset to a comparative bioactivity profile analysis, in order to evaluate how inconsistent phenotype definitions change subsequent mode-of-action analyses.

Table 2 Difference and agreement in phenotype annotations between manual and automatic phenotype detection. Automated classification in many cases agrees with the manual classification, particularly in phenotypes which are easier to define (such as general morphology). However, for melanophore migration (highlighted in bold) it can be seen that there is significant disagreement between the two annotations. This was the purpose of investigating the reason behind different annotations further, and evaluating the impact of different annotations on subsequent bioactivity spectra analysis. It was found that consistent annotations give statistically superior results which are also easier to interpret, hence on this particular dataset automated annotations seem to be advantageous

Phenotypic annotation and agreement between manual and automated annotations	Absolute numbers		Percentage	
	Identical	Different	Identical	Different
Pigmentation	41	28	59.42	40.58
General morphology	51	18	73.91	26.09
Eye development	36	33	52.17	47.83
Melanophore migration	26	43	37.68	62.32
Melanophore morphology	40	29	57.97	42.03
Blistering/oedema	46	23	66.67	33.33

Mode-of-action analysis for the melanophore migration phenotype

Thus far we have demonstrated the importance of consistent definitions for phenotype classification. In this section, we will show the impact different annotations have on generating subsequent models for *in silico* mode of action analysis (while the conclusions drawn can likely be transferred also to other, experimental mode of action analyses). In particular, we generated decision trees (see Data analysis section of Materials and methods) for both manually and automatically annotated melanophore migration phenotypes to explore the impact of this disagreement in annotation. For this analysis, the predicted bioactivity spectra were used as attributes for the classifier, from which the derived bioactivity profiles were used to analyse the difference in mode-of-action analysis for the active compounds.

The resulting C4.5 (ref. 57) classification trees are shown in Fig. 5 (manual annotation) and 6 (automated annotation). Starting at the top (root) of each tree, each node comprises a protein target being assessed for whether a query compound is predicted to bind ("yes") to the said target or not ("no"). Depending on the prediction, arrows then lead to the assessment of another target (node) or an outcome (leaf). At each leaf, the first number signifies how many compounds follow this predicted bioactivity profile while the second number highlights how many compounds are misclassified.

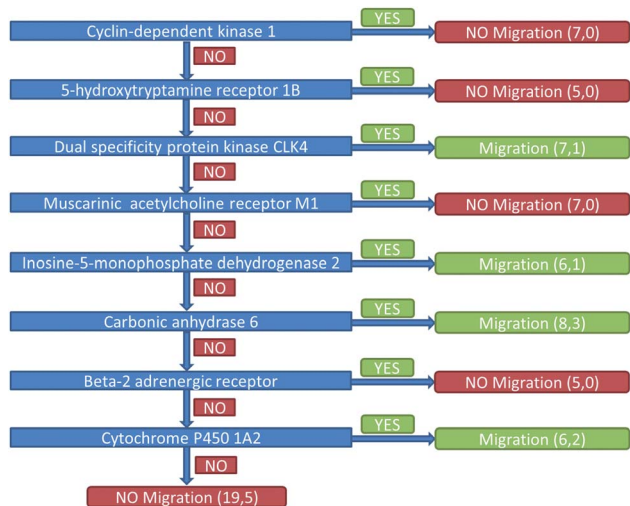


Fig. 5 Mode-of-action decision tree resulting from manual phenotype annotation for all active compounds (originally annotated with a phenotype). At each node (protein target) chosen by the algorithm, a compound predicted to be active ('yes') or not ('no') is either classified (showing the melanophore migration phenotype or not) or forwarded to the next node (protein target) on the next level of the tree. The first number on each leaf signifies how many compounds follow a particular bioactivity profile, whereas the second the number of these compounds which are misclassified. We have found that the tree shown here, derived from manual annotations, performs statistically worse in phenotype classification than the one based on automated annotations (shown in Fig. 6), as well as being less supported by the literature. Hence, we conclude that on the dataset evaluated here automated phenotype classification seems to be more appropriate than manual annotation.

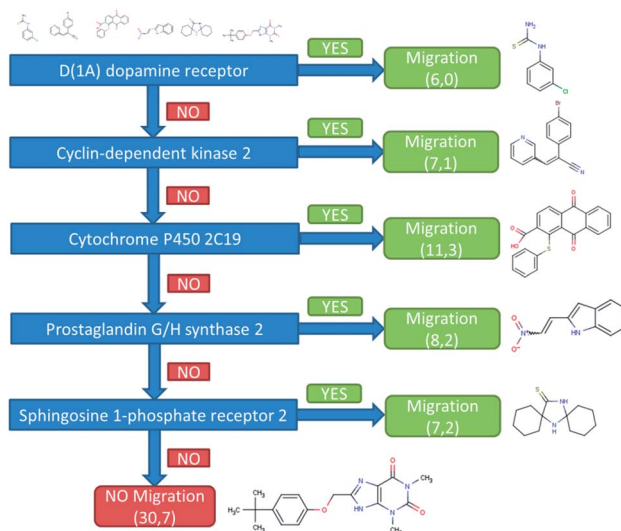


Fig. 6 Mode-of-action decision tree based on automated annotations. It can be observed that compared to the tree based on manual annotations (Fig. 5) a smaller tree is required to explain a large part of the phenotype, while giving at the same time better statistical results. Combined with the fact that the targets identified in this tree have more support in the scientific literature of being associated with the phenotype, we conclude that automated phenotype annotation leads to more consistent results, which are important for the annotations themselves, but also for subsequent mode-of-action analysis.

Overall, the final decision trees generated using manual and automated annotation shown do not seem to differ significantly in performance regarding correctly annotated instances (83% and 79% for manual and automated annotation respectively). However, the classification accuracy using 10-fold cross-validation improved from 47.1% (this is due to the small number of molecules in the active set, the imbalance in instances annotated as eliciting the phenotype and possibly inconsistent phenotype classification) in the case of manual annotations to 56.5% in the case of automated and consistent phenotype annotations. For the classification tree derived from automated annotation, we can see that at every node, activity on a particular target leads to the compound being classified as eliciting the migration phenotype, whereas inactivity leads to a further node. This signifies that the algorithm has located several individual modes-of-action from the bioactivity profiles which can cause the melanophore migration phenotype. It can also be observed that the number of leaves decreased from 9 to 6, the tree size from 17 to 11 and the tree depth from 8 to 5, comprising a tree that is simpler and hence easier to interpret. Hence overall we conclude that the mode-of-action analysis following automated phenotype classification gives a more consistent picture than the identical analysis following manual annotations. In the following we will now investigate how meaningful the analyses are in both cases from the biological side.

In the decision tree in Fig. 5 (derived from manually annotated phenotypes), predicted activity (indicated by the 'Yes' labels in the figure) on dual specificity protein kinase CLK4, inosine-5-monophosphate dehydrogenase 2, carbonic

anhydrase 6 as well as cytochrome P450 1A2 has been detected by our algorithm for compounds causing the melanophore migration phenotype. (For the following discussion it should be noted that the decision tree does not take into account agonism or antagonism on the protein targets, hence we cannot predict the sign of the effect observed.) No literature support could be found for connections of dual specificity protein kinase CLK4 and inosine-5-monophosphate dehydrogenase (IMPDH) 2 with this phenotype. Mutations in the IMPDH1 gene, however, have been shown to induce the RP10 form of autosomal dominant retinitis pigmentosa.⁵⁸ Regarding the remaining two targets for which predicted activity has been classified as causing the melanophore migration phenotype, carbonic anhydrase (CA) 6 and cytochrome P450 1A2, both may have indirect involvement in the phenotype. In particular, CA activity has been shown to be increased in the retinal pigmented epithelium in rat,⁵⁹ whereas another CA member, CA9, has been associated with cell migration.⁶⁰ Finally, for cytochrome P450 1A2, we cannot infer a direct relationship in the mechanism of action of these compounds but there may be involvement in metabolism. An example of such an indirect link is the potential inhibition of melatonin elimination or metabolism (which contracts pigment-containing melanophores in frogs) by fluvoxamine *via* cytochrome P450 1A2 or 2C19.⁶¹

In the second tree (automatically annotated phenotypes), the predicted targets used to separate between compounds causing the melanophore migration phenotype are the dopamine D1a receptor, cyclin-dependent kinase 2, the cytochrome P450 2C19, prostaglandin G/H synthase 2 and sphingosine 1-phosphate receptor 2. In particular, activation of the dopamine D1a receptor may be responsible for the aggregation of melanophores shown to be mediated by dopamine in *Pseudopleuronectes americanus*,⁶² as well as blocking the release of melanophore-stimulating hormone from neuroendocrine melanotrope cells in *Xenopus laevis*.⁶³ Dispersal of pigment was also caused by dopamine in retinal pigment epithelium (RPE) cells in *Lepomis cyanellus*.⁶⁴ The next protein target used in the tree is cyclin-dependent kinase 2, which is known to be involved in melanocyte survival.⁶⁵ Melanosome transport and synthesis are thought to be regulated by the microphthalmia-associated transcription factor (MITF), whose role influences the expression of cyclin-dependent kinase inhibitors.⁶⁶ As for the predicted enzyme cytochrome P450 2C19, similar to cytochrome P450 1A2 (see above) we can only infer an indirect relationship *via* melatonin elimination or metabolism inhibition.⁶¹ At the next level of the decision tree, the algorithm has selected prostaglandin G/H synthase 2 (cyclooxygenase-2) to separate the compounds causing melanophore migration from the inactive compounds in the set. Prostaglandin G/H synthase 2 is expressed in RPE cells in both humans⁶⁷ and rat.⁶⁸ While this target is hence linked to pigmentation itself, to our knowledge no literature has reported its involvement in migration. On the other hand, the final target selected in this analysis, sphingosine 1-phosphate (S1P) receptor 2 has a well-documented involvement in cell migration and more specifically in smooth muscle cells.^{69–71} Amphibian melanophores have been shown to be functionally modified smooth muscle cells, thereby lending

support to this prediction.⁷² Finally, it is suggested that SP1 may activate the extracellular signal-regulated protein kinase, which in turn inhibits melanin synthesis through MITF degradation.⁷³ Hence, overall a majority of targets from this decision tree can be linked to the phenotype observed.

Following the evaluation of the predicted bioactivity profiles between both decision trees, we can conclude that there is more literature support for the classification based on automated phenotype annotation. In addition to the improved phenotype classification results this leads us to the conclusion that the definition of consistent phenotypes is crucial, both for the quality of annotations themselves, as well as for the quality of the subsequent mode-of-action analysis.

Conclusions

In this work, we investigated the interplay between the consistency of phenotype definitions in phenotypic readouts and their impact on subsequent *in silico* mode-of-action analysis. To this end, we used both manual and automatic phenotype annotations on a chemical genetic screen of *Xenopus laevis* tadpoles treated with compounds from NCI diversity set II,⁴⁵ and compared predicted mode-of-action analyses of poly-pharmacological nature between both approaches.

It was found that there was a wide variety in agreement and disagreement between automated and manual classification approaches, between 73.9% in the case of the general morphology phenotype and 37.6% in the case of the melanophore migration phenotype. The automated categorisation improved the decision tree classification accuracy of the melanophore migration phenotype by 9.4% while at the same time reducing its size by eight nodes and the number of leaves and depth by three, rendering the model both more accurate and easier to interpret. For many targets predicted to be involved in this phenotype literature support could be found (such as the dopamine D1a receptor, cyclin-dependent kinase 2, the cytochrome P450 2C19, prostaglandin G/H synthase 2 and the sphingosine 1-phosphate receptor 2), while the remainder would be testable novel mode-of-action hypotheses.

Overall we conclude that a consistent phenotype definition is important for subsequent mode-of-action studies, both when considering the follow-up analysis of individual compounds, as well as when analyzing the mode-of-action of groups of compounds which are associated with the same phenotype.

Declarations

The authors declare that there are no conflicts of interest. All experiments were performed in compliance with the relevant laws and institutional guidelines at the University of East Anglia. The research has been approved by the local ethical review committee according to UK Home Office regulations.

Acknowledgements

This research was supported by Eli Lilly (GD), EPSRC (GD), University of East Anglia (AH and KH), John Innes Centre (AH),

AstraZeneca (AH), John Jarrold Trust studentship (KH) and Unilever (AB).

References

- 1 J. Kotz, Phenotypic screening, take two, *J. SciBX*, 2012, 5, 1–3.
- 2 Y. Feng, T. J. Mitchison, A. Bender, D. W. Young and J. A. Tallarico, Multi-parameter phenotypic profiling: using cellular effects to characterize small-molecule compounds, *Nat. Rev. Drug Discovery*, 2009, 8, 567–578.
- 3 S. A. Haney, P. LaPan, J. Pan and J. Zhang, High-content screening moves to the front of the line, *Drug Discovery Today*, 2006, 11, 889–894.
- 4 H. Morgan, *et al.*, EuroPhenome: a repository for high-throughput mouse phenotyping data, *Nucleic Acids Res.*, 2010, 38, D577–D585.
- 5 G. P. Aithal, *et al.*, Case definition and phenotype standardization in drug-induced liver injury, *Clin. Pharmacol. Ther.*, 2011, 89, 806–815.
- 6 C. Laggner, *et al.*, Chemical informatics and target identification in a zebrafish phenotypic screen, *Nat. Chem. Biol.*, 2012, 8, 144–146.
- 7 D. W. Young, *et al.*, Integrating high-content screening and ligand-target prediction to identify mechanism of action, *Nat. Chem. Biol.*, 2008, 4, 59–68.
- 8 R. E. Kälin, N. E. Bänziger-Tobler, M. Detmar and A. W. Brändli, An *in vivo* chemical library screen in *Xenopus* tadpoles reveals novel pathways involved in angiogenesis and lymphangiogenesis, *Blood*, 2009, 114, 1110–1122.
- 9 G. N. Wheeler and A. W. Brändli, Simple vertebrate models for chemical genetics and drug discovery screens: lessons from zebrafish and *Xenopus*, *Dev. Dyn.*, 2009, 238, 1287–1308.
- 10 M. L. Tomlinson, A. E. Hendry and G. N. Wheeler, Chemical genetics and drug discovery in *Xenopus*, *Methods Mol. Biol.*, 2012, 917, 155–166.
- 11 M. L. Tomlinson, M. Rejzek, M. Fidock, R. Field and G. N. Wheeler, Chemical genomics identifies compounds affecting *Xenopus laevis* pigment cell development, *Mol. Biosyst.*, 2009, 5, 376–384.
- 12 V. C. Abraham, D. L. Taylor and J. R. Haskins, High content screening applied to large-scale cell biology, *Trends Biotechnol.*, 2004, 22, 15–22.
- 13 A. E. Carpenter, *et al.*, CellProfiler: image analysis software for identifying and quantifying cell phenotypes, *Genome Biol.*, 2006, 7, R100.
- 14 B. Bayraktar, B. Rajwa and J. P. Robinson, Feature extraction for cellular shape analysis in high-content screening (HCS) applications, *Proc. SPIE*, 2005, 5699, 342–353.
- 15 Z. Zhang, Y. Ge, D. Zhang and X. Zhou, High-content analysis in monastrol suppressor screens. A neural network-based classification approach, *Methods Inf. Med.*, 2011, 50, 265–272.
- 16 E. Krausz, High-content siRNA screening, *Mol. Biosyst.*, 2007, 3, 232–240.
- 17 B. Neumann, *et al.*, High-throughput RNAi screening by time-lapse imaging of live human cells, *Nat. Methods*, 2006, 3, 385–390.
- 18 E. K. Kieserman, C. Lee, R. S. Gray, T. J. Park and J. B. Wallingford, High-magnification *in vivo* imaging of *Xenopus* embryos for cell and developmental biology, *Cold Spring Harb. Protoc.*, 2010, DOI: 10.1101/pdb.prot5427.
- 19 H. Y. Kim and L. A. Davidson, Investigating morphogenesis in *Xenopus* embryos: imaging strategies, processing, and analysis, *Cold Spring Harb. Protoc.*, 2013, 2013, 298–304.
- 20 R. Yelin, *et al.*, Multimodality optical imaging of embryonic heart microstructure, *J. Biomed. Opt.*, 2007, 12, 1–28.
- 21 T. Goda, *et al.*, Genetic screens for mutations affecting development of *Xenopus tropicalis*, *PLoS Genet.*, 2006, 2, e91.
- 22 A. A. Rana, C. Collart, M. J. Gilchrist and J. C. Smith, Defining synphenotype groups in *Xenopus tropicalis* by use of antisense morpholino oligonucleotides, *PLoS Genet.*, 2006, 2, e193.
- 23 K. Dooley and L. I. Zon, Zebrafish: a model system for the study of human disease, *Curr. Opin. Genet. Dev.*, 2000, 10, 252–256.
- 24 A. Vogt, *et al.*, Automated image-based phenotypic analysis in zebrafish embryos, *Dev. Dyn.*, 2009, 238, 656–663.
- 25 T. Annala, *et al.*, ZebiAT, an image analysis tool for registering zebrafish embryos and quantifying cancer metastasis, *BMC Bioinf.*, 2013, 14, S5.
- 26 S. Xia, Y. Zhu, X. Xu and W. Xia, Computational techniques in zebrafish image processing and analysis, *J. Neurosci. Methods*, 2013, 213, 6–13.
- 27 R. Mikut, *et al.*, Automated processing of zebrafish imaging data: a survey, *Zebrafish*, 2013, 10, 401–421.
- 28 P. S. Kutchukian, *et al.*, Inside the mind of a medicinal chemist: the role of human bias in compound prioritization during drug discovery, *PLoS One*, 2012, 7, e48476.
- 29 M. S. Lajiness, G. M. Maggiora and V. Shanmugasundaram, Assessment of the consistency of medicinal chemists in reviewing sets of compounds, *J. Med. Chem.*, 2004, 47, 4891–4896.
- 30 M. A. Bray, A. N. Fraser, T. P. Hasaka and A. E. Carpenter, Workflow and metrics for image quality control in large-scale high-content screens, *J. Biomol. Screen*, 2012, 17, 266–274.
- 31 S. Liggi, *et al.*, Extensions to *In Silico* Bioactivity Predictions Using Pathway Annotations and Differential Pharmacology Analysis: Application to *Xenopus laevis* Phenotypic Readouts, *Mol. Inf.*, 2013, 32(11–12), 1009–1024.
- 32 I. Cortes-Ciriano, *et al.*, Experimental validation of *in silico* target predictions on synergistic protein targets, *MedChemComm*, 2013, 4, 278.
- 33 A. Subramanian, *et al.*, Gene set enrichment analysis: A knowledge-based approach for interpreting genome-wide, *Proc. Natl. Acad. Sci. U. S. A.*, 2005, 102, 15545–15550.
- 34 A. Koutsoukas, *et al.*, From *in silico* target prediction to multi-target drug design: Current databases, methods and applications, *J. Proteomics*, 2011, 74, 2554–2574.

- 35 M. J. Keiser, *et al.*, Relating protein pharmacology by ligand chemistry, *Nat. Biotechnol.*, 2007, **25**, 197–206.
- 36 M. J. Keiser, *et al.*, Predicting new molecular targets for known drugs, *Nature*, 2009, **462**, 175–181.
- 37 T. M. Steindl, D. Schuster, C. Laggner and T. Langer, Parallel screening: a novel concept in pharmacophore modeling and virtual screening, *J. Chem. Inf. Model.*, 2006, **46**, 2146–2157.
- 38 D. Schuster, C. Laggner, T. M. Steindl and T. Langer, Development and validation of an in silico P450 profiler based on pharmacophore models, *Curr. Drug Discovery Technol.*, 2006, **3**, 1–48.
- 39 M. Glick, J. L. Jenkins, J. H. Nettles, H. Hitchings and J. W. Davies, Enrichment of high-throughput screening data with increasing levels of noise using support vector machines, recursive partitioning, and Laplacian-modified naive bayesian classifiers, *J. Chem. Inf. Model.*, 2006, **46**, 193–200.
- 40 A. Koutsoukas, *et al.*, *In silico* target predictions: comparing multiclass Naïve Bayes and Parzen-Rosenblatt Window and the definition of a benchmarking dataset for target prediction, *J. Chem. Inf. Model.*, 2013, **53**, 1957–1966.
- 41 Nidhi, M. Glick, J. W. Davies and J. L. Jenkins, Prediction of biological targets for compounds using multiple-category Bayesian models trained on chemogenomics databases, *J. Chem. Inf. Model.*, 2006, **46**, 1124–1133.
- 42 F. Nigsch, A. Bender, J. L. Jenkins and J. B. O. Mitchell, Ligand-target prediction using Winnow and naive Bayesian algorithms and the implications of overall performance statistics, *J. Chem. Inf. Model.*, 2008, **48**, 2313–2325.
- 43 J. Mestres, E. Gregori-Puigjané, S. Valverde and R. V. Solé, Data completeness—the Achilles heel of drug-target networks, *Nat. Biotechnol.*, 2008, **26**, 983–984.
- 44 D. Vidal and J. Mestres, *In Silico* Receptorome Screening of Antipsychotic Drugs, *Mol. Inf.*, 2010, **29**, 543–551.
- 45 NCI Repositories, Diversity Set Information, http://ntp.nhl.nih.gov/branches/dscb/div2_explanation.html, accessed 30 May 2013.
- 46 Open Source Computer Vision, OpenCV, 2013, <http://opencv.org>.
- 47 J. Canny, A computational approach to edge detection, *IEEE Trans. Pattern. Anal. Mach. Intell.*, 1986, **8**, 679–698.
- 48 G. Bradski and A. Kaehler, Image Processing (Morphology), in *Learning OpenCV: Computer Vision with the OpenCV Library*, O'Reilly Media, 2008, p. 115.
- 49 S. Suzuki and K. Abe, Topological Structural Analysis of Digitized Binary Images by Border Following, *Comput Vision Graph*, 1985, **46**, 32–46.
- 50 G. Bradski and A. Kaehler, Image Processing (Smoothing), in *Learning OpenCV: Computer Vision with the OpenCV Library*, O'Reilly Media, 2008, p. 110.
- 51 P. V. C. Hough, Machine Analysis of Bubble Chamber Pictures, in *Proc. Int. Conf. High Energy Accel. Instrum.*, 1959.
- 52 R. O. Duda and P. E. Hart, Use of the Hough Transformation to Detect Lines and Curves in Pictures, *Commun. ACM*, 1972, **15**, 11–15.
- 53 H. K. Yuen, J. Princen, J. Illingworth and J. Kittler, A Comparative Study of Hough Transform Methods for Circle Finding, *Image Vis. Comput.*, 1990, **8**, 71–77.
- 54 M. R. Berthold, N. Cebron, F. Dill and T. R. Gabriel, KNIME: The Konstanz information miner, in *Studies in Classification, Data Analysis, and Knowledge Organization (GfKL 2007)*, Springer, 2007, pp. 319–326.
- 55 A. Gaulton, *et al.*, ChEMBL: a large-scale bioactivity database for drug discovery, *Nucleic Acids Res.*, 2011, **44**, 1–8.
- 56 M. Hall, *et al.*, *The WEKA Data Mining Software: An Update*, SIGKDD Explor Newsl 11, 2009.
- 57 J. R. Quinlan, *C4.5: Programs for Machine Learning*, Morgan Kaufmann Publishers, 1993.
- 58 S. J. Bowne, *et al.*, Mutations in the inosine monophosphate dehydrogenase 1 gene (IMPDH1) cause the RP10 form of autosomal dominant retinitis pigmentosa, *Hum. Mol. Genet.*, 2002, **11**, 559–568.
- 59 M. Eichhorn, M. Schreckenberger, E. R. Tamm and E. Lütjen-Drecoll, Carbonic anhydrase activity is increased in retinal pigmented epithelium and choriocapillaris of RCS rats, *Graefes Arch. Clin. Exp. Ophthalmol.*, 1996, **234**, 258–263.
- 60 H. J. Shin, *et al.*, Carbonic anhydrase IX (CA9) modulates tumor-associated cell migration and invasion, *J. Cell Sci.*, 2011, **124**, 1077–1087.
- 61 P. R. Shankar, *et al.*, Melatonin, the hormone of darkness: A ray of Hope for Many Diseases, *Pharmacologyonline*, 2006, **2**, 274–289.
- 62 D. Burton, Differential *in vivo* Sensitivity of Melanophores and Xanthophores to Catecholamines in Winter Flounder (*Pseudopleuronectes americanus* Walbaum) Integumentary Patterns, *J. Exp. Biol.*, 1985, **114**, 649–659.
- 63 E. P. C. T. De Rijk, F. J. C. van Strien and E. W. Roubos, Demonstration of Coexisting Catecholamine (Dopamine), Amino Acid (GABA), and Peptide (NPY) Involved in Inhibition of Melanocyte Cell Activity in *Xenopus Levis*: A Quantitative Ultrastructural, Immunocytochemical Study, *J. Neurosci.*, 1992, **12**, 864–871.
- 64 U. Druenner and B. Burnside, Pigment Granule Migration in Isolated Cells of the Teleost Retinal Pigment Epithelium, *Invest. Ophthalmol. Visual Sci.*, 1986, **27**, 1634–1643.
- 65 C. Wasmeier, A. N. Hume, G. Bolasco and M. C. Seabra, Melanosomes at a glance, *J. Cell Sci.*, 2008, **121**, 3995–3999.
- 66 J. Vachtenheim and J. Borovanský, “Transcription physiology” of pigment formation in melanocytes: central role of MITF, *Exp. Dermatol.*, 2010, **19**, 617–627.
- 67 M. S. Chin, C. N. Nagineni, L. C. Hooper, B. Detrick and J. J. Hooks, Cyclooxygenase-2 Gene Expression and Regulation in Human Retinal Pigment Epithelial Cells, *Invest. Ophthalmol. Visual Sci.*, 2001, **42**, 2338–2346.
- 68 C. T. Beuckmann, *et al.*, Lipocalin-Type Prostaglandin D Synthase (beta-Trace) Is Located in Pigment Epithelial Cells of Rat Retina and Accumulates within Interphotoreceptor Matrix, *J. Neurosci.*, 1996, **16**, 6119–6124.
- 69 S. Inoue, *et al.*, Regulation of arterial lesions in mice depends on differential smooth muscle cell migration: a

- role for sphingosine-1-phosphate receptors, *Vasc. Surg.*, 2007, **46**, 756–763.
- 70 L. Becciolini, *et al.*, Sphingosine 1-phosphate inhibits cell migration in C2C12 myoblasts, *Biochim. Biophys. Acta*, 2006, **1761**, 43–51.
- 71 W. I. Leong and J. D. Saba, S1P metabolism in cancer and other pathological conditions, *Biochimie*, 2010, **92**, 716–723.
- 72 S. Salim and S. A. Ali, *Melanophores: Smooth Muscle Cells in Disguise*, in *Current Basic and Pathological Approaches to the Function of Muscle Cells and Tissues – From Molecules to Humans*, InTech, 2012, DOI: 10.5772/48256.
- 73 D. S. Kim, Sphingosine-1-phosphate decreases melanin synthesis *via* sustained ERK activation and subsequent MITF degradation, *J. Cell Sci.*, 2003, **116**, 1699–1706.